



HAL
open science

Electrochemical Approach for the Molecular Catalytic Activation of N-O Bond: Application to Nitrous Oxide and Pyridine N-Oxide Molecules

Rana Deeba

► **To cite this version:**

Rana Deeba. Electrochemical Approach for the Molecular Catalytic Activation of N-O Bond: Application to Nitrous Oxide and Pyridine N-Oxide Molecules. Other. Université Grenoble Alpes [2020-..], 2023. English. NNT: 2023GRALV080 . tel-04515370

HAL Id: tel-04515370

<https://theses.hal.science/tel-04515370>

Submitted on 21 Mar 2024

HAL is a multi-disciplinary open access archive for the deposit and dissemination of scientific research documents, whether they are published or not. The documents may come from teaching and research institutions in France or abroad, or from public or private research centers.

L'archive ouverte pluridisciplinaire **HAL**, est destinée au dépôt et à la diffusion de documents scientifiques de niveau recherche, publiés ou non, émanant des établissements d'enseignement et de recherche français ou étrangers, des laboratoires publics ou privés.

THÈSE

Pour obtenir le grade de

DOCTEUR DE L'UNIVERSITÉ GRENOBLE ALPES

École doctorale : CSV- Chimie et Sciences du Vivant

Spécialité : Chimie inorganique et Bio inorganique

Unité de recherche : Département de Chimie Moléculaire

Approche électrochimique de l'activation moléculaire catalytique de liaisons N-O : Application aux molécules protoxyde d'azote et pyridine N-oxyde

Electrochemical Approach for the Molecular Catalytic Activation of N-O Bond: Application to Nitrous Oxide and Pyridine N-Oxide Molecules

Présentée par :

Rana DEEBA

Direction de thèse :

Sylvie CHARDON

DIRECTRICE DE RECHERCHE, Université Grenoble Alpes

Directrice de thèse

Cyrille COSTENTIN

PROFESSEUR DES UNIVERSITES, Université Grenoble Alpes

Co-directeur de thèse

Rapporteurs :

Marine DESAGE- EL MURR

PROFESSEURE DES UNIVERSITES, Université de Strasbourg

Ally AUKAULOO

PROFESSEUR DES UNIVERSITES, Université Paris-Saclay

Thèse soutenue publiquement le **27 octobre 2023**, devant le jury composé de :

Sylvie CHARDON

DIRECTRICE DE RECHERCHE, CNRS délégation Alpes

Directrice de thèse

Cyrille COSTENTIN

PROFESSEUR DES UNIVERSITES, Université Grenoble Alpes

Co-directeur de thèse

Victor MOUGEL

ASSISTANT PROFESSOR, ETH Zürich

Examinateur

Jérôme CHAUVIN

PROFESSEUR DES UNIVERSITES, Université Grenoble Alpes

Président

Marine DESAGE- EL MURR

PROFESSEURE DES UNIVERSITES, Université de Strasbourg

Rapporteuse

Ally AUKAULOO

PROFESSEUR DES UNIVERSITES, Université Paris-Saclay

Rapporteur



Acknowledgments

‘‘Alone we can do so little; together we can do so much’’ is a well known proverb by Hellen Keller and I strongly believe that completing a PhD requires the support of many great people around. I can’t believe a journey of three years is coming to an end and I can’t believe that I am fulfilling one of my first list dreams of pursuing a PhD. When I embarked to the PhD journey three years ago, little did I know the profound experiences that lay ahead. But I insisted on learning, challenging myself and working hard. I used to consider everyday is a new opportunity to learn new things. I failed and did many mistakes but I never gave up, continued to learn and progress day by day.

First and foremost, I would like to thank deeply my supervisors, Sylvie Chardon and Cyrille Costentin. From the initial stages of starting the PhD to the final submission of my thesis, their unwavering presence and wealth of wisdom have been instrumental in shaping my academic growth. I highly valued the biweekly meetings and discussions we held, which not only served as crucial checkpoints to keep me on track, but also provided me with plenty of encouragement. I am profoundly grateful for the immeasurable contributions they made to my development in the field of electrochemistry. Your guidance and encouragement have been invaluable! Together we have wrote six articles in well published journals and I am grateful and thankful for achieving this success since it will enrich my future professional career.

I am incredibly grateful for the opportunity to be a part of an exceptional research institute ‘‘Département de Chimie Moléculaire’’ working within well known research team ‘‘EMPRE’’ in the field of molecular electrochemistry and redox photochemistry using well developed methods and techniques to study in depth reaction mechanisms for small molecules activation. I thank all the members of this team researchers, postdoc and PhD students!

I would like also to express my gratitude to the committee jury members of my CSI, Christophe Bucher, Murielle Chavarot Kerlidou and Jérôme Fortage for following up my research progress of the first and second year. The discussion with them always led to fruitful ideas and always gave me more encouragement and motivation.

Furthermore I would like to thank the committee jury members for accepting to be part of my PhD defense jury. Ally Aukauloo, Marine Desage-El Murr, Victor Mougel and Jérôme Chauvin.

I also had the chance to be working with three, hard working intelligent internship students, Titouan, Camille and Alexandra. You have worked hard and with perseverance to achieve publishable results. Thank you deeply!

I am also thankful for Selim and Florian for always being ready to help. Thankful for Florian for his patience, time and support he has given me to train to use the GC, HPLC and for doing the EPR analysis and to overcome technical difficulties I had during my experiments.

I am grateful for the Institut de Chimie Moléculaire de Grenoble including the NMR and PSM for providing facilities to do analysis most especially Amélie Durand and Rodolphe Gueret thank you for your patience and help.

I would like to thank our collaborators at the LCMCE (NIMBE)-CEA Paris Saclay including Thibault Cantat, Emmanuel Nicolas, Lucile Anthore Dalion and the former PhD student Marianne Kjellberg together with JOLIOT CEA institut including Annamaria Quaranta for sharing fruitful ideas and discussions which helped a lot to reach the proposed mechanism of N_2O reduction by rhenium complex.

I also had the chance to meet a very kind, intelligent visiting researchers in our lab Elina Laurila and Hua Liang. Thank you for the nice time and evenings we spent together around in the city.

I am also indebted to my exceptional lab mates. I am proud to say that we became more than just lab partners, but good friends. I have met many friends throughout those three years. Emiliano former phd student was one of my first friends I have met, we used to hangout during the weekends in the city sharing jokes and stories. Lionie M2 internship student I thank her for the hiking adventures we did in the mountains. Mélanie is a great colleageu, we helped and supported each other a lot during the PhD. I would like to thank Chukuka and Samuel former PhD students we used always to hang around and spend nice summer evenings until late time talking and laughing. I would like also to thank Lorna for always coming out with new plans, and gathering of all the lab mates at her house which made me feel that I have another family away from home. I thank also Kabibi, Valentin, Eder, Baptiste, Richard, Jonathan, Damien, Adrian, Thomas, Ludivine, Irene, Rayhane, Alex, Walaa, Fakourou, Océane, Funmilola, Subash, Lili, Guanqi, Leticia, Fatima and Charbel.

Lastly, I want to express my deepest gratitude to my family who believed in my abilities and gave me support. Your encouragement played an integral role in my accomplishments. To my mom, dad, and my sister Rita: Thank you for everything!

Abstract

Due to increasing concerns regarding global warming an interest in $\text{N}_2\text{O}(\text{g})$ reduction is gradually increasing in the recent days. N_2O has been categorized as the greatest contributor to the stratospheric ozone depletion and is regarded as the third most significant anthropogenic greenhouse gas. Reduction of N_2O to N_2 gas is therefore of interest. Despite being a thermodynamically good oxidant, N_2O is a kinetically inert molecule. Hence its use as an oxidant requires harsh conditions ($> 200^\circ\text{C}$) heterogeneous catalysis. Enzymes, namely N_2O reductase enzymes, have been reported to be able to reduce nitrous oxide, and Cu based molecular models of these enzymes active sites have been proposed and used as stoichiometric reagents to reduce N_2O . More generally, binding and activation of N_2O at transition metal complex centers has been studied and reviewed, but only few examples of reactions with N_2O occur under homogeneous and mild reaction conditions. In most cases, N_2O reacts with highly reactive organometallic species via oxygen atom transfer. This reactivity has enabled the development of transition metal-catalyzed transformations where N_2O is deoxygenated in the presence of reductants such as Grignard reagents, phosphines, aldehydes, alcohols, or CO.

It is surprising to observe that, besides these few examples, there have been very few attempts to catalyze the electrochemical reduction of N_2O to N_2 with molecular catalysts as it can also be viewed as a prototypical example of N-O bond deoxygenation. For that reason, we have decided in this thesis to undergo a thorough investigation of the N_2O to N_2 electrochemical conversion with a molecular catalytic approach under ambient conditions in organic solvent and performing in depth mechanistic analysis using spectroelectrochemical techniques. Our initial reasoning is based on analogies between N_2O and CO_2 (both molecules are isoelectronic with a central electrophilic atom). N_2O should bind to the open coordination site on reduced form of a transition metal complex (rhenium and manganese) and transfer of electrons should occur from the metal to the electrophilic center of N_2O in the presence of an acid acting as proton source to facilitate the breaking of the N-O bond while stabilizing the oxygen. In this context the electrons used for the reduction of N_2O were obtained electrochemically via the use of homogenous molecular catalysts acting as electron shuttles from the electrode to the substrate and creating open coordination site for (N_2O) binding to the reduced form of the catalyst.

Simpler homogeneous catalysis was also be realized by the use of redox catalysts (organic aromatic molecules) in which the catalyst acquires the electrons via an outer-sphere manner from the electrode acting heterogeneously and delivers them via an outersphere manner

with no chemical interaction with N_2O . This allows to set a benchmark for catalysis. However chemical catalysis is more interesting in the sense that the catalyst should be designed to allow chemical interaction between the reduced active form of the catalyst and the substrate.

Numerous advances have been made in recent years in understanding the activation of C-O, O-O, P-O bonds, but less has focused on the activation of N-O bonds. It is the purpose of this thesis to contribute to explore this field which is not only limited to N-O activation in N_2O but also opens new directions for the deoxygenation of N-oxides which is discussed in the last section of this thesis.

Résumé

En raison des préoccupations croissantes concernant le réchauffement climatique, l'intérêt pour la réduction du $\text{N}_2\text{O}(\text{g})$ s'est progressivement accru ces dernières années. Le N_2O est considéré comme le principal responsable de la dégradation de la couche d'ozone stratosphérique et comme le troisième gaz à effet de serre anthropique le plus important. La réduction du N_2O en gaz N_2 est donc intéressante. Bien qu'il soit un bon oxydant thermodynamiquement parlant, le N_2O est une molécule cinétiquement inerte. Son utilisation en tant qu'oxydant nécessite donc une catalyse hétérogène dans des conditions difficiles ($> 200^\circ\text{C}$). Des enzymes, à savoir les N_2O réductases, ont été signalées comme étant capables de réduire l'oxyde nitreux, et des molécules à base de Cu, modèles des sites actifs de ces enzymes, ont été proposés et utilisés comme réactifs stœchiométriques pour réduire le N_2O . Plus généralement, la liaison et l'activation du N_2O au niveau des centres métalliques des complexes de métaux de transition ont été étudiées et examinées, mais seuls quelques exemples de réactions avec le N_2O se produisent dans des conditions de réaction homogènes et douces. Dans la plupart des cas, le N_2O réagit avec des espèces organométalliques très réactives par transfert d'atomes d'oxygène. Cette réactivité a permis le développement de transformations catalysées par des métaux de transition où le N_2O est désoxygéné en présence de réducteurs tels que les réactifs de Grignard, les phosphines, les aldéhydes, les alcools ou le CO.

Il est surprenant de constater qu'en dehors de ces quelques exemples, il y a eu très peu de tentatives pour catalyser la réduction électrochimique de N_2O en N_2 à l'aide de catalyseurs moléculaires, car elle cette méthode peut également être considérée comme un exemple de prototype de réaction de désoxygénation de la liaison N-O. Pour cette raison, nous avons décidé dans cette thèse de procéder à une étude approfondie de la conversion électrochimique de N_2O en N_2 avec une approche de catalyse moléculaire dans des conditions ambiantes dans un solvant organique et d'effectuer une analyse mécanistique approfondie en utilisant des techniques spectroélectrochimiques. Notre raisonnement initial est basé sur des analogies entre le N_2O et le CO_2 (les deux molécules sont isoélectroniques avec un atome électrophile central). Le N_2O devrait se lier au site vacant du métal de la forme réduite d'un complexe de métaux de transition (rhénium et manganèse) et le transfert d'électrons devrait se produire du métal vers le centre électrophile du N_2O en présence d'un acide agissant comme source de protons pour faciliter la rupture de la liaison N-O tout en stabilisant l'oxygène. Dans ce contexte, les électrons utilisés pour la réduction du N_2O sont obtenus par voie électrochimique via l'utilisation de catalyseurs

moléculaires en solutions homogènes agissant comme des navettes d'électrons de l'électrode au substrat (N_2O) lié à la forme réduite du catalyseur.

Une catalyse homogène plus simple a également été réalisée par l'utilisation de catalyseurs redox (molécules aromatiques organiques) qui acquièrent les électrons, via un transfert en sphère externe, de l'électrode agissant de manière hétérogène et les délivrent, sans interaction chimique au N_2O via une réaction en sphère externe). Cela permet d'apporter une réaction électrochimique de référence en catalyse. Cependant, la catalyse chimique est plus intéressante dans le sens où le catalyseur doit être conçu pour permettre une interaction chimique entre la forme active réduite du catalyseur et le substrat.

De nombreuses avancées ont été réalisées ces dernières années dans la compréhension de l'activation des liaisons C-O, O-O, P-O, mais l'activation des liaisons N-O a été moins étudiée. L'objectif de cette thèse est de contribuer à l'exploration de ce domaine qui n'est pas seulement limité à l'activation des liaisons N-O dans le N_2O mais qui ouvre également de nouvelles directions pour la désoxygénation des N-oxydes, ce qui est discuté dans la dernière partie de cette thèse.

Table of Abbreviations

Ar	Argon
bpy	2,2'-bipyridine
CV	Cyclic voltammetry
diam.	Diameter
CPE	Controlled potential electrolysis
DISP	Disproportionation
DMF	Dimethylformamide
dmbpy	Dimethylbipyridine
EDG/EWG	Electron donating /electron withdrawing group
ET	Electron transfer
FTIR	Fourier transform infrared
FE	Faradaic efficiency
GC	Gas chromatography
GCE	Glassy carbon electrode
HPLC	High performance liquid chromatography
HER	Hydrogen evolution reaction
LSV	Linear scan voltammetry
MLCT/LLCT	Metal-to-ligand /ligand-to-ligand charge transfer
MS	Mass spectrometry
NMR	Nuclear magnetic resonance
PCET	Proton coupled electron transfer
PNO	Pyridine N-oxide
RDE	Rotating disk electrode
SEC	Spectroelectrochemistry
sh	Shoulder
SCE	Saturated calomel electrode
TON/TOF	Turnover number /Turnover frequency
TPP	Tetraphenylporphyrin
UV-vis	Ultraviolet-visible
WE	Working electrode
Yrs	Years

Table of Contents

Acknowledgments	1
Abstract	5
Résumé	7
Table of Abbreviations	11
Chapter I : General Introduction	21
1. Nitrous oxide gas.....	22
2. Nitrous oxide no laughing matter	22
3. Properties of N ₂ O and its reactivity.....	24
4. Transforming nitrous oxide / mitigation strategies	25
4.1 Natural Strategies	25
4.2 Nitrous oxide use in synthetic organic and inorganic chemistry	27
5. Principles of molecular catalysis of electrochemical reactions.....	35
6. State of art of the catalysis of the electrochemical reduction of N ₂ O	36
7. Thesis objectives and scope	39
Chapter II: Outer-Sphere Activation of N-O Bond in N₂O: Redox Catalysis	45
1. Introduction	46
2. Homogeneous redox catalysis: experimental results.....	48
2.1 Cyclic Voltammetry analysis under argon and N ₂ O effect of scan rate	48
2.2 Minimizing Ohmic Drop.....	50
2.3 Effect of addition of water	51
2.4 Selectivity of the redox catalytic process: electrolysis	53
3. Homogeneous redox catalysis: kinetic analysis	54
4. Direct reduction of N ₂ O	58
5. Comparison of direct reduction and homogeneous redox reduction of N ₂ O	59

6. Deactivation of the catalyst by co-substrate: Application to 4-cyanopyridine	61
7. Conclusion.....	64

Chapter III: Homogeneous Chemical Catalysis of Electrochemical

Molecular Reduction of N₂O 69

1. Introduction	70
2. Chemical homogeneous catalysis vs. redox catalysis	71
3. Electrochemical reduction of N ₂ O mediated by Fe tetraphenylporphyrin catalysts	72
4. Electrochemical reduction of N ₂ O mediated by [Re(bpy-R)(CO) ₃ X].....	74
4.1 Motive for the choice of rhenium complexes.....	74
4.2 Rhenium complexes considered	76
5. Electrochemical reduction of N ₂ O mediated by [Mn(bpy-R)(CO) ₃ X]	86
6. Contrasts between Rhenium and Manganese bipyridine complexes towards electrocatalytic reduction of N ₂ O	89
7. Electrochemical reduction of N ₂ O mediated by Ru, Rh and Os complexes	89
8. Conclusion.....	93

Chapter IV: Mechanistic Analysis for the Electrochemical Molecular

Reduction of N₂O by Rhenium Complexes: Spectroelectrochemical

Studies..... 99

1. Introduction	100
2. [Re ⁰ (bpy ^{•-})(CO) ₃] ⁻ in the electrochemical reduction of CO ₂ and N ₂ O.....	101
3. Electrochemical reduction of N ₂ O by electrogenerated [Re ⁰ (bpy ^{•-})(CO) ₃] ⁻ species. 102	
3.1 Infrared and UV-vis spectroelectrochemistry of [Re(bpy)(CO) ₃ Cl]	102
3.2 Infrared and UV-vis Spectroelectrochemistry of [Re(bpy)(CO) ₃ (OH)]	104
3.3 Reactivity of the bi-reduced species [Re ⁰ (bpy ^{•-})(CO) ₃] ⁻ with N ₂ O	107
4. Behavior of [Re(bpy)(CO) ₃ (MeCN)]PF ₆ under N ₂ O atmosphere.....	112
5. Behavior of mono-reduced species of [Re(bpy)(CO) ₃ Cl] and [Re(bpy)(CO) ₃ (OH)] with N ₂ O.....	117

6. Overall recap of the electrochemical reduction of N ₂ O by [Re(bpy)(CO) ₃ X] ⁿ⁺ (X = CH ₃ CN, Cl ⁻ and OH ⁻ , n = 0 or 1)	121
7. Conclusion.....	125
Chapter V: Extension to Catalysis of Pyridine N-Oxide	
Electrochemical Reduction	131
1. Introduction	132
2. Properties of Pyridine N-oxide and the State of Art:	132
3. Results and Discussion.....	133
3.1 Cyclic Voltammetry Overview:	133
3.2 Reaction of PNO with the mono-reduced species	134
3.3 Bi-reduced species with PNO	138
3.4 Controlled potential electrolysis: Product Analysis.....	140
4. Conclusion :.....	145
Chapter VI: Conclusions and Perspectives.....	149
Chapter VII: Experimental Part.....	155
Methods and Instrumentation.....	156
1. Cyclic voltammtery.....	156
2. Linear scan voltammetry.....	156
3. Exhaustive electrolysis at controlled potential for SEC.....	156
4. Controlled potential electrolysis described in (Chapter II and III)	157
5. Determination of solubility of N ₂ O.....	157
6. Quantification of electrolysis reaction product of N ₂ O reduction	159
7. Quantification of electrolysis reaction product of pyridine N-oxide reduction...	160
Chapter II.....	160
1. Aromatic redox catalysts.....	160
2. Ohmic drop correction	162
Chapter III	162

Synthesis and characterization	162
Chapter IV: Evaluation of rate constants	165
Evaluation of $k_{ap}^{mono,ACN}$:	165
Evaluation of $k_{ap}^{mono,OH}$:	166
Evaluation of $k_{ap}^{mono,Cl}$:	167

Chapter I : General Introduction

1. Nitrous oxide gas

Nitrous oxide, commonly known as laughing gas, discovered more than 200 yrs ago in 1772 by English scientist Joseph Priestley, is an oxide of nitrogen with the formula N_2O and molecular weight of 44.01. At room temperature, it is a colorless non-flammable diamagnetic gas, with a weak pleasant odor and sweetish flavor. On the one hand, nitrous oxide has significant medical uses; especially in surgery and dentistry, for its anesthetic and pain reducing effects. Very preliminary results have shown that it can be used for the treatment of resistant major depression.¹ However high doses of N_2O or long-term contact (days) significantly decrease vitamin B12 (cobalamin) function causing bone marrow depression, macrocytic anemia and neuropsychiatric disorders.² More technical applications include its utilization as whipping agent for cream or as fuel additive for rockets and motors. In laboratory conditions nitrous oxide is generally prepared either by thermal decomposition of ammonium nitrate or by the reaction of potassium nitrosyl sulfate with sulfuric acid.

2. Nitrous oxide no laughing matter

Nitrogen (N) is a colorless and odorless element. It is the most abundant element in the earth atmosphere: approximately 78 % of the atmosphere is dinitrogen. Nitrogen is important to all living things including humans, it is one of the essential primary nutrients for many biological macromolecules, counting proteins, nucleic acids (DNA and RNA) and chlorophyll.

What is the nitrogen cycle? The nitrogen cycle is a repeating cycle of processes during which nitrogen moves through both living and non-living things: the atmosphere, soil, water, plants, animals and bacteria. N_2O is crucial link in the nitrogen cycle and should be reduced to dinitrogen (N_2) to complete this cycle and limit the accumulation of N_2O in the atmosphere (Figure I.2 1).

Nitrous oxide is a potent greenhouse gas. It has been regarded as the third most important anthropogenic greenhouse gas and the largest remaining anthropogenic activities source of stratospheric ozone depleting substances throughout the 21st century³ with a steady state life time of about 120 yrs.⁴ The presence of atmospheric N_2O was not established until 1938 when Aryal investigated absorption bands in the infrared solar spectrum.⁵ Its absorption capacity of infrared radiation 200 times greater than that of CO_2 . N_2O is a by-product of several fundamental natural reactions of the N cycle: nitrification, denitrification, and chemo-denitrification⁶ (Figure I.2 1). The complete denitrification pathway consists of a chain of individual steps carried out by separate enzymes beginning with nitrite reductase (NiR) to nitric

oxide reductase (NOR) and ending with nitrous oxide reductase (N₂OR) to release dinitrogen gas as shown in (Scheme I.2 1).

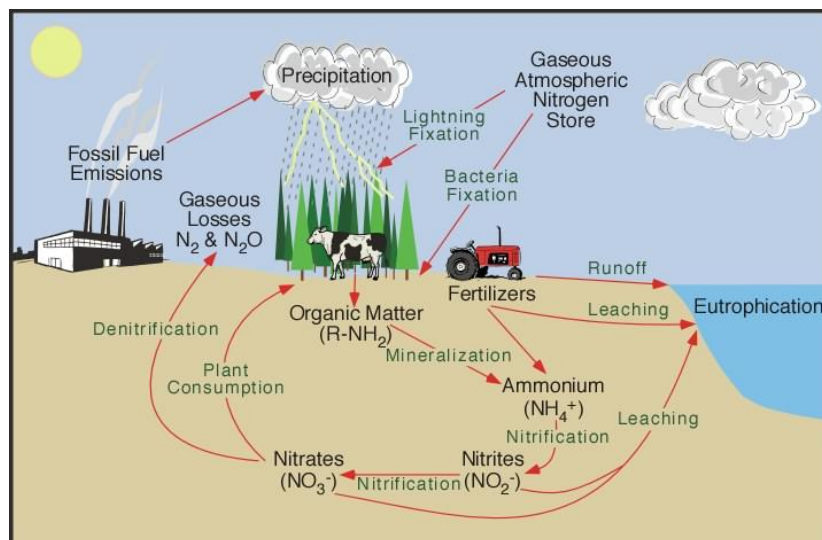
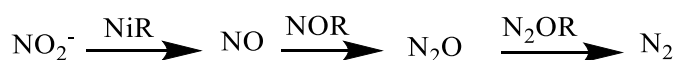


Figure I.2 1 : Nitrogen Cycle from Climate program office website.



Scheme I.2 1 : Complete denitrification pathway to dinitrogen gas.

Sustaining a world population of eight billion has required dramatic increases in the consumption of synthetic nitrogen fertilizers, cultivation of nitrogen-fixing crops, and deposition of NO_x from combustion of fossil fuels along with adipic and nitric acid production processes. These processes increase the availability of mineralized nitrogen (for example NH₄⁺ and NO₃⁻) and lead to N₂O emission through microbially mediated nitrification or denitrification in both terrestrial and aquatic ecosystems.⁷ Also human alteration accelerated dramatically with the discovery of the Haber–Bosch process, the chemical process that synthetically transforms atmospheric dinitrogen (N₂) gas into ammonia (NH₃) based fertilizers to increase crop production to provide food to sustain growing population.⁸ Figure I.2 2 shows both sources of N₂O emissions; natural predominantly terrestrial and anthropogenic chiefly from agriculture where both of them contribute to the high levels of N₂O in the atmosphere. Less than 1% of atmospheric N₂O is removed annually from the atmosphere, primarily by photolysis and oxidative reactions in the stratosphere. Nitrous oxide is also destroyed (and produced) by denitrification in nearly anoxic environments and, possibly, as recently suggested, by an uncharacterized process in forest soils under drought; again, however, the influence of

these processes on the lifetime of N₂O is probably small. Therefore, it is of utmost importance to limit N₂O production by lowering its emission and by implementing processes that can degrade it to chemical species with low environmental impact, currently drawing increased attention in the last decades. Mitigation of N₂O is thus crucial for both, slowing down global warming and improving the health of all living population.

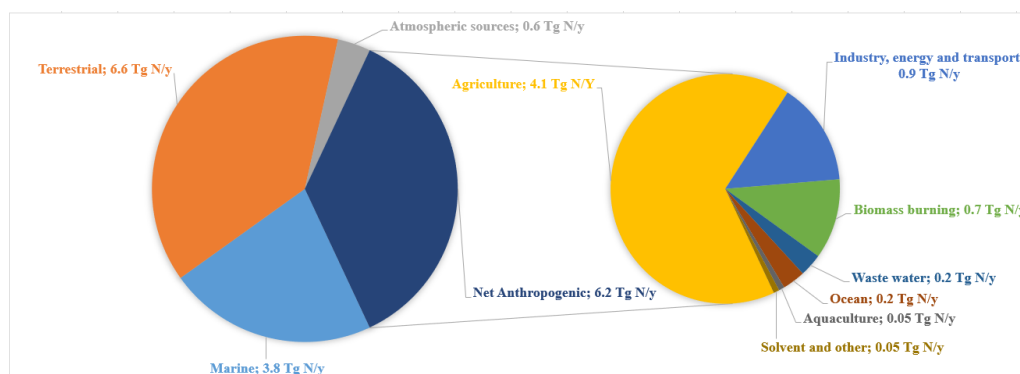
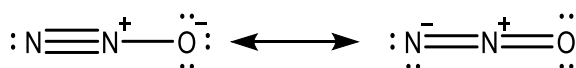
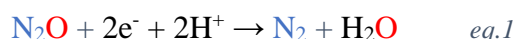


Figure 1.2.2 : Natural versus anthropogenic emissions of N₂O updated in 2013. ³

3. Properties of N₂O and its reactivity

N₂O is a linear asymmetrical molecule with different resonance structures which explains its electronic and structural properties (Scheme I.3.1).⁹ Contrary to carbon dioxide (CO₂), a symmetrical molecule, N₂O has a dipole moment of 0.166 Debye with a point group C ∞ v, and the interatomic N-N and N-O distances are shorter than the average values for a double bond, 1.128 Å and 1.184 Å respectively. The N-N bond order is about 2.7 and that of N-O about 1.6 so that the latter is more probable to be broken first. This molecule is thermodynamically a potent oxidant given its reduction potential of ($E^0(\text{N}_2\text{O}/\text{N}_2) = 2.01 \text{ V vs. SCE at pH } 0; \text{ eq } 1$)¹⁰ but the reaction has impressive kinetic inertness with high activation barrier of around 250 kJ/mol for its thermal decomposition.¹¹ This activation barrier can be overcome through coordination and activation by metal ions. However, N₂O is in general a poor ligand to transition metals owing to its weak σ -donating and π -accepting capabilities.¹²



Scheme I.3.1 : Representation of molecular model and resonance structures of the linear N₂O molecule.

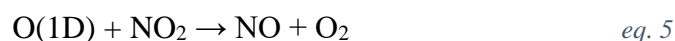
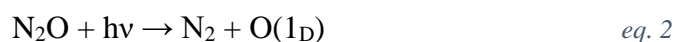
4. Transforming nitrous oxide / mitigation strategies

Mitigation of nitrous oxide: could be important to tackle global warming and improve air quality. However, it is not realistic to think that an artificial chemical transformation of N₂O could have an impact on N₂O in the atmosphere. However, for our fundamental chemical approach, it is interesting to note that nitrous oxide has stimulated a lot of research interest regarding its reactivity modes and transformation. Oxidation reactions involving N₂O as an oxidant typically result in the release of dinitrogen which is environmentally benign side product and transfer of an oxygen atom. Nitrous oxide can also act as nitrogen atom donor for the formation of azides. Below are presented interesting examples for the synthetic use of nitrous oxide in organic and inorganic chemistry where the transfer of oxygen is the most common observed form of reactivity but not the only one.

4.1 Natural Strategies

4.1.1 *Decomposition of N₂O through photolysis: Ozone layer depletion*

N₂O can be decomposed in the middle stratosphere through photolysis to N₂ and oxygen atom in an excited singlet state O(1D) (eq 2) contributing as the dominant ozone depleting agent of the 21st century.¹³ A minor fraction of N₂O will react with O(1D) forming nitric oxide (eq. 3) responsible for ozone depletion.



This reaction was identified as the major source of reactive nitrogen (NO_x) which then reacts with ozone in a catalytic cycle, whereby single NO molecule can destroy 10³-10⁵ ozone molecules before being converted to a less reactive molecule. Hence the net reaction catalyzed by NO can be represented as follows:



Only a minor fraction of N₂O after undergoing photolysis in the stratosphere reacts with reactive oxygen forming nitric oxides. Removal of N₂O from the atmosphere can however occur via three enzymes pre-existing in nature which serve as molecular catalysts reported to be efficient to reduce N₂O.

4.1.2 Enzymes

The removal of nitrous oxide from the atmosphere might only be efficiently performed by an enzymatic activity, in which three enzymes have been reported in the literature that use nitrous oxide as a substrate: nitrogenase, multi-copper oxidase and nitrous oxide reductase (N₂OR). These three enzymes are metalloproteins but do not share a similar catalytic center nor these centers have in their composition a similar metal.¹⁴

Nitrogenase is a metalloenzyme with a complex FeMo cofactor, also named M-cluster (MoFe₇S₉C-homocitrate), that catalyzes the reduction of N₂ to ammonia (NH₃). Early studies have shown that this enzyme can interact also with N₂O with the same redox form of nitrogenase producing N₂ gas which also acts as a substrate to produce ammonia. Hence mechanistic studies showed that N₂O is reduced by nitrogenase to dinitrogen gas which is then reduced by the enzyme to ammonia.^{15,16}

Multicopper oxidase produced in *E. coli* is a metallo-oxidase for Fe²⁺ and Cu⁺. The natural substrate of this enzyme is the molecular oxygen. However, this enzyme has evolved to have the potential to use nitrous oxide in the oxidation of iron with higher turnover numbers (TONs) than the one attained for molecular oxygen.¹⁷

The third reported enzyme, a nitrous oxide reductase (N₂OR), is a copper enzyme with active site of four copper ions with a bridging (μ 4) sulfide ligand. It is the most efficient enzyme for the reduction of nitrous oxide in the biological denitrification process, a key step in the global nitrogen cycle. It has a 'CuA' center, a binuclear copper center, acting as the electron transferring center from c-type cytochrome to the catalytic center 'CuZ' which is a tetranuclear copper sulfide center unique in nature (Figure I.4.1.2 1). The large activation barrier for the reduction of N₂O (250 kJ/mol), which is the last step of denitrification pathway,¹⁸ can be overcome by taking place at the special metal center of this catalyst CuZ. A CuZ-N₂O complex is formed in which the two copper atoms (Cu_I and Cu_{IV}) are directly involved in bridged N₂O binding, bending the ligand to a configuration that resembles the transition state and leading to N₂O reduction by two electrons. The other atoms of the CuZ cluster maintain the needed structural motif and make Cu_I and Cu_{IV} better electron donors to enhance the back-bonding required for N₂O activation. After the N-O bond cleavage, the catalytic cycle (Scheme I.4.1.2 1) consists of a sequence of alternating one electron reduction and protonation steps which return the CuZ cluster to the fully reduced (4Cu_I) state for future turnovers.^{19,20}

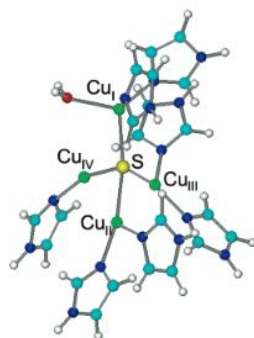
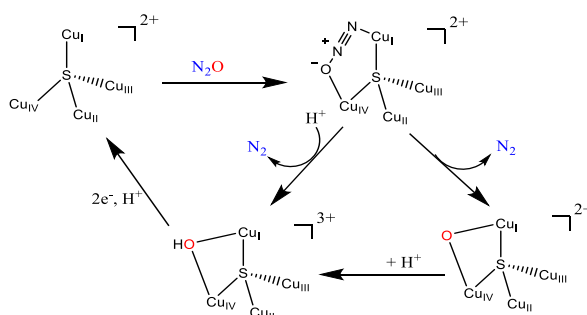


Figure I.4.1.2 1 : Structure of CuZ site of N₂OR²⁰ "Reprinted with permission from [J. Am. Chem. Soc. 2006, 128, 1, 278–290]. Copyright [2005] American Chemical Society."

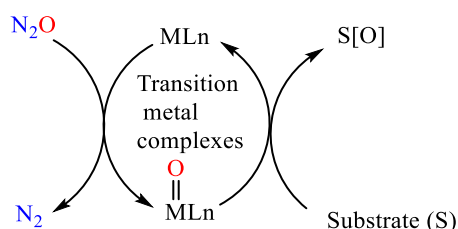


Scheme I.4.1.2 1 : Proposed mechanism for the reduction of N₂O by nitrous oxide reductase at the active site.¹⁰

4.2 Nitrous oxide use in synthetic organic and inorganic chemistry

4.2.1 Oxidation reactions with N₂O

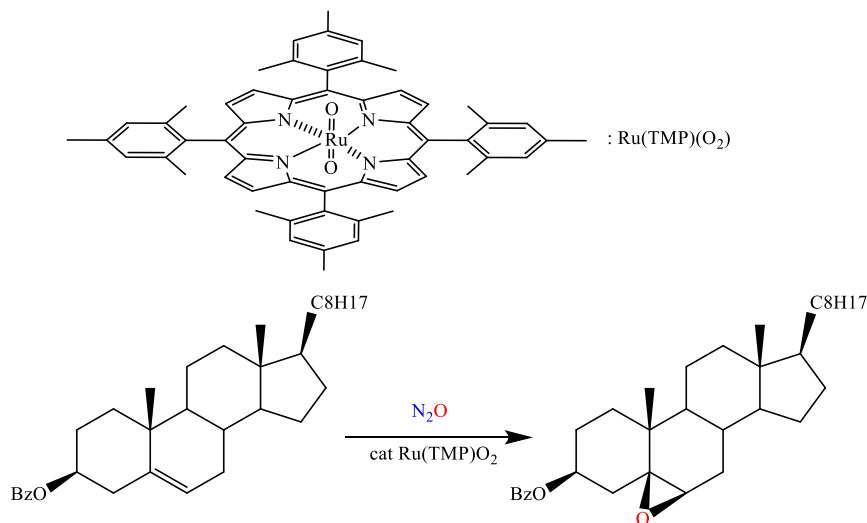
As mentioned above nitrous oxide is a very strong oxidant from a thermodynamic point of view. However, from kinetic point, it has an inert character. Additionally, it is a poor ligand towards transition metals. This low intrinsic reactivity is advantageous because it allows performing selective oxidation reactions which proceed via oxygen atom transfer as shown in the generic catalytic cycle (Scheme I.4.2.1 1) with the release of environmentally benign by-product dinitrogen. Transition metal complexes are employed as catalysts in order to lower the activation energy for the reduction of nitrous oxide.



Scheme I.4.2.1 1 : Metal catalyzed oxidation reactions with N₂O.

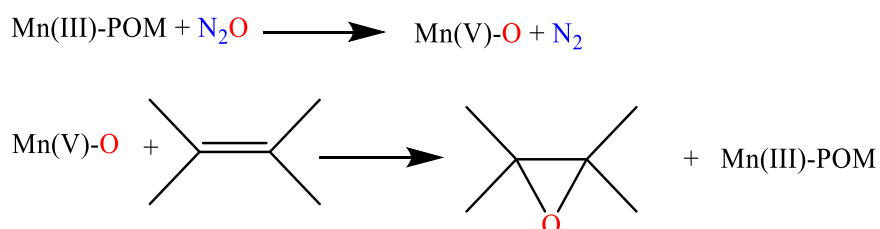
Yamada et al., reported in 2000 the first successful catalytic epoxidation of olefins using ruthenium porphyrin complexes as catalysts for the epoxidation of olefins cholesteryl benzoate

in the presence of nitrous oxide with 5 mol% RuTMP(O₂) (TMP = tetramesitylporphyrinato) catalyst (Scheme I.4.2.1 2).²¹



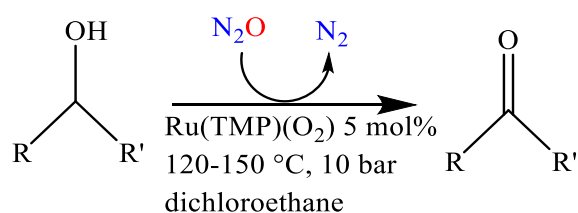
Scheme I.4.2.1 2 : N₂O oxidation of cholesteryl benzoate at 100 °C in chlorobenzene under 10 atm N₂O by dioxo-ruthenium complex.²¹

In 2002 Neumann et al., reported highly selective epoxidation of alkenes (>99.9%) catalyzed by [Mn^{III}₂ZnW(Zn₂W₉O₃₄)₂]¹⁰⁻, a manganese-substituted polyoxometalate (POM) ‘sandwich’ structure in a glass pressure tube at 1 atm N₂O and 150 °C in fluorobenzene as solvent based on the following reaction (Scheme I.4.2.1 3).²²



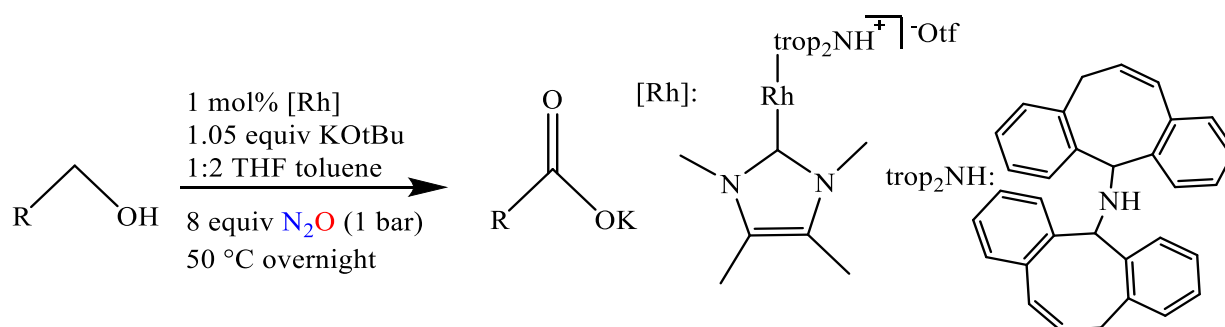
Scheme I.4.2.1 3 : Direct activation of N₂O by Mn(III) polyoxometalate.

N₂O was also used for the oxidation of alcohols. Yamada et al., in 2001 reported the use of RuTMP(O₂) catalyst (5 mol%), already used for epoxidation: they tried it for the oxidation of primary alcohols (benzylic) and secondary to aldehydes and ketones (Scheme I.4.2.1 4).^{23,24}



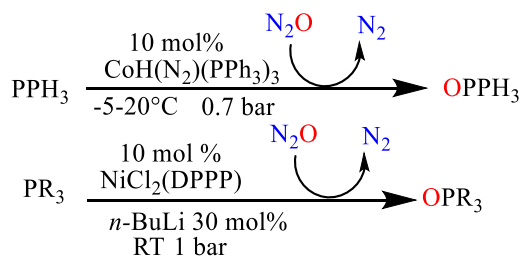
Scheme I.4.2.1 4 : Oxidation of alcohols by N₂O in the presence of dioxoruthenium catalyst.

In 2016, Grützmacher et al., reported Rh-catalyzed dehydrogenative coupling of alcohols using N₂O as a hydrogen acceptor, which proceeds by metal–ligand cooperation and which was the most active catalyst for the oxidation of wide range of primary alcohols in the presence of N₂O as oxidant to form carboxylic acids (Scheme I.4.2.1 5).²⁵



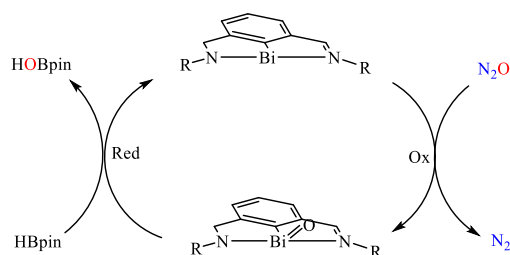
Scheme I.4.2.1 5 : Alcohol esterification process using N₂O as an oxygen donor in the presence of rhodium catalyst complex.

N₂O has also been used as an oxidant for the oxidation of phosphines to phosphine oxides in which CoH(N₂)(PPh₃)₃ was able to catalyze the oxidation of PPh₃ to give OPPh₃ as reported by Yamamoto et al.^{26,27} The reaction was performed under ambient conditions and atleast six turnovers were achieved. Also, NiCl₂(DPPP) (DPPP = 1,3-bis(diphenylphosphino)propane) has been reported by Suzuki et al.,²⁸ to be efficient for the oxidation of phosphines to phosphine oxides by N₂O with high yields (Scheme I.4.2.1 6).



Scheme I.4.2.1 6 : Metal catalyzed oxidation of phosphines by N₂O.

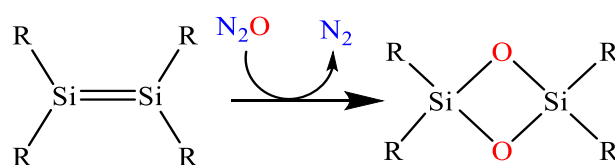
Catalytic activation of N₂O under mild conditions was performed by Cornella et al., at a low valent Bi redox platform (Bi^I ⇌ Bi^{III}) by the use of bismuthinidene catalysts, aided by pinacolborane (HBpin) as reducing agent featuring high TON and TOF (Scheme I.4.2.1 7).²⁹



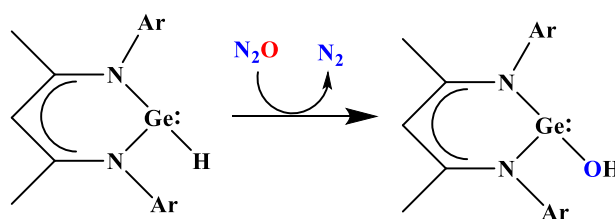
Scheme I.4.2.1 7 : Catalytic N_2O deoxygenation via a Bi^I/Bi^{III} redox cycle.

Focusing on the use of N_2O in synthetic inorganic chemistry we present here a few examples reported in the literature. Low valent silicon,^{30,31,32} germanium³³ compounds are suited substrates for the activation of N_2O . In addition, catalytic metal free deoxygenation of N_2O was recently reported by Cantat et al.,³⁴ using disilanes as reducing agents with catalytic amount of fluoride anions and alkoxides at ambient temperature and pressure. Disilanes are easier to activate than hydrogen (will be discussed in the following section) because of high exophilicity of silicon, since the bond dissociation energy of $Me_3SiSiMe_3$ is lower compared to H_2 . However, this reaction must be carried out in strictly anhydrous conditions to prevent competitive reduction of H_2O to H_2 (Scheme I.4.2.1 8).

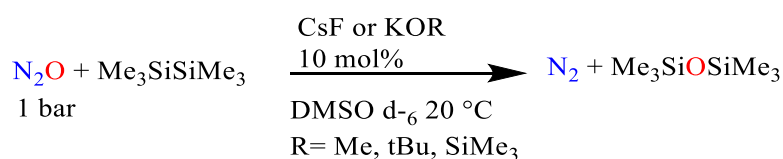
Roesky and Stalke 2011³²



Roesky and Schulzke 2011³³



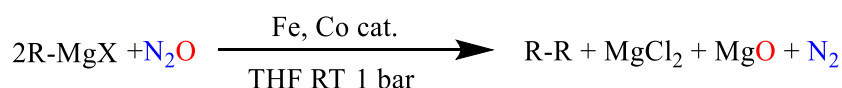
Cantat et al., 2019³⁴



Scheme I.4.2.1 8 : Oxidation of low valent silicon and germanium compounds by N_2O .

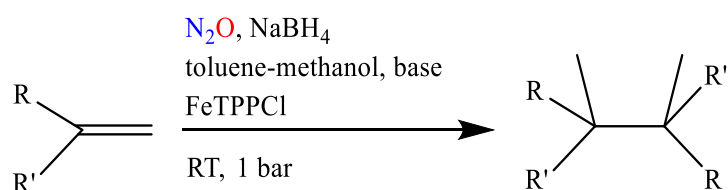
4.2.2 Metal catalyzed homo-coupling reactions of Grignard reagents with N₂O

In 2013 Severin et al., reported the oxidative carbon-carbon coupling reactions under mild conditions with high selectivity and TON using different transition-metal salts as potential catalysts Li₂CuCl₄, Li₂MnCl₄, CoCl₂, FeCl₃ and [Fe(acac)₃]. The best results were obtained with Co and Fe salts (Scheme I.4.2.2 1).³⁵



Scheme I.4.2.2 1 : Oxidative homo-coupling of Grignard reagents with N₂O and Co or Fe complexes.

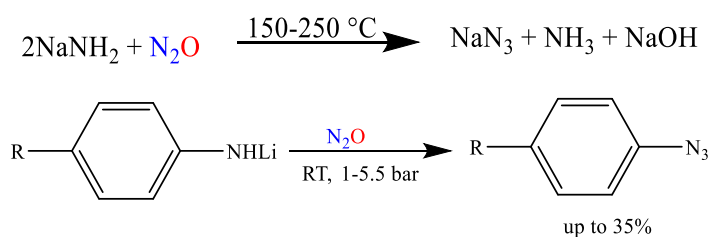
Reduction of N₂O was also performed with alkene-alkene coupling catalyzed by metalloporphyrins (Fe, Mn and Co) in the presence of NaBH₄ as a reductant as reported by Higuchi et al. in 2013³⁶ (Scheme I.4.2.2 2). The best results were obtained with iron tetraphenyl porphyrinato complex (FeTPPCL), following the reduction of FeTPPCL by NaBH₄ then dimerization of the alkene and formation of highly reduced [Fe(TPP)]⁻ species. These species undergo oxidation by N₂O releasing N₂ to regenerate back Fe(III) porphyrin and closing the catalytic cycle. Interestingly, this work indicates that FeTPPCL is potentially a molecular catalyst for the reduction N₂O into N₂ via electrogeneration of Fe(I)TPPCL which will be discussed more in details in Chapter III.



Scheme I.4.2.2 2 : Reductive coupling of olefins by NaBH₄, N₂O in the presence of FeTPPCL complex.

4.2.3 Nitrous oxide as a nitrogen donor atom

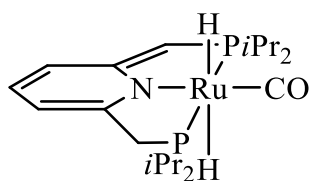
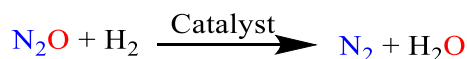
Nitrous oxide can also act as N atom donor as reported in 1892 by Wislicenus³⁷ for the synthesis of sodium azide by the exposure of NaNH₂ to N₂O at elevated temperatures. Nowadays this reaction is used by industry to produce sodium azide on a larger scale.³⁸ Amides of aromatic amines can also be converted into azides. Meier reported the reaction of lithium anilide with N₂O to give azobenzene, biphenyl, and a small amount of a yellow oil, assumed to be phenyl azide.³⁹ The reaction was later optimized by Koga and Anselme⁴⁰ to increase the amount of phenyl azide produced (Scheme I.4.2.3 1).



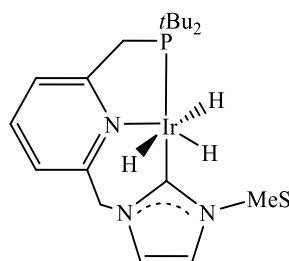
Scheme I.4.2.3 1 : Synthesis of azides by the reaction of amides with N_2O .

4.2.4 Reduction of N_2O by dihydrogen

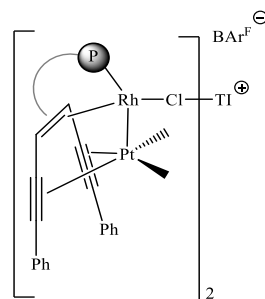
Reduction of nitrous oxide using dihydrogen, which is driven by release of dinitrogen and water, is considered an attractive reductive process. However, a major disadvantage of the utilization of H_2 is the hazard posed by mixtures of the two gases (H_2 and N_2O).⁴¹ Finding an efficient catalyst is challenging. The catalyst must be highly selective for N_2O in the presence of hydrogen. Moreover, over-reduction by dihydrogen can inhibit the catalytic efficiency and the catalyst should be able to remain active in the presence of large excess of H_2O produced. Below are presented efficient molecular catalysts for the reduction of N_2O gas under mild conditions with high TONs (Scheme I.4.2.4 1).^{42,43,44}



Milstein TON = 417



Suárez TON = 525



Grützmacher TON = 587

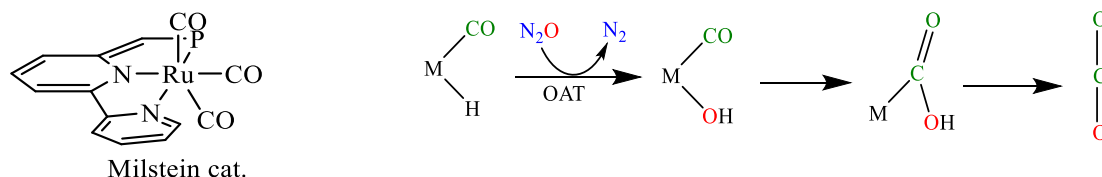
Scheme I.4.2.4 1 : Homogenous reduction of N_2O with H_2 using different catalysts.

4.2.5 Reduction of N_2O with CO as reductant

Carbon monoxide and nitrous oxide gases emitted into the atmosphere create the heat-reflective layer that keeps the Earth at a livable temperature linked to climate change and global warming.

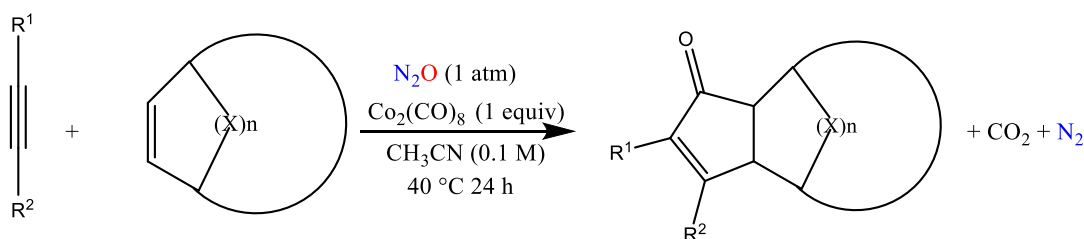
In 2019 Milstein et al., reported the reduction of N_2O using CO as a reductant in the presence of ruthenium carbonyl hydride pincer catalyst complexes under mild conditions to

which he proposed that this reaction occurs via oxygen atom transfer (OAT) from N_2O to the Ru–H bond to form a Ru–OH intermediate, followed by intramolecular OH attack on an adjacent CO ligand, forming CO_2 and N_2 with high TONS (Scheme I.4.2.5 1).⁴⁵



Scheme I.4.2.5 1 : Proposed mechanism for homogenous reaction of N_2O and coordinated CO.

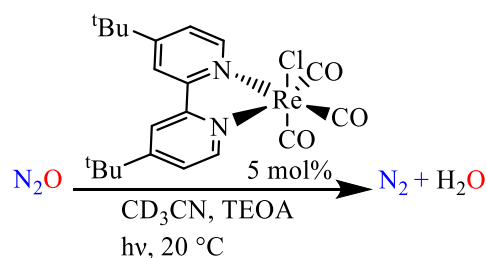
The same year Geary et al., reported the reduction of N_2O using Pauson–Khand cycloaddition of alkynes, alkenes [2 + 2 + 1] promoted by cobalt carbonyl and nitrous oxide which removed CO ligand from the cobalt complex to bring out cyclopentenones in moderate to good yields, carbon dioxide and nitrogen gas (Scheme I.4.2.5 2).⁴⁶



Scheme I.4.2.5 2 : Cobalt-Mediated Pauson–Khand Cycloadditions.

4.2.6 Photocatalytic deoxygenation of N_2O

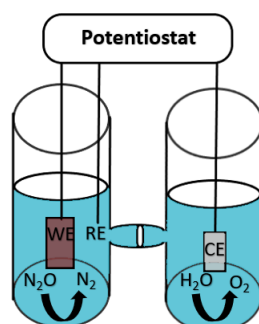
Photocatalytic deoxygenation of nitrous oxide was recently reported by Cantat et al.,⁴⁷ They have identified efficient photocatalytic activity of the rhenium $[Re(4,4'-tBu-bpy)(CO)_3Cl]$ complex under ambient conditions ($20^\circ C$ and 1 bar) in the presence of triethanolamine (TEOA) as sacrificial electron donor and later on extending their studies to the activation of N-O bond in pyridine N-oxides which represents much greater challenge compared to nitrous oxide reduction (Scheme I.4.2.6 1).



Scheme I.4.2.6 1 : Photo-deoxygenation of N_2O catalyzed by Re complex.

4.2.7 Conclusion

As already stated, nitrous oxide is very inert gas, and its chemical activation under ambient conditions is a very challenging task. In most cases, as illustrated above, the use of N_2O corresponds to its reductive deoxygenation to N_2 , the leaving oxygen being or not incorporated in the substrate. Focusing on the deoxygenation of N_2O , it appears that it usually requires harsh conditions high temperature with heterogeneous catalysts,^{48,49} high pressure⁵⁰ in addition to the use of oxophilic and energy intensive reductants such as phosphines, organoboranes or organosilanes generating phosphine oxides, boroxanes, or siloxanes which demand high energy cost to recycle them. If the fate of the leaving oxygen is not crucial, i.e. if it is not aiming to incorporate it in the oxidized species, then, an electrochemical approach for N_2O reductive deoxygenation can be considered. In such a case, reduction (N_2O to N_2 conversion) and oxidation might be operated in separated compartments and the electrochemical reduction of N_2O can be optimized (Scheme I.4.2.7 1). The goal is then to search for a selective, clean and energy thrifty electrochemical process. In that regard, molecular electrochemical catalysis could be an interesting approach using electrons as external energy source for the activation of N-O bond in N_2O . This is one of the main topics which will be discussed throughout this thesis.



Scheme I.4.2.7 1 : Schematic representation of the electrochemical cell with reduction of N_2O taking place in the working electrode compartment.

5. Principles of molecular catalysis of electrochemical reactions

In this section, we will briefly recall few simple concepts regarding the catalysis of an electrochemical reaction, focusing on a reduction process. First, we distinguish ‘electrocatalysis’ and ‘molecular catalysis’.

We define ‘electrocatalysis’ as a process in which the electrode material is chemically involved in the catalytic process. This implies that specific interactions exist between the substrate and/or the products of the electrochemical reaction with the electrode material.

Alternatively, molecular catalysis involves an ‘innocent’ electrode material being simply an outersphere electron donor. Electrons are transferred to the catalyst molecules (P) homogeneously dispersed in the solution bathing the electrode and these molecules could then transfer the electrons to the substrate (A) either by an innersphere process then corresponding to ‘chemical catalysis’ or by an outersphere process corresponding to ‘redox catalysis’. If the molecular catalyst is indeed homogeneously dispersed in the solution, both processes are referred to as ‘homogeneous chemical catalysis’ or ‘homogeneous redox catalysis’. In addition to that, if the catalyst molecules are immobilized in a mono or multilayer coating the electrode surface this corresponds to heterogeneous molecular catalysis.⁵¹ (Figure I.5 1)

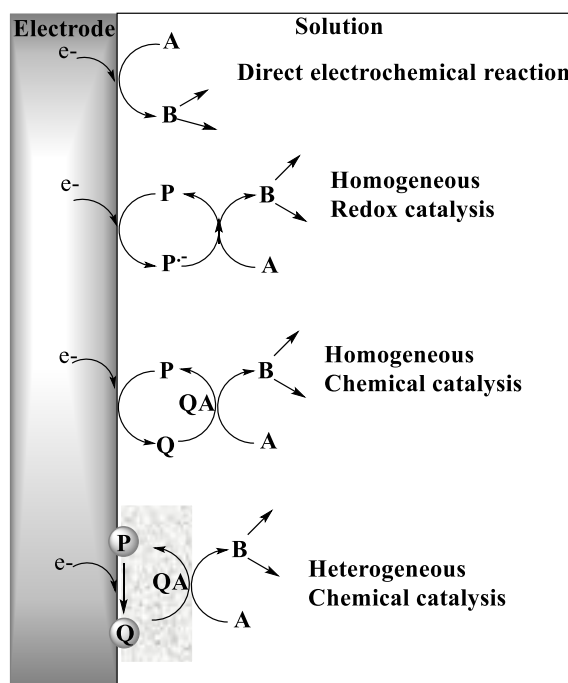


Figure I.5 1 : Schematic representation of the various types of molecular catalysis of electrochemical reactions.

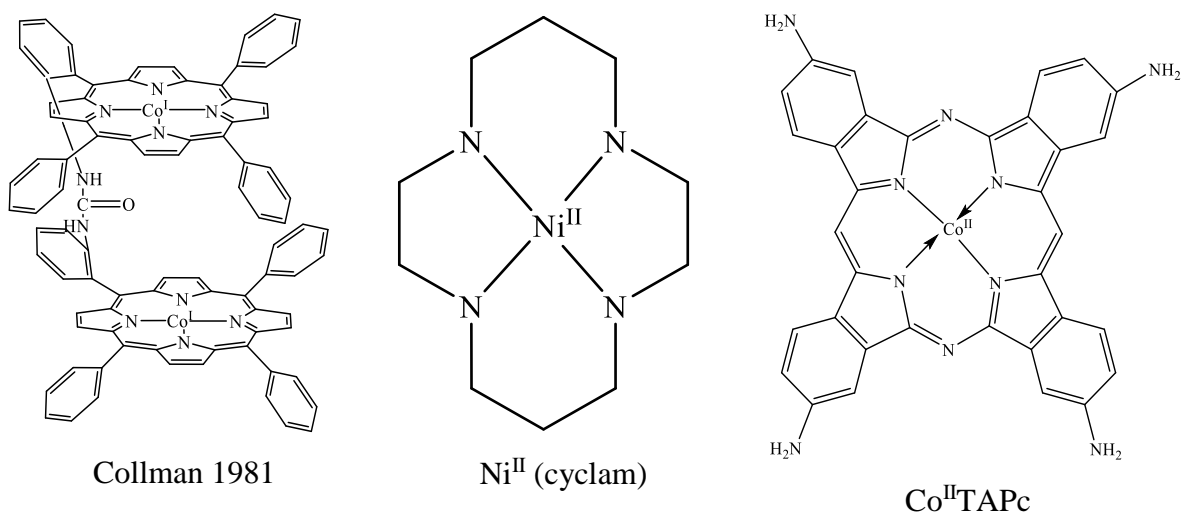
6. State of art of the catalysis of the electrochemical reduction of N₂O

Why is there a need for catalysis to reduce N₂O to N₂? Without catalysis, reduction of N₂O implies the generation of N₂O^{•-} radical anion which demands applying a very negative electrode potential (as will be shown later on in this thesis). Indeed, N₂O^{•-} is a very highly energetic species. Therefore, the purpose of catalysis is to avoid the formation of N₂O^{•-} in the two electron process leading to N₂.

Avoiding the formation of N₂O^{•-} can be achieved by the use of catalysts via electrocatalysis or molecular catalytic approaches. Beginning with electrocatalytic process involving the electrode material, we note that, among the electrocatalytic metals, palladium, platinum, indium or iridium have led to some successes with regard to N₂O reduction. However, they remain expensive materials. Moreover, the selectivity of the reaction in an aqueous medium in particular (competition with the production of hydrogen) remains problematic with abundant metals.^{8,52} Jiao et al., recently reported the electrochemical reduction of gaseous nitrogen oxides (NO and N₂O) at ambient conditions using a series of commercial transition metal catalysts such as Fe, Co, Ni, Cu, Pd, Ag, and Pt particles deposited onto a gas diffusion layer (GDL), which is critical for providing hydrophobicity and electrical conductivity. They have shown that Cu is highly selective toward NH₃ formation with >80% FE in NO electroreduction and Co, Cu, and Ag achieved high N₂ FE at high rates, and suppression of hydrogen Evolution Reaction (HER) was critical.⁵³ Deciphering mechanisms with such heterogeneous systems is more difficult than in the case of molecular catalysis due to the lack of knowledge and control on the elusive electrode surface states.

Molecular electrochemical catalysis processes for N₂O reduction were scarcely reported in the literature. In 1981 Collman et al.,⁵⁴ reported a face-to-face Co porphyrin as catalyst for N₂O to N₂ reduction. They propose a simultaneous interaction of the two-metal center with N₂O, whereby each metal provides one electron. Proton sources are necessary to capture and stabilize the nitrous oxide oxygen. However, a very weak acid is required in order to avoid side reactions since protons are undesirable as they can react with Co(I) to form hydrides. Therefore, they have showed that the rate of the electrocatalytic reaction of N₂O by the cobalt porphyrins is sensitive to the presence of hydroxide and substituents on the porphyrin ring. In addition to the presence of proton donors and the geometric proximity of the two electroactive metal centers in the catalyst molecule. Surprisingly, there was no follow-up on the initial paper.

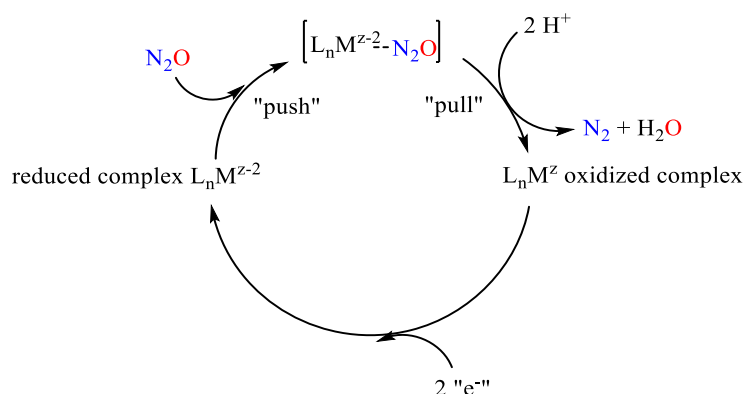
In 1990 Taniguchi et al.,⁵⁵ reported the reduction of N_2O to N_2 using mercury electrodes in the presence of nickel macrocyclic polyamines = (1,4,8,12(or 11)-tetra-azacyclopenta(or tetra)decane with extremely large TOF and yields close to 100% in aqueous solution. However, the mechanism of N_2O reduction is not clear since mercury seems to be playing a role in this process. Cobalt(II) tetraaminophthalocyanine (Co^{II} TAPc) adsorbed on a graphite electrode were also studied for the reduction of N_2O in aqueous medium however the selectivity of the reaction depends on the pH of the solution; below pH 5 the two processes of N_2O and H_2O reduction interfere. A simple mechanism in which N_2O interacts with the reduced Co^I adsorbed at the surface forming an adduct was proposed.⁵⁶ However, the mechanistic analysis presents inconsistencies and deserves to be deepened in order to better define the factors controlling the activation of the N-O bond.



Scheme I.6 1 : Molecular catalysts previously studied for the reduction of N_2O .

It is surprising to observe that, besides these few examples (Scheme I.6 1), there have been very few attempts to catalyze the electrochemical reduction of N_2O to N_2 with molecular catalysts as it can also be viewed as a prototypical example of N-O bond deoxygenation. For that reason, we have decided to undergo a thorough investigation of the N_2O to N_2 electrochemical conversion with a molecular electrocatalytic approach with the following reasoning for the activation of N-O bond at ambient conditions in organic solvent. Our reasoning is based on analogies between N_2O and CO_2 (both molecules are isoelectronic with a central electrophilic atom) N_2O should bind to the reduced form of a transition metal complex (rhenium and manganese) and transfer of electrons should occur from the electron rich metal center to the electrophilic center of N_2O in the presence of an acid acting as proton source to

facilitate the breaking of the N-O bond while stabilizing the oxygen. This activation pathway is called “push-pull” type strategy. In this context the electrons used for the reduction of N_2O were obtained electrochemically by the use of homogenous molecular catalysts acting as electron shuttles from the electrode to the substrate (N_2O) after binding to the reduced form of the catalyst (Scheme I.6 2). However, this putative mechanism might not be the one taking place. It is a question that needs to be acknowledged in this thesis.



Scheme I.6 2 : Our strategy used for the activation of N_2O using transition metal complexes.

Simpler homogeneous catalysis can also be realized by the use of redox catalysts (organic aromatic molecules) in which the catalyst acquires the electrons via an outer-sphere manner from the electrode acting heterogeneously and delivers them via an outersphere manner with no chemical interaction with N_2O . However chemical catalysis is more interesting in the sense that the catalyst should be designed to allow chemical interaction between the reduced active form of the catalyst and the substrate. Usually, better efficiencies and selectivity are expected with chemical catalysis compared to redox catalysis. Actually, because it does not avoid formation of $N_2O^{\bullet-}$, one may wonder why redox catalysis may be superior to simple direct reduction of N_2O . It is another question that will be discussed in this thesis.

Being able to distinguish between redox and chemical catalysis is very important for designing an efficient selective catalyst; In order to discriminate between them, as shown later an activation driving force relationship have to be deciphered. To do so rate constants have to be obtained by the help of either cyclic voltammetry analysis (which gives us a fast response and is suitable for fast catalytic processes) or spectroelectrochemical measurements (UV-vis, FTIR) which allows investigating slow process.

7. Thesis objectives and scope

As discussed above the aim of this fundamental research project is to study the activation of N-O bond in N_2O molecule using electrochemical approach coupled with spectrochemical measurements with the goal to decipher mechanisms to be able to design better catalytic systems in the future.

Chapter II will focus on redox catalysis using organic aromatic molecules leading to either anion or dianion radical species upon one or two successive electron transfers. These catalysts function as redox catalysts (outersphere electron transfer) and will serve as benchmark for chemical catalysts. Later in this Chapter, we will take specifically 4-cyanopyridine as redox catalyst and we will study the effect of water (co-substrate) on catalyst deactivation in the presence of N_2O .

Chapter III will focus on chemical catalysis. First, we will use Fe porphyrins as molecular catalysts then we will move to low valent rhenium and manganese bipyridyl transition metal complexes as catalysts aiming to study the selectivity of these catalysts by running controlled potential electrolysis and product analysis, then extending our studies to other complexes such as ruthenium, rhodium and osmium in organic solvents. Last section of this Chapter includes work performed by an L1 internship student Titouan Montceau.

Chapter IV will focus on thorough mechanistic investigation of the reduction of N_2O by rhenium complexes. It will include spectroelectrochemistry analysis and investigation of the reaction product obtained upon addition of N_2O to the reduced active species, focusing on inhibition pathways and how to circumvent this inhibition of the catalyst by the co-product produced.

Chapter V will take insights from Chapters III and IV and will open new directions for the activation of N-O bond in pyridine N-oxide molecule. This Chapter includes results achieved by a master 1 internship student Alexandra Collard.

Finally, in Chapter VI we will conclude the thesis and draw some perspectives for future work.

References:

- (1) Nagele, P.; Duma, A.; Kopec, M.; Gebara, M. A.; Parsoei, A.; Walker, M.; Janski, A.; Panagopoulos, V. N.; Cristancho, P.; Miller, J. P.; et al. Nitrous Oxide for Treatment-Resistant Major Depression: A Proof-of-Concept Trial. *Biol Psychiatry* **2015**, *78* (1), 10-18. DOI: 10.1016/j.biopsych.2014.11.016.
- (2) Sanders, Robert D.; Weimann, J.; Maze, M.; Warner, David S.; Warner, Mark A. Biologic Effects of Nitrous Oxide: A Mechanistic and Toxicologic Review. *Anesthesiology* **2008**, *109* (4), 707-722. DOI: 10.1097/ALN.0b013e3181870a17.
- (3) Davidson, E. A.; Kanter, D. Inventories and scenarios of nitrous oxide emissions. *Environmental Research Letters* **2014**, *9* (10). DOI: 10.1088/1748-9326/9/10/105012.
- (4) Hsu, J. C.; Prather, M. J. Global long-lived chemical modes excited in a 3-D chemistry transport model: Stratospheric N₂O, NO_y, O₃ and CH₄ chemistry. *Geophysical Research Letters* **2010**, *37*. DOI: 10.1029/2009GL042243, 2010.
- (5) Aryal, B.; Gurung, R.; Camargo, A. F.; Fongaro, G.; Treichel, H.; Mainali, B.; Angove, M. J.; Ngo, H. H.; Guo, W.; Puadel, S. R. Nitrous oxide emission in altered nitrogen cycle and implications for climate change. *Environ Pollut* **2022**, *314*, 120272. DOI: 10.1016/j.envpol.2022.120272.
- (6) Firestone, M. K.; Davidson, E. A.; Andreae, M. O.; Schimel, D. S. Microbiological basis of NO and N₂O production and consumption in soil. 1989.
- (7) Montzka, S. A.; Dlugokencky, E. J.; Butler, J. H. Non-CO₂ greenhouse gases and climate change. *Nature* **2011**, *476* (7358), 43-50. DOI: 10.1038/nature10322.
- (8) Erisman, J. W.; Sutton, M. A.; Galloway, J.; Klimont, Z.; Winiwarter, W. How a century of ammonia synthesis changed the world. *Nature Geoscience* **2008**, *1* (10), 636-639. DOI: 10.1038/ngeo325.
- (9) Pauling, L. The Electronic Structure of the Normal Nitrous Oxide Molecule. *Proc Natl Acad Sci U S A* **1932**, *18* (7), 498-499. DOI: 10.1073/pnas.18.7.498.
- (10) Gómez, R.; Weaver, M. J. Reduction of Nitrous Oxide on Iridium Single-Crystal Electrodes. *Langmuir* **2002**, *18* (11), 4426-4432. DOI: 10.1021/la015700b.
- (11) Vaughan, G. A.; Rupert, P. B.; Hillhouse, G. L. Selective O-atom transfer from nitrous oxide to hydride and aryl ligands of bis(pentamethylcyclopentadienyl)hafnium derivatives. *Journal of the American Chemical Society* **2002**, *124* (18), 5538-5539. DOI: 10.1021/ja00252a047.
- (12) Tolman, W. B. Binding and activation of N₂O at transition-metal centers: recent mechanistic insights. *Angew Chem Int Ed Engl* **2010**, *49* (6), 1018-1024. DOI: 10.1002/anie.200905364.
- (13) Ravishankara, A. R.; Daniel, J. S.; Portmann, R. W. Nitrous Oxide: The Dominant Ozone-Depleting Substance Emitted in the 21st Century. *Science* **2009**, *326* (5949), 123-125. DOI: 10.1126/science.1176985.
- (14) Pauleta, S. R.; Carepo, M. S. P.; Moura, I. Source and reduction of nitrous oxide. *Coordination Chemistry Reviews* **2019**, *387*, 436-449. DOI: 10.1016/j.ccr.2019.02.005.
- (15) Liang, J.; Burris, R. H. Interactions among nitrogen, nitrous oxide, and acetylene as substrates and inhibitors of nitrogenase from *Azotobacter vinelandii*. *Biochemistry* **1988**, *27* (18), 6726-6732. DOI: 10.1021/bi00418a013.
- (16) Rivera-Ortiz, J. M.; Burris, R. H. Interactions among substrates and inhibitors of nitrogenase. *Journal of Bacteriology* **1975**, *123* (2), 537-545. DOI: 10.1128/jb.123.2.537-545.1975.
- (17) Liang, J.; Burris, R. H. N₂O reduction and HD formation by nitrogenase from a nifV mutant of *Klebsiella pneumoniae*. **1989**, *171* (6), 3176-3180. DOI: 10.1128/jb.171.6.3176-3180.1989.
- (18) Jones, C. A. Hernán Cortés: Letters from Mexico. Translated and edited by A. R. Pagden, with an Introduction by J. H. Elliott. *Journal of Latin American Studies* **2009**, *7* (1), 147-148. DOI: 10.1017/s0022216x00016722.
- (19) Gorelsky, S. I.; Ghosh, S.; Solomon, E. I. Mechanism of N₂O reduction by the μ₄-S tetranuclear CuZ cluster of nitrous oxide reductase. *J Am Chem Soc* **2006**, *128* (1), 278-290. DOI: 10.1021/ja055856o.
- (20) Ghosh, S.; Gorelsky, S. I.; DeBeer George, S.; Chan, J. M.; Cabrito, I.; Dooley, D. M.; Moura, J. J. G.; Moura, I.; Solomon, E. I. Spectroscopic, Computational, and Kinetic Studies of the μ₄-Sulfide-Bridged Tetranuclear CuZ Cluster in N₂O Reductase: pH Effect on the Edge Ligand and Its Contribution to Reactivity. *Journal of the American Chemical Society* **2007**, *129* (13), 3955-3965. DOI: 10.1021/ja068059e.
- (21) Yamada, T.; Hashimoto, K.; Kitaichi, Y.; Suzuki, K.; Ikeno, T. Nitrous Oxide Oxidation of Olefins Catalyzed by Ruthenium Porphyrin Complexes. *Chemistry Letters* **2001**, *30* (3), 268-269. DOI: 10.1246/cl.2001.268.
- (22) Ben-Daniel, R.; Weiner, L.; Neumann, R. Activation of nitrous oxide and selective epoxidation of alkenes catalyzed by the manganese-substituted polyoxometalate, [Mn^{III}₂ZnW(Zn₂W₉O₃₄)₂]¹⁰⁻. *J. Am. Chem. Soc.* **2002**, *124* (30), 8788-8789. DOI: 10.1021/ja0259077.
- (23) Kentaro, H.; Yasunori, K.; Hirotsuka, T.; Taketo, I.; Tohru, Y. Nitrous Oxide Oxidation of Secondary and Benzylic Alcohols Using Ruthenium Complex Catalyst. *Chemistry Letters* **2001**, *30* (9), 922-923. DOI: 10.1246/cl.2001.922.

- (24) Stuchinskaya, T. L.; Kozhevnikov, I. V. Novel efficient catalysts based on Ru or Pd oxide for selective liquid-phase oxidation of alcohols with nitrous oxide. *Catalysis Communications* **2003**, *4* (12), 609-614. DOI: 10.1016/j.catcom.2003.09.005.
- (25) Gianetti, T. L.; Annen, S. P.; Santiso-Quinones, G.; Reiher, M.; Driess, M.; Grützmacher, H. Nitrous Oxide as a Hydrogen Acceptor for the Dehydrogenative Coupling of Alcohols. *Angewandte Chemie International Edition* **2016**, *55* (5), 1854-1858. DOI:10.1002/anie.201509288.
- (26) Pu, L. S.; Yamamoto, A.; Ikeda, S. Catalytic reduction of nitrous oxide with nitrogentris(triphenylphosphine)cobalt hydride. *Journal of the Chemical Society D: Chemical Communications* **1969**, (5), 189b-190. DOI: 10.1039/C2969000189B.
- (27) Yamamoto, A.; Kitazume, S.; Pu, L. S.; Ikeda, S. Synthesis and properties of hydridodinitrogentris(triphenylphosphine)cobalt(I) and the related phosphine-cobalt complexes. *Journal of the American Chemical Society* **1971**, *93* (2), 371-380. DOI: 10.1021/ja00731a012.
- (28) Tohru, Y.; Kyosuke, S.; Kentaro, H.; Taketo, I. N₂O Oxidation of Phosphines Catalyzed by Low-Valent Nickel Complexes. *Chemistry Letters* **1999**, *28* (10), 1043-1044. DOI: 10.1246/cl.1999.1043.
- (29) Pang, Y.; Leutzsch, M.; Nothling, N.; Cornella, J. Catalytic Activation of N₂O at a Low-Valent Bismuth Redox Platform. *J. Am. Chem. Soc.* **2020**, *142* (46), 19473-19479. DOI: 10.1021/jacs.0c10092.
- (30) Maity, B.; Koley, D. Mechanistic investigation of the reactivity of disilene with nitrous oxide: A DFT study. *J. Mol. Graph. Model.* **2014**, *51*, 50-63. DOI: 10.1016/j.jmgm.2014.04.011.
- (31) Wiberg, N.; Niedermayer, W.; Polborn, K.; Mayer, P. Reactivity of the Isolable Disilene R*PhSi=SiPhR* (R*=Si^tBu₃). *Chemistry – A European Journal* **2002**, *8* (12), 2730-2739. DOI:10.1002/1521-3765(20020617)8:12<2730::AID-CHEM2730>3.0.CO;2-Q.
- (32) Khan, S.; Michel, R.; Koley, D.; Roesky, H. W.; Stalke, D. Reactivity Studies of a Disilene with N₂O and Elemental Sulfur. *Inorganic Chemistry* **2011**, *50* (21), 10878-10883. DOI: 10.1021/ic201419m.
- (33) Jana, A.; Roesky, H. W.; Schulzke, C. Reactivity of germanium(II) hydride with nitrous oxide, trimethylsilyl azide, ketones, and alkynes and the reaction of a methyl analogue with trimethylsilyl diazomethane. *Dalton Transactions* **2010**, *39* (1), 132-138. DOI: 10.1039/B914164B.
- (34) Anthore-Dalion, L.; Nicolas, E.; Cantat, T. Catalytic Metal-Free Deoxygenation of Nitrous Oxide with Disilanes. *ACS Catalysis* **2019**, *9* (12), 11563-11567. DOI: 10.1021/acscatal.9b04434.
- (35) Kiefer, G.; Jeanbourquin, L.; Severin, K. Oxidative Coupling Reactions of Grignard Reagents with Nitrous Oxide. *Angewandte Chemie International Edition* **2013**, *52* (24), 6302-6305. DOI:10.1002/anie.201302471.
- (36) Saito, S.; Ohtake, H.; Umezawa, N.; Kobayashi, Y.; Kato, N.; Hirobe, M.; Higuchi, T. Nitrous oxide reduction-coupled alkene-alkene coupling catalysed by metalloporphyrins. *Chem. Commun. (Camb)* **2013**, *49* (79), 8979-8981. DOI: 10.1039/c3cc43912g.
- (37) Wislicenus, W. *Ber. Dtsch. Chem. Ges.* **1892**, *25* (1892).
- (38) J. Haase. *Organic Azides, Syntheses and Applications*. S. Bräse and K. Banert John Wiley & Sons, Weinheim **2010**, 29-51.
- (39) Meier, R. Reaktionen metallorganischer Verbindungen mit Stickoxydul. *Chemische Berichte* **1953**, *86* (12), 1483-1492. DOI:10.1002/cber.19530861203.
- (40) Koga, G.; Anselme, J. P. The formation of azides by the reaction of amine anions with nitrous oxide. *Chemical Communications (London)* **1968**, (8), 446-447. DOI: 10.1039/C19680000446.
- (41) Wang, L.-Q.; Li, T.; Ma, H.-H. Explosion behaviors of hydrogen-nitrous oxide mixtures at reduced initial pressures. *Process Safety and Environmental Protection* **2021**, *153*, 11-18. DOI: 10.1016/j.psep.2021.07.010.
- (42) Zeng, R.; Feller, M.; Ben-David, Y.; Milstein, D. Hydrogenation and Hydrosilylation of Nitrous Oxide Homogeneously Catalyzed by a Metal Complex. *J. Am. Chem. Soc.* **2017**, *139* (16), 5720-5723. DOI: 10.1021/jacs.7b02124.
- (43) Ortega-Lepe, I.; Sánchez, P.; Santos, L. L.; Lara, P.; Rendón, N.; López-Serrano, J.; Salazar-Pereda, V.; Álvarez, E.; Paneque, M.; Suárez, A. Catalytic Nitrous Oxide Reduction with H₂ Mediated by Pincer Ir Complexes. *Inorganic Chemistry* **2022**, *61* (46), 18590-18600. DOI: 10.1021/acs.inorgchem.2c02963.
- (44) Jurt, P.; Abels, A. S.; Gamboa-Carballo, J. J.; Fernandez, I.; Le Corre, G.; Aebli, M.; Baker, M. G.; Eiler, F.; Müller, F.; Worle, M.; et al. Reduction of Nitrogen Oxides by Hydrogen with Rhodium(I)-Platinum(II) Olefin Complexes as Catalysts. *Angew. Chem. Int. Ed. Engl.* **2021**, *60* (48), 25372-25380. DOI: 10.1002/anie.202109642.
- (45) Zeng, R.; Feller, M.; Diskin-Posner, Y.; Shimon, L. J. W.; Ben-David, Y.; Milstein, D. CO Oxidation by N₂O Homogeneously Catalyzed by Ruthenium Hydride Pincer Complexes Indicating a New Mechanism. *J Am Chem Soc* **2018**, *140* (23), 7061-7064. DOI: 10.1021/jacs.8b03927.
- (46) Ricker, J. D.; Mohammadrezaei, V.; Crippen, T. J.; Zell, A. M.; Geary, L. M. Nitrous Oxide Promoted Pauson-Khand Cycloadditions. *Organometallics* **2018**, *37* (24), 4556-4559. DOI: 10.1021/acs.organomet.8b00810.
- (47) Kjellberg, M.; Ohleier, A.; Thuéry, P.; Nicolas, E.; Anthore-Dalion, L.; Cantat, T. Photocatalytic deoxygenation of N–O bonds with rhenium complexes: from the reduction of nitrous oxide to pyridine N-oxides. *Chemical Science* **2021**, *12* (30), 10266-10272. DOI: 10.1039/D1SC01974K.

-
- (48) Parmon, V. N.; Panov, G. I.; Uriarte, A.; Noskov, A. S. Nitrous oxide in oxidation chemistry and catalysis: application and production. *Catalysis Today* **2005**, *100* (1-2), 115-131. DOI: 10.1016/j.cattod.2004.12.012.
- (49) Konsolakis, M. Recent Advances on Nitrous Oxide (N₂O) Decomposition over Non-Noble-Metal Oxide Catalysts: Catalytic Performance, Mechanistic Considerations, and Surface Chemistry Aspects. *ACS Catalysis* **2015**, *5* (11), 6397-6421. DOI: 10.1021/acscatal.5b01605.
- (50) Poh, S.; Hernandez, R.; Inagaki, M.; Jessop, P. G. Oxidation of Phosphines by Supercritical Nitrous Oxide. *Organic Letters* **1999**, *1* (4), 583-586. DOI: 10.1021/ol9906918.
- (51) Savéant, J. M. Molecular catalysis of electrochemical reactions. Mechanistic aspects. *Chem Rev* **2008**, *108* (7), 2348-2378. DOI: 10.1021/cr068079z.
- (52) Kudo, A.; Mine, A. Electrocatalysis for N₂O reduction on metal electrodes. *Journal of Electroanalytical Chemistry* **1996**, *408* (1-2), 267-269. DOI: 10.1016/0022-0728(96)04630-x.
- (53) Ko, B. H.; Hasa, B.; Shin, H.; Zhao, Y.; Jiao, F. Electrochemical Reduction of Gaseous Nitrogen Oxides on Transition Metals at Ambient Conditions. *Journal of the American Chemical Society* **2022**, *144* (3), 1258-1266. DOI: 10.1021/jacs.1c10535.
- (54) Collman, J. P.; Marrocco, M.; Elliott, C. M.; L'Her, M. Electrocatalysis of nitrous oxide reduction. *Journal of Electroanalytical Chemistry and Interfacial Electrochemistry* **1981**, *124* (1-2), 113-131. DOI: 10.1016/s0022-0728(81)80289-6.
- (55) Taniguchi, I.; Shimpuku, T.; Yamashita, K.; Ohtaki, H. Electrocatalytic reduction of nitrous oxide to dinitrogen at a mercury electrode using Ni(II) complexes of macrocyclic polyamines. *Journal of the Chemical Society, Chemical Communications* **1990**, (13), 915-917. DOI: 10.1039/C39900000915.
- (56) ZHANG, J.; TSE, Y.-H.; LEVER, A. B. P.; PIETRO, W. J. Electrochemical Reduction of Nitrous Oxide (N₂O) Catalysed by Tetraaminophthalocyanatocobalt(II) Adsorbed on a Graphite Electrode in Aqueous Solution. *Journal of Porphyrins and Phthalocyanines* **1997**, *01* (04), 323-331. DOI :10.1002/(SICI)1099-1409(199710)1:4<323::AID-JPP46>3.0.CO;2-Q.

Chapter II: Outer-Sphere Activation of N-O Bond in N₂O: Redox Catalysis

This Chapter includes work I have published as the first co-author:

- Homogeneous Molecular Catalysis of the Electrochemical Reduction of N₂O to N₂: Redox vs. Chemical Catalysis. Deeba, R.; Chardon-Noblat, S.; Costentin, C. *Chem. Sci.*, **2021**, *12*, 12726–12732. DOI:10.1039/D1SC03044B.
- Molecular Catalysis of Electrochemical Reactions: Competition between Reduction of the Substrate and Deactivation of the Catalyst by a Cosubstrate Application to N₂O Reduction. Deeba, R.; Chardon-Noblat, S.; Costentin, C., *ChemElectroChem*, **2021**, *8*, 3740 – 3744. DOI: 10.1002/celc.202100.

1. Introduction

This Chapter reports an original type of homogenous catalysis, not yet detailed in the literature, that performs the reduction of nitrous oxide employing a series of organic aromatic molecules as catalysts. We thought that N_2O could be reduced via an outersphere electron transfer as it is the case in pulse radiolysis in which hydrated electrons (e^-)_{aq} have been used to reduce N_2O which dissociates to give N_2 and $\text{O}^{\bullet-}$, which readily reacts with H_2O to give OH^{\bullet} radicals and OH^- in aqueous medium.^{1,2} However, our study is in acetonitrile and the formation and evolution of $\text{N}_2\text{O}^{\bullet-}$ anion radical (if it exists) might be different than in water. In the majority of reported cases of N_2O deoxygenation, dinitrogen is released and the oxygen atom is transferred either to the metal of a complex,³ inserted into a metal ligand bond, a metal carbon^{4,5} or a metal hydride bond^{6,7} or, transferred catalytically to an oxygen atom acceptor. In this case of homogeneous catalysis, because we will use simple outersphere electron donors as reductant and water as a source of protons, nitrous oxide reduction might result in the release of dinitrogen gas and hydroxide or water. Our goal here is thus to investigate the outersphere electron reduction of N_2O with homogeneous electron donors and to compare it to the direct reduction of N_2O at a glassy carbon electrode.

Let us briefly recall the basic principle of redox homogeneous catalysis. We consider P/Q (Figure I.5 1 Chapter I) as a reversible couple and the standard potential of which is less negative than the irreversible onset potential of the direct electrochemical reaction of the substrate (e.g. N_2O) at the working electrode (WE) surface. The catalyst (P) acquires the electrons via an outersphere manner from the electrode and delivers them via an outersphere manner with no chemical interaction with the substrate yielding the reaction products and regenerating the oxidized form of the catalyst that is then reduced again leading to a catalytic process. In cyclic voltammetry, an increase of the current is observed in the presence of substrate at a potential where P is reduced into Q, in view of the fact that electrons from the electrode are replaced by the reduced form of the catalyst Q constantly regenerated at the electrode. Herein we use as catalysts organic aromatic molecules leading to radical anion or dianion reductive species upon one or two successive one-electron reversible electron transfers.

We recall here the cyclic voltammetry (CV) response of simple one-electron step catalytic system. With excess of substrate, the CV response is given by the following analytical expression:⁸

$$\frac{1}{\sqrt{\pi}} \int_0^{\xi} \frac{\psi \exp[-\lambda_{CV}(\xi - \eta)]}{\sqrt{\xi - \eta}} d\eta = \frac{1}{1 + \exp(\xi)} \quad (1)$$

with the dimensionless current and potential being respectively $\psi = \frac{i}{FSC_P^0 \sqrt{DFv/RT}}$ and

$\xi = F(E_{P/Q}^0 - E)/RT$. Importantly, the CV response is governed by a single dimensionless

parameter $\lambda_{CV} = \frac{kC_A^0}{Fv/RT}$ measuring the ratio of the timescale of the CV and the timescale of

the homogeneous reaction. As illustrated in Figure II.1 1 (showing the different type of CVs),

for small values of λ_{CV} , the CV trace corresponds to the simple reversible nernstian wave

indicating that no catalysis takes place in the timescale of the CV. In other words, CV is not a

useful technique to investigate slow catalytic processes, keeping in mind that scan rates smaller than 20 mV/s should be avoided to prevent interference of natural convection perturbing the

semi-infinite planar diffusion regime. As λ_{CV} is increased the CV loses its reversibility and

reaches a canonical S-shape at large values of λ_{CV} . This last behavior corresponds to pure-

kinetics conditions resulting from a mutual compensation of diffusion of Q and its reaction with

the substrate so that the catalytic reaction only takes place within a thin diffusion-reaction layer

close to the electrode surface. The CV plateau current is thus given by $i_{pl} = FSC_P^0 \sqrt{DkC_A^0}$ giving

a simple direct access to the evaluation of the rate constant, hence showing that CV is a

convenient technique to investigate fast catalytic processes.

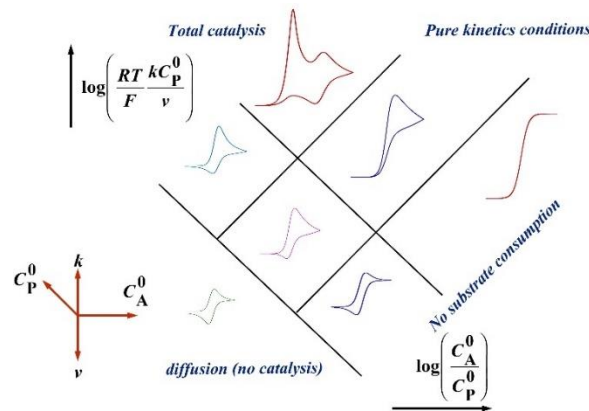


Figure II.1 1: Kinetic zone diagram for one electron catalytic reduction showing the expected shapes of the cyclic voltammetry responses as a function of the two dimensionless parameters for a first order catalytic reaction in substrate C_A (bulk substrate concentration) and C_P (bulk catalyst concentration) and v is the scan rate. ⁹

2. Homogeneous redox catalysis: experimental results

2.1 Cyclic Voltammetry analysis under argon and N₂O effect of scan rate

The chosen aromatic species (see Table VII 1 in the experimental part) give upon reduction stable radical anion species (able to act as outersphere electron donors) with increasing reducing power as the standard potential is more and more negative. The rationale is thus that upon using aromatic species, with negative enough standard potential, they should be able to reduce N₂O. This is what has been observed experimentally. The corresponding standard potentials (E°) are calculated from the midpoint of the anodic and cathodic peak wave potentials, recorded from CVs plotted at scan rate of 0.1 V/s at a 3 mm diameter glassy carbon (GC) electrode in CH₃CN + 0.1 M *n*-NBu₄PF₆ (Table II.2.1 1).

Catalyst	E° (V vs. SCE)
Terephthalonitrile	-1.65
Phthalonitrile	-1.73
Perylene	-1.73
Benzophenone	-1.82
4-cyanopyridine	-1.85
1-naphthonitrile	-1.94
9,10-diphenylanthracene	-1.93
Anthracene	-2.03
9,10-dimethylanthracene	-2.05
9,10-dicyanoanthracene	-0.95 / -1.56
Phenazine	-1.21 / -1.55
Fluorenone	-1.33 / -1.88

Table II.2.1 1: Standard potentials of redox catalysts.

A catalytic current is observed in the presence of N₂O (saturated solution, 1 atm, 280 mM solubility in acetonitrile)(cf. experimental part Determination of solubility of N₂O), with catalysts which standard potentials are negative to *ca.* -1.62 V vs SCE. No catalytic current is observed with 9,10-dicyanoanthracene or phenazine. In all cases where a catalytic current is observed raising the scan rate allows reaching a plateau current independent on scan rate indicating pure kinetics conditions (Figure II.2.1 1).⁹

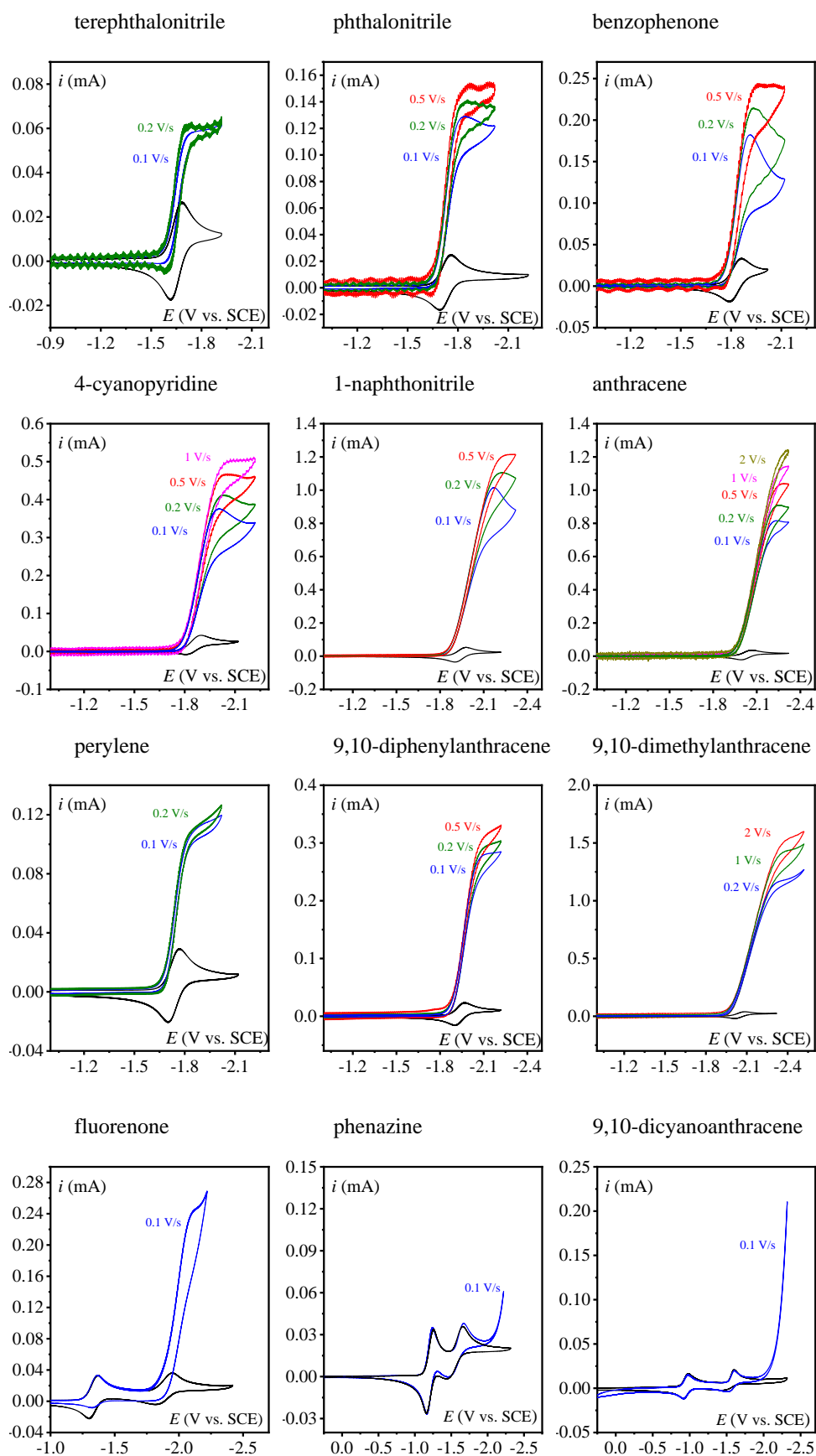
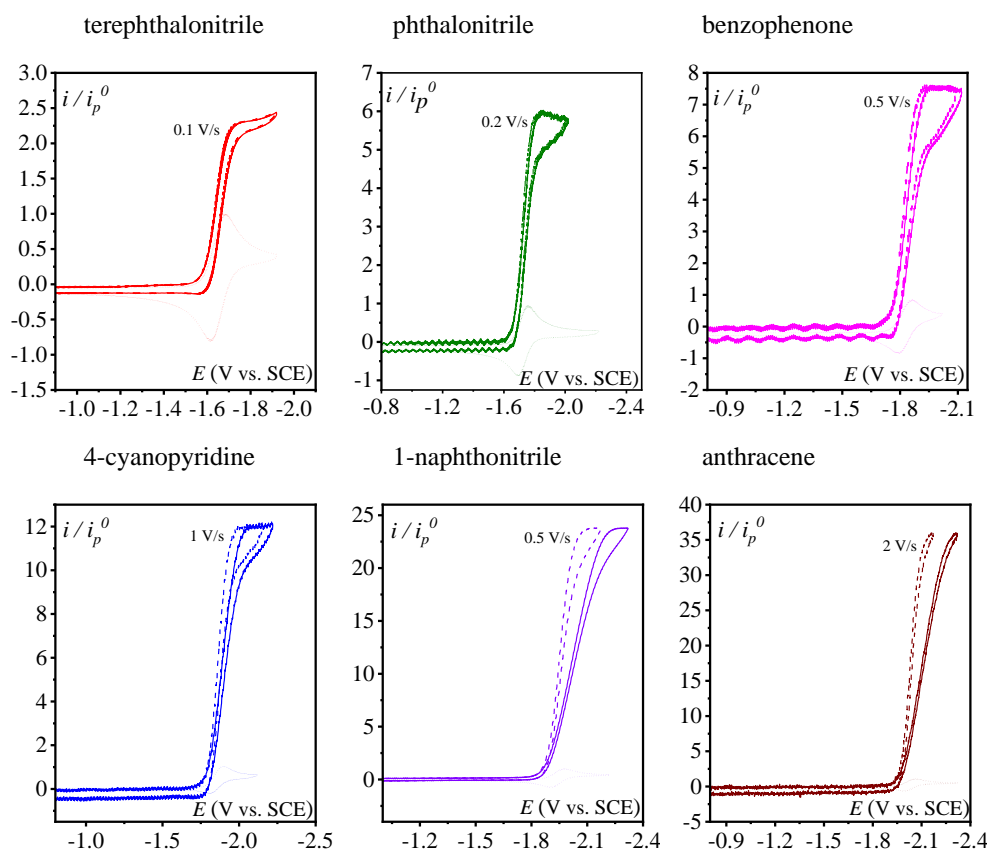


Figure II.2.1: CVs of the catalysts (1 mM) under argon at 0.1 V/s (black) and under N_2O , in CH_3CN with $n-Bu_4NPF_6$ (0.1 M) on a 3 mm diam. GC electrode.

2.2 Minimizing Ohmic Drop

Electrocatalytic solutions have an intrinsic resistance R_{sol} in the electrochemical cell which is equal to $R_c + R_u$ (c corresponds for compensated and u for uncompensated). While potentiostats compensates for R_c there remains a portion of uncompensated resistance (R_u) between the WE and the reference electrode. If R_u wasn't compensated by the positive feedback, then the potential that the instrument records might not be the potential experienced by the analyte and so a shift of the catalytic wave might be observed as shown in the CVs below (Figure II.2.2 1) especially with high currents intensity. This ohmic drop has to be minimized in order to be able to obtain accurate kinetic and mechanistic information which will be discussed in the coming section. The catalytic CVs shown below have also been corrected for ohmic drop using the formula $E-Ri$ considering a resistance of 120Ω (cf. experimental part Ohmic drop correction).



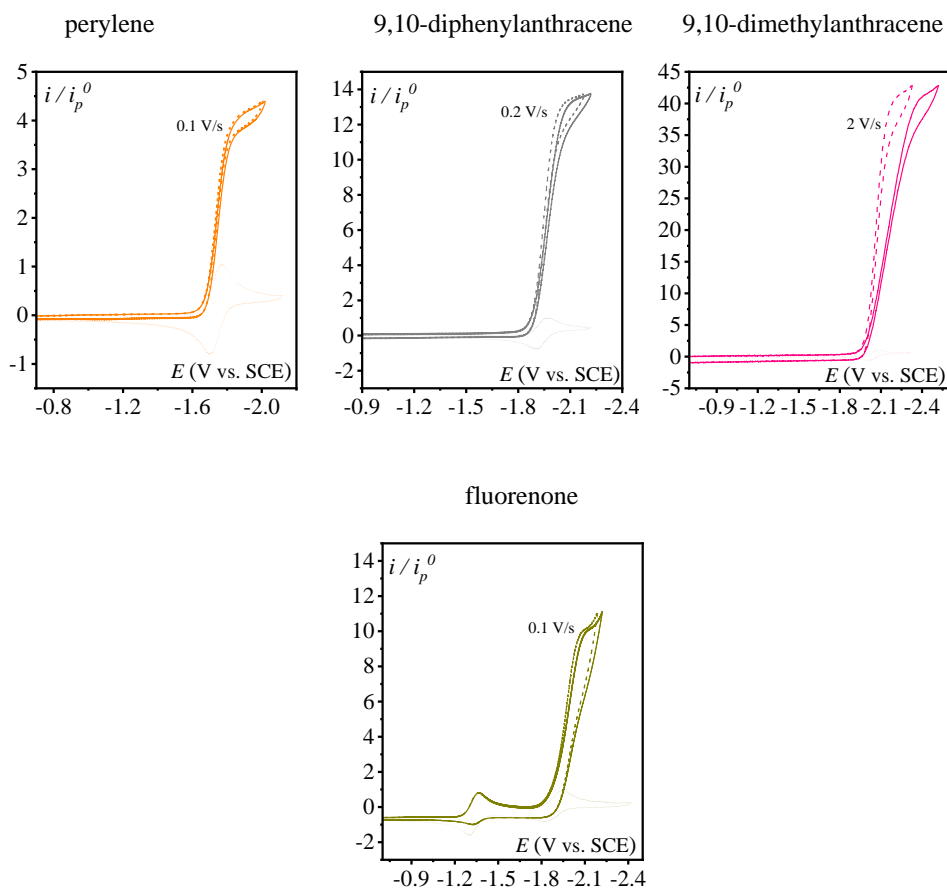
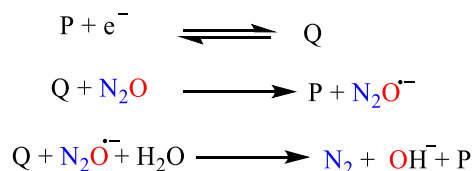


Figure II.2.2 1: Homogeneous catalysis of the electrochemical reduction of N_2O by organic molecule radical anions or dianions. Normalized CVs of the catalyst under argon at 0.1 V/s (short dot) and under N_2O (full line) and after ohmic drop correction (dashed line) at a scan rate that permits the catalytic plateau current to be reached, in CH_3CN with $n-Bu_4NPF_6$ (0.1 M) on a 3 mm diam. GCE. $i_p^0 = 0.446FSC_{cat}^0 \sqrt{DFv/RT}$. s is the electrode surface area, C_{cat}^0 is the catalyst concentration, D the catalyst diffusion coefficient, F the Faraday, R the gas constant, T the temperature.

2.3 Effect of addition of water

The effect of addition of water was then studied showing no to little effect on the catalytic current indicating that the outersphere rate determining step is not coupled to proton transfer (Figure II.2.3 1). Water is required to stabilize the oxygen atom after the rupture of the N-O bond based on the following proposed mechanism (Scheme II.2.3 1).



Scheme II.2.3 1: Mechanism for the reduction of N_2O with electrogenerated organic catalysts Q .

For 4-cyanopyridine, which will be studied broadly at the end of this Chapter, water showed detrimental effect on catalysis of N_2O reduction.

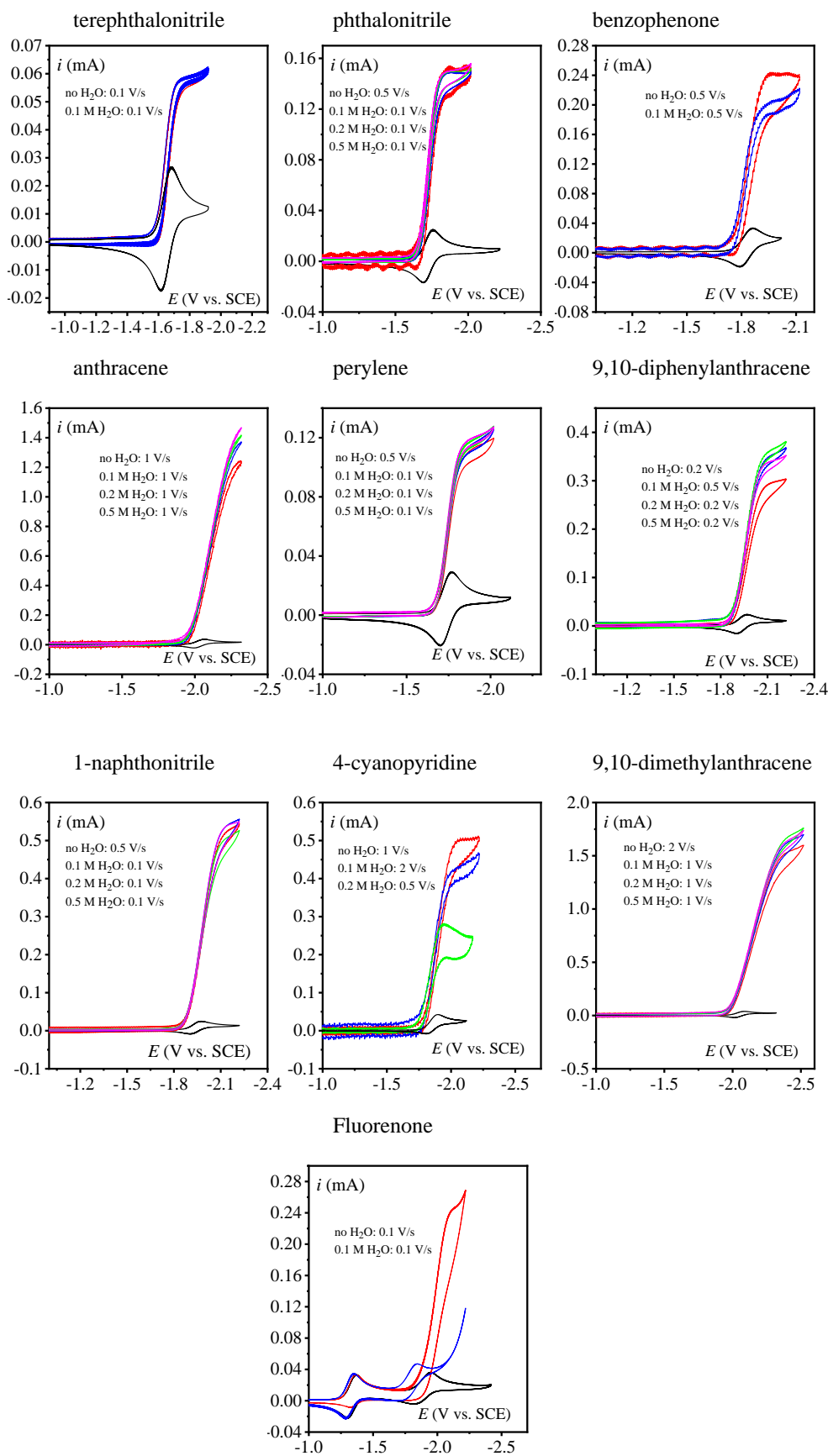


Figure II.2.3 1: Normalized CVs of the catalysts (1 mM) under argon at 0.1 V/s (black line) and under N_2O with or without addition of water in CH_3CN with $n-Bu_4NPF_6$ (0.1 M) on a 3 mm diameter GC electrode.

Likewise, in the case of fluorenone with the addition of 100 mM H₂O the catalytic current intensity was suppressed and the potential peak became less negative by *ca.* 100 mV. This observation suggests the reaction of intermediate organic radical anions or dianions with water, is preventing its ability to reduce N₂O. We conclude that there is a competition between the reaction of N₂O and water with the organic radical anions. This reaction might lead to a neutral radical which is immediately reduced leading to ECE process (electrochemical, chemical, electrochemical or catalyst hydrogenation DISP disproportionation) and thus the deactivation of the catalyst.

2.4 Selectivity of the redox catalytic process: electrolysis

The selectivity and the stoichiometry of the catalytic process were probed by running short controlled potential electrolysis (CPE) under N₂O in acetonitrile in the presence of 100 mM of H₂O on a 1 cm² glassy carbon electrode and 1 mM catalyst concentration for the following representative catalysts as well as for the direct electrochemical reduction of N₂O on glassy carbon electrode (Figure II.2.4 1). Results are gathered in the Table II.2.4 1. In all cases N₂ is the only product obtained in a quantitative faradaic yield corresponding to the consumption of two moles of electron per mole of mole of N₂O reduced, thus leading to the overall reaction: $\text{N}_2\text{O} + 2\text{e}^- + \text{H}_2\text{O} \rightarrow \text{N}_2 + 2\text{OH}^-$

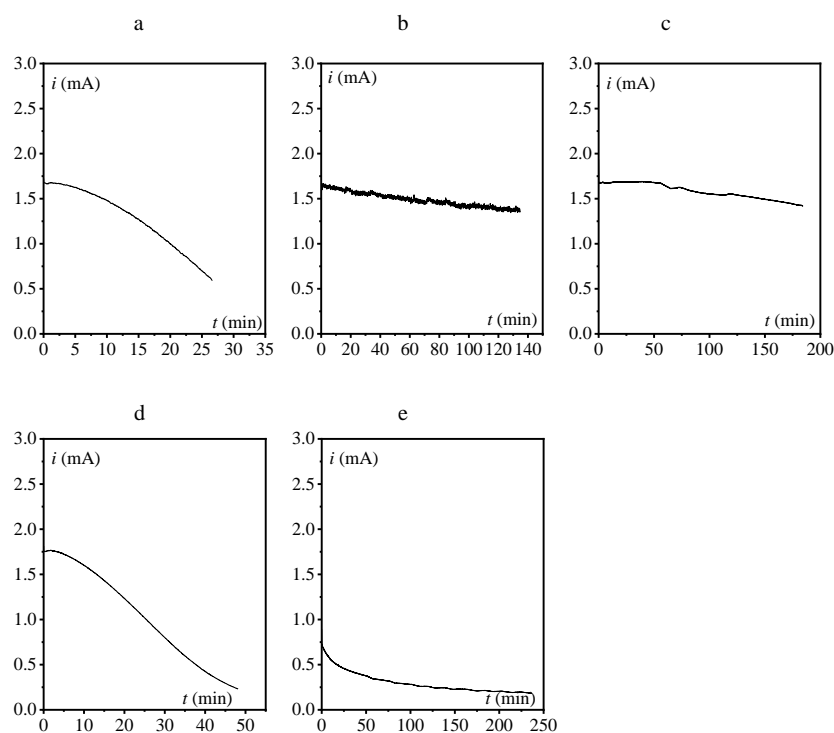


Figure II.2.4 1: Current vs. time for controlled potential electrolysis for (a) phthalonitrile, (b) benzophenone, (c) perylene, (d) 4-cyanopyridine and (e) direct reduction of N₂O.

Redox organic catalyst	Applied Potential (V vs. SCE)	Charge passed (C)	Faradaic yield (%)
Phthalonitrile	-1.87	2.45	74
Benzophenone	-1.87	17	117
Perylene	-1.87	17.47	101
4-cyanopyridine	-1.87	3.0	109
No catalyst	-2.17	4.22	123

Table II.2.4 1: N₂O reduction electrolysis.

3. Homogeneous redox catalysis: kinetic analysis

The experimental results obtained from CV and CPE show that electrogenerated organic based radical anions are able to reduce N₂O to N₂ with a rate determining step that do not involve proton transfer. Hence in the reaction sequence proposed in Scheme II.3 1, we can assume that the first chemical step is rate determining.

The rate constant k , corresponding to the initial chemical step for the reduction of N₂O by electrogenerated radical anions or dianions, can be obtained from the plateau current measured in CV considering that a stoichiometry of two electrons is required to reduce N₂O as attested from the electrolysis experiments. This stoichiometric factor has to be included in the expression of the plateau current given below:

$$\frac{i_{pl}}{i_p^0} = 2.24 \sqrt{\frac{RT}{Fv}} \sqrt{2k} \quad (2)$$

Here it is referred to a two-electron process in which the second electron transfer is occurring in solution as opposed to at the electrode surface. This assumption is justified a posteriori given the slowness of the overall process, the one electron reduced N₂O intermediate is produced far away from the electrode so that it is further reduced in solution and not at the electrode surface. Figure II.3 1 demonstrates a good agreement of the fit of the forward catalytic response with equation (2) with i_p^0 is the peak current corresponding to the catalyst under argon, E_{cat}^0 : standard potential of the redox catalyst couple, F : the Faraday, R : the gas constant, T : temperature

$$\frac{i}{i_p^0} = \frac{i_{pl}/i_p^0}{1 + \exp\left[\frac{F}{RT}(E - E_{cat}^0)\right]} \quad (3)$$

CVs were plotted based on the above derived equation (3) showing exact fitting with the CVs corrected for ohmic drop done on raw experimental data.

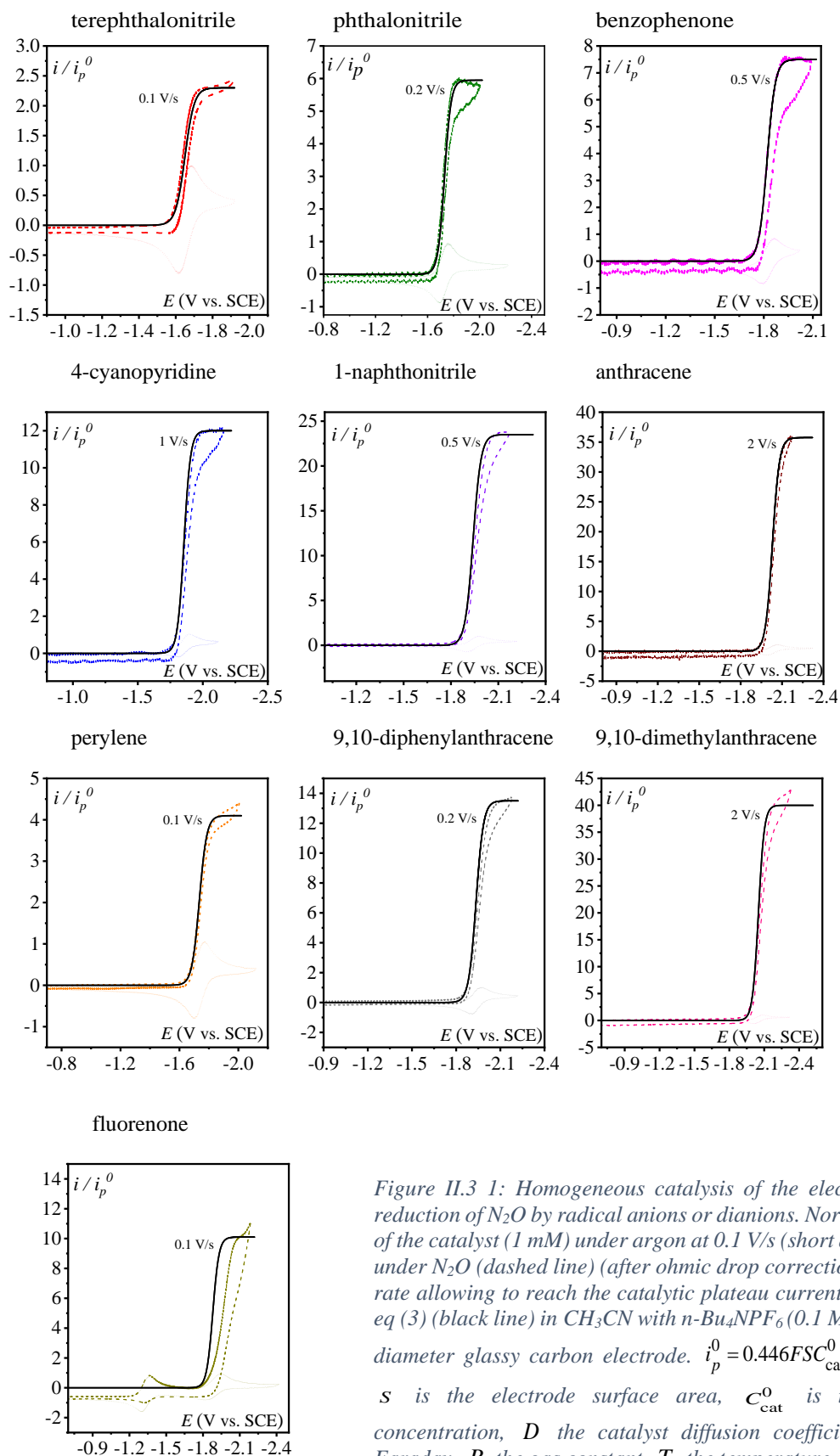


Figure II.3 1: Homogeneous catalysis of the electrochemical reduction of N_2O by radical anions or dianions. Normalized CVs of the catalyst (1 mM) under argon at 0.1 V/s (short dot line) and under N_2O (dashed line) (after ohmic drop correction) at a scan rate allowing to reach the catalytic plateau current, fitting with eq (3) (black line) in CH_3CN with $n-Bu_4NPF_6$ (0.1 M) on a 3 mm diameter glassy carbon electrode. $i_p^0 = 0.446FSC_{cat}^0 \sqrt{DFv/RT}$. s is the electrode surface area, C_{cat}^0 is the catalyst concentration, D the catalyst diffusion coefficient, F the Faraday, R the gas constant, T the temperature.

This indicates that the half-wave potential is equivalent to the catalyst's standard potential, which is a well-established criterion for two-electron processes in which the catalysis's first chemical step really determines the process's rate.¹⁰ However, when fluorenone dianion is utilized as a reductant, there is a change in the match with equation (3). Presumably, this is due to the fact that the equivalent redox pair-radical anion/dianion is not Nernstian., i.e., the electron transfer is not fast enough to form the radical anion at equilibrium.

Figure II.3 2 shows how the rate constant changes in relation to catalyst couple's standard potential. There seems to be a relationship between the catalyst's standard potential and the rate constant: the more negative the standard potential, the larger the rate constant following an activation driving force correlation shown as black dashed line in Figure II.3 2 with average slope of:

$$\frac{\partial \log k}{\partial E_{cat}^0} = -\frac{F}{RT \ln 10} \alpha_{ap} \quad (4)$$

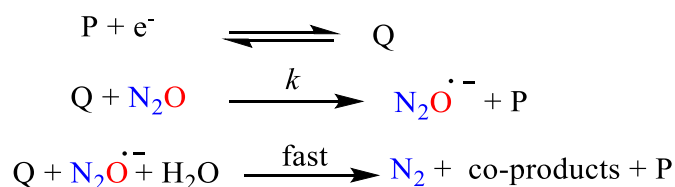
This results in an apparent transfer coefficient of $\alpha_{ap} \approx 0.35$. Such correlation can be simplified as corresponding to anionic species acting outer-sphere electron donors to N₂O to form intermediate which is (N₂O^{•-}) and this reaction is characterized by a large reorganization energy λ .^{11,12} A quadratic relationship is anticipated within the framework of Marcus-Hush theory for electron transfer between the activation energy ΔG^\ddagger and standard free energy of the reaction $\Delta G^0 = F \left(E_{cat}^0 - E_{N_2O/N_2O^{\bullet-}}^0 \right)$:

$$\Delta G^\ddagger = \frac{\lambda}{4} \left(1 + \frac{\Delta G^0}{\lambda} \right)^2 \quad (5)$$

$$\text{with } k = Z_{\text{hom}} [N_2O] \exp \left(-\frac{\Delta G^\ddagger}{RT} \right) \quad (6)$$

where Z_{hom} is the pre-exponential factor for the homogeneous bimolecular electron transfer between radical anions or dianions and N₂O. We anticipate that this factor won't change during the course of the series. Furthermore, we suppose that the contribution of the electron donor to the total reorganization energy λ remains little and insignificant throughout the series. Within

this context $\frac{\Delta G^0}{\lambda} = 2\alpha - 1$ and taking the averaged value $\alpha_{ap} \approx 0.35$, we obtain that $\frac{\Delta G^0}{\lambda} \approx -0.3$ in the range of driving force investigated with the reduced organic molecules. The reorganization energy is the sum of the contribution of the internal reorganization energy λ_i and the solvent contribution λ_0 . The internal reorganization energy required for reduction of N_2O to $N_2O^{\bullet-}$ has been evaluated from theoretical calculations¹ as being $\lambda_i \approx 1.8$ eV due to the bending of the N-N-O angle from 180° to 133° and due to the stretching of both N-N and N-O bonds. Due to the molecule's tiny radius, it is also anticipated that the solvent's reorganization energy is also expected to be quite large. Taking, λ_0 (eV) $\approx 3/a(\text{\AA})$ $a \approx 2$ \AA radius of N_2O , we obtain $\lambda \approx 3.3$ eV and therefore ΔG^0 is in the range of -1 eV. It takes such a large driving force defeat the intrinsic activation energy $\Delta G_0^\ddagger = \lambda/4$. An approximate calculation of the standard potential of $N_2O/N_2O^{\bullet-}$ redox couple is $E_{N_2O/N_2O^{\bullet-}}^0 \approx -0.82$ V vs SCE as, standard potentials of the electron donors are around -1.82 V vs SCE. Taking this value and $\lambda \approx 3.3$ eV, the experimental data are fitted with equations (5) and (6) leading to $Z_{hom}[N_2O] \approx 3 \cdot 10^8$ s⁻¹. Therefore, it is reasonable to propose that the initial step is a simple outersphere electron transfer. Hence the proposed mechanism is (Scheme II.3 1):



Scheme II.3 1 : Proposed mechanism for the reduction of N_2O by radical anions (Q).

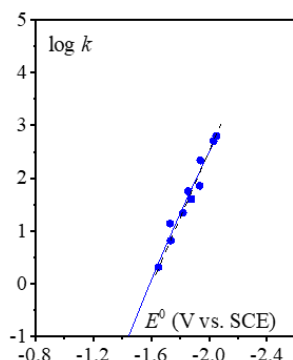


Figure II.3 2: Variation of the rate constant of electron transfer between N_2O and catalysts (Q).

4. Direct reduction of N₂O

The direct reduction of N₂O was studied on glassy carbon electrode. Due to the slow reduction rate, the current is purely kinetic, i.e., not perturbed by mass transport and hence independent of scan rate (Figure II.4 1).

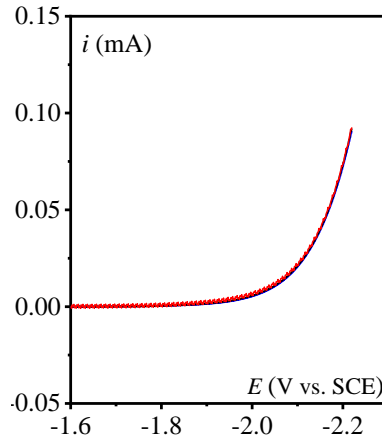


Figure II.4 1 : CVs of the direct reduction of N₂O in CH₃CN + 0.1 M nBu₄NPF₆ on a 3 mm diameter glassy carbon electrode $v = 0.1$ (blue), 0.2 (black) and 0.5 (red)V/s. Current is offset zero at -1.6 V to subtract the scan rate dependent capacitive contribution.

After accounting for ohmic drop, the kinetics can be plotted in the form of a Tafel plot, i.e. $\log(i)$ vs. E . (Figure II.4 3). The plot is only valid for potentials negative to -1.92 V vs. SCE for the current to be significantly above the background current, i.e. larger than 1 mA.

It is not surprising that the direct electroreduction of N₂O occurs at a non-electrocatalytic glassy carbon electrode with significant overpotential due to the large reorganization energy (Figure II.4 2). It is consistent with the finding that the electrochemical transfer coefficient α_{elec} , obtained from the averaged slope of the Tafel plot, is much below 0.5, i.e., $\alpha_{elec} = -\frac{RT \ln 10}{F} \frac{\partial \log i}{\partial E} = 0.34$. In the light of this,¹³ the direct electroreduction of N₂O can be described in the frame of electrochemical electron transfer theory expressed as:

$$\frac{i}{2FS} = Z_{el} [N_2O] \exp \left[-\frac{\lambda_{el}}{RT} \left(1 + \frac{F \left(E - E_{N_2O/N_2O^{\bullet-}}^0 \right)}{\lambda_{el}} \right)^2 \right] \quad (7)$$

where Z_{el} is the pre-exponential factor for the heterogeneous electron transfer and λ_{el} is the electrochemical reorganization energy. Noting that

$$\alpha_{el} \approx \frac{1}{2} \left(1 + \frac{F \left(E - E^0_{N_2O/N_2O^{\bullet-}} \right)}{\lambda_{el}} \right) \approx 0.34 \text{ at potentials around } -2.12 \text{ V vs. SCE and taking}$$

the standard potential evaluated above, we get $\lambda_{el} \approx 4 \text{ eV}$ and the fitting of the Tafel plot with equation (7) leads to $Z_{el}[N_2O] = 0.16 \text{ mol cm}^{-2} \text{ s}^{-1}$ (Figure II.4 3)

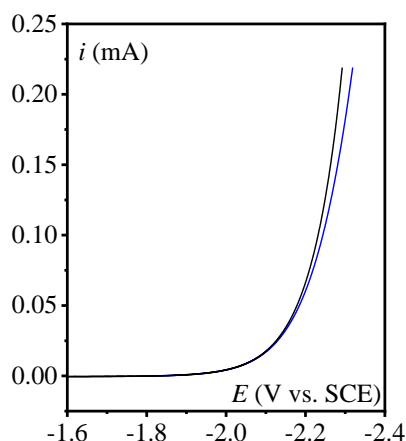


Figure II.4 2: CVs of direct reduction of N_2O in CH_3CN with $n-Bu_4NPF_6$ (0.1 M) on a 3 mm diameter GC electrode. $v = 0.1 \text{ V/s}$ blue: with ohmic drop correction. Black: with no ohmic drop correction.

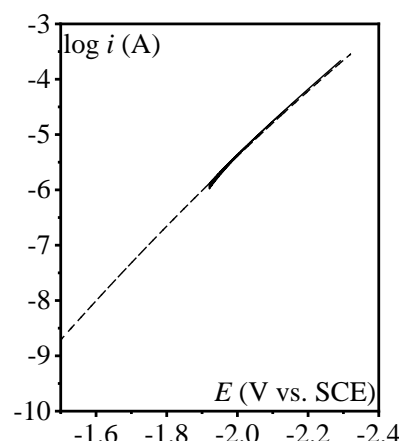


Figure II.4 3: Tafel plot obtained from the direct reduction of N_2O . Dashed line fitting with equation (7).

5. Comparison of direct reduction and homogeneous redox reduction of N_2O

In both cases, the electrode electron transfer and the homogeneous electron transfer have an outersphere character (Figure II.5 1). The two of them obey Marcus-Hush-Levich type activation driving force with similar intrinsic barriers. What makes it possible to obtain a current of higher intensity at less negative potential in redox catalysis compared to the direct reduction of N_2O ?

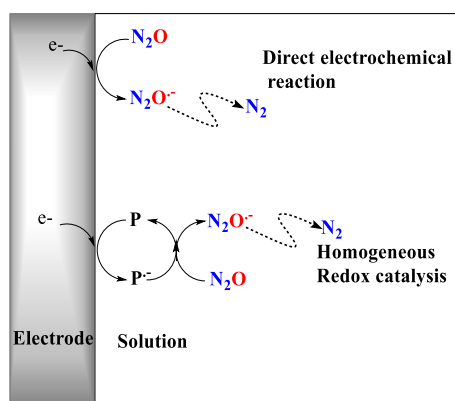


Figure II.5 1: Schematic representation of direct electrochemical reduction and homogeneous redox catalysis of N_2O .

The answer is that the electrons transferred in redox catalysis are dispersed in a three-dimensional space rather than to be confined within a two-dimensional space as in the case of direct reduction.¹⁴ This amount to compare the catalytic current at $E = E_{cat}^0$ for a given catalyst, i.e. when half of the catalyst has been converted at the electrode surface to its reduced form, i.e.

$$\frac{i_{cat}}{FS} = \frac{C_{cat}^0 \sqrt{D}}{\sqrt{2} k} Z_{hom} [N_2O] \exp \left[-\frac{\lambda}{RT} \left(\frac{\lambda + F \left(E_{cat}^0 - E_{N_2O/N_2O^{\bullet-}}^0 \right)}{\lambda} \right)^2 \right] \quad (8)$$

and the direct reduction current given by equation (7) with $E = E_{cat}^0$ (Figure II.5 2).

Consequently the corresponding ratio $\frac{i_{cat}}{i}$ is the result of two terms. The first term is

$$\rho = \frac{Z_{hom} C_{cat}^0 \sqrt{D/k}}{2\sqrt{2} Z_{el}} \quad \text{and considers the number of active catalysts, i.e. outersphere}$$

molecular reductants, in the diffusion reaction layer which size is $\sqrt{D/k}$. Thus it contrasts the necessity for the substrate N_2O to pick up electrons from the electrode at the Helmholtz outer plane for the direct reduction with the effect of electrons dispersing in the diffusion-reaction layer to. Taking $C_{cat}^0 = 1 \text{ mM}$, $D = 10^{-5} \text{ cm}^2\text{s}^{-1}$, the ratio ρ is plotted as function of the catalyst standard potential (Figure II.5 3). This demonstrates that electron spreading in a diffusion reaction layer is only advantageous in terms of collision efficiency between the electron donor and the substrates at potentials positive to -1.72 V vs. SCE . This physical catalytic effect decreases as the catalyst's standard potential becomes more negative, which is caused by an increase in the homogeneous rate constant and a corresponding decrease in the size of the diffusion reaction layer, which inturn reduced the number of electrons dispersed in the solution. As a result, there is a self-limitation of the physical catalytic effect. Consequently a comparison of (Figure II.5 2 and Figure II.5 3) shows that redox catalysis is more efficient than direct reduction at potentials negative to -1.92 V vs. SCE and it shows that the term ρ is unfavourable for redox catalysis. It reveals that the second term of the ratio $\frac{i_{cat}}{i}$ is

responsible for $\frac{i_{cat}}{i}$ being larger than 1 at potentials negative to -1.92 V vs. SCE. The main catalytic effect of the homogenous donors resides in the fact that $\lambda < \lambda_{el}$, making the exponential term of $\frac{i_{cat}}{i}$ ratio much larger than 1.

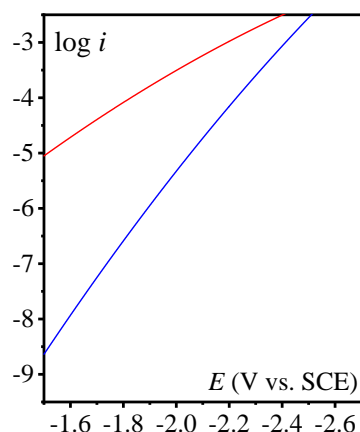


Figure II.5 2 : Comparison of the calculated direct reduction of N_2O (blue) from equation (7) with $S = 0.07 \text{ cm}^2$, $z_{el}[N_2O] = 0.16 \text{ mol cm}^{-2} \text{ s}^{-1}$, $\lambda_{el} \approx 4 \text{ eV}$ and $E_{N_2O/N_2O^{\bullet-}}^0 \approx -0.82 \text{ V vs SCE}$, and of the redox catalytic current (red) from equation (8) with $c_{cat}^0 = 1 \text{ mM}$, $D = 10^{-5} \text{ cm}^2 \text{ s}^{-1}$, $S = 0.07 \text{ cm}^2$, $z_{hom}[N_2O] = 3 \cdot 10^8 \text{ s}^{-1}$, $\lambda = 3.3 \text{ eV}$ and $E_{N_2O/N_2O^{\bullet-}}^0 \approx -0.82 \text{ V vs SCE}$ considering an infinity of catalysts with $E = E_{cat}^0$.

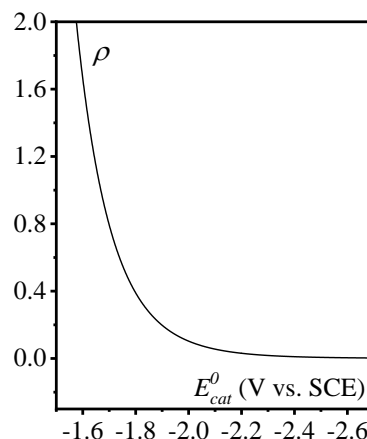


Figure II.5 3 : Plot of ρ as function of $E = E_{cat}^0$, k is obtained from equations (5) and (6).

6. Deactivation of the catalyst by co-substrate: Application to 4-cyanopyridine

Chemical evolution of a designed molecular catalyst could lead to variety of situations with divergent consequences on the catalytic process extending from a dead-end (chemical conversion of the active form of the catalyst into in-active molecule) and might be the contrast in other cases leading to the acceleration of catalysis (chemical modification of the precursor or/and active catalyst into a more active form) or conversion of molecular catalysis to electrocatalysis process via electrodeposition of an active catalytic species on the working electrode surface, metallic for example.¹⁵ A significant issue in homogeneous catalysis, is the problem of catalyst deactivation which has also been a continuing subject of interest in molecular catalysis of electrochemical reactions.

While we were investigating the effect of the different aromatic organic molecules on the reduction of nitrous oxide in the presence of water as proton donor, a deactivation process was observed upon increasing the concentration of water with 4-cyanopyridine as a catalyst. We have investigated more about this effect and we used CV as an analytical tool providing a formal kinetic analysis. We studied the effect of water addition on the reversible reduction of 4-cyanopyridine looking at how it loses its reversibility with increasing water concentration due to an electro-hydrogenation ($2e^-/2H^+$ process) of 4-cyanopyridine. The first wave partially chemically reversible due to substantial amount of water in acetonitrile or the supporting electrolyte, starts to lose its reversibility, while the electron stoichiometry increases above 1 (Figure II.6 1). The latter eventually becomes fully irreversible wave and reaches a two-electron stoichiometry. These variations reflect the protonation of the radical anion $P^{\bullet-}$, yielding the neutral radical PH^{\bullet} , which is usually easier to reduce than the starting molecule P. It is reduced, as soon as it is produced, into PH^- , which protonates rapidly to give PH_2 (Scheme II.6 1).

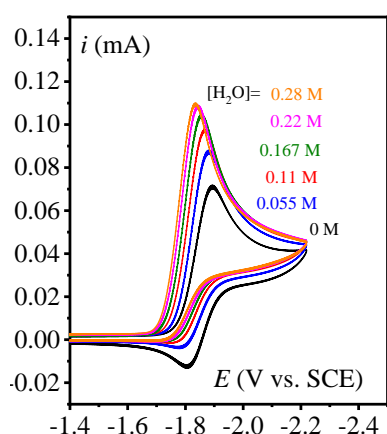
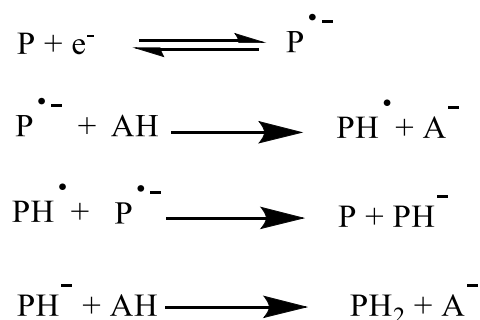


Figure II.6 1: CVs of 4-cyanopyridine 1.75 mM in CH_3CN with $n-Bu_4NPF_6$ (0.1 M) on a 3 mm diameter glassy carbon electrode. $v = 0.1$ V/s under argon with additional amount of water.



Scheme II.6 1: Mechanism for 4-cyanopyridine hydrogenation (DISP) by proton donor AH.

Then we studied how the catalytic effect of 4-cyanopyridine on nitrous oxide gas reduction is diminished with increasing water concentration due to competing reaction with the co-substrate (water) which deactivates the catalyst via its electro-hydrogenation (Figure II.6 2).

The electrochemical generation of the reduced form of the catalyst $P^{\bullet-}$ makes it more basic than the starting compound (P). Therefore, a competition occurs in the diffusion reaction layer between the reaction of $P^{\bullet-}$ with N_2O assumed to be in excess and the reaction of $P^{\bullet-}$ with

H₂O (protonation) also assumed to be in excess as well. The protonated catalyst PH^{•-} is reduced in solution and finally protonated a second time as shown in (Scheme II.6 2).

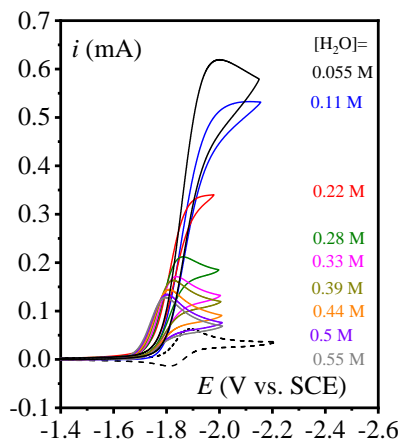
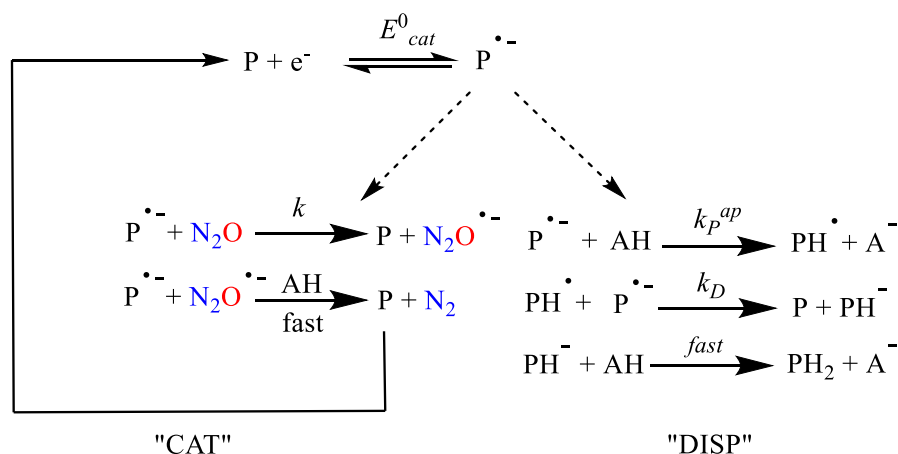


Figure II.6 2 : CVs of 4-cyanopyridine in CH₃CN with n-Bu₄NPF₆ (0.1 M) on a 3 mm diameter glassy carbon electrode. $v = 0.1$ V/s. (a) 1.45 mM under N₂O with increasing additional amount of water Dashed CV: under argon with no water added.



Scheme II.6 2 : Mechanism for competition between catalysis (CAT) and catalytic hydrogenation (DISP).

It was observed that with increasing concentration of H₂O, there is no enhancement of the catalytic current. This indicates that the outersphere rate determining step is not coupled to proton transfer. We have observed increase in the pseudo-first order rate constant for the reaction of P^{•-} with H₂O with increasing concentration of H₂O. Then plotting $\log k_P^{ap}$ vs. $\log [\text{H}_2\text{O}]$ gives a line in which from the slope we were able to infer that the reaction order with water is four. This means that the protonation of P^{•-} occurs via a cluster of four water molecules for the proton transfer to occur irreversibly (Figure II.6 3).

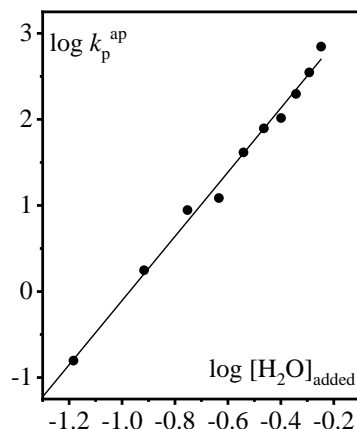


Figure II.6 3 : Variation of k_p^{ap} as a function of increasing concentration of water.

7. Conclusion

Electrochemically generated radical anions of twelve different organic aromatic molecules were studied for their ability to reduce N_2O to N_2 gas via an outersphere electron transfer in polar aprotic medium (acetonitrile). The catalytic enhancement of the cyclic voltammetric peaks of these catalysts is used to determine the rate constant of the electron transfer from these aromatic anion radicals to N_2O which corresponds to the rate determining step, as a function of the catalyst standard potential. It has emerged that there is a correlation between the standard potential and the rate constant; the catalytic efficiency in terms of currents decreases when the standard potential of the redox catalyst becomes less and less negative. An important driving force is required to drive the reaction due to the large reorganization energy. From the activation driving force quadratic relationship, the standard potential of $N_2O/N_2O^{\cdot-}$ was evaluated. We have shown that redox catalysis is more efficient than the direct reduction of N_2O at non-catalytic glassy carbon electrode due to the smaller reorganization energy. Finally, we have also shown that addition of a co-substrate (here water) can have deleterious effect via a degradation of the catalyst activity through a competitive hydrogenation of the catalyst.

References:

- (1) Takahashi, K.; Ohgami, S.; Koyama, Y.; Sawamura, S.; Marin, T. W.; Bartels, D. M.; Jonah, C. D. Reaction rates of the hydrated electron with N₂O in high temperature water and potential surface of the N₂O⁻ anion. *Chemical Physics Letters* **2004**, *383* (5-6), 445-450. DOI: 10.1016/j.cplett.2003.11.050.
- (2) Chantry, P. J. Formation of N₂O⁻ via Ion-Molecule Reactions in N₂O. *The Journal of Chemical Physics* **1969**, *51* (8), 3380-3384. DOI: 10.1063/1.1672522.
- (3) Bottomley, F.; Lin, I. J. B.; Mukaida, M. Reactions of dinitrogen oxide (nitrous oxide) with dicyclopentadienyltitanium complexes including a reaction in which carbon monoxide is oxidized. *Journal of the American Chemical Society* **1980**, *102* (16), 5238-5242. DOI: 10.1021/ja00536a020.
- (4) Matsunaga, P. T.; Hillhouse, G. L.; Rheingold, A. L. Oxygen-atom transfer from nitrous oxide to a nickel metallacycle. Synthesis, structure, and reactions of [cyclic] (2,2'-bipyridine)Ni(OCH₂CH₂CH₂CH₂). **1993**, *115* (5), 2075-2077. DOI: 10.1021/ja00058a085.
- (5) Matsunaga, P. T.; Mavropoulos, J. C.; Hillhouse, G. L. Oxygen-atom transfer from nitrous oxide (NNO) to nickel alkyls. Syntheses and reactions of nickel(II) alkoxides. *Polyhedron* **1995**, *14* (1), 175-185. DOI: 10.1016/0277-5387(94)00330-H.
- (6) Yu, H.; Jia, G.; Lin, Z. Theoretical Studies on O-Insertion Reactions of Nitrous Oxide with Ruthenium Hydride Complexes. *Organometallics* **2008**, *27* (15), 3825-3833. DOI: 10.1021/om8000845.
- (7) Ortega-Lepe, I.; Sánchez, P.; Santos, L. L.; Lara, P.; Rendón, N.; López-Serrano, J.; Salazar-Pereda, V.; Álvarez, E.; Paneque, M.; Suárez, A. Catalytic Nitrous Oxide Reduction with H₂ Mediated by Pincer Ir Complexes. *Inorganic Chemistry* **2022**, *61* (46), 18590-18600. DOI: 10.1021/acs.inorgchem.2c02963.
- (8) Savéant, J.-M. Costentin, C. Elements of Molecular and Biomolecular Electrochemistry. Vol. Chapter 1; 2019; pp 6-10. John Wiley, 2019. ISBN: 978-1-119-29233-3.
- (9) Savéant, J. M. Molecular catalysis of electrochemical reactions. Mechanistic aspects. *Chem. Rev* **2008**, *108* (7), 2348-2378. DOI: 10.1021/cr068079z.
- (10) Costentin, C.; Savéant, J.-M. Multielectron, Multistep Molecular Catalysis of Electrochemical Reactions: Benchmarking of Homogeneous Catalysts. *ChemElectroChem* **2014**, *1* (7), 1226-1236. DOI: 10.1002/celec.201300263.
- (11) Lexa, D.; Savéant, J. M.; Su, K. B.; Wang, D. L. Chemical vs. redox catalysis of electrochemical reactions. Reduction of trans-1,2-dibromocyclohexane by electrogenerated aromatic anion radicals and low oxidation state metalloporphyrins. *Journal of the American Chemical Society* **1987**, *109* (21), 6464-6470. DOI: 10.1021/ja00255a036.
- (12) Kojima, H.; Bard, A. J. Determination of rate constants for the electroreduction of aromatic compounds and their correlation with homogeneous electron transfer rates. **1975**, *97* (22), 6317-6324. DOI: 10.1021/ja00855a005.
- (13) Marcus, R. A. On the Theory of Electron-Transfer Reactions. VI. Unified Treatment for Homogeneous and Electrode Reactions. *The Journal of Chemical Physics* **2004**, *43* (2), 679-701. DOI: 10.1063/1.1696792.
- (14) Savéant, J.-M. Costentin, C. Elements of Molecular and Biomolecular Electrochemistry. Vol. Chapter 5; 2019; p 287. John Wiley, 2019. ISBN: 978-1-119-29233-3.
- (15) Lee, K. J.; McCarthy, B. D.; Dempsey, J. L. On decomposition, degradation, and voltammetric deviation: the electrochemist's field guide to identifying precatalyst transformation. *Chemical Society Reviews* **2019**, *48* (11), 2927-2945, DOI: 10.1039/C8CS00851E.

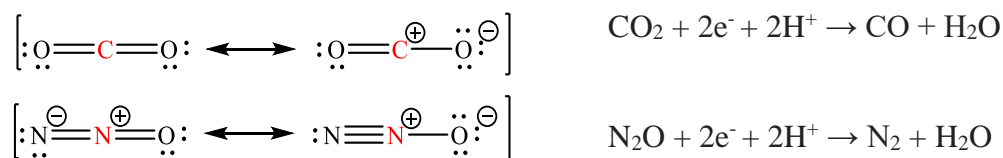
Chapter III: Homogeneous Chemical Catalysis of Electrochemical Molecular Reduction of N₂O

This Chapter includes work I have published as the first co-author:

- Effective Homogeneous Catalysis of Electrochemical Reduction of Nitrous Oxide to Dinitrogen at Rhenium Carbonyl Catalysts. Deeba, R.; Molton, F.; Chardon-Noblat, S.; Costentin, C. *ACS Catalysis*. **2021**, *11*, 6099-6103. DOI: 10.1021/acscatal.1c01197.

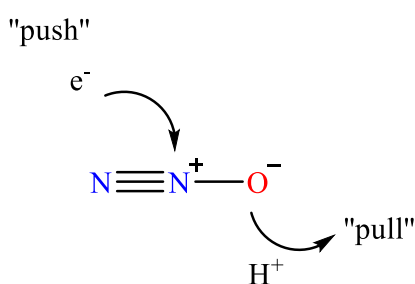
1. Introduction

N₂O is an inert molecule with analogies to CO₂: these two molecules are isoelectronic and have a central electrophilic atom. Their reduction to two electrons leads to the rupture of an N-O or C-O bonds and to the stabilization of oxygen atom via two protons Scheme III.1 1.



Scheme III.1 1 : Analogy between structural formula and two-electron reduction of CO₂ and N₂O

Thus, we decide to apply the strategy developed for the activation of the C-O bond of CO₂ to the activation of the N-O bond of N₂O. Using reduced transition metal complexes via ‘‘electron push-pull’’ type bond breaking mechanism (Scheme III.1 2) where the catalytic active species of the transition metal complex bind to N₂O ‘‘pushes’’ electrons to the electrophilic center of N₂O while an acid (Brønsted) makes it possible to assist to break the N-O bond while stabilizing the oxygen by ‘‘pulling’’ electron density to weaken the bond.¹ This push-pull mechanism is also used in nature by nickel iron carbon monoxide dehydrogenases enzymes [NiFe] CODHs for instance, in the synthesis of acetyl coenzyme A, from CO₂ reduction to CO.² In order to perform this type of electron transfer the need of chemical catalysis is necessary.



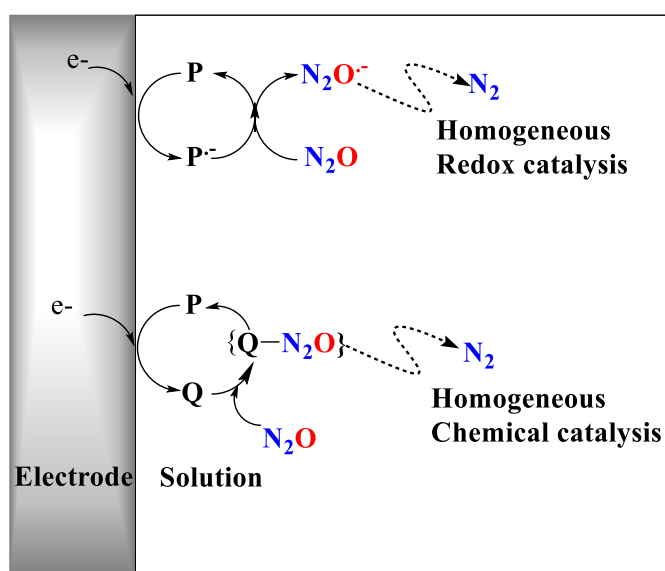
Scheme III.1 2 : Push pull mechanism.

In this Chapter, we will describe results of our attempts to find molecular catalysts for the electrochemical reduction of N₂O to N₂ which could be potentially chemical catalysts (as opposed to the redox catalysts described in Chapter II). After recalling the difference between chemical catalysis and redox catalysis we will thus describe results with various catalysts: iron

tetraphenylporphyrin, rhenium bipyridine tricarbonyl, manganese bypyridine tricarbonyl, and finally, various ruthenium, rhodium and osmium complexes. Mechanisms will not be described in detail in this Chapter. We will focus on mechanistic studies with rhenium bypyridine tricarbonyl complexes in Chapter IV.

2. Chemical homogeneous catalysis vs. redox catalysis

In contrast to redox catalysis where the catalyst acts as an outersphere electron transfer agent as discussed in Chapter II, chemical catalysis involves more intimate interaction between the active form of the catalyst and the substrate; that is transient formation of an adduct between the active form of the catalyst and the reactant to allow innersphere transfer of electrons. This results in lower activation energy compared to an outersphere electron transfer for the same driving force. This adduct has then to be cleaved or after additional electron exchanges to give eventually the products and regenerating the catalyst.³ Catalysis then results from chemical rather than physical reasons. For chemical catalysis to prevail over redox catalysis conditions have to be realized: first the formation of an adduct has to be faster than the outersphere electron transfer from the reduced form of the catalyst to the substrate; second the adduct formed between the active form of the catalyst and the substrate should transform rapidly for the regeneration of the catalyst. The advantage of this chemical interaction gives chance for higher product selectivity compared to redox catalysis. Scheme III.2 1 illustrates the difference between redox and chemical catalysis for the deoxygenation of N_2O as a substrate into N_2 gas.



Scheme III.2 1 : Homogeneous redox and chemical catalysis.

3. Electrochemical reduction of N₂O mediated by Fe tetraphenylporphyrin catalysts

Iron tetraphenyl porphyrin (FeTPP) complexes have been reported as efficient catalysts for CO₂ electroreduction. Fe(0) porphyrins, electrochemically generated from Fe(III) by three successive one-electron uptakes at a glassy carbon electrode, are efficient because of their high turnover frequency, high selectivity for CO₂ to CO conversion and robust provided that they are coupled with lewis or Brønsted acids.^{4,5,6} In this regard we report the use of FeTPP/Cl as catalyst in DMF for the reduction of N₂O. In the absence of N₂O as well as proton donors this complex exhibits three successive waves corresponding to the reversible Fe^{III/II}, Fe^{II/I} and Fe^{I/0} redox couples (Figure III.3 1).

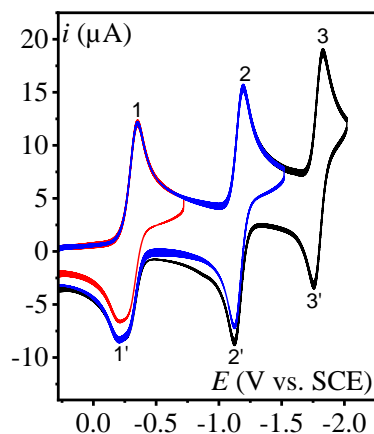


Figure III.3 1 : CVs of 1 mM of FeTPP/Cl under Ar in DMF + 0.1 M n-Bu₄NPF₆ at 0.1 V/s on a 3 mm diam. GCE.

Under 1 atm of N₂O and in the absence of proton source, catalysis is observed at the level of Fe^{I/0} wave, and the third wave becomes irreversible and increases in intensity (Figure III.3 2). A second intense catalytic wave appeared at more negative potential but its onset is close to the direct reduction of N₂O at glassy carbon electrode (Figure III.3 3).

This catalysis can be enhanced by the use of phenol as Brønsted acid in which an increase in the catalytic wave at the position of Fe^{I/0} redox system was observed with increasing concentration of phenol (Figure III.3 4). A control CVs experiment for the behavior of phenol in the presence of FeTPP/Cl under argon was made showing lower current intensities at the level of the third wave compared to the ones under N₂O, because FeTPP/Cl is also known for its ability to reduce phenol with the release of hydrogen gas (Figure III.3 5).⁷

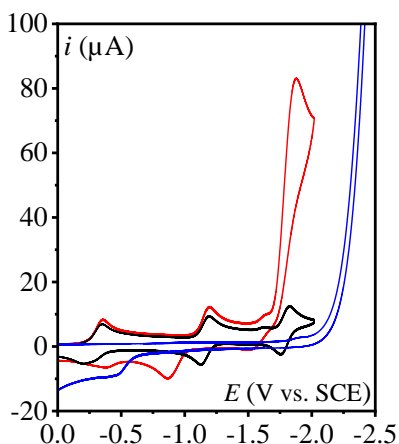


Figure III.3 2 : CVs of direct reduction of N_2O (blue), 1 mM FeTPPCL under Ar (black) and under N_2O (red) in DMF + 0.1 M $n-Bu_4NPF_6$ at 0.1 V/s on a 3 mm diam. GCE.

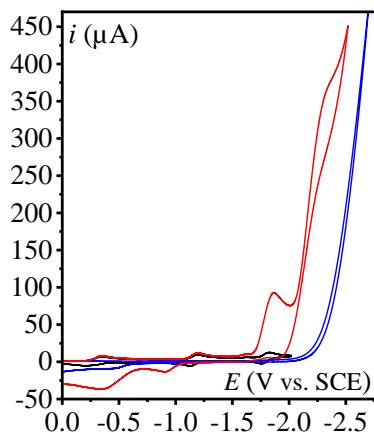


Figure III.3 3 : CVs of direct reduction of N_2O (blue), 1 mM FeTPPCL under Ar (black) and under N_2O (red) in DMF + 0.1 M $n-Bu_4NPF_6$ at 0.1 V/s on a 3 mm diam. GCE.

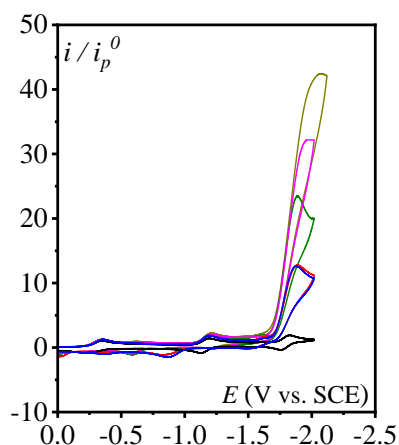


Figure III.3 4 : Normalized CVs of FeTPPCL under Ar (black), under N_2O (blue), in the presence of PhOH, concentration (mM): 1 (red), 19.9 (olive), 50 (magenta) and 100 (dark yellow) respectively in DMF + 0.1 M $n-Bu_4NPF_6$ at 0.1 V/s on a 3 mm diam. GCE.

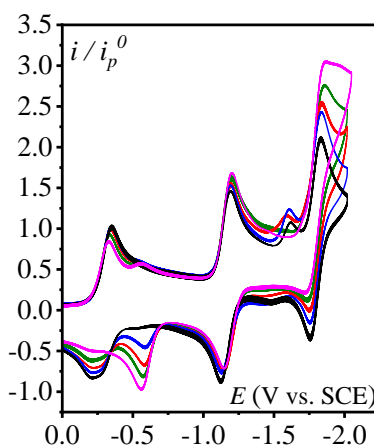


Figure III.3 5 : Normalized CVs of FeTPPCL under Ar (black), in the presence of PhOH, concentration (mM): 5 (blue), 20 (red), 50.1 (olive) and 100.1 (magenta) respectively in DMF + 0.1 M $n-Bu_4NPF_6$ at 0.1 V/s on a 3 mm diam. GCE.

CPE was performed at -1.82 V vs. SCE in a solution containing 1 mM FeTPPCL in the presence of 115 mM PhOH in DMF under 1 atm of N_2O on a carbon felt electrode with apparent surface area (S_{app}) of 6.53 cm² (Figure III.3 6). A stable current density of 11.63 mA was measured for 76 min leading to a linear increase of charge passed over time (Figure III.3 7). Gas chromatography (GC) analysis of the gas headspace allows determination of the quantity of N_2 produced at the end of the electrolysis indicating selective transformation of the N_2O to N_2 with 85% faradaic yield where no H_2 gas was detected.

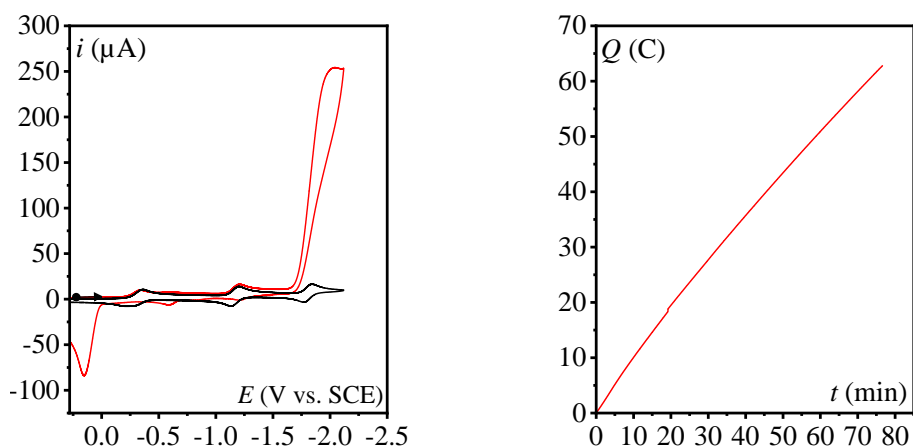


Figure III.3 6 : CVs 1 mM FeTPPCl under Ar (black) and under N_2O + 110 mM PhOH (red) in DMF + 0.1 M $n-Bu_4NPF_6$ at 0.1 V/s on a 3 mm diam. GCE.

Figure III.3 7 : CPE at -1.82 V of a solution of DMF + 0.1 M $n-Bu_4NPF_6$ with FeTPPCl (1 mM) under N_2O on a carbon felt. Charge passed as a function of time.

4. Electrochemical reduction of N_2O mediated by $[Re(bpy-R)(CO)_3X]$

4.1 Motive for the choice of rhenium complexes

The reduction of carbon dioxide is a process of fundamental importance both for the activation of C-O bond and also as potentially sustainable source of renewable fuels and commodity chemicals. This requires the discovery of catalysts providing low energy and polyelectronic pathways with high efficiency. A variety of homogeneous catalysts have been used for the electrocatalytic CO_2 reduction. A particularly efficient promising catalyst, *fac*- $[Re(bpy)(CO)_3Cl]$, originally reported by Lehn et al. in 1984, was found to catalyze CO_2 reduction to CO on a GCE in a 9 :1 DMF / H_2O solution at (-1.49 V vs. SCE) making 300 catalytic cycles during 14 h without loss of activity and with high current efficiency corresponding to a FE of 98% CO .⁸ This seminal paper laid the foundation for the subsequent research on rhenium and manganese tricarbonyl complexes as catalysts for CO_2 reduction.^{9,10,11,12,13}

Lehn's discovery captured the interest of Meyer group, who reported in 1985 the electrocatalytic reduction of CO_2 in acetonitrile solvent by *fac*- $[Re(bpy)(CO)_3Cl]$ resulting in the production of CO with FE > 85 %. They have studied the behavior of this complex under argon and CO_2 by CV and CPE. Under argon the complex shows first a reversible reduction of the bipyridyl ligand (waves A,F; Figure III.4.1 1) followed by a second irreversible reduction of $[Re^I(bpy^{\bullet-})(CO)_3Cl]^-$ (wave C). A dimer $[Re^0(bpy)(CO)_3]_2$ is generated and a reversible wave at ~ -1.4 V vs. SCE is observed when reversing the potential (waves B,D). They have

proposed two distinct pathways for the reduction of CO₂; a slower 1e⁻ pathway and a more rapid 2e⁻ pathway (Scheme III.4.1 1).

The first electron pathway proceeds through the penta coordinated mono-reduced species [Re^I(bpy^{•-})(CO)₃] or the hexacoordinated solvated one [Re^I(bpy^{•-})(CO)₃(MeCN)] in the presence of CO₂ thus suppressing the formation of the dimer and forming CO and CO₃²⁻. The second two electron pathway, which is more rapid, involves the reaction of the bi-reduced species [Re⁰(bpy^{•-})(CO)₃]⁻ with CO₂ which results in the high current response corresponding to the production of CO in high yields in the presence of oxide ion acceptor ‘‘A’’ to pull the oxygen atom from CO₂. This oxide acceptor can be a proton that can be extracted from acetonitrile or even from the supporting electrolyte via Hofmann degradation whose fate in the reaction was still unknown at that time (Scheme III.4.1 1).

The CV of *fac*-[Re(bpy)(CO)₃Cl] under CO₂ showed no change of the bpy based reduction (first wave). The onset of the catalytic current occurs at -1.4 V vs. SCE and continues through the potential region of the second reduction and the two-electron reduction of the dimer [Re⁰(bpy)(CO)₃]₂ as shown below (Figure III.4.1 1).¹⁴

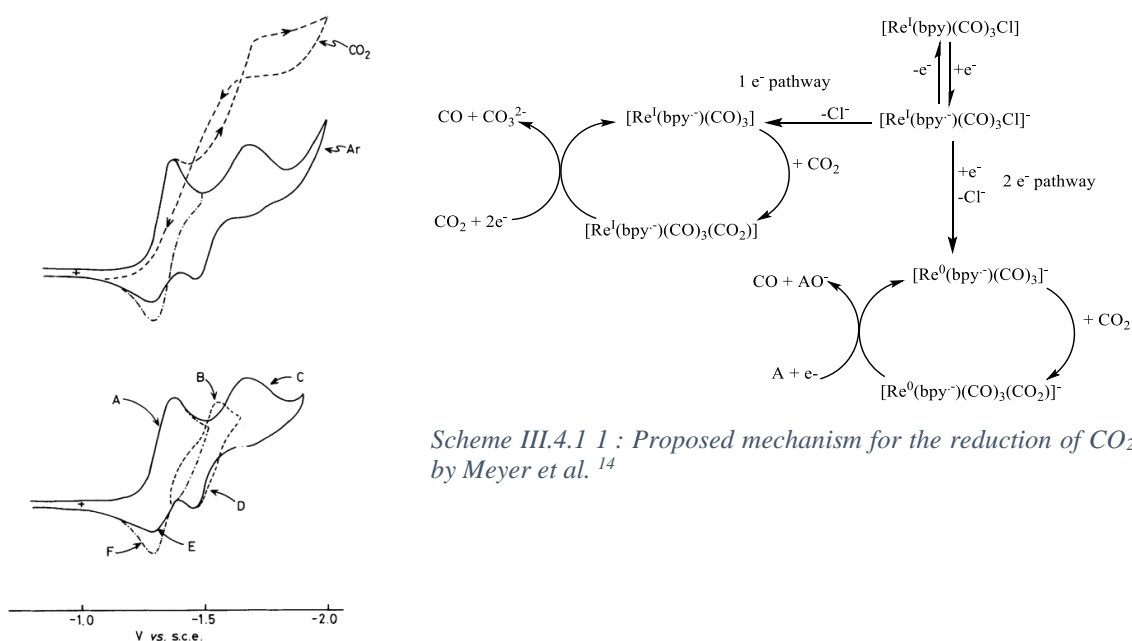


Figure III.4.1 1: CVs of [Re(bpy)(CO)₃Cl] in CH₃CN under Ar (full line) and under CO₂ (dotted line) above and CV below under Ar.¹⁴

Based on the history of the rhenium complexes in acting as highly active, selective and robust electrochemical molecular catalyst for the conversion of CO₂ to CO, it was clear that this catalyst fitted our requirements and was a source of inspiration for the reductive deoxygenation

of N₂O into N₂ gas. In this context, CV and preparative scale CPE (detection and quantification of the reduction product: N₂, by GC to assess FE), are the techniques of choice for analyzing the mechanisms involved, the methodology developed applying perfectly to bielectronic processes. These techniques can be complemented by spectroelectrochemistry (SEC) which will be discussed thoroughly in Chapter IV.

4.2 Rhenium complexes considered

The behavior of a range of Re complexes *fac*-[Re(R-bpy)(CO)₃X]ⁿ⁺ (X = Cl⁻, Br⁻, OH⁻ or MeCN, n=0 or 1) with different R substituents (electron withdrawing and donating) were studied under argon and N₂O atmosphere using CV as an analytical tool to investigate the effect of the bpy substituents electron-donating nature, as well as the labile ligand (X). We selected a sample of 10 complexes we synthesized or which were already synthesized in the laboratory (Figure III.4.2 1). The complexes with bpy-H with X= Cl⁻, Br⁻ were synthesized by simple complexation reaction: refluxing of the rhenium pentacarbonyl chloro or bromo complex with the ligand (bpy or 4,4'-OMebpy) in toluene. The bpy-H with CH₃CN was synthesized starting from bpy-H with Br⁻ or Cl⁻: precipitation of Br⁻ by reflux with AgOTf then followed by metathesis in the presence of excess NH₄PF₆ to exchange counter anion OTf⁻ by PF₆⁻. The bpy-H with OH⁻ was synthesized starting from [Re(bpy)(CO)₃(OTf)] obtained from [Re(bpy)(CO)₃Br] by refluxing in acetone in the presence of equimolar quantity of AgOTf to precipitate AgBr. Then this complex was refluxed in the presence of excess KOH in a mixture of water and acetone leading to the precipitation of the Re hydroxo complex.

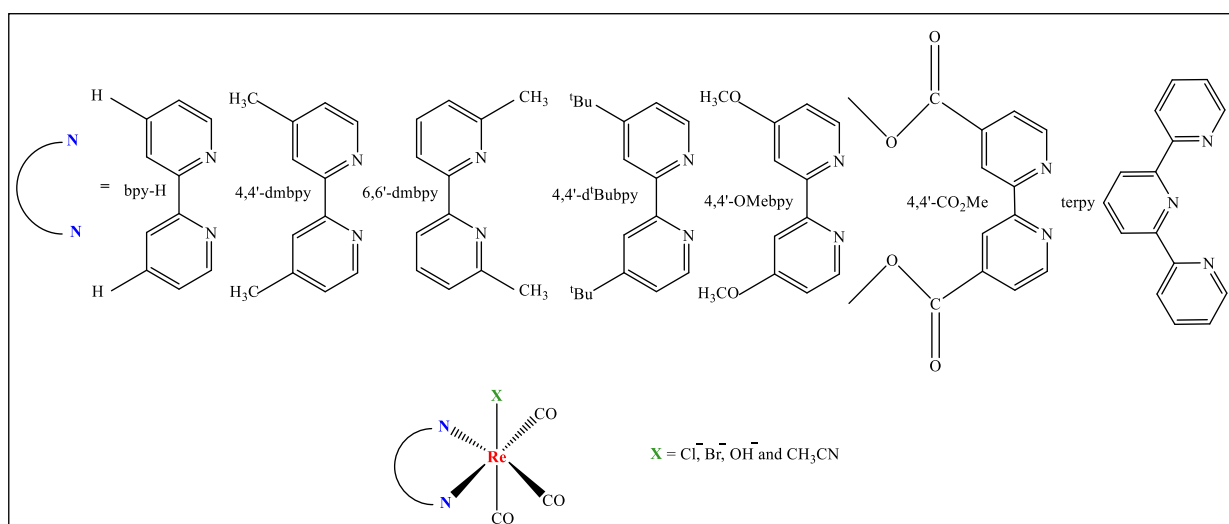


Figure III.4.2 1 : Rhenium complexes included in this study.

4.2.1 Cyclic Voltammetry under Inert Atmosphere

Under argon each complex displays a reversible one electron wave corresponding to bpy based reduction which renders the first reduction wave to be relatively insensitive to replacing chloride by bromide. This wave shifts towards more negative potential with more electron donating substituents (-R) on the bpy reflecting the difficulty in reducing the more electron rich compounds compared to the reference bpy-H complex (Figure III.4.2.1 3).

The second reduction wave is irreversible or quasi-reversible. It is a $\text{Re}^{\text{I}/0}$ based reduction, usually less than one electron as attested by linear scan voltammetry (Figure III.4.2.1 1) except reaching one electron for $[\text{Re}(4,4'\text{-CO}_2\text{Mebpy})(\text{CO})_3\text{Cl}]$ and $[\text{Re}(\text{bpy})(\text{CO})_3(\text{OH})]$ with OH^- . This second reduction is in competition with spontaneous dehalogenation of the bpy centered mono-reduced species before they undergo second reduction, to give five-coordinate $\text{Re}(0)$ complex. The later can react with itself to form a metal-bonded $\text{Re}^0\text{-Re}^0$ dimer $[\text{Re}^0(\text{bpy})(\text{CO})_3]_2$, revealed on CV when reversing the potential at -1.40 V showing a reversible system corresponding to the redox couple $[\text{Re}(\text{bpy})(\text{CO})_3]_2^{0/-}$ with $E_{1/2} = -1.54\text{ V}$ (Figure III.4.2.1 2). In our study, catalysts with electron donating groups (EDG; CH_3 , $t\text{Bu}$ and OMe) showed redox activities at more negative potential compared to the reference bpy-H catalyst. This indicates that EDGs at 4,4'-position of the bpy ligand disfavored the reduction of mono-reduced species $[\text{Re}(\text{R-bpy}^{\bullet-})(\text{CO})_3\text{X}]$. In contrast electron withdrawing group (EWGs; methyl ester CO_2Me on the 4,4'- position of the bpy, shifted the second reduction potential towards less negative values, showing that the mono-reduced species are easier to be reduced compared to the reference bpy-H complex (Figure III.4.2.1 3).

In addition to the change of bpy substituents we also considered the effect of the labile ligand X (Cl^- , Br^- , OH^- , MeCN) and we have found that the chloro and the bromo complexes have almost identical CV responses, with the Br^- complex having slightly less negative second reduction potential (by 40 mV) than Cl^- , attributed to the increase in the lability of Br^- to Cl^- due to the higher atomic radius of the former rendering the bond easier to break. However, with OH^- ligand the second reduction is more shifted towards negative potential (by 310 mV) than Cl^- since it is a strong σ -donor coordinating ligand difficult to decoordinate. The neutral ligand CH_3CN results in complexes easier to reduce, as the first and second reduction potentials are less negative in comparison to the complexes with Cl^- and Br^- and is not the same as any of the other complexes (Table III.4.2.1 1). These results are consistent with what was previously reported in the literature.^{10,15}

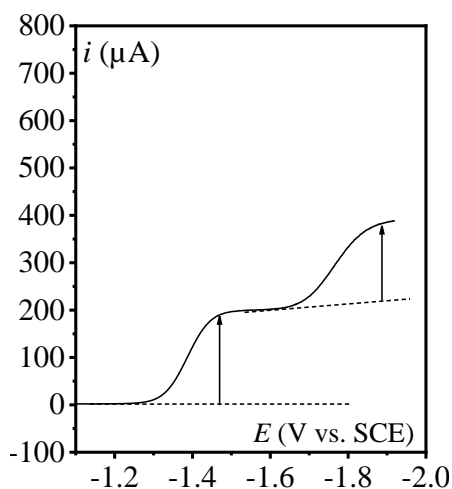


Figure III.4.2.1 1 : Linear scan voltammetry of 1 mM $[\text{Re}(\text{bpy})(\text{CO})_3\text{Cl}]$ under Ar at 10 mV/s on a 5 mm diam. GC RDE at 1000 rpm.

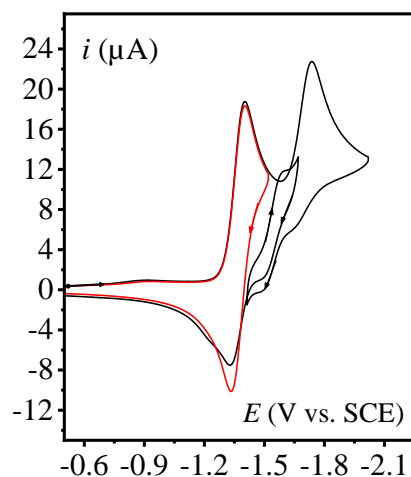


Figure III.4.2.1 2 : CV of 1 mM $[\text{Re}(\text{bpy})(\text{CO})_3\text{Cl}]$ under Ar in $\text{CH}_3\text{CN} + 0.1 \text{ M n-Bu}_4\text{NPF}_6$ at 0.05 V/s on a 3 mm diam. GCE.

Table III.4.2.1 1 : Reduction Potentials for the *fac*- $[\text{Re}(\text{R-bpy})(\text{CO})_3\text{X}]$ in this study.

Complex	1 st peak reduction potential (V vs. SCE) ^a	2 nd peak reduction potential (V vs. SCE) ^a
$[\text{Re}(\text{bpy})(\text{CO})_3(\text{MeCN})]\text{PF}_6$	-1.26	-1.47
$[\text{Re}(\text{bpy})(\text{CO})_3\text{Cl}]$	-1.41	-1.67
$[\text{Re}(\text{bpy})(\text{CO})_3\text{Br}]$	-1.41	-1.63
$[\text{Re}(\text{bpy})(\text{CO})_3(\text{OH})]$	-1.44	-1.98
$[\text{Re}(4,4'\text{-dmbpy})(\text{CO})_3\text{Cl}]$	-1.50	-1.75
$[\text{Re}(6,6'\text{-dmbpy})(\text{CO})_3\text{Cl}]$	-1.48	-1.77
$[\text{Re}(4,4'\text{-}^t\text{Bubpy})(\text{CO})_3\text{Cl}]$	-1.49	-1.82
$[\text{Re}(\text{terpy})(\text{CO})_3\text{Cl}]$	-1.41	-1.74
$[\text{Re}(4,4'\text{-OMebpy})(\text{CO})_3\text{Cl}]$	-1.52	-1.80
$[\text{Re}(4,4'\text{-CO}_2\text{Mebpy})(\text{CO})_3\text{Cl}]$	-1.01	-1.27

^a First reduction potential is the peak maximum for the first cathodic wave and the second reduction is the peak maximum for the second cathodic wave. All scans were performed at 100 mV/s in acetonitrile with $\text{n-Bu}_4\text{NPF}_6$ 0.1 M. Pt wire counter electrode and reference electrode Ag wire in 10 mM AgNO_3 solution + 0.1 M nBu_4NPF_6 in CH_3CN .

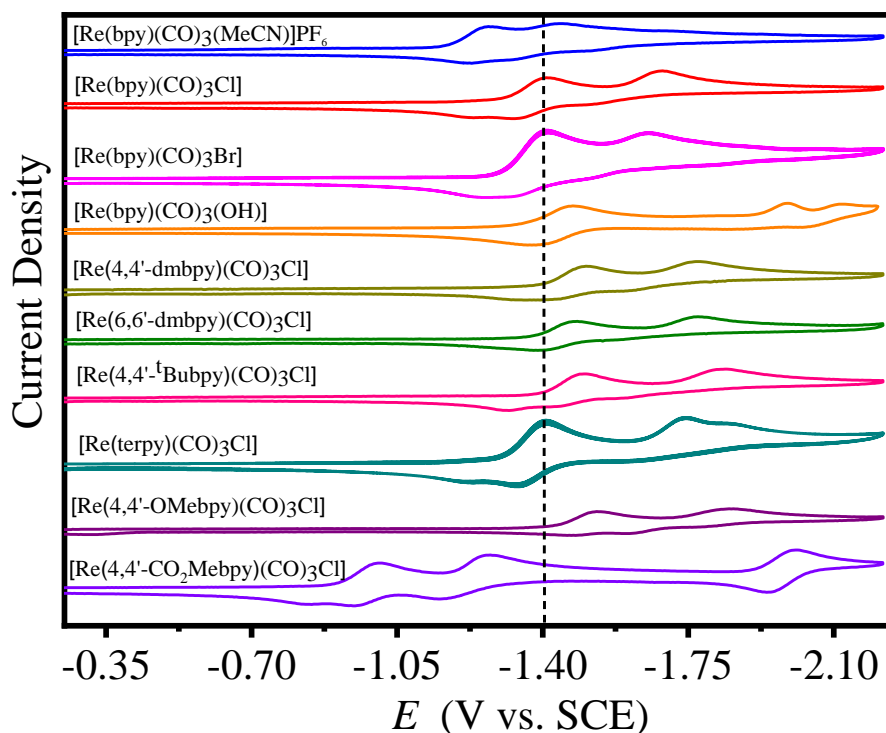


Figure III.4.2.1 3 : CVs under Ar of $[Re^I(R\text{-}bpy)(CO)_3X]$ 1 mM at 0.1 V/s.

4.2.2 Cyclic voltammetry under N_2O atmosphere without proton source

Each complex was studied under saturated N_2O conditions (1 atm, 280 mM in CH_3CN) to investigate the effect of bpy substituents and the labile ligand on the catalytic current response without any added proton source besides residual water already present in the solvent or the supporting electrolyte.

In the presence of N_2O , on the time scale of the CV (Figure III.4.2.2 1), the first reduction wave remains unchanged, corresponding to the reversible one-electron reduction centered on the R-bpy ligand except in the $[Re^I(bpy)(CO)_3(MeCN)]PF_6$ and $[Re^I(bpy)(CO)_3Br]$ complexes whichever lose their reversibility presumably due to the interaction of N_2O with the mono-reduced species $[Re^I(bpy^{\bullet-})(CO)_3Br]^-$ and $[Re^I(bpy)(CO)_3(MeCN)]^0$, as it will be discussed thoroughly in the upcoming Chapter IV.

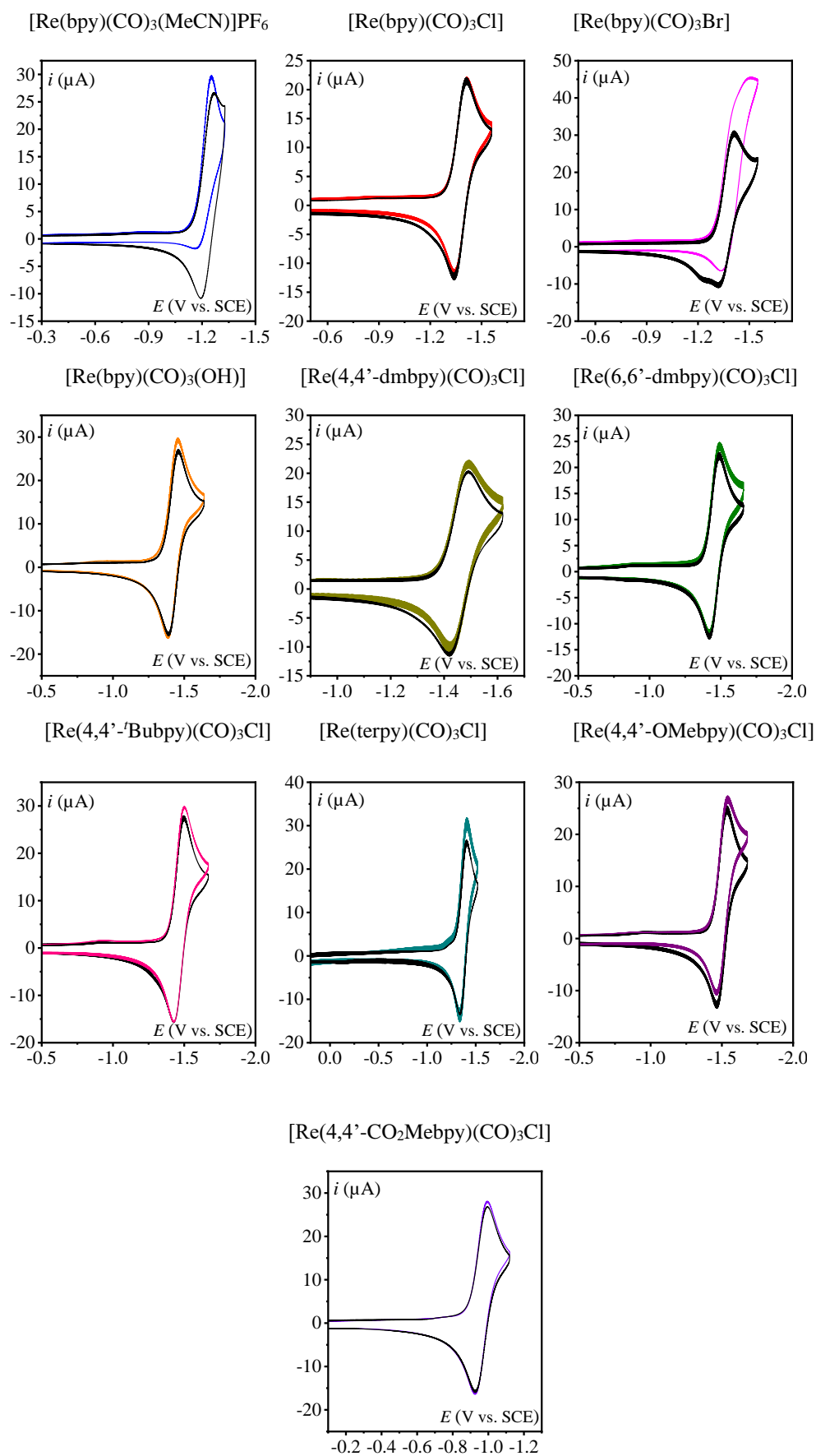


Figure III.4.2.2 1 : CVs of the first reduction system of $[Re^I(R-bpy)(CO)_3X]$ under Ar (black) and N_2O (colored) in $CH_3CN + 0.1 M n-Bu_4NPF_6$ at $0.1 V/s$ on a $3 mm$ diam. GCE.

The stoichiometry of the second wave, which is below one electron under argon reaches a one to two electron stoichiometry per rhenium atom as attested by the linear scan voltammetry on a rotating disk electrode (RDE) under N_2O for $[Re(bpy)(CO)_3(MeCN)]$ (Figure III.4.2.2 2 and Figure III.4.2.2 3) and $[Re(bpy)(CO)_3Cl]$ (Figure III.4.2.2 4 and Figure III.4.2.2 5). This was also true for other Re complexes with substituents on the bipyridyl ligand (Figure III.4.2.2 6).

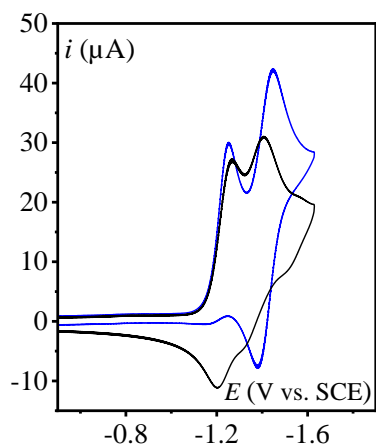


Figure III.4.2.2 2: CVs of 1 mM $[Re(bpy)(CO)_3(MeCN)]PF_6$ under Ar (black) and under N_2O (blue) in $CH_3CN + 0.1 M n-Bu_4NPF_6$ at 0.1 V/s on a 3 mm diam. GCE.

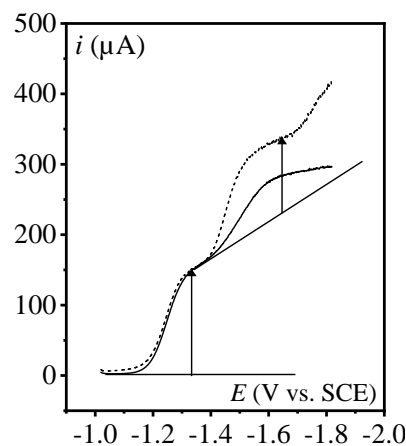


Figure III.4.2.2 3: Linear scan voltammetry at 10 mV/s on a 5 mm diam. GC RDE at 1000 rpm under Ar (full line) and under N_2O (dotted line).

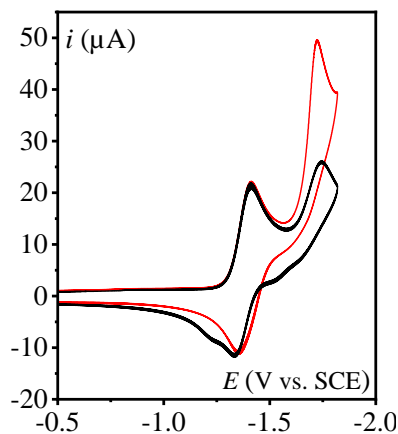


Figure III.4.2.2 4: CVs of 1 mM $[Re(bpy)(CO)_3Cl]PF_6$ under Ar (black) and under N_2O (blue) in $CH_3CN + 0.1 M n-Bu_4NPF_6$ at 0.1 V/s on a 3 mm diam. GCE.

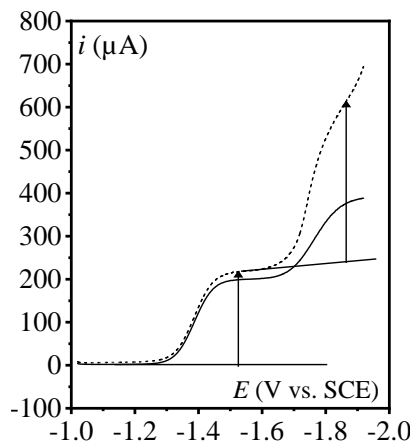


Figure III.4.2.2 5: Linear scan voltammetry at 10 mV/s on a 5 mm diameter GC RDE at 1000 rpm under Ar (full line) and under N_2O (dotted line).

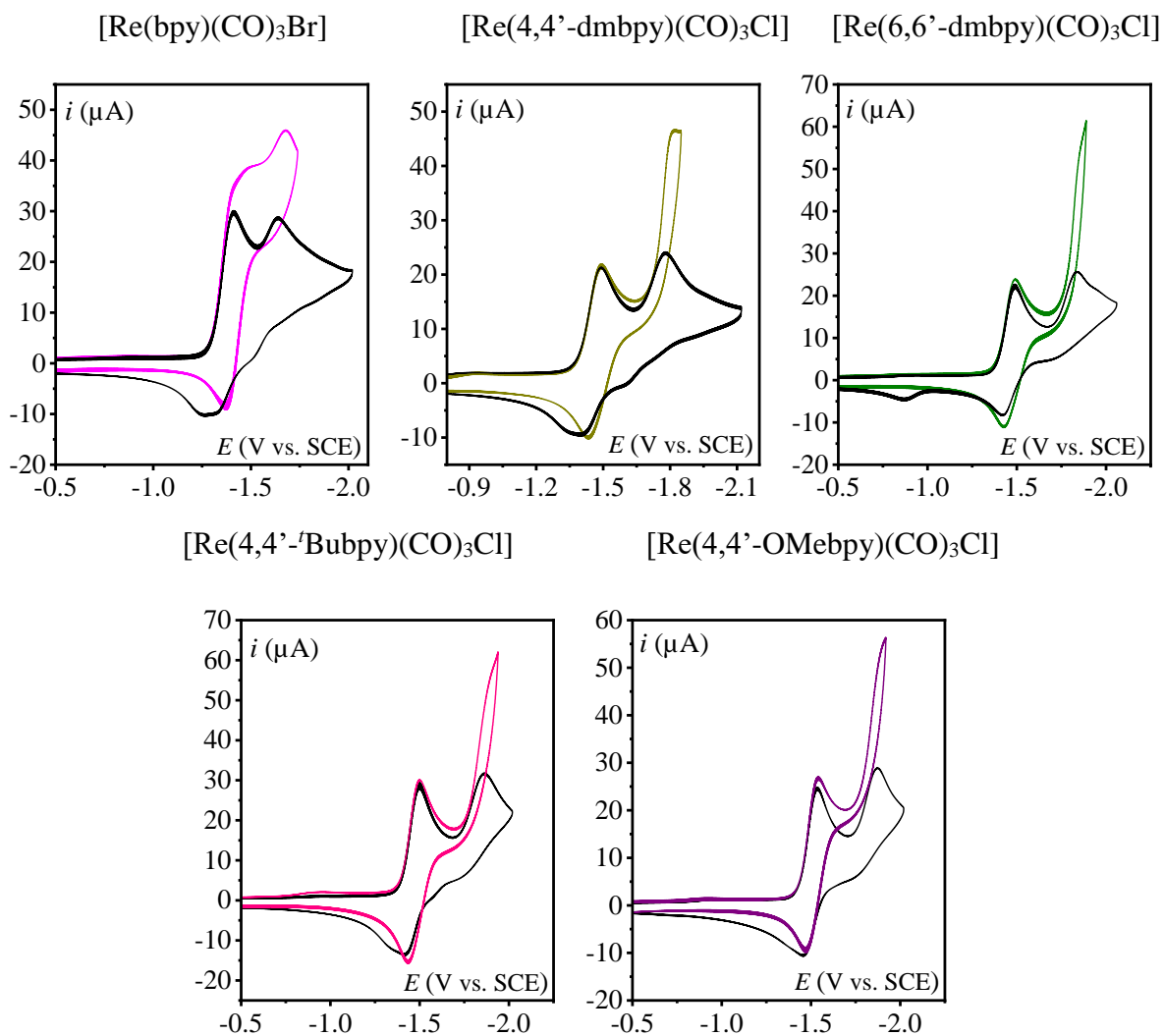


Figure III.4.2.2 6 : CVs of the 1st and 2nd reduction system of $[Re^I(R\text{-}bpy)(CO)_3X] 1 \text{ mM}$ under Ar (black) and N_2O (colored) in $CH_3CN + 0.1 \text{ M } n\text{-}Bu_4NPF_6$ at 0.1 V/s on a 3 mm diam. GCE.

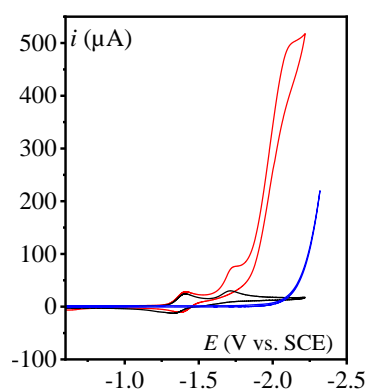


Figure III.4.2.2 7 : CVs of direct reduction of N_2O (blue), $1 \text{ mM } [Re(bpy)(CO)_3Cl]$ under Ar (black) and under N_2O (red) in $CH_3CN + 0.1 \text{ M } n\text{-}Bu_4NPF_6$ at 0.1 V/s on a 3 mm diam. GCE.

A new large wave appears at more negative potential which wasn't present under argon. This large catalytic wave occurs at a potential which is less negative than the direct reduction of N_2O indicating that the overpotential has been reduced. for the ref bpy-H (Figure III.4.2.2 7). The catalytic wave almost exhibits the characteristic canonical S-shape of a fast catalytic process in the presence of excess of substrate (N_2O) (Figure III.4.2.2 8).

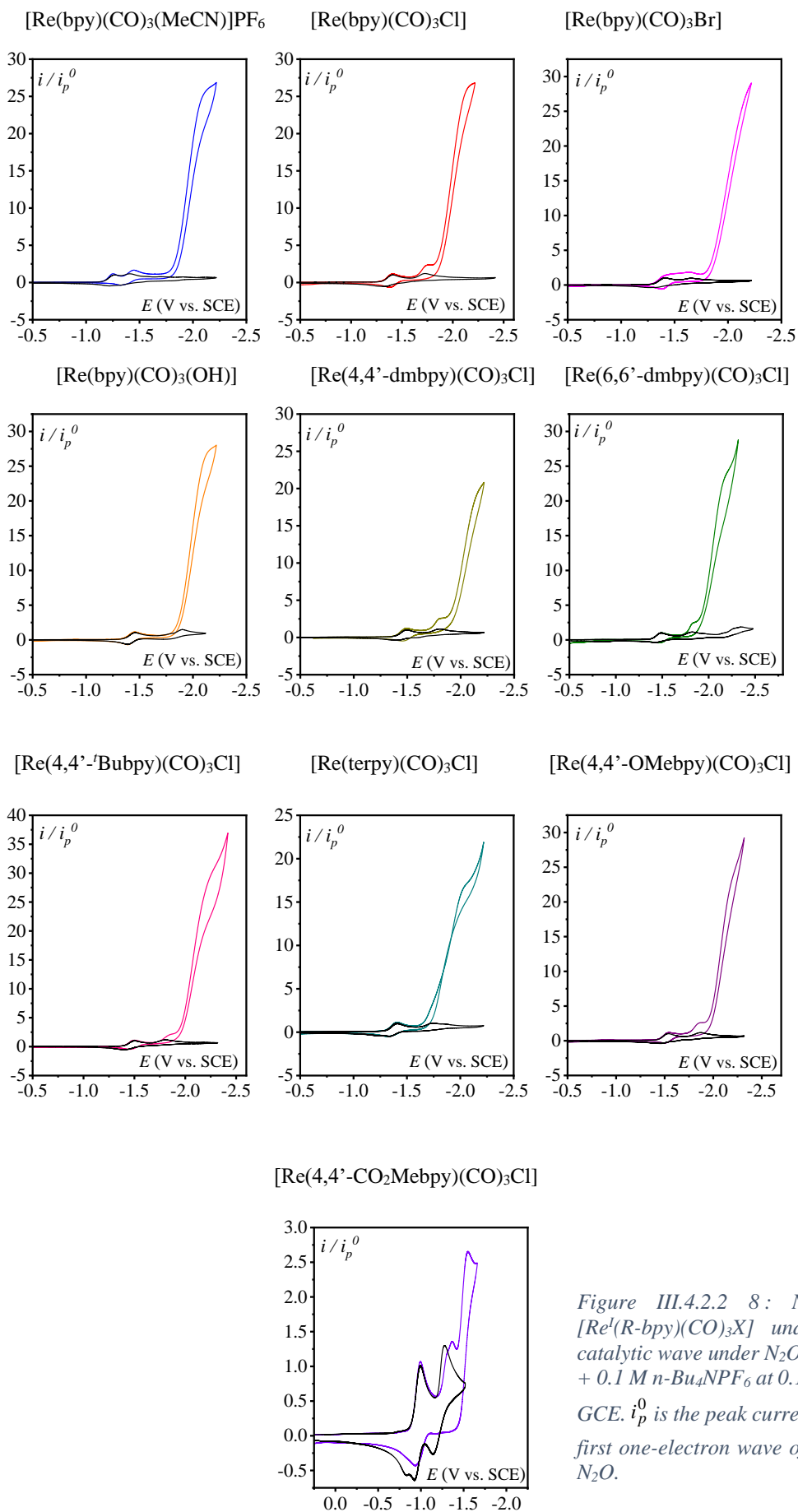
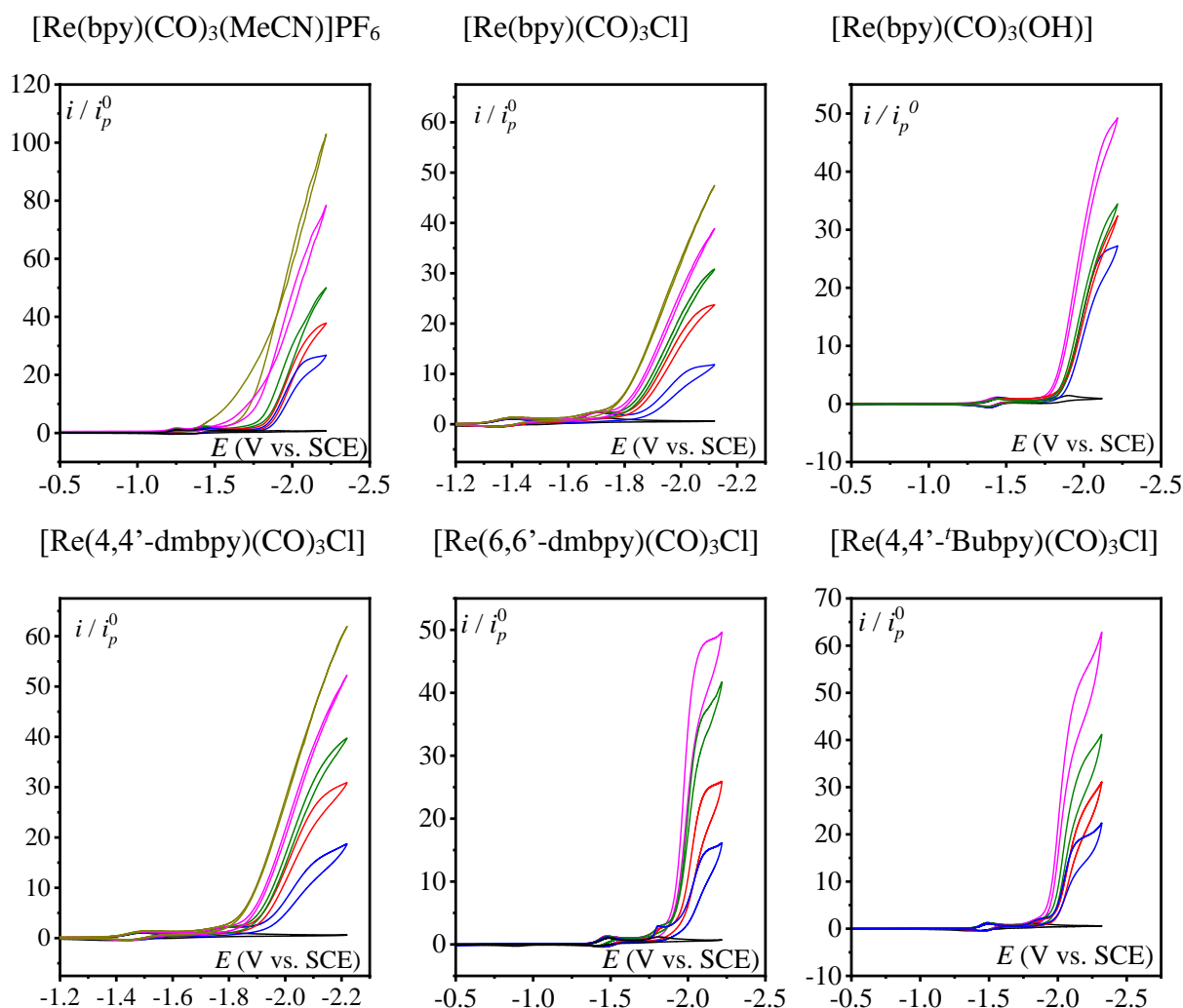


Figure III.4.2.2 8: Normalized CVs of [Re^I(R-bpy)(CO)₃X] under Ar (black), the catalytic wave under N₂O (colored), in CH₃CN + 0.1 M n-Bu₄NPF₆ at 0.1 V/s on a 3 mm diam. GCE. i_p^0 is the peak current corresponding of a first one-electron wave of each catalyst under N₂O.

As expected, it is observed at more negative potential with complexes with EDGs on the bpy ligand compared to the ref bpy-H complex and it is more intense with the former compared to the latter one. However, with the methyl ester (CO₂Me) EWG, the catalytic current intensity is much less intense and occurs at less negative potential compared to the complexes with EDGs on the -bpy ligand (Figure III.4.2.2 8).

4.2.3 Effect of water addition on the catalytic wave

In order to decrease the overpotential and improve the catalytic response of the electrocatalyst for N₂O reduction a proton source is required. Without an explicitly added proton source, the catalyst must scavenge protons from “adventitious water” in the solution coming from the electrolyte (n-Bu₄NPF₆) or CH₃CN solvent. When a proton source is explicitly added, the strength of the proton donor may affect the selectivity and activity of the catalyst. We have used water as a weak proton donor (pK_a = 38–41 in CH₃CN).¹⁶ A cathodic shift of the onset of the catalytic current is observed along with increase in the plateau current with increasing the concentration of water added (Figure III.4.2.3 1).



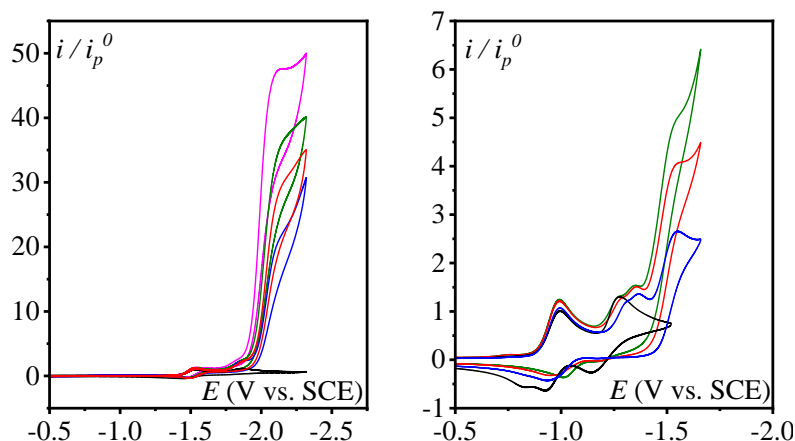


Figure III.4.2.3 1: Normalized CVs of 1 mM [Re^I(R-bpy)(CO)₃X] under Ar (black), under N₂O (blue), and with increasing amounts of water with concentration (mM) : 100 (red), 200 (olive), 500 (magenta), 1000 (dark yellow), in CH₃CN + 0.1 M n-Bu₄NPF₆ at 0.1 V/s on a 3 mm diam. GCE. i_p^0 is the peak current corresponding of a first one-electron wave of each catalyst under N₂O.

4.2.4 Controlled Potential Electrolysis

In order to check the selectivity, stoichiometry of the catalytic process and the faradaic efficiency, CPE associated with gas chromatography (GC) analysis was performed at -1.72 V vs. SCE in a solution containing 0.5 mM [Re(bpy)(CO)₃Cl] under 1 atm of N₂O on a 1 cm² GCE in MeCN / H₂O (90/10 v/v) mixture. A stable current density of ca. 7.5 mA /cm² was measured for 90 min leading to a linear increase of charge passed over time (Figure III.4.2.4 1).

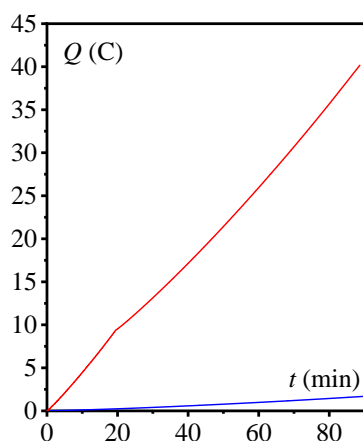


Figure III.4.2.4 1: CPE at -1.72 V vs. SCE of a solution of CH₃CN / H₂O (90 / 10) + 0.1 M n-Bu₄NPF₆ with [Re(bpy)(CO)₃Cl] (0.5 mM) under N₂O atmosphere on a 1 cm² GCE. Charge passed as a function of time in the presence (red) and in absence of catalyst (blue).

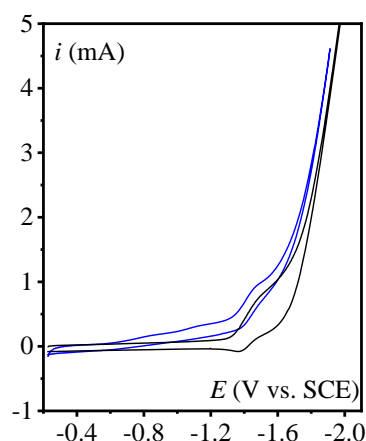


Figure III.4.2.4 2: CVs run on the GC plate of 0.5 mM [Re(bpy)(CO)₃Cl] under N₂O atmosphere at 0.1 V/s in CH₃CN / H₂O (90 / 10) + 0.1 M n-Bu₄NPF₆. (Black) before and (blue) after electrolysis at -1.72 V.

GC analysis of the electrolysis cell headspace allows determination of the quantity of N₂ produced after passing 20, 33.5 and 40 C giving FE for N₂ close to 100 % with no detection of

H₂ gas. No significant degradation of the catalyst was observed as manifested by the CVs run before and after the electrolysis (Figure III.4.2.4 2). Control experiment at -1.72 V without Re-bpy complex in the presence of N₂O + 10 % H₂O confirmed no reduction of N₂O.

5. Electrochemical reduction of N₂O mediated by [Mn(bpy-R)(CO)₃X]

A very interesting finding in the electrocatalytic reduction of CO₂ was the discovery of a particular substitution of manganese (Mn) for Re in *fac*-[Re(R-bpy)(CO)₃Cl] complexes. Mn is the third most abundant transition metal *ca.* 10 million times more abundant in the earth's crust and much cheaper than Re, accordingly it could be a good idea for the development of such type of catalyst complexes.¹⁷ Johnson et al. originally reported that the bi-reduced species of the Mn complex [Mn⁻¹(bpy)(CO)₃]⁻ does not react with CO₂ and so these complexes were not considered for CO₂ electroreduction for a long time.¹³ However, Chardon-Noblat et al. showed in 2011 that, while no current enhancement was observed in the cyclic voltammogram of *fac*-[Mn(R-bpy)(CO)₃Br] (R= Me or H) under CO₂, dramatic changes were observed when water, as proton source, was added in solution (5 % volume) resulting in strong enhancement of the cathodic current at the second reduction system where [Mn⁻¹(bpy)(CO)₃]⁻ is formed (Figure III.5 1). This addition of water is important to exhibit CO₂ reactivity and thus catalytic turnover in electrocatalysis. Controlled potential electrolysis at -1.42 V vs. SCE, gave in to quantitative faradaic efficiency for the production of CO.¹⁸

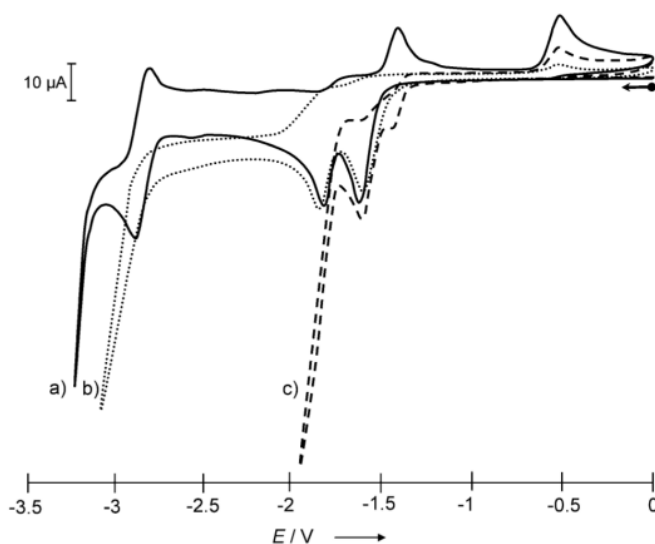
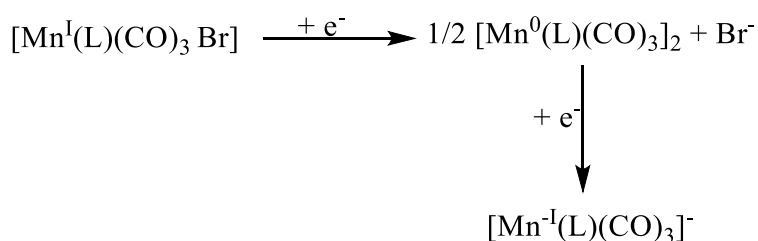


Figure III.5 1 : CVs of [Mn(bpy)(CO)₃Br] in CH₃CN + *n*-Bu₄NClO₄ under Ar (full line), under CO₂ (dotted) and under CO₂ with 5 % H₂O dashed line at 0.1 V/s on GCE¹⁷.

Under argon the complex undergoes two successive reversible reductions corresponding to the respective formation of the dimer [Mn⁰(L)(CO)₃]₂ which then undergoes reduction giving

the bi-reduced species known as the active catalytic species $[\text{Mn}^{-1}(\text{L})(\text{CO})_3]^-$ as revealed in the following Scheme III.5 1.



Scheme III.5 1 : Mechanism proposed for the formation of active catalytic species of $[\text{Mn}^{-1}(\text{L})(\text{CO})_3]^-$ ¹⁷.

Kubiak et al. reported in 2014, two Mn complexes with bulky bpy substituents: $[\text{Mn}(\text{mesbpy})(\text{CO})_3\text{Br}]$ and $[\text{Mn}(\text{mesbpy})(\text{CO})_3(\text{MeCN})](\text{OTf})$ (mesbpy = 6,6'-dimesityl-2,2'-bpy). They have been used to prevent dimerization process in the catalytic cycle. Under N_2 these complexes give a single reversible two electron reduction wave forming $[\text{Mn}(\text{mesbpy})(\text{CO})_3]^-$ at a potential 300 mV less negative than the typical bpy-Mn complexes. However, introducing these bulky ligands didn't decrease the overpotential, in fact it was shifted towards more negative potential compared to the typical bpy-Mn complex since the formed intermediate $\text{Mn}(\text{I})\text{-CO}_2\text{H}$ required one more electron to initiate catalysis.¹⁹

We have tested the catalytic activity of two manganese complexes for the reduction of N_2O , $[\text{Mn}(\text{bpy})(\text{CO})_3\text{Cl}]$ and $[\text{Mn}(\text{dmbpy})(\text{CO})_3\text{Cl}]$ (with dmbpy = 4,4'-Me₂bpy) which were available in the lab from previous synthesis. The catalytic wave occurs at more negative potential than that for the formation of $[\text{Mn}^{-1}(\text{L})(\text{CO})_3]^-$ which is produced at a potential of -1.52 V vs. SCE and is observed with both catalysts $[\text{Mn}(\text{bpy})(\text{CO})_3\text{Cl}]$ and $[\text{Mn}(\text{dmbpy})(\text{CO})_3\text{Cl}]$ at ca. -1.85 V vs. SCE, i.e. at slightly less negative potential compared to $[\text{Re}(\text{bpy})(\text{CO})_3\text{Cl}]$ and $[\text{Re}(\text{dmbpy})(\text{CO})_3\text{Cl}]$ but the catalytic plateau current is much smaller than the later ones (Figure III.5 2 and Figure III.5 3).

A second intense catalytic wave is observed at more negative potentials but its onset is close to the direct reduction of N_2O on GCE (Figure III.5 4 and Figure III.5 5). The catalytic wave which occurs at less negative potential is only slightly sensitive to the addition of water. We have observed that with increasing concentration of H_2O there is slight increase in the intensity of the catalytic wave (Figure III.5 6 and Figure III.5 7).

Controlled potential electrolysis at -1.72 V was applied passing a charge of 12.8 C over a course of 4 h in the absence of light, and with sustained current at 0.5 mA/cm² gave a quantitative production of N_2 with FE = 91%. Also release of CO was observed during the

electrolysis detected after the first GC injection at 3.3 C but it seems that even though de-carbonylation was observed, catalysis was still sustained and this shows that the new species formed are also active towards N_2O reduction.

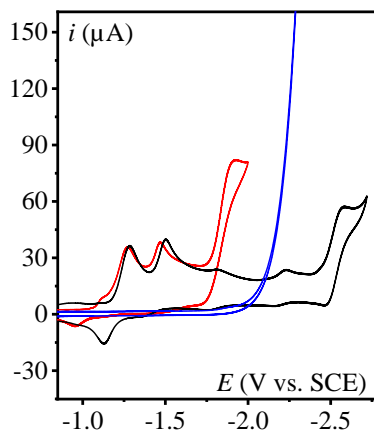


Figure III.5 2 : CVs of direct reduction of N_2O (blue), 1 mM $[Mn(bpy)(CO)_3Br]$ under Ar (black) and under N_2O (red) in $CH_3CN + 0.1 M n-Bu_4NPF_6$ at 0.1 V/s on a 3 mm diam. GCE.

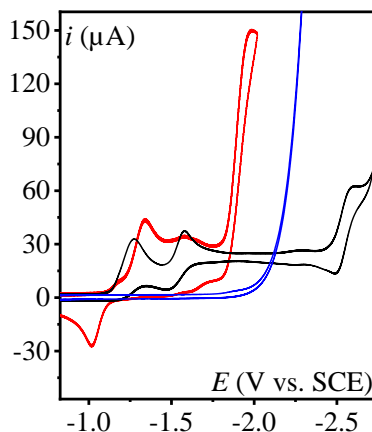


Figure III.5 3 : CVs of direct reduction of N_2O (blue), 1 mM $[Mn(dmbpy)(CO)_3Br]$ under Ar (black) and under N_2O (red) in $CH_3CN + 0.1 M n-Bu_4NPF_6$ at 0.1 V/s on a 3 mm diam. GCE.

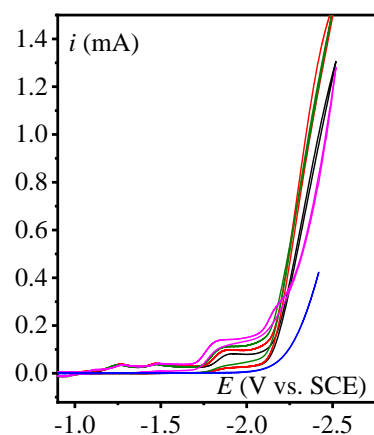


Figure III.5 4 : CVs of direct reduction of N_2O (blue), $[Mn(bpy)(CO)_3Br]$ 1 mM under 1 atm of N_2O (black), with increasing amounts of water with concentration (mM): 100 (red), 200 (olive), 500 (magenta) in $CH_3CN + 0.1 M n-Bu_4NPF_6$ at 0.1 V/s on a 3 mm diam. GCE.

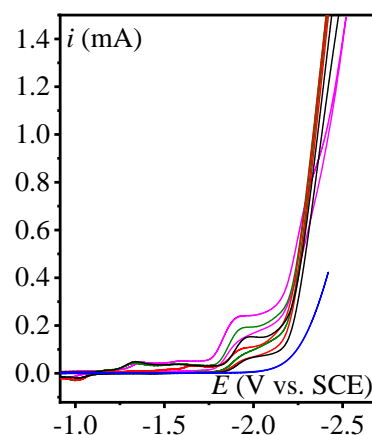


Figure III.5 5 : CVs of direct reduction of N_2O (blue), $[Mn(dmbpy)(CO)_3Br]$ 1 mM under 1 atm of N_2O (black), with increasing amounts of water with concentration (mM): 100 (red), 200 (olive), 500 (magenta) in $CH_3CN + 0.1 M n-Bu_4NPF_6$ at 0.1 V/s on a 3 mm diam. GCE.

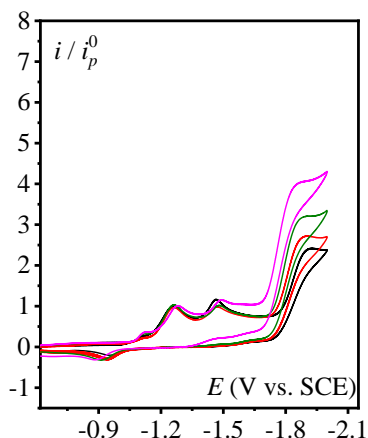


Figure III.5 6 : Normalized CVs of $[Mn(bpy)(CO)_3Br]$ under 1 atm of N_2O (black), with increasing amounts of water with concentration (mM): 100 (red), 200 (olive), 500 (magenta) in $CH_3CN + 0.1 M n-Bu_4NPF_6$ at 0.1 V/s on a 3 mm diam. GCE.

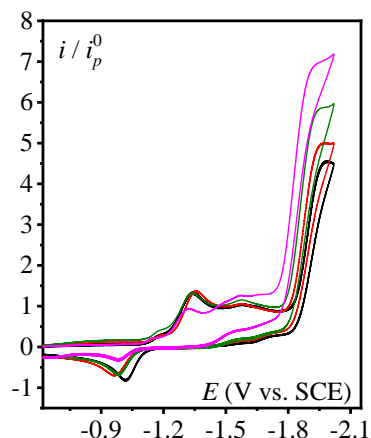


Figure III.5 7 : Normalized CVs of $[Mn(bpy)(CO)_3Br]$ under 1 atm of N_2O (black), with increasing amounts of water with concentration (mM): 100 (red), 200 (olive), 500 (magenta) in $CH_3CN + 0.1 M n-Bu_4NPF_6$ at 0.1 V/s on a 3 mm diam. GCE.

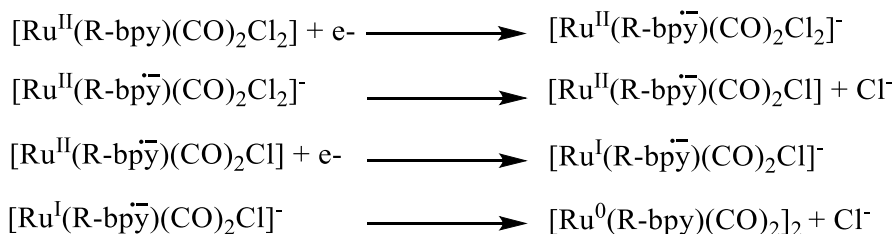
6. Contrasts between Rhenium and Manganese bipyridine complexes towards electrocatalytic reduction of N_2O

Under argon and on the time scale of the CV (100 mV/s) rapid dimerization occurs for the typical manganese bipyridyl complexes upon one electron reduction after the loss of Br^- . In contrast relatively limited or partial dimerization is observed for rhenium bipyridyl complexes. Under N_2O and in the absence of added proton source catalysis is weak for the Mn complexes compared to the rhenium complexes which showed much higher catalytic currents in the presence of residual water source. Also, this catalytic wave is shifted towards less negative potential for Mn complexes compared to the rhenium complexes. In addition, according to a smaller catalytic current (close to a plateau), we can anticipate that the chemical step rate constants for the reaction with N_2O is lower in the case of Mn compared to the Re complexes. Hence, we will have either to choose catalysts which significantly operate at lower overpotential but give a lower catalytic current and lower rate constants or choose catalysts with higher catalytic current intensities but demanding more energy potential.

7. Electrochemical reduction of N_2O mediated by Ru, Rh and Os complexes

The ruthenium complexes of compounds have received much attention over the past decades especially for carbon dioxide reduction. The Ru complexes discussed below were

previously synthesized in our lab. The cyclic voltammograms of $[\text{Ru}(\text{bpy})(\text{CO})_2\text{Cl}_2]$ and $[\text{Ru}(4,4'\text{-dmbpy})(\text{CO})_2\text{Cl}_2]$ exhibit an irreversible 2 e- cathodic peak at -1.22 V and -1.26 V corresponding to the formation of the Ru dimer and a weak anodic peak at ~ -0.002 V and -0.069 V respectively corresponding to the oxidation of the dimer (Scheme III.7 1) leading to the breaking of the Ru-Ru bond. (Figure III.7 1 and Figure III.7 2).



Scheme III.7 1 : Proposed mechanism for the behavior of $[\text{Ru}(\text{R-bpy})(\text{CO})_2\text{Cl}_2]$ under Ar.

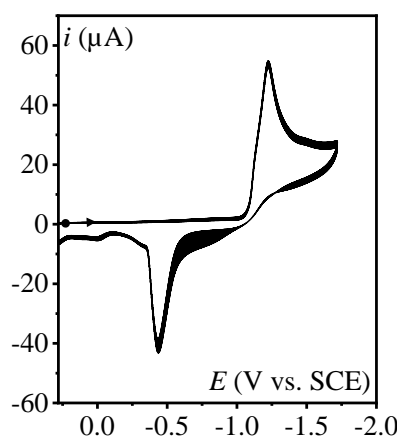


Figure III.7 1 : CVs of $[\text{Ru}(\text{bpy})(\text{CO})_2\text{Cl}_2]$ 1 mM under Ar in $\text{CH}_3\text{CN} + 0.1 \text{ M } n\text{-Bu}_4\text{NPF}_6$ at 0.1 V/s on a 3 mm diam. GCE.

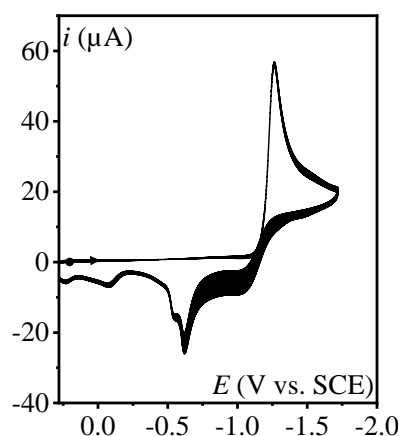


Figure III.7 2 : CVs of $[\text{Ru}(\text{dmbpy})(\text{CO})_2\text{Cl}_2]$ 1 mM under Ar in $\text{CH}_3\text{CN} + 0.1 \text{ M } n\text{-Bu}_4\text{NPF}_6$ at 0.1 V/s on a 3 mm diam. GCE.

The $[\text{Ru}(\text{bpy})(\text{CO})_2\text{Cl}_2]$ complex under N_2O displays a strong cathodic peak with onset potential at -1.54 V (red) less negative than the direct reduction of N_2O (blue) (Figure III.7 3). Same behavior is observed with $[\text{Ru}(\text{dmbpy})(\text{CO})_2\text{Cl}_2]$ but shifted slightly towards more negative potential consistent with the electron donating effect of the dimethyl and towards less negative potential with the isopropyl ester ($\text{CO}_2\text{-iPr}$) substituent on the bipyridine ligand (Figure III.7 4).

Accordingly high current intensities were obtained with the ruthenium complexes under N_2O observed at a position which is less negative than the direct reduction of N_2O . Thus, these complexes might function as catalysts for the electrochemical reduction of N_2O which seems to be promising. These preliminary results should open new directions for the development of

modified film electrodes which proved to be efficient heterogeneous molecular catalysts for the reduction of carbon dioxide in water and in organic solvents.^{20,21,22,23}

Figure III.7 3 : CVs of direct reduction of N_2O (blue), 1 mM $[Ru(bpy)(CO)_2Cl_2]$ under Ar (black) and under N_2O (red) in $CH_3CN + 0.1 M n-Bu_4NPF_6$ at 0.1 V/s on a 3 mm diam. GCE.

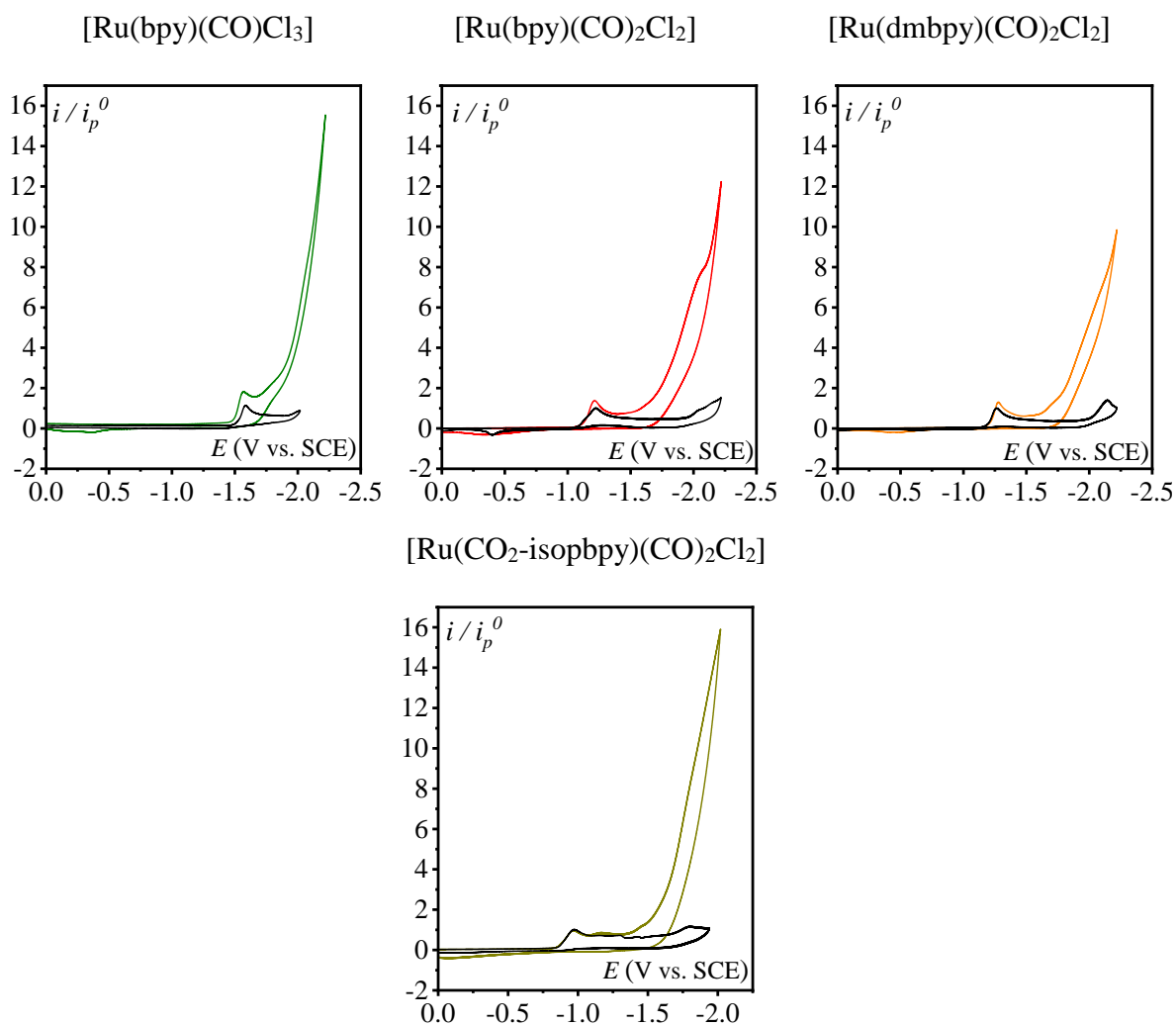
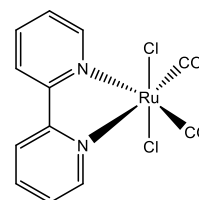
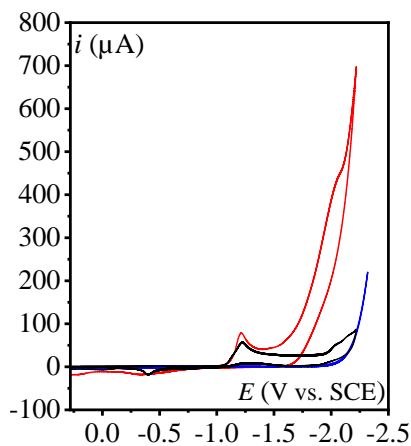


Figure III.7 4 : Normalized CVs of 1 mM $[Ru(R-bpy)(CO)_xCl_y]$ under Ar (black), the catalytic wave under N_2O (colored) in $CH_3CN + 0.1 M n-Bu_4NPF_6$ at 0.1 V/s on a 3 mm diam. GCE. i_p^0 is the peak current corresponding of a first one-electron wave of each catalyst under N_2O .

Building on the success of ruthenium complexes, polypyridyl osmium complexes have also been studied for CO₂ reduction. In 1987 Meyer et al., reported the use of [Os(bpy)₂(CO)H]PF₆ for the molecular electrochemical reduction of carbon dioxide observing the release of CO as dominant product under anhydrous conditions. But in the presence of water formate was formed. In this thesis we have used polypyridyl osmium carbonyl chloride [Os(bpy)₂(CO)Cl]PF₆ as a catalyst to screen it for the reduction of N₂O.

Our CV analysis of this complex, previously synthesized in our group, showed the appearance of high current intensity which wasn't present under Ar. In addition, this increase in current occurs at a potential less negative than the direct reduction of N₂O. Moreover, we have tested rhodium complexes as they were previously reported by Meyer and co-workers in 1985²⁴ and 1988,²⁵ and also in our team for the CO₂ERR.²⁶ Current enhancement was observed in the presence of the rhodium phenanthroline pentamethyl cyclopentadienyl perchlorate complex [Rh(phen)(MeCp)]ClO₄ under N₂O atmosphere (Figure III.7 5).

In conclusion these preliminary results obtained will pave the way for the development and design of new catalysts to be used in the future in N-O bond activation.

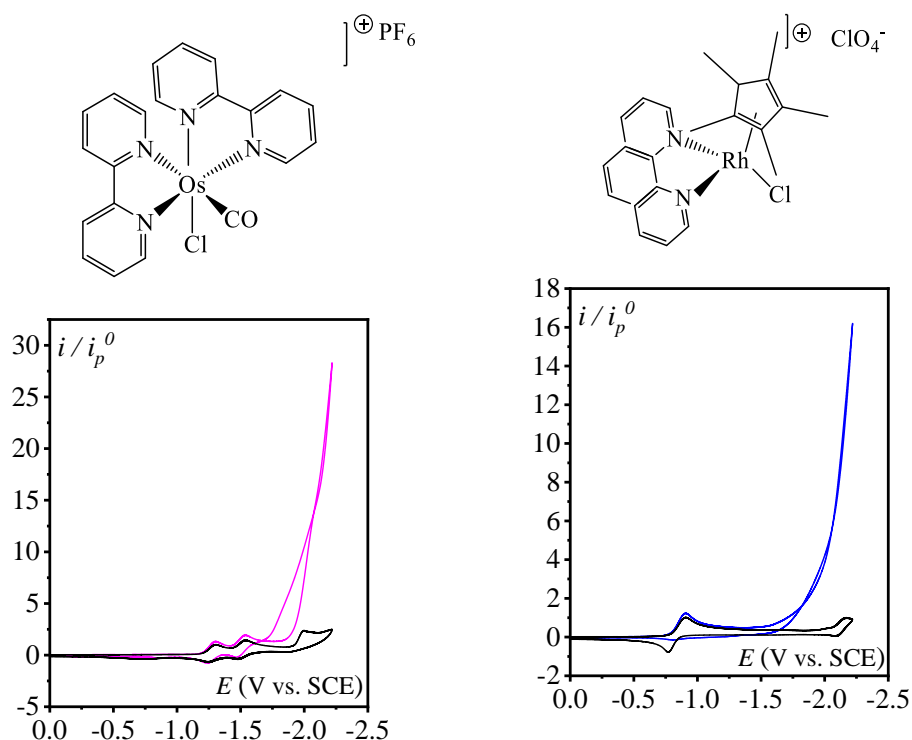


Figure III.7 5 : Normalized CVs of [Os(bpy)₂(CO)Cl]PF₆ and [Rh(phen)(Cp*)]ClO₄ under Ar (black), the catalytic wave under N₂O (colored) in CH₃CN + 0.1 M n-Bu₄NPF₆ at 0.1 V/s on a 3 mm diam. GCE. i_p^0 is the peak current corresponding of a first one-electron wave of each catalyst under N₂O.

8. Conclusion

In this chapter, we have reported a series of transition metal complexes as molecular catalysts and studied their catalytic activity for N_2O reduction in organic solvents. Beginning with the commercial iron porphyrin (FeTPPCl) very well-known catalysts for CO_2 reduction has proved to be efficient and selective catalysts for N_2O reduction with no concomitant reduction of phenol to H_2 . Then, a series of Re complexes *fac*-[Re(R-bpy)(CO)₃X] were explored. A systematic study of the effect of labile ligands, substituents on the bipyridyl ligand and the effect of Brønsted acid (H_2O) was conducted. Also, these catalysts showed to be stable, selective catalysts for N_2O reduction in the presence of water to form N_2 gas. Water (proton source) showed to be beneficial to enhance the catalytic chemical rate and lowered the overpotential by 500 mV (Figure III.8 1). Water also assists the electrochemical limiting event. Indeed, in the subsequent Chapter we will show the N-O bond breaking is followed by proton coupled electron transfer (PCET) to facilitate the removal of the OH^- ligand after the reduction of N_2O by the bi-reduced species.

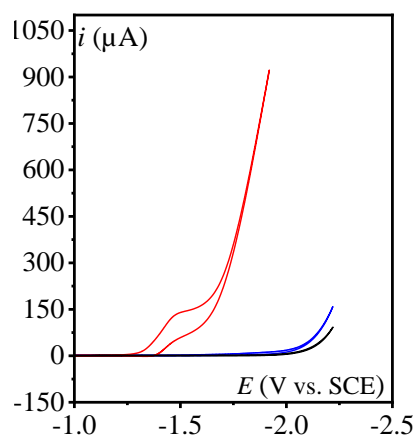


Figure III.8 1 : CVs of direct reduction of N_2O (black), $N_2O + 10\% H_2O$ under (blue) and $1 \text{ mM } [Re(bpy)(CO)_3Cl]$ $N_2O + 10\% H_2O$ (red) in $CH_3CN + 0.1 \text{ M } n\text{-Bu}_4\text{NPF}_6$ at 0.1 V/s on a 3 mm diam. GCE .

Next, we studied Mn complexes belonging to the same column as Re and they also showed catalytic activity towards N_2O deoxygenation but with catalytic currents lower than that of Re and at less negative potential. Finally, we studied other complexes in different group in the periodic table Ru, Os and Rh and the results obtained were preliminary studies which will be further matured in the future.

The studies reported in this Chapter are qualitative and so far do not allow for discussing the mechanism and its particular, the outersphere or innersphere character of the mechanism. Nonetheless, cyclic voltammograms give some information in that regard. Indeed, in most cases

(actually all cases except FeTPP), the catalytic wave developed at a potential where there is no wave in the absence of N_2O . This is an indication that the mechanism is not a redox catalysis process but involve species resulting from interaction of the catalyst and N_2O . We have thus decided to investigate in details the mechanism in the case of rhenium bipyridine tricarbonyl complexes in the following Chapter IV.

References:

- (1) Bhugun, I.; Lexa, D.; Savéant, J.-M. Catalysis of the Electrochemical Reduction of Carbon Dioxide by Iron(0) Porphyrins: Synergistic Effect of Weak Brønsted Acids. *Journal of the American Chemical Society* **1996**, *118* (7), 1769-1776. DOI: 10.1021/ja9534462.
- (2) Mondal, B.; Song, J.; Neese, F.; Ye, S. Bio-inspired mechanistic insights into CO₂ reduction. *Current Opinion in Chemical Biology* **2015**, *25*, 103-109. DOI:10.1016/j.cbpa.2014.12.022.
- (3) Lexa, D.; Savéant, J. M.; Su, K. B.; Wang, D. L. Chemical vs. redox catalysis of electrochemical reactions. Reduction of trans-1,2-dibromocyclohexane by electrogenerated aromatic anion radicals and low oxidation state metalloporphyrins. *Journal of the American Chemical Society* **1987**, *109* (21), 6464-6470. DOI: 10.1021/ja00255a036.
- (4) Costentin, C.; Robert, M.; Savéant, J. M.; Tatin, A. Efficient and selective molecular catalyst for the CO₂-to-CO electrochemical conversion in water. *Proceedings of the National Academy of Sciences U S A* **2015**, *112* (22), 6882-6886. DOI: 10.1073/pnas.1507063112.
- (5) Azcarate, I.; Costentin, C.; Robert, M.; Savéant, J.-M. Dissection of Electronic Substituent Effects in Multielectron–Multistep Molecular Catalysis. Electrochemical CO₂-to-CO Conversion Catalyzed by Iron Porphyrins. *The Journal of Physical Chemistry C* **2016**, *120* (51), 28951-28960. DOI: 10.1021/acs.jpcc.6b09947.
- (6) Boutin, E.; Merakeb, L.; Ma, B.; Boudy, B.; Wang, M.; Bonin, J.; Anxolabéhère-Mallart, E.; Robert, M. Molecular catalysis of CO₂ reduction: recent advances and perspectives in electrochemical and light-driven processes with selected Fe, Ni and Co aza macrocyclic and polypyridine complexes. *Chemical Society Reviews* **2020**, *49* (16), 5772-5809, DOI: 10.1039/D0CS00218F.
- (7) Bhugun, I.; Lexa, D.; Savéant, J.-M. Homogeneous Catalysis of Electrochemical Hydrogen Evolution by Iron(0) Porphyrins. *Journal of the American Chemical Society* **1996**, *118* (16), 3982-3983. DOI: 10.1021/ja954326x.
- (8) Hawecker, J.; Lehn, J.-M.; Ziessel, R. Electrocatalytic reduction of carbon dioxide mediated by Re(bipy)(CO)₃Cl (bipy = 2,2'-bipyridine). *Journal of the Chemical Society, Chemical Communications* **1984**, (6), 328-330. DOI: 10.1039/C39840000328.
- (9) Hawecker, J.; Lehn, J.-M.; Ziessel, R. Photochemical and Electrochemical Reduction of Carbon Dioxide to Carbon Monoxide Mediated by (2,2'-Bipyridine)tricarbonylchlororhenium(I) and Related Complexes as Homogeneous Catalysts. *Helvetica Chimica Acta* **1986**, *69* (8), 1990-2012. DOI:10.1002/hlca.19860690824.
- (10) Smieja, J. M.; Kubiak, C. P. Re(bipy-tBu)(CO)₃Cl-improved catalytic activity for reduction of carbon dioxide: IR-spectroelectrochemical and mechanistic studies. *Inorg. Chem.* **2010**, *49* (20), 9283-9289. DOI: 10.1021/ic1008363.
- (11) Smieja, J. M.; Benson, E. E.; Kumar, B.; Grice, K. A.; Seu, C. S.; Miller, A. J.; Mayer, J. M.; Kubiak, C. P. Kinetic and structural studies, origins of selectivity, and interfacial charge transfer in the artificial photosynthesis of CO. *Proceeding National Academy of Sciences U S A* **2012**, *109* (39), 15646-15650. DOI: 10.1073/pnas.1119863109.
- (12) Elgrishi, N.; Chambers, M. B.; Wang, X.; Fontecave, M. Molecular polypyridine-based metal complexes as catalysts for the reduction of CO₂. *Chemical Society Reviews* **2017**, *46* (3), 761-796. DOI: 10.1039/C5CS00391A.
- (13) Johnson, F. P. A.; George, M. W.; Hartl, F.; Turner, J. J. Electrocatalytic Reduction of CO₂ Using the Complexes [Re(bpy)(CO)₃L]_n (n = +1, L = P(OEt)₃, CH₃CN; n = 0, L = Cl⁻, Otf⁻; bpy = 2,2'-Bipyridine; Otf⁻ = CF₃SO₃) as Catalyst Precursors: Infrared Spectroelectrochemical Investigation. *Organometallics* **1996**, *15* (15), 3374-3387. DOI: 10.1021/om960044+.
- (14) Sullivan, B. P.; Bolinger, C. M.; Conrad, D.; Vining, W. J.; Meyer, T. J. One- and two-electron pathways in the electrocatalytic reduction of CO₂ by fac-Re(bpy)(CO)₃Cl (bpy = 2,2'-bipyridine). *J. Chem. Soc., Chem. Commun.* **1985**, (20), 1414-1416. DOI: 10.1039/c39850001414.
- (15) Clark, M. L.; Cheung, P. L.; Lessio, M.; Carter, E. A.; Kubiak, C. P. Kinetic and Mechanistic Effects of Bipyridine (bpy) Substituent, Labile Ligand, and Brønsted Acid on Electrocatalytic CO₂ Reduction by Re(bpy) Complexes. *ACS Catalysis* **2018**, *8* (3), 2021-2029. DOI: 10.1021/acscatal.7b03971.
- (16) Rountree, E. S.; McCarthy, B. D.; Eisenhart, T. T.; Dempsey, J. L. Evaluation of Homogeneous Electrocatalysts by Cyclic Voltammetry. *Inorganic Chemistry* **2014**, *53* (19), 9983-10002. DOI: 10.1021/ic500658x.
- (17) Yaroshevsky, A. A. Abundances of chemical elements in the Earth's crust. *Geochemistry International* **2006**, *44* (1), 48-55. DOI: 10.1134/S001670290601006X.
- (18) Bourrez, M.; Molton, F.; Chardon-Noblat, S.; Deronzier, A. [Mn(bipyridyl)(CO)₃Br]: An Abundant Metal Carbonyl Complex as Efficient Electrocatalyst for CO₂ Reduction. *Angewandte Chemie International Edition* **2011**, *50* (42), 9903-9906. DOI:10.1002/anie.201103616.
- (19) Sampson, M. D.; Nguyen, A. D.; Grice, K. A.; Moore, C. E.; Rheingold, A. L.; Kubiak, C. P. Manganese Catalysts with Bulky Bipyridine Ligands for the Electrocatalytic Reduction of Carbon Dioxide: Eliminating

-
- Dimerization and Altering Catalysis. *Journal of the American Chemical Society* **2014**, *136* (14), 5460-5471. DOI: 10.1021/ja501252f.
- (20) Collomb-Dunand-Sauthier, M.-N.; Deronzier, A.; Ziessel, R. Electrocatalytic reduction of CO₂ in water on a polymeric [$\{\text{Ru}^0(\text{bpy})(\text{CO})_2\}$](bpy = 2,2'-bipyridine) complex immobilized on carbon electrodes. *Journal of the Chemical Society, Chemical Communications* **1994**, (2), 189-191. DOI: 10.1039/C39940000189.
- (21) Collomb-Dunand-Sauthier, M. N.; Deronzier, A.; Ziessel, R. Electrochemical elaboration of thin films of poly[Ru^{II}(L)(CO)₂Cl₂] (L = 4-(2-pyrrol-1-ylethyl)-4'-methyl-2,2'-bipyridine or 4,4'-bis((3-pyrrol-1-ylpropyloxy)carbonyl)-2,2'-bipyridine): photochemical properties and photoimaging. *The Journal of Physical Chemistry* **1993**, *97* (22), 5973-5979. DOI: 10.1021/j100124a032.
- (22) Chardon-Noblat, S.; Deronzier, A.; Ziessel, R.; Zsoldos, D. Electroreduction of CO₂ catalyzed by polymeric [Ru(bpy)(CO)₂]_n films in aqueous media: Parameters influencing the reaction selectivity. *Journal of Electroanalytical Chemistry* **1998**, *444* (2), 253-260. DOI:10.1016/S0022-0728(97)00584-6.
- (23) Ishida, H.; Fujiki, K.; Ohba, T.; Ohkubo, K.; Tanaka, K.; Terada, T.; Tanaka, T. Ligand effects of ruthenium 2,2'-bipyridine and 1,10-phenanthroline complexes on the electrochemical reduction of CO₂. *Journal of the Chemical Society, Dalton Transactions* **1990**, (7), 2155-2160. DOI: 10.1039/DT99000002155.
- (24) Bolinger, C. M.; Sullivan, B. P.; Conrad, D.; Gilbert, J. A.; Story, N.; Meyer, T. J. Electrocatalytic reduction of CO₂ based on polypyridyl complexes of rhodium and ruthenium. *Journal of the Chemical Society, Chemical Communications* **1985**, (12), 796-797. DOI: 10.1039/C39850000796.
- (25) Bolinger, C. M.; Story, N.; Sullivan, B. P.; Meyer, T. J. Electrocatalytic reduction of carbon dioxide by 2,2'-bipyridine complexes of rhodium and iridium. *Inorganic Chemistry* **1988**, *27* (25), 4582-4587. DOI: 10.1021/ic00298a016.
- (26) Caix, C.; Chardon-Noblat, S.; Deronzier, A. Electrocatalytic reduction of CO₂ into formate with $[(\eta^5\text{Me}_5\text{C}_5)\text{M}(\text{L})\text{Cl}]^+$ complexes (L = 2,2'-bipyridine ligands; M Rh(III) and Ir(III)). *Journal of Electroanalytical Chemistry* **1997**, *434* (1), 163-170. DOI:10.1016/S0022-0728(97)00058-2.

Chapter IV: Mechanistic Analysis for the Electrochemical Molecular Reduction of N₂O by Rhenium Complexes: Spectroelectrochemical Studies

This Chapter includes work I have published as the first co-author:

- Importance of Ligand Exchange in the Modulation of Molecular Catalysis: Mechanism of the Electrochemical Reduction of Nitrous Oxide with Rhenium Bipyridyl Carbonyl Complexes. Deeba, R.; Chardon-Noblat, S.; Costentin, C. *ACS Catal.* **2023**, 13, 12, 8262–8272. DOI : 10.1021/acscatal.3c01495.

1. Introduction

As discussed at the beginning of Chapter III, chemical catalysis involves intimate interaction between the active form of the catalyst and the substrate. This leads to the formation of an adduct that is formation of chemical bonding to facilitate “exchange” of electrons.

In the matter of transition metal complexes to act as chemical catalysts this requires getting a free or open coordination site on the metal center to achieve this type of chemical bonding and to sustain catalysis. Thus, regeneration of this active or free site on the metal center is necessary to allow the rebinding of the substrate and to sustain the catalysis. However, in some cases the generation of strong coordinating ligand as a product or co-product can be detrimental for the catalyst which results in slow down catalysis or demand more energy potential to remove this strong coordinating ligand, making it difficult the regeneration once more of the free site.

Examples of catalyst deactivation include $[\text{Ni}(\text{cyclam})](\text{PF}_6)_2$ (cyclam = 1,4,8,11-tetraazacyclotetradecane) used for the homogeneous reduction of CO_2 forming Ni(I) carbonyl $[\text{Ni}(\text{cyclam})(\text{CO})]^+$ and a Ni(II) coordinated hydroxycarbonyl ligand, $[\text{Ni}(\text{cyclam})(\text{CO}_2\text{OH})]^+$ corresponding to the deactivated form of the catalyst. However the addition of $[\text{Ni}(\text{TMC})]^+$ (TMC = 1,4,8,11-tetramethyl-1,4,8,11-tetraazacyclotetradecane) can act as CO scavenger to regenerate the active catalyst resulting in increased catalytic current.¹ Another example is the electrochemical reduction of N_2 to NH_3 by Mo and Re complexes which leads to the formation of stable metal nitrides. These latter then require additional reductions to release NH_3 via three proton coupled electron transfers PCET.^{2,3,4} In other cases catalysis is not inhibited but self-modulated as shown in the reductive dechlorination of alkyl chlorides by vitamin B12, cobalamins whereby the production of free chlorides shifts the potential required to reduce the alkylcobalt(III) complex towards more negative potential.⁵

In this Chapter we will study in detail the mechanism of electrochemical reduction of N_2O gas using $[\text{Re}(\text{bpy})(\text{CO})_3\text{X}]^{n+}$ ($\text{X} = \text{CH}_3\text{CN}, \text{Cl}^-$, $n = 0$ or 1) as catalyst metal complexes. We will reveal a ligand exchange route which decelerates catalysis. We will indeed show that the bi-reduced species $[\text{Re}^0(\text{bpy}^{\bullet-})(\text{CO})_3]^-$, electrogenerated by two sequential one-electron reductions from these complexes, reacts by redox reaction with N_2O to form the hydroxo complex $[\text{Re}^I(\text{bpy})(\text{CO})_3(\text{OH})]$. Since hydroxide is a co-product, strong ligand produced during the reaction, then it can bind to the metal center and this makes the regeneration of the free coordination site on the Re(0) center more energetically difficult. However, we have found that

adding an excess of free chlorides in the electrolyte facilitates the displacement of the OH^- ligand to regenerate the free coordination site on the metal center. Such in-depth mechanistic studies were realized by well-established electrochemical methods such as cyclic voltammetry, controlled potential electrolysis along with spectroelectrochemical measurements (SEC).

2. $[\text{Re}^0(\text{bpy}^{\bullet-})(\text{CO})_3]^-$ in the electrochemical reduction of CO_2 and N_2O

Starting from $[\text{Re}(\text{bpy})(\text{CO})_3\text{Cl}]$, two sequential one electron reductions lead to the catalytic active state species $[\text{Re}^0(\text{bpy}^{\bullet-})(\text{CO})_3]^-$ having a vacant coordination site to allow the binding of N_2O or CO_2 for their reduction. The interaction of the bi-reduced species with CO_2 leads to the formation of η^1 -bound CO_2 adduct at the Re center giving carboxylate species intermediate which upon protonation gives rise to $\text{Re-CO}_2\text{H}$ and this can react with a second proton to liberate water and produce tetracarbonyl cationic intermediate. Finally, the release of CO can occur upon further reduction regenerating the catalytically active species (Scheme IV.2 1).^{6,7,8} Since N_2O and CO_2 are analogous molecules one can envision a nucleophilic attack of the reduced metal center to the electrophilic N atom as in the case of CO_2 . However, this is not the case since binding of the metal center occurs probably through the oxygen atom as it will be discussed in the following sections.

Additionally, in the case of N_2O , sustained catalysis is not initiated at the potential of electrogeneration of the bi-reduced species on the time scale of the cyclic voltammetry. The catalytic wave is shifted towards more negative potential as revealed in Figure IV.2 1. As will be shown in the following, the catalytic wave in the CV corresponds to the potential of release of OH^- from the $[\text{Re}(\text{bpy})(\text{CO})_3(\text{OH})]$ formed by the chemical reaction of N_2O and the bi-reduced species. Below are the different proposed mechanisms for the electrochemical reduction of CO_2 and N_2O by the bi-reduced species $[\text{Re}^0(\text{bpy}^{\bullet-})(\text{CO})_3]^-$ (Scheme IV.2 1).

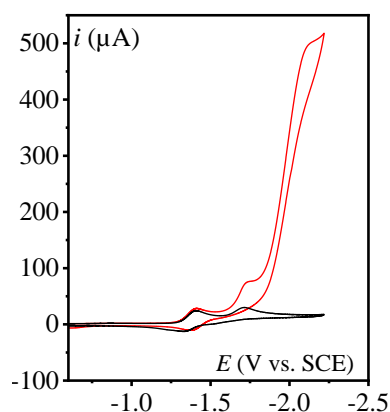
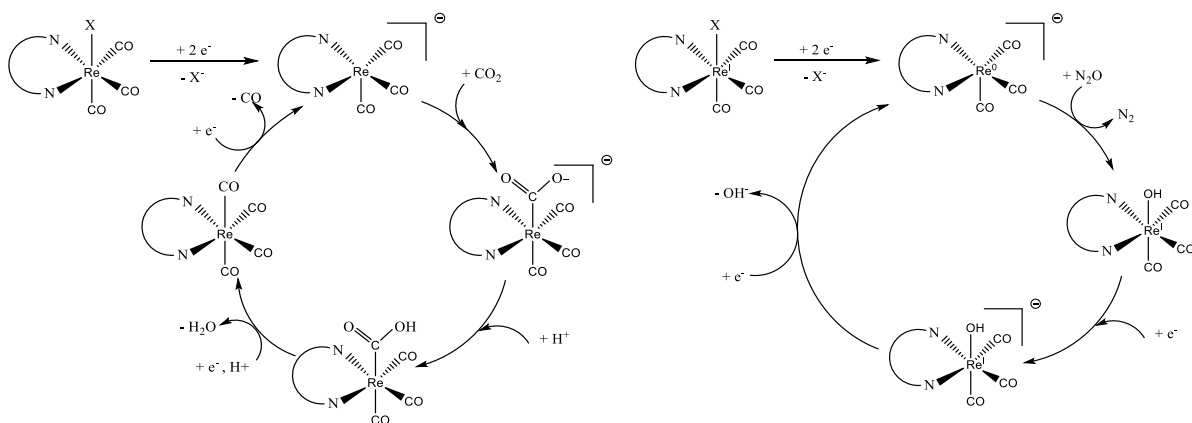


Figure IV.2 1 : CVs of 1 mM $[\text{Re}(\text{bpy})(\text{CO})_3\text{Cl}]$ under Ar (black) and N_2O (red) in CH_3CN + 0.1 M $n\text{-Bu}_4\text{NPF}_6$ at 0.1 V/s on a 3 mm diam. GCE.



Scheme IV.2.1 : Proposed mechanism for the electrocatalytic reduction of CO_2 and N_2O by $[\text{Re}^I(\text{bpy})(\text{CO})_3\text{X}]$.

3. Electrochemical reduction of N_2O by electrogenerated $[\text{Re}^0(\text{bpy}^{\bullet-})(\text{CO})_3]^-$ species

In order to prove that there is a reaction between N_2O and the bi-reduced active catalytic species $[\text{Re}^0(\text{bpy}^{\bullet-})(\text{CO})_3]^-$, electrogeneration of the bi-reduced species followed by addition of N_2O was performed.

Electrogeneration of the bi-reduced species: Setting up the best experimental conditions took time to electrogenerate the bi-reduced species. It turned out that working under inert atmosphere (Ar) inside the glove box and using carbon felt having large electroactive surface area as WE was helpful to perform exhaustive reductive electrolysis to electrogenerate quantitatively the bi-reduced species and to make the reaction faster with as less degradation as possible. Other methods can also be used to generate the bi-reduced species chemically by using potassium intercalated graphite (KC_8) as a reductant and 18-crown-6 to stabilize the anion in THF solvent;^{9,10} we have favored using the electrochemical method since we have the control of the charge passed and also to avoid the presence of excess of residual KC_8 in the solvent.

Preliminary to the study of the reaction between the bi-reduced species and N_2O , we will first discuss the characterization of the mono- and bi-reduced species involved in the process by SEC measurements.

3.1 Infrared and UV-vis spectroelectrochemistry of $[\text{Re}(\text{bpy})(\text{CO})_3\text{Cl}]$

As already recalled in Chapter III, $[\text{Re}(\text{bpy})(\text{CO})_3\text{Cl}]$ in solution shows a reversible one electron wave with $E_{1/2} = -1.36$ V corresponding to bipyridine based reduction followed by an irreversible or quasi-reversible one electron wave Re based reduction associated with loss of

Cl^- . This second reduction is in competition with spontaneous dehalogenation of the bpy centered monoreduced species, which can dimerize to form a metal bonded Re-Re dimer observed by the initiation of the second cyclical scan at -1.40 V giving the dimer anion couple as shown in Figure IV.3.1 1 based on the mechanism proposed in Scheme IV.3.1 1.

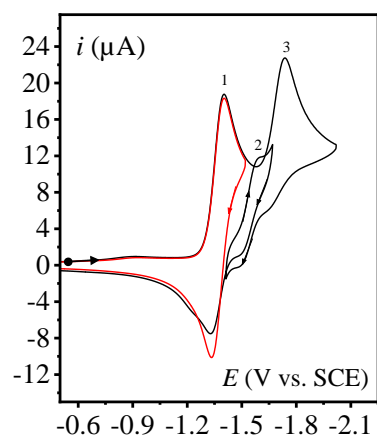
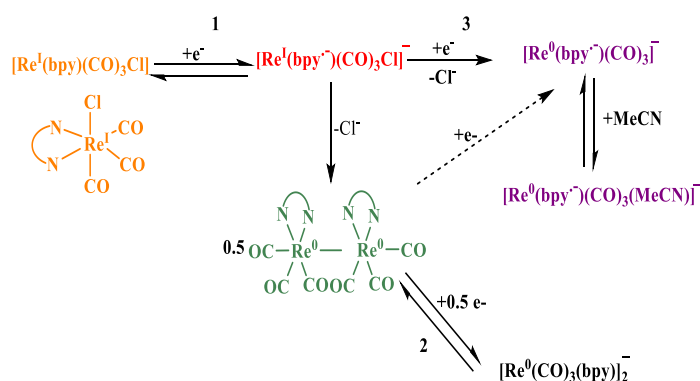


Figure IV.3.1 1: CVs of 1 mM $[\text{Re}(\text{bpy})(\text{CO})_3\text{Cl}]$ under Ar in CH_3CN + 0.1 M $n\text{-Bu}_4\text{NPF}_6$ at 0.05 V/s on a 3 mm diam. GCE.



Scheme IV.3.1 1: Proposed mechanism for the two one electron reductions of $[\text{Re}(\text{bpy})(\text{CO})_3\text{Cl}]$.

The $[\text{Re}(\text{bpy})(\text{CO})_3\text{Cl}]$ complex shows three $\nu(\text{CO})$ bands in its FTIR spectrum in acetonitrile electrolyte at rest potential (2023, 1917 and 1897 cm^{-1}).¹¹ The three facial carbonyl groups are a strong reporter of the electronic structure at the metal center as shown in Figure IV.3.1 3.

The ground state UV-vis spectrum of this complex shows a broad absorption band at high wavelength assigned to a $\text{Re} \rightarrow \pi^*$ bpy singlet metal to ligand charge transfer (MLCT; $\lambda_{\text{max}} = 370\text{ nm}$) which is affected by changing the polarity of the solvent while high energy feature at $\lambda_{\text{max}} < 300\text{ nm}$ is associated with a bpy based $\pi \rightarrow \pi^*$ transition LL charge transfer (LLCT). MLCT are less intense and are always red shifted compared to the $\pi \rightarrow \pi^*$ absorptions¹² as shown in Figure IV.3.1 2 (black spectrum).

When a potential was applied ($E_{\text{app}} = -1.42\text{ V}$) to a solution of $[\text{Re}(\text{bpy})(\text{CO})_3\text{Cl}]$, at a potential slightly more negative than the first reversible wave, the metal-metal bonded dimer $[\text{Re}_2(\text{bpy})_2(\text{CO})_6]$ was formed as a major product. The latter shows two intense absorption bands at 590 and 780 nm, giving a dark green colored solution characteristic of the dimeric species, and a shift of the $\nu(\text{CO})$ bands towards lower energy, with four characteristic $\nu(\text{CO})$ of the dimer ($1986, 1949, 1883$ and 1851 cm^{-1}), is observed.¹³ This dimer can be further reduced at more negative potential ($E_{\text{app}} = -1.82\text{ V}$) to give the the five coordinated bi-reduced complex

$[\text{Re}^0(\text{bpy}^{\bullet-})(\text{CO})_3]^-$. This product exhibits an intense dark purple color solution with a broad and intense absorption band at 570 nm with shoulders (sh) at 522, 636, 689 and 755 nm. Two intense $\nu(\text{CO})$ vibrations at 1943 and 1838 cm^{-1} and also smaller $\nu(\text{CO})$ bands at 1988 and 1869 cm^{-1} (six-coordinated anion $[\text{Re}^0(\text{bpy}^{\bullet-})(\text{CO})_3(\text{MeCN})]^-$) characterize the resulting solution (Figure IV.3.1 3). The absorption band between 500 and 600 nm might be assigned more probably to an electronic transition with a partial $\text{bpy}^{2-} \rightarrow \text{Re}^{\text{I}}$ CT character as shown in Figure IV.3.1 2, in agreement with previous reported work in the literature.^{8,14}

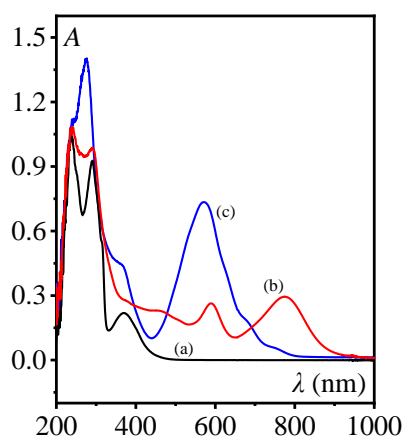


Figure IV.3.1 2 : Absorption spectra obtained during two successive reductive electrolysis of 0.6 mM $[\text{Re}(\text{bpy})(\text{CO})_3\text{Cl}]$ in acetonitrile + 0.1 M $n\text{-Bu}_4\text{NPF}_6$. (a) initial, at applied potential are (b) -1.47 V and (c) -1.82 V, $l = 1$ mm quartz probe.

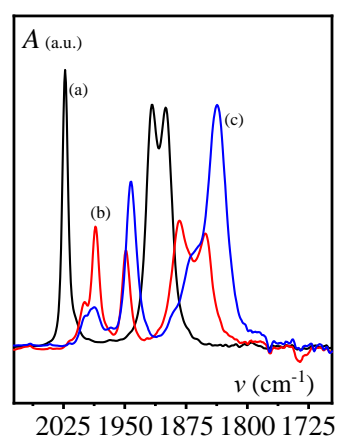
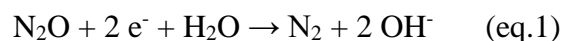


Figure IV.3.1 3 : $\nu(\text{CO})$ FTIR spectral changes following two successive reductive electrolysis of $[\text{Re}(\text{bpy})(\text{CO})_3\text{Cl}]$ (0.6 mM) in acetonitrile + 0.1 M $n\text{-Bu}_4\text{NPF}_6$. (a) initial, at applied potential are (b) -1.47 V and (c) -1.82 V.

3.2 Infrared and UV-vis Spectroelectrochemistry of $[\text{Re}(\text{bpy})(\text{CO})_3(\text{OH})]$

The reduction of N_2O to N_2 , with water as a proton source, gives hydroxide ions OH^- that can be a strong coordinating ligand to the Re center. Moreover, DFT calculations, carried out by our collaborators at CEA-Saclay working on the photoreduction of N_2O with Re equivalent complexes, showed that, after the binding of N_2O to the bi-reduced species, N_2O is reduced to nitrogen gas by two electrons giving also OH^- (eq.1) ions which coordinate to the vacant site on the Re center.



Therefore, we have synthesized the $[\text{Re}(\text{bpy})(\text{CO})_3(\text{OH})]$ complex, (cf experimental part, Synthesis and characterization) and we have characterized it by CV, UV-vis and FTIR spectroscopies. CV analysis was made inside the glovebox in acetonitrile solvent with $n\text{-Bu}_4\text{NPF}_6$ as supporting electrolyte giving first a reversible reduction with $E_{1/2} = -1.43$ V, then a second reduction wave with $E_{\text{pc}} = -1.97$ V, a third wave with $E_{\text{pc}} = -2.11$ V and a fourth wave with $E_{\text{pc}} = -2.60$ V as shown in Figure IV.3.2 1.

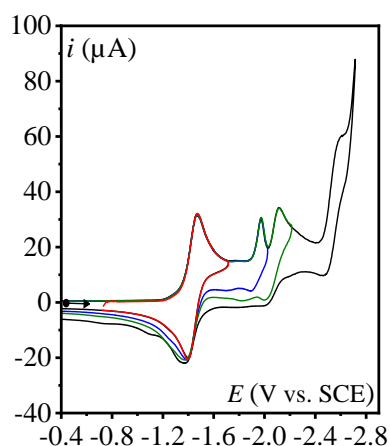


Figure IV.3.2 1 : CVs of 1 mM $[\text{Re}(\text{bpy})(\text{CO})_3(\text{OH})]$ under Ar in $\text{CH}_3\text{CN} + 0.1 \text{ M } n\text{-Bu}_4\text{NPF}_6$ at 0.1 V/s on a 3 mm diam. GCE.

We have observed that the CV run outside the glovebox in less dry conditions under Ar shows the second and the third reduction waves combine into a singly partially reversible one electron reduction wave at less negative potential $E_{\text{pc}} = -1.93 \text{ V}$. This suggests a PCET-type process for the second reduction whereby the OH^- ligand is protonated before being released from the complex. Figures below show the difference in the CVs of the $[\text{Re}(\text{bpy})(\text{CO})_3(\text{OH})]$ run outside (Figure IV.3.2 2) and inside the glovebox (Figure IV.3.2 3) respectively.

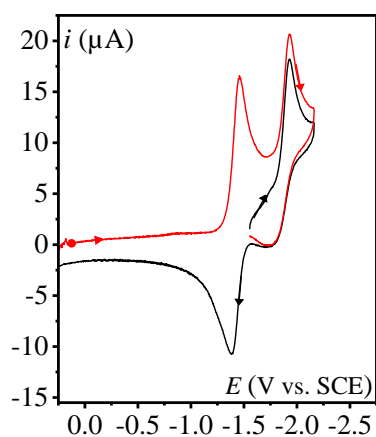


Figure IV.3.2 2 : CVs of 1 mM $[\text{Re}(\text{bpy})(\text{CO})_3(\text{OH})]$ under Ar in $\text{CH}_3\text{CN} + 0.1 \text{ M } n\text{-Bu}_4\text{NPF}_6$ at 0.1 V/s on a 3 mm diam. GCE outside the glovebox.

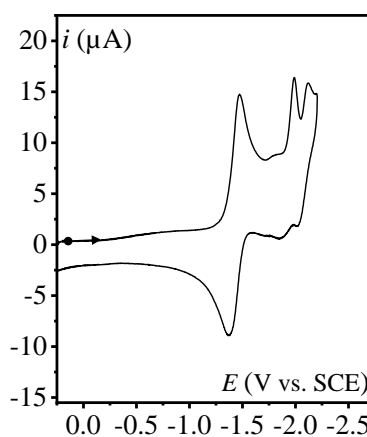


Figure IV.3.2 3 : CV of 1 mM $[\text{Re}(\text{bpy})(\text{CO})_3(\text{OH})]$ under Ar in $\text{CH}_3\text{CN} + 0.1 \text{ M } n\text{-Bu}_4\text{NPF}_6$ at 0.1 V/s on a 3 mm diam. GCE inside the glovebox.

Exhaustive electrolysis was done inside the glovebox on the first reversible wave $E_{\text{app}} = -1.52 \text{ V}$ following the experiment by UV-vis spectroscopy. The evolution of the spectra showed no formation of the dimer suggesting the difficulty in removing OH^- ligand; indeed, it

is a strong donating ligand compared to MeCN and Cl^- as observed by comparing the redox potentials of the first reduction waves shown in Table IV.3.2 1.

Complex	1 st reduction peak potential (vs. SCE)
$[\text{Re}(\text{bpy})(\text{CO})_3(\text{MeCN})]^+$	-1.26 V
$[\text{Re}(\text{bpy})(\text{CO})_3\text{Cl}]$	-1.41 V
$[\text{Re}(\text{bpy})(\text{CO})_3(\text{OH})]$	-1.45 V

Table IV.3.2 1 : First reduction potential of $[\text{Re}(\text{bpy})(\text{CO})_3\text{X}]$ complexes.

Then shifting the potential at the level of the second reduction wave led to the bi-reduced species as characterized by UV-vis (Figure IV.3.2 4) and FTIR analysis (Figure IV.3.2 5) (blue spectra). This shows that the generation of the bi-reduced species $[\text{Re}^0(\text{bpy}^{\bullet-})(\text{CO})_3]^-$ occurs at more negative potential compared to $[\text{Re}(\text{bpy})(\text{CO})_3\text{Cl}]$ and $[\text{Re}(\text{bpy})(\text{CO})_3(\text{MeCN})]\text{PF}_6$.

Table IV.3.2 2 shows the spectroscopic UV-vis and FTIR data of the different rhenium complexes at resting state and single and double reduced oxidation states.

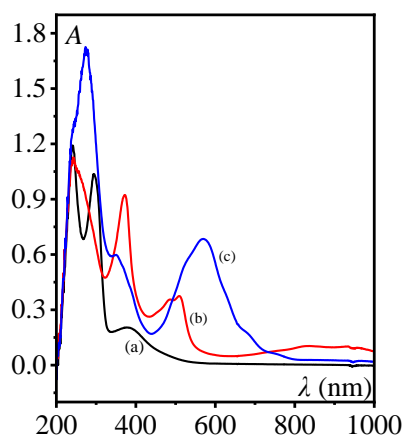


Figure IV.3.2 4 : absorption spectra obtained during two successive reductive electrolysis of 0.87 mM $[\text{Re}(\text{bpy})(\text{CO})_3(\text{OH})]$ in acetonitrile + 0.1 M $n\text{-Bu}_4\text{NPF}_6$. (a) initial, at applied potential (b) -1.52 V and (c) -1.97 V, $l = 1$ mm quartz probe.

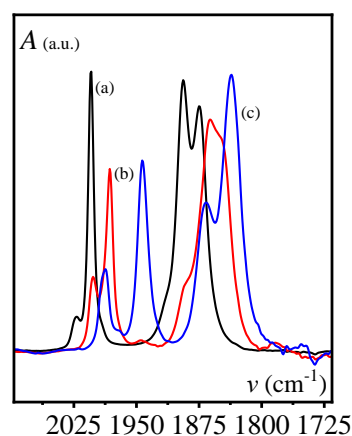


Figure IV.3.2 5 : $\nu(\text{CO})$ FTIR spectral changes following two successive reductive electrolysis of $[\text{Re}(\text{bpy})(\text{CO})_3(\text{OH})]$ (0.87 mM) in acetonitrile + 0.1 M $n\text{-Bu}_4\text{NPF}_6$. (a) initial, at applied potential (b) -1.52 V and (c) -1.97 V.

<i>Spectroscopic properties</i>	<i>Complexes</i>	
UV-Vis λ_{max} , nm	$[\text{Re}^{\text{I}}(\text{bpy})(\text{CO})_3\text{Cl}]$	240, 291, 371
	$[\text{Re}^{\text{I}}(\text{bpy})(\text{CO})_3(\text{MeCN})](\text{PF}_6)$	244, 306, 316, 346(sh)
	$[\text{Re}^{\text{I}}(\text{bpy})(\text{CO})_3(\text{OH})]$	245, 296, 382
	$[\text{Re}^{\text{I}}(\text{bpy}^{\bullet-})(\text{CO})_3\text{Cl}]^-$	502
	$[\text{Re}^{\text{I}}(\text{bpy}^{\bullet-})(\text{CO})_3(\text{OH})]^-$	370, 484, 508
	$[\text{Re}^0(\text{bpy}^{\bullet-})(\text{CO})_3(\text{MeCN})]^-$	496
	$[\text{Re}^0(\text{bpy})(\text{CO})_3]_2$	590, 780
	$[\text{Re}^0(\text{bpy}^{\bullet-})(\text{CO})_3]^-$	572
	FTIR $\nu(\text{CO})$, cm^{-1}	$[\text{Re}^{\text{I}}(\text{bpy})(\text{CO})_3\text{Cl}]$
$[\text{Re}^{\text{I}}(\text{bpy})(\text{CO})_3(\text{MeCN})]\text{PF}_6$		2041, 1938 (br)
$[\text{Re}^{\text{I}}(\text{bpy})(\text{CO})_3(\text{OH})]$		2005, 1894, 1875
$[\text{Re}^0(\text{bpy})(\text{CO})_3]_2$		1986, 1949, 1883, 1851
$[\text{Re}^0(\text{bpy}^{\bullet-})(\text{CO})_3]^-$		1943, 1838 (br)
$[\text{Re}^0(\text{bpy}^{\bullet-})(\text{CO})_3(\text{MeCN})]^-$		1988, 1869
$[\text{Re}^{\text{I}}(\text{bpy}^{\bullet-})(\text{CO})_3(\text{OH})]^-$		2001, 1982, 1859, 1845

Table IV.3.2 2 : Spectroscopic data.

3.3 Reactivity of the bi-reduced species $[\text{Re}^0(\text{bpy}^{\bullet-})(\text{CO})_3]^-$ with N_2O

N_2O gas dissolved in an acetonitrile solution (solubility in acetonitrile: 280 mM) was prepared by well degassing a CH_3CN solution with Ar and then N_2O gas to ensure the saturation and as well the gas phase with N_2O and to bring out dissolved oxygen (air). The solubility of N_2O in different solvents (MeCN, THF, H_2O) was experimentally determined using vacuum triggered flash desolubilization method previously reported for studying the solubility of CO_2 in different solvents (cf. experimental part Determination of solubility of N_2O).¹⁵

The $\text{CH}_3\text{CN} + \text{N}_2\text{O}_{\text{sat}}$ flask was firmly closed and entered into the glovebox. Then, a volume of N_2O dissolved in acetonitrile was added using gas tight Hamilton Microsyringe to the solution of the bi-reduced $[\text{Re}^0(\text{bpy}^{\bullet-})(\text{CO})_3]^-$ species (0.6 mM) while stirring. This led to a known concentration of N_2O in the electrolyte solution (1.5 mM), calculated from the dilution factor of the saturated solution. The evolution of the bi-reduced species when N_2O was added was monitored in-situ by UV-vis absorption spectroscopy using quartz probe. Spectral changes for the reaction of N_2O with the five-coordinated anion showed rapid decay following the absorbance at 570 nm of the absorption of the Re anionic species to almost half of the initial absorbance after 0.5 s with isosbestic points at 355, 477 and 755 nm; Figure IV.3.3 1). Rapid change in color from intense purple to red-orange was observed following the addition of N_2O . This indicates a fast reaction between $[\text{Re}^0(\text{bpy}^{\bullet-})(\text{CO})_3]^-$ and N_2O .

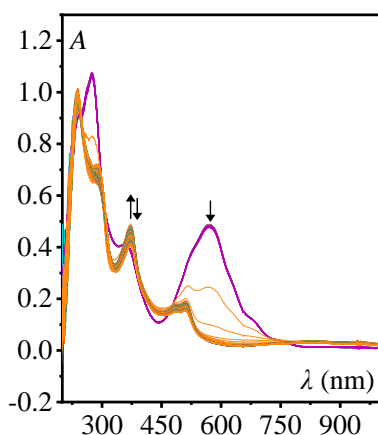


Figure IV.3.3 1 : Evolution of UV-vis spectra taken every 0.5 s, $l = 1$ mm, 0.6 mM solution of $[\text{Re}^0(\text{bpy}^{\bullet-})(\text{CO})_3]^-$ in $\text{CH}_3\text{CN} + 0.1$ M $n\text{-Bu}_4\text{NPF}_6$ with the addition of 1.5 mM of N_2O . In purple initial $t=0$, after addition of N_2O from $t=0.5$ s and > orange, $l = 1$ mm quartz probe.

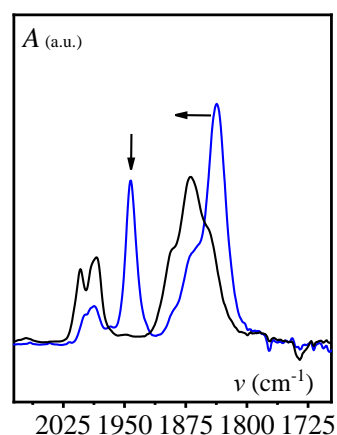


Figure IV.3.3 2 : FTIR spectra collected before (blue) and after addition of 1.5 mM N_2O (black) in CH_3CN .

The reaction leads to a complex exhibiting a shift of $\nu(\text{CO})$ towards higher values with complete disappearance of the characteristic $\nu(\text{CO})$ at 1942 cm^{-1} (Figure IV.3.3 2). We note here that we didn't observe the formation of the dimer which could be formed from $[\text{Re}^I(\text{bpy}^{\bullet-})(\text{CO})_3]$ indicating an inner-sphere ET process rather than an outer-sphere process. This will be confirmed by the kinetic analysis in the following sections. The shift of the carbonyl bands in IR suggests a decrease in the electron density on the metal center which decreases the back donation from the metal to the CO ligands, strengthening more the C-O bond thus increasing the carbonyl stretching frequency. Comparison with authentic samples, we revealed that the carbonyl bands obtained correspond to a mixture of $[\text{Re}^I(\text{bpy}^{\bullet-})(\text{CO})_3(\text{OH})]^-$ and $[\text{Re}^I(\text{bpy})(\text{CO})_3(\text{OH})]$ (vide infra).

The reaction is fast and it can be controlled by mass transport which depends on the stirring of the solution. Nonetheless, based on the decay of the bi-reduced species a lower limit of the pseudo-first-order rate constant can be estimated as $k_{ap} \approx 1.4\text{ s}^{-1}$ (Figure IV.3.3 3). This gives a lower limit of the pseudo-first-order rate constant *ca.* $k_{ap}^{bi} = 250\text{ s}^{-1}$ for a saturated solution of $[\text{N}_2\text{O}] = 280\text{ mM}$.

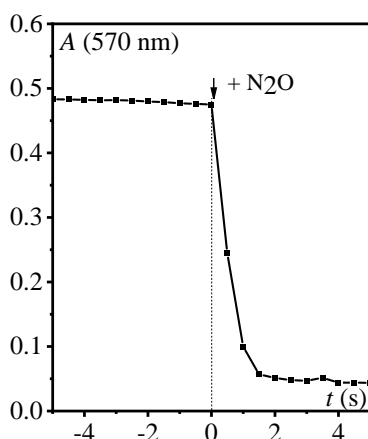


Figure IV.3.3 3 : Time evolution of the absorbance at 570 nm of the bi-reduced species $[Re^0(bpy^{\bullet-})(CO)_3]^-$ following the addition of N_2O .

Cyclic voltammograms were recorded before and after addition of N_2O to the solution of the bi-reduced species showing the appearance of a reversible system with $E_{1/2} = -1.43$ V as well as a new irreversible wave at *ca.* -2.00 V which wasn't spotted before adding N_2O (Figure IV.3.3 4). The reversible wave matches the redox behavior of the synthesized $[Re(bpy)(CO)_3(OH)]$. The second wave is at the same potential as the catalytic wave observed for $[Re(bpy)(CO)_3Cl]$ under N_2O (Figure IV.2 1). Note that, if a larger quantity of N_2O is added, this wave is larger. Hence it can be concluded that the species formed in solution after addition of N_2O is still a competent catalyst for N_2O reduction upon reduction at *ca.* -2 V.

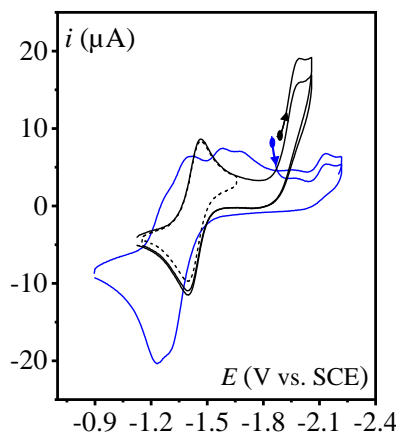


Figure IV.3.3 4 : CVs of 0.6 mM $[Re^0(bpy^{\bullet-})(CO)_3]^-$ before (blue) and after reaction with N_2O 1.5 mM (black) in $CH_3CN + 0.1$ M $n-Bu_4NPF_6$ at 0.1 V/s on a 3 mm diam. GCE.

Successive application of constant oxidative and reductive potential at -1.22 V and -1.52 V respectively to the final solution obtained after addition of N_2O to the solution of the bi-reduced species was followed by FTIR (Figure IV.3.3 5) UV-vis (Figure IV.3.3 6). After each step, both UV-vis and FTIR characterizations showed similar features to

$[\text{Re}(\text{bpy})(\text{CO})_3(\text{OH})]$ and $[\text{Re}^{\text{I}}(\text{bpy}^{\bullet-})(\text{CO})_3(\text{OH})]^-$. Thus, the FTIR data of the solution obtained directly after addition of N_2O to the bi-reduced species gives a mixture of the mono-reduced and neutral form of $[\text{Re}(\text{bpy})(\text{CO})_3(\text{OH})]$. We can thus conclude that a fast reaction is observed between the bi-reduced species and N_2O and we propose the following mechanism of action of the bi-reduced species towards N_2O reduction (Scheme IV.3.3 1).

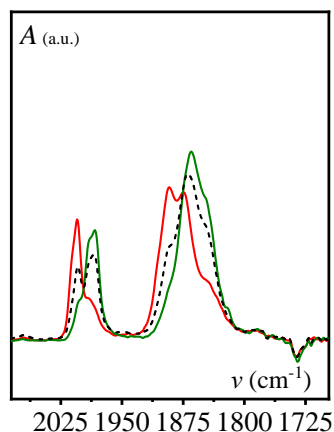


Figure IV.3.3 5 : IR spectra after addition of N_2O to the $[\text{Re}^0(\text{bpy}^{\bullet-})(\text{CO})_3]^-$ solution (dotted line), after $E_{\text{app}} = -1.22$ V (red line) and -1.52 V (green line).

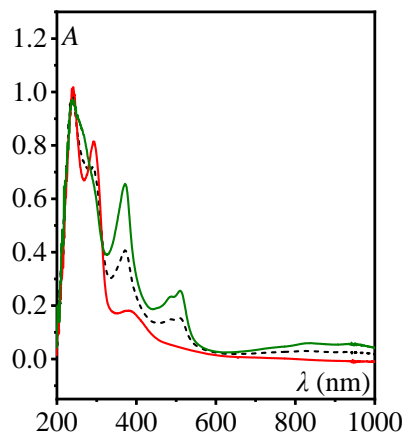
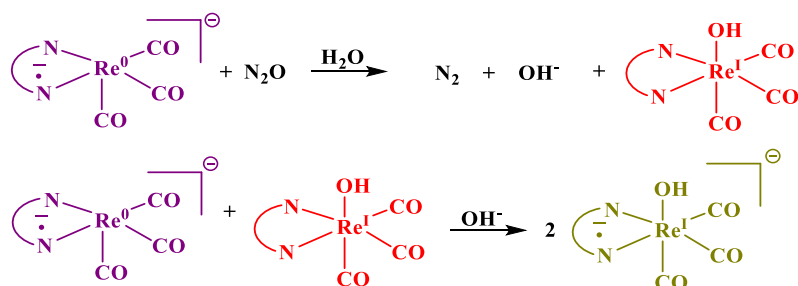


Figure IV.3.3 6 : UV-vis spectra after addition of N_2O to the $[\text{Re}^0(\text{bpy}^{\bullet-})(\text{CO})_3]^-$ solution (dotted line), after $E_{\text{app}} = -1.22$ V (red line) and -1.52 V (green line), $l = 1$ mm quartz probe.



Scheme IV.3.3 1 : Proposed mechanism for the reaction of N_2O with the bi-reduced species $[\text{Re}^0(\text{bpy}^{\bullet-})(\text{CO})_3]^-$.

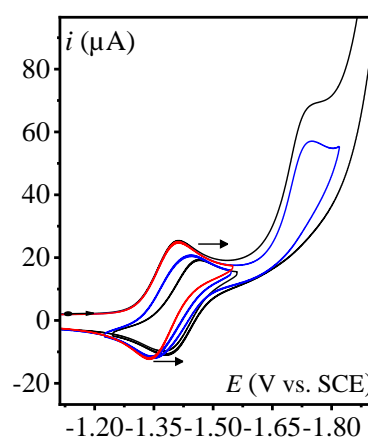
Our results show that the bi-reduced species is able to efficiently reduce N_2O , however, at the potential where $[\text{Re}^0(\text{bpy}^{\bullet-})(\text{CO})_3]^-$ is generated which corresponds to the second reduction wave of $[\text{Re}(\text{bpy})(\text{CO})_3\text{Cl}]$ no substantial catalysis is observed on the time scale of the CV (Figure IV.3.3 7). Rather than a catalytic wave, a reduction wave of *ca.* 1.5-2 electrons per rhenium center was observed as shown by the linear scan voltammetry on a RDE (see Chapter III Figure III.4.2.2 5). What is the reason behind lack of catalysis at the potential of the second wave and why it is not the same as the case for carbon dioxide reduction by the Re complexes which takes place at the second reduction wave? Our results reveal that the reason behind the lack of efficient catalysis is that the free coordination site on the Re center was

coordinated by hydroxide after the first turnover of the reaction of N₂O with the bi-reduced species, thus forming a stable species that, at this potential, cannot regenerate back the active species, namely the bi-reduced species.

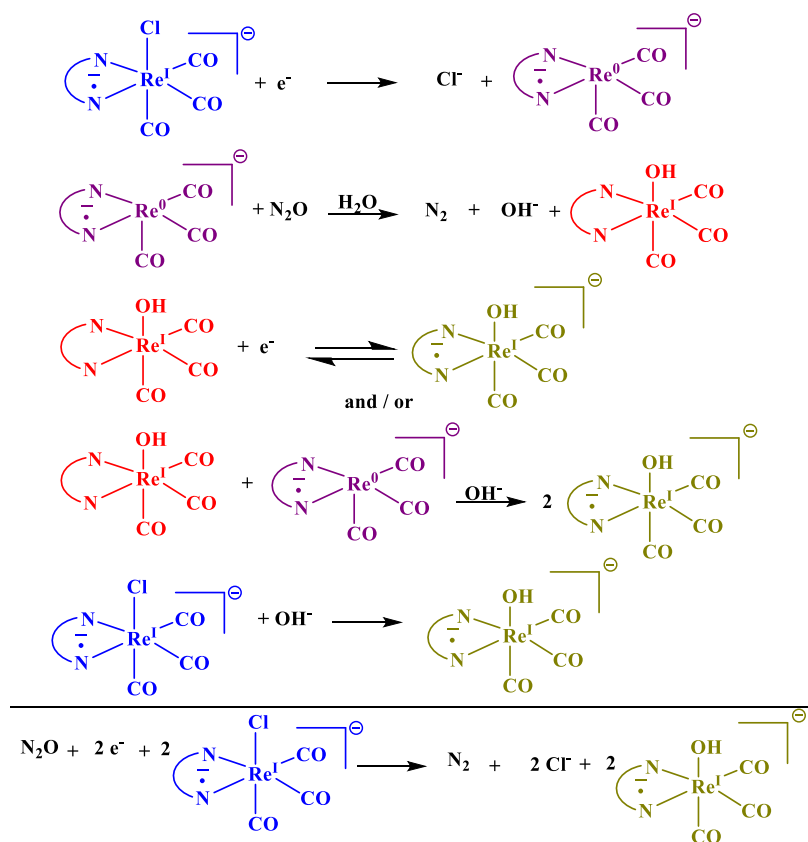
The overall reaction (ECE) process at the level of the second reduction wave of [Re(bpy)(CO)₃Cl] under N₂O thus corresponds to a net reduction of 0.5 N₂O per Re complex followed by a ligand exchange on the Re center corresponding to an electron transfer followed by a chemical step then electron transfer because, at the level of the second wave, the [Re(bpy)(CO)₃(OH)] complex is also reduced (Scheme IV.3.3 2). The fast release of hydroxide requires further reduction at a more negative potential, hence corresponding to the third wave where the catalysis of N₂O is observed. This additional reduction regenerates the bi-reduced species [Re⁰(bpy^{•-})(CO)₃]⁻ via a PCET type reaction. Displacement of hydroxide is thus a requirement to get catalysis at lower overpotential.

As a further confirmation of the proposed mechanism, we note that a shift of the first reversible system towards more negative potential is observed under N₂O atmosphere when reversing the potential at the level of the anodic wave. This shift is more remarkable when passing through the catalytic wave compared to stopping at the potential of the second wave then reversing the current. The reversible system obtained when plotting the CV and passing through the catalytic current corresponds to E_{1/2} = -1.43 V which corresponds to E_{1/2} of redox couple [Re(bpy)(CO)₃(OH)]^{I/0} as shown in Figure IV.3.3 7. Finally, we note that the potential at which the active catalytic bi-reduced species is formed depends on the nature of the labile ligand X present in the initial complex [Re(bpy)(CO)₃X]. Therefore, in the following, we will investigate the role of the labile ligand X.

Figure IV.3.3 7: CVs of 1 mM [Re(bpy)(CO)₃Cl] under N₂O running the CV through the catalytic wave (black), running the CV through the second reduction wave (blue) (both black and blue CVs were reversed at -1.2 V) first reversible reduction wave (red) in CH₃CN + 0.1 M n-Bu₄NPF₆ at 0.1 V/s on a 3 mm diameter GCE.



The scheme below shows the proposed mechanism taking place at the level of the second reduction wave of $[\text{Re}(\text{bpy})(\text{CO})_3\text{Cl}]$ under N_2O atmosphere revealing the increase in the current intensity at the level of this wave reaching almost two electrons. (Scheme IV.3.3 2)



Scheme IV.3.3 2 : Proposed mechanism for the reduction of N_2O at the level of the second reduction wave.

4. Behavior of $[\text{Re}(\text{bpy})(\text{CO})_3(\text{MeCN})]\text{PF}_6$ under N_2O atmosphere

We first recall the electrochemical behavior of $[\text{Re}^{\text{I}}(\text{bpy})(\text{CO})_3(\text{MeCN})]^+$ under Ar, which shows a partially reversible one electron wave ($E_{\text{pc}} = -1.27$ V and $E_{1/2} = -1.23$ V) followed by a second quasi or irreversible reduction at $E_{\text{pc}} = -1.41$ V due to the rapid loss of MeCN and formation of the dimer $[\text{Re}(\text{bpy})(\text{CO})_3]_2$ whose oxidation is observed at -0.10 V (Figure IV.4 1). The first and second reductions of the dimer ($E_{\text{pc}} = -1.57$ and -1.72 V respectively) are easier to be observed in the case of this complex compared to $[\text{Re}(\text{bpy})(\text{CO})_3\text{Cl}]$ due to the shift of the first two reduction peaks towards less negative potential. Generation of the bi-reduced species $[\text{Re}^0(\text{bpy}^{\bullet-})(\text{CO})_3]^-$ occurs at less negative potential than $[\text{Re}(\text{bpy})(\text{CO})_3\text{Cl}]$. A shift of around 300 mV is observed because CH_3CN is more labile (or less σ -donnor) compared to chloride. Scheme IV.4 1 illustrates the proposed mechanism of $[\text{Re}(\text{bpy})(\text{CO})_3(\text{MeCN})]\text{PF}_6$ behavior.

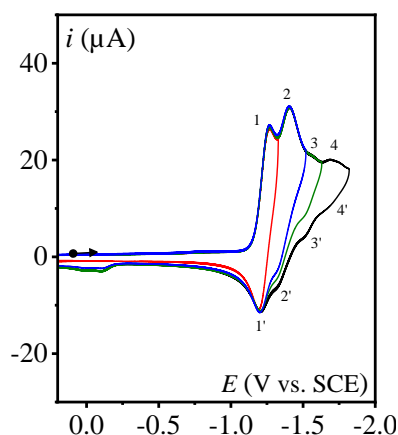
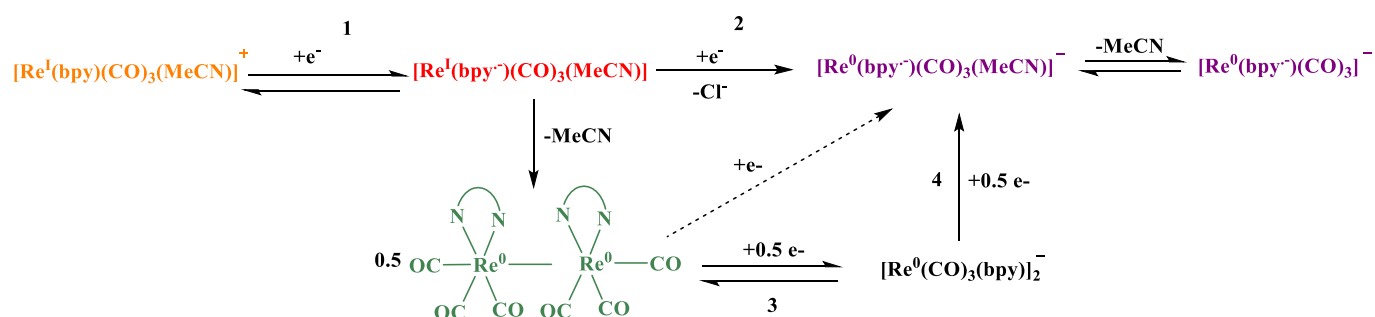


Figure IV.4 1 : CVs of 1 mM $[\text{Re}(\text{bpy})(\text{CO})_3(\text{MeCN})]\text{PF}_6$ under Ar in $\text{CH}_3\text{CN} + 0.1 \text{ M } n\text{-Bu}_4\text{NPF}_6$ at 0.1 V/s on a 3 mm diam. GCE.



Scheme IV.4 1 : Proposed mechanism for the two electrons reduction of $[\text{Re}(\text{bpy})(\text{CO})_3(\text{MeCN})]\text{PF}_6$ under Ar.

In the presence of N_2O the CV of $[\text{Re}(\text{bpy})(\text{CO})_3(\text{MeCN})]^+$ shows first an irreversible wave which slightly increases in intensity compared to the wave under argon but remains monoelectronic and then a reversible system is observed with $E_{1/2} = -1.42 \text{ V}$ (Figure IV.4 2). Finally, a catalytic wave is attained at the same position as the Re complex with chloride, bromide or hydroxide. In all these complexes the catalytic wave is triggered at the potential corresponding to the release of OH^- from $[\text{Re}^{\text{I}}(\text{bpy}^{\bullet-})(\text{CO})_3(\text{OH})]^-$ which was formed on a pre-catalytic wave (Figure IV.4 3).

The loss of reversibility of the first wave of $[\text{Re}(\text{bpy})(\text{CO})_3(\text{MeCN})]^+$ under N_2O led us to the proposal that N_2O might also be reactive at the time scale of the CV with the so-called mono-reduced species $[\text{Re}^{\text{I}}(\text{bpy}^{\bullet-})(\text{CO})_3(\text{MeCN})]$ or presumably $[\text{Re}^{\text{I}}(\text{bpy}^{\bullet-})(\text{CO})_3]$ before it dimerizes. Increasing the scan rate partially restores the reversibility of the first wave on the CV as shown in Figure IV.4 4. This indicates that the pseudo-first order rate constant is of the order of $k_{ap}^{\text{mono,ACN}} \approx 10 \text{ s}^{-1}$ (cf. experimental part) which is smaller than the corresponding rate

constant for the reaction of the bi-reduced species with N_2O (250 s^{-1}) for a saturated solution of $[N_2O] = 280 \text{ mM}$.

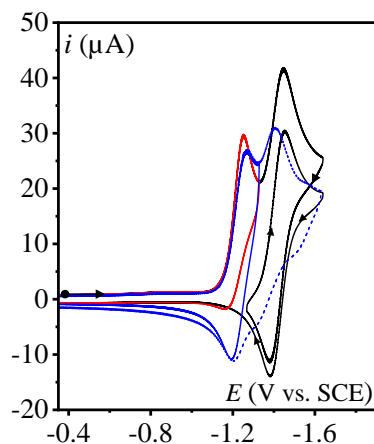


Figure IV.4 2 : CVs of $[Re(bpy)(CO)_3(MeCN)]PF_6$ under argon (blue) full line first reversible wave, dotted line CV run to -1.6 V , under N_2O (red) first reduction wave and black CV run to -1.6 V and reversing the current at -1.2 V , in $CH_3CN + 0.1 \text{ M } n\text{-Bu}_4NPF_6$ at 0.1 V/s on a 3 mm diam. GCE.

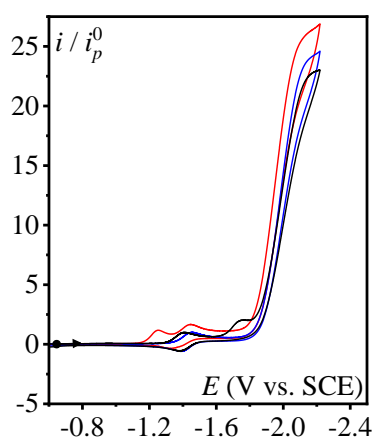


Figure IV.4 3 : Normalized CVs of $[Re(bpy)(CO)_3X]$ under N_2O , $X = CH_3CN$ (red), $X = Cl^-$ (black) and $X = OH^-$ (blue) in $CH_3CN + 0.1 \text{ M } n\text{-Bu}_4NPF_6$ at 0.1 V/s on a 3 mm diam. GCE.

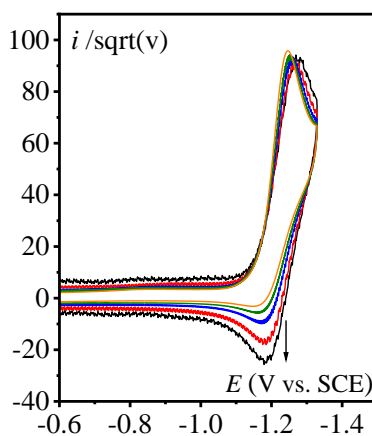


Figure IV.4 4 : Normalized CVs by \sqrt{v} of $[Re(bpy)(CO)_3(MeCN)]PF_6$ in $CH_3CN + 0.1 \text{ M } n\text{-Bu}_4NPF_6$ on a 3 mm diam. GCE under N_2O atmosphere at 0.05 (orange), 0.1 (green), 0.2 (blue), 0.5 (red) and 1 (black) V/s .

Exhaustive electrolysis was thus performed on the first reduction wave of $[Re(bpy)(CO)_3(MeCN)]^+$, with N_2O already present in the solution, in the glovebox to investigate the nature of the species obtained. CVs run after electrolysis showed no to little decrease in the intensity of the catalytic current (Figure IV.4 5) and here again a reversible system with $E_{1/2} = -1.43 \text{ V}$ was observed (Figure IV.4 6). The FTIR with major $\nu(CO)$ at 2005 , 1894 and 1877 cm^{-1} (Figure IV.4 7) and the UV-vis (Figure IV.4 8) obtained characterize the formation of the $[Re^I(bpy)(CO)_3(OH)]$. We also note that no dimer was formed indicating that

reaction of N_2O with $[\text{Re}^{\text{I}}(\text{bpy}^{\bullet-})(\text{CO})_3]^+$ is faster than the dimerization reaction (Re(0)-Re(0) bond formation).

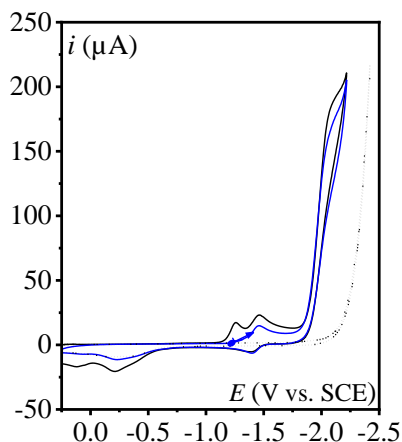


Figure IV.4 5 : CVs of direct reduction of N_2O (black short dot) with $0.53 \text{ mM } [\text{Re}(\text{bpy})(\text{CO})_3(\text{MeCN})]\text{PF}_6$ in the presence of $280 \text{ mM } \text{N}_2\text{O}$ in the solution before (black) and after $E_{\text{app}} = -1.2 \text{ V}$ (blue), in $\text{CH}_3\text{CN} + 0.1 \text{ M } n\text{-Bu}_4\text{NPF}_6$ at 0.1 V/s on a 3 mm diam. GCE

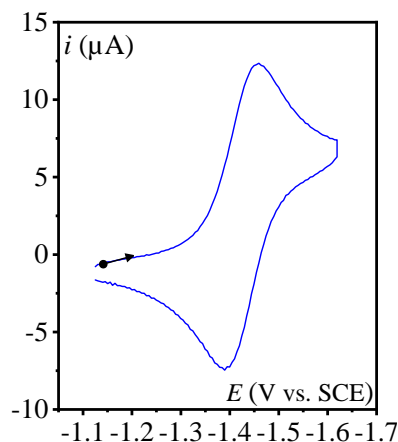


Figure IV.4 6 : CV of the reversible system obtained after $E_{\text{app}} = -1.20 \text{ V}$ in $\text{CH}_3\text{CN} + 0.1 \text{ M } n\text{-Bu}_4\text{NPF}_6$ at 0.1 V/s on a 3 mm diam. GCE

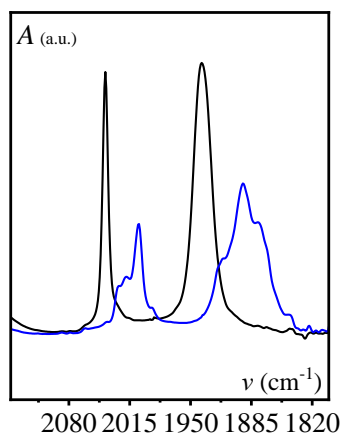


Figure IV.4 7 : FTIR spectra of $0.53 \text{ mM } [\text{Re}(\text{bpy})(\text{CO})_3(\text{MeCN})]\text{PF}_6$ before (black) and after $E_{\text{app}} = -1.22 \text{ V}$ (blue) in the presence of N_2O in solution.

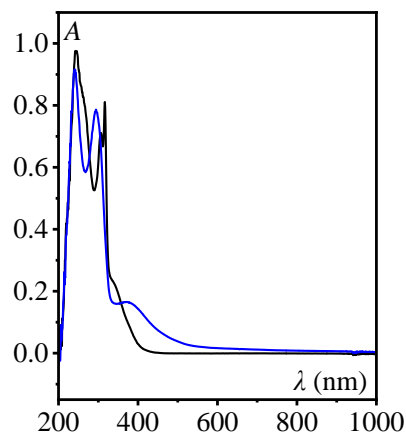


Figure IV.4 8 : UV-vis spectra of $0.53 \text{ mM } [\text{Re}(\text{bpy})(\text{CO})_3(\text{MeCN})]\text{PF}_6$ before (black) and after $E_{\text{app}} = -1.22 \text{ V}$ (blue) in the presence of N_2O in solution $l = 1 \text{ mm}$ quartz probe.

CPE was also performed under the continuous flow of N_2O through the cell at -1.22 V monitoring the UV-vis evolution in the bulk. It showed quantitative transformation of $[\text{Re}^{\text{I}}(\text{bpy})(\text{CO})_3(\text{MeCN})]^+$ to $[\text{Re}^{\text{I}}(\text{bpy})(\text{CO})_3(\text{OH})]$ with the formation of an isosbestic point at $\lambda_{\text{max}} = 362 \text{ nm}$ showing clean transformation without formation of intermediates (Figure IV.4 9 and Figure IV.4 10). This indicates that the reaction of N_2O and the mono-reduced species $[\text{Re}^{\text{I}}(\text{bpy}^{\bullet-})(\text{CO})_3(\text{MeCN})]$ is fast and takes place in the diffusion

reaction layer which thickness is roughly $\mu \approx \sqrt{D/k_{\text{ap}}^{\text{mono,ACN}}} \approx 7 \mu\text{m}$ with $D \approx 5 \cdot 10^{-6} \text{ cm}^2/\text{s}$ the

rhodium complex diffusion coefficient and $k_{ap}^{mono,ACN} \approx 10 \text{ s}^{-1}$ the pseudo-first order rate constant.¹⁶

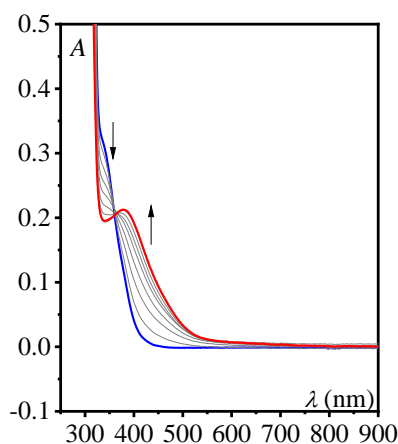


Figure IV.4 9 : Evolution of the UV-vis spectrum (1 spectrum/250 s) $l = 1 \text{ mm}$ of the bulk solution upon electrolysis at -1.22 V of 1 mM $[\text{Re}(\text{bpy})(\text{CO})_3(\text{MeCN})]\text{PF}_6$ in CH_3CN + 0.1 M $n\text{Bu}_4\text{NPF}_6$ under flux of N_2O . Blue is the initial spectrum and red is the final spectrum. "Reprinted with permission from [ACS Catal. 2023, 13, 12, 8262–8272]. Copyright [2023] American chemical Society".

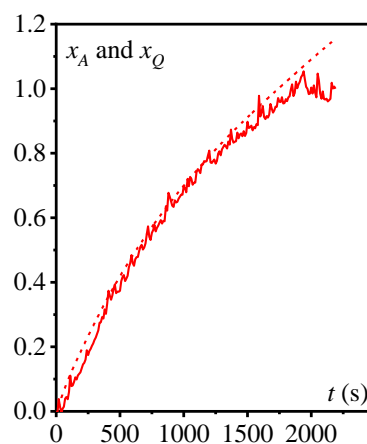
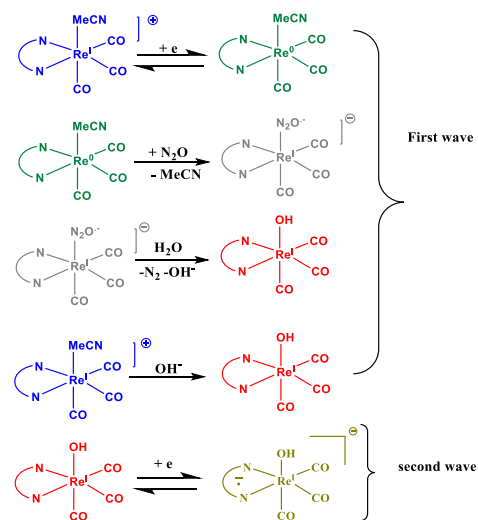


Figure IV.4 10 : Full red line normalized absorption at 450 nm $X_A = A/A_0$ ($t > 2000\text{s}$) and dashed line normalized charge consumed $X_Q = Q/nF$. "Reprinted with permission from [ACS Catal. 2023, 13, 12, 8262–8272]. Copyright [2023] American chemical Society".

We can now rationalize the CV of $[\text{Re}^{\text{I}}(\text{bpy})(\text{CO})_3(\text{MeCN})]\text{PF}_6$ in the presence of N_2O . It exhibits a first mono-electronic irreversible wave corresponding to the net reduction of 0.5 equivalent of N_2O and substitution of acetonitrile by hydroxide on the $\text{Re}(\text{I})$. It is followed by the reversible mono-electronic reduction of $[\text{Re}^{\text{I}}(\text{bpy})(\text{CO})_3(\text{OH})]$. The stoichiometry of the waves was attested by RDE as shown in Chapter III (Figure III.4.2.2 3). Thus we can propose a mechanism of action on the time scale of the CV (Scheme IV.4 2).

Scheme IV.4 2 : Proposed mechanism for the behavior of $[\text{Re}^{\text{I}}(\text{bpy})(\text{CO})_3(\text{MeCN})]^+$ in the presence of N_2O (first and second reduction wave).



5. Behavior of mono-reduced species of $[\text{Re}(\text{bpy})(\text{CO})_3\text{Cl}]$ and $[\text{Re}(\text{bpy})(\text{CO})_3(\text{OH})]$ with N_2O

After the observation of the reaction of the mono-reduced species of $[\text{Re}(\text{bpy})(\text{CO})_3(\text{MeCN})]\text{PF}_6$ with N_2O we decided to investigate on the behavior of the mono-reduced species of $[\text{Re}(\text{bpy})(\text{CO})_3\text{Cl}]$ and $[\text{Re}(\text{bpy})(\text{CO})_3(\text{OH})]$ complexes with N_2O . On the time scale of the CV the first reversible reduction of $[\text{Re}(\text{bpy})(\text{CO})_3(\text{OH})]$ and $[\text{Re}(\text{bpy})(\text{CO})_3\text{Cl}]$ remains unchanged under N_2O (Figure IV.5 1 and Figure IV.5 2).

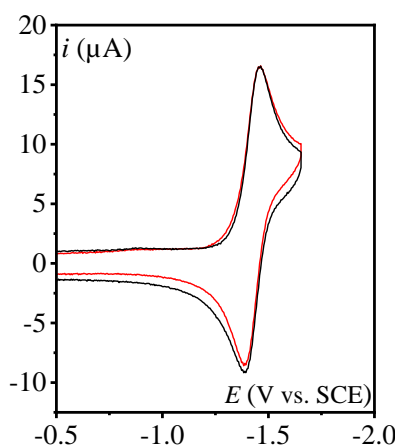


Figure IV.5 1 : CVs of $[\text{Re}(\text{bpy})(\text{CO})_3(\text{OH})]$ under Ar (black) and under N_2O (red) in $\text{CH}_3\text{CN} + 0.1 \text{ M } n\text{-Bu}_4\text{NPF}_6$ at 0.1 V/s on a 3 mm diam. GCE.

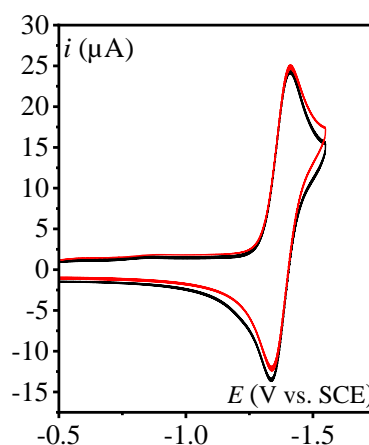


Figure IV.5 2 : CVs of $[\text{Re}(\text{bpy})(\text{CO})_3\text{Cl}]$ under Ar (black) and under N_2O (red) in $\text{CH}_3\text{CN} + 0.1 \text{ M } n\text{-Bu}_4\text{NPF}_6$ at 0.1 V/s on a 3 mm diam. GCE.

We performed CPE at the potential of the first reduction wave of the $[\text{Re}(\text{bpy})(\text{CO})_3\text{Cl}]$ in the presence of N_2O in the glovebox using carbon felt as WE and monitoring the progress of the reaction by in-situ UV-vis and FTIR. No formation of the dimer was observed. It is at variance with the electrolysis made without N_2O under Ar which leads to the formation of the dimer $[\text{Re}^0(\text{bpy})(\text{CO})_3]_2$. This confirms that N_2O coordinates to the vacant site after the slow dehalogenation of the $[\text{Re}^I(\text{bpy}^{\bullet-})(\text{CO})_3\text{Cl}]^-$. Figure IV.5 3 shows the direct reduction of N_2O and the behavior of the catalyst in the presence of N_2O . On the same figure is shown the CV plotted after $E_{\text{app}} = -1.37 \text{ V vs. SCE}$ revealing that the catalytic wave remained at the same position; it didn't change compared to before electrolysis but the second wave has completely disappeared. A shift of the first reversible wave towards slightly more negative potential was observed shown in (blue) with $E_{1/2} = -1.43 \text{ V}$ and it occurs at the same potential as the reversible system of the $[\text{Re}(\text{bpy})(\text{CO})_3(\text{OH})]^{I/0}$ complex shown in (Figure IV.5 4).

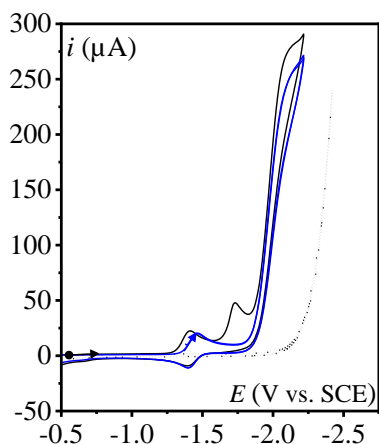


Figure IV.5 3 : CVs of direct reduction of N_2O (black short dot) with 1 mM $[Re(bpy)(CO)_3Cl]$ in the presence of N_2O in the solution before (black) and after $E_{app} = -1.37$ V (blue), in CH_3CN solution in the presence of 280 mM N_2O + 0.1 M $n-Bu_4NPF_6$ at 0.1 V/s on a 3 mm diameter GCE.

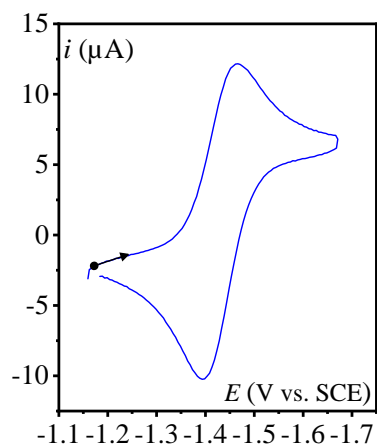


Figure IV.5 4 : Reversible reduction system obtained after $E_{app} = -1.37$ V in CH_3CN solution in the presence of 280 mM N_2O + 0.1 M $n-Bu_4NPF_6$ at 0.1 V/s on a 3 mm diameter GCE.

Figure IV.5 5 shows the FTIR vibrations of the $\nu(CO)$ / at 2006, 1895 and 1877 cm^{-1} has shifted towards lower wavenumbers, similar values to the ones obtained with an authentic sample of $[Re(bpy)(CO)_3(OH)]$. UV-vis data obtained after electrolysis also confirms formation of $[Re(bpy)(CO)_3(OH)]$ (Figure IV.5 6).

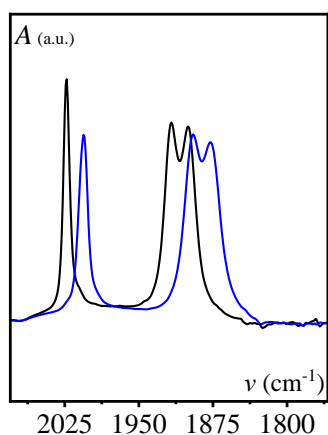


Figure IV.5 5 : FTIR spectra of 1 mM $[Re(bpy)(CO)_3Cl]$ before (black) and after $E_{app} = -1.37$ V (blue) in the presence of 280 mM N_2O .

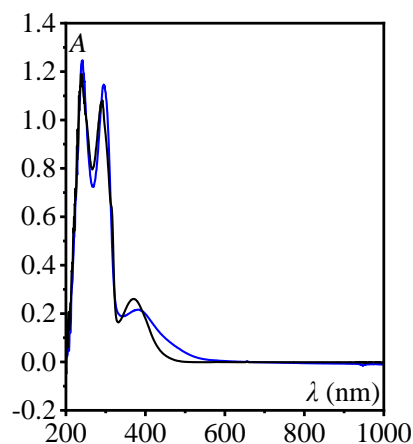


Figure IV.5 6 : UV-vis spectra of 1 mM $[Re(bpy)(CO)_3Cl]$ before (black) and after $E_{app} = -1.37$ V (blue) in the presence of 280 mM N_2O $l = 1$ mm quartz probe.

CPE was also performed under continuous flow of N_2O at -1.37 V monitoring the UV-vis evolution in the bulk. We observe in the first 15 min, decrease in the concentration of $[Re(bpy)(CO)_3Cl]$ along with the formation of $[Re(bpy)(CO)_3(OH)]$ without formation of the dimer and also no observation of $[Re^I(bpy^{\bullet-})(CO)_3Cl]^-$ which shows that this species once

formed at the electrode surface does not accumulate in the bulk solution but reacts with N₂O. However, this reaction is slow enough for not taking place on the CV time scale. After that, we observe the appearance of a new compound with a broad absorption band in the visible region. It was attributed to a degraded product of the rhenium complex.

Direct evaluation of the pseudo-first order rate constant of the reaction of N₂O with [Re^I(bpy^{•-})(CO)₃Cl]⁻ is not possible because electrogeneration of a solution of this species is unachievable since it's dehalogenation leads directly to the dimer. Moreover, the targeted reaction is too slow to take place on the time scale of the CV. Nonetheless, a lower limit $k_{ap}^{mono,Cl}$ can be estimated from the absence of observation of [Re^I(bpy^{•-})(CO)₃Cl]⁻ in the bulk which gives an estimated value of $k_{ap}^{mono,Cl} > 0.5 \text{ s}^{-1}$ (cf. experimental part).

Electrolysis at -1.37 V was also performed in a tight closed cell under N₂O in the presence of [Re(bpy)(CO)₃Cl]. GC analysis of the electrolysis cell headspace allows determination of the quantity of N₂ produced and reveals that after passing a charge of 10 C the faradaic yield for N₂O to N₂ conversion is 100 %.

Starting now from [Re(bpy)(CO)₃(OH)], electrolysis at -1.42 V was performed under a flux of N₂O monitoring the UV-vis evolution using in situ UV-vis probe. A prolonged current was observed passing a charge of 12 C after 4 h of electrolysis corresponding to 9.2 moles of electron per mole of rhenium. UV-vis monitoring of the solution shows that [Re(bpy)(CO)₃(OH)] is slowly converted in the bulk. This indicates that once [Re^I(bpy^{•-})(CO)₃(OH)]⁻ is formed close to the electrode surface it reacts with N₂O on its way back to the bulk giving back [Re(bpy)(CO)₃(OH)]. After 15 min of applying constant potential the [Re(bpy)(CO)₃(OH)] started to be converted in the bulk into a new compound with a broad absorption band in the visible region. This could suggest a decarbonylation reaction of the Re complex or a degradation of the catalyst.

To better characterize the behavior of N₂O with the mono-reduced species [Re^I(bpy^{•-})(CO)₃(OH)]⁻, a solution of the mono-reduced species (0.8 mM) was electrogenerated by applying a constant potential at -1.52 V then adding a slight excess of 1.16 mM N₂O gas dissolved in acetonitrile solution. A fast decay in the UV-vis evolution at 508 nm was observed upon addition of N₂O to the solution of the mono-reduced species; this fast decay is probably due to the reaction of N₂O with bi-reduced species due to slight over reduction of [Re(bpy)(CO)₃(OH)]. Then a slow decay was observed which corresponds to the

reaction of $[\text{Re}^{\text{I}}(\text{bpy}^{\bullet-})(\text{CO})_3(\text{OH})]^-$ with N_2O . An estimation of the pseudo first order rate constant for the reaction of $[\text{Re}^{\text{I}}(\text{bpy}^{\bullet-})(\text{CO})_3(\text{OH})]^-$ and N_2O from the UV-vis evolution gave $k_{\text{ap}}^{\text{mono,OH}} = 0.04 \text{ s}^{-1}$ (cf. experimental part). We thus conclude that the electrochemical reduction of N_2O by $[\text{Re}^{\text{I}}(\text{bpy}^{\bullet-})(\text{CO})_3(\text{OH})]^-$ is a slow process which is attributed to the difficulty of replacing the hydroxide by N_2O in $[\text{Re}^{\text{I}}(\text{bpy}^{\bullet-})(\text{CO})_3(\text{OH})]^-$ along with decarbonylation reaction which can be detrimental for the catalyst.

In order to prolong the catalytic activity of the mono-reduced species of $[\text{Re}(\text{bpy})(\text{CO})_3\text{Cl}]$ towards N_2O reduction and to slow down its degradation, addition of free chlorides Et_4NCl could be a good idea to sustain catalysis by preventing hydroxide coordination to the Re center and / or displacing hydroxide by chloride. Electrolysis at -1.37 V of $[\text{Re}(\text{bpy})(\text{CO})_3\text{Cl}]$ through a continuous flux of N_2O in the presence of 100 mM Et_4NCl gave higher current compared to the electrolysis run in the absence of Et_4NCl because excess of chloride allows the regeneration of $[\text{Re}^{\text{I}}(\text{bpy}^{\bullet-})(\text{CO})_3\text{Cl}]^-$ allowing to do more than one catalytic cycle (Figure IV.5 7). After a while and due to the deoxygenation of N_2O to N_2 accompanied with the release of OH^- this slows the regeneration of $[\text{Re}^{\text{I}}(\text{bpy}^{\bullet-})(\text{CO})_3\text{Cl}]^-$.

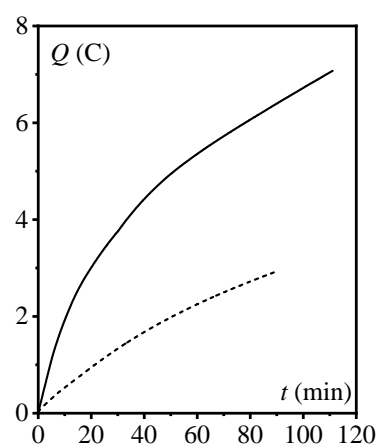


Figure IV.5 7 : Charge consumed upon electrolysis at -1.37 V of $[\text{Re}(\text{bpy})(\text{CO})_3\text{Cl}]$ 0.88 mM in $\text{CH}_3\text{CN} + 0.1 \text{ M}$ $n\text{-Bu}_4\text{NPF}_6$ under N_2O with 100 mM Et_4NCl (full line) and in the absence of Et_4NCl (dotted). "Reprinted with permission from [ACS Catal. 2023, 13, 12, 8262–8272]. Copyright [2023] American chemical Society".

The time evolution of the charge passed was initially fast due to an innersphere process but then kept increasing at slower pace when $[\text{Re}(\text{bpy})(\text{CO})_3(\text{OH})]$ is dominant in the bulk after 30 min of electrolysis (Figure IV.5 7-Figure IV.5 8). Also, after some times during electrolysis we start to observe a product with broad absorption band in the visible region which we attribute to the degraded product due to the decarbonylation of the complex (Figure IV.5 9).

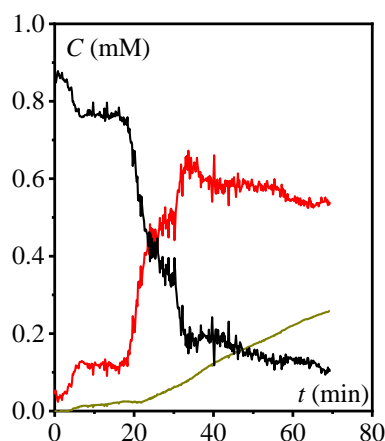


Figure IV.5 8: Time evolution of the species $[\text{Re}(\text{bpy})(\text{CO})_3\text{Cl}]$ (black), $[\text{Re}(\text{bpy})(\text{CO})_3(\text{OH})]$ (red) and the degraded product (dark yellow) monitored by in-situ UV-vis probe in the bulk during electrolysis $E_{\text{app}} = -1.37$ V of 0.88 mM $[\text{Re}(\text{bpy})(\text{CO})_3\text{Cl}] + 100$ mM Et_4NCl under the flux of N_2O . "Reprinted with permission from [ACS Catal. 2023, 13, 12, 8262–8272]. Copyright [2023] American chemical Society".

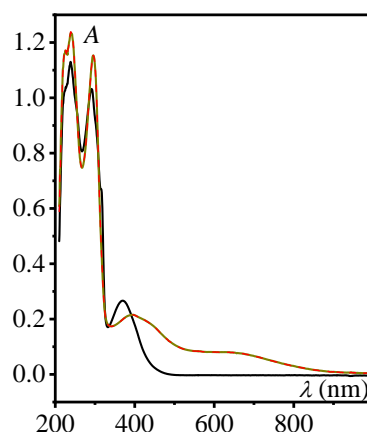
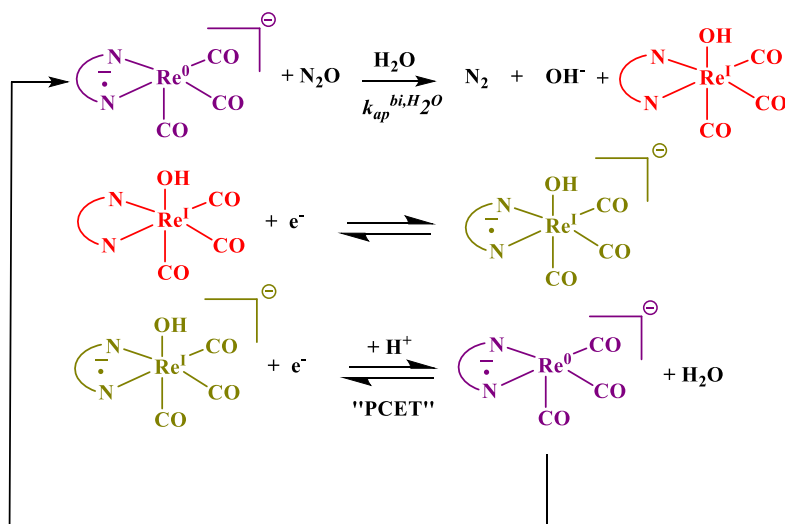


Figure IV.5 9: 0.88 mM $[\text{Re}(\text{bpy})(\text{CO})_3\text{Cl}]$ (black) and degraded complex observed during electrolysis (dark yellow). "Reprinted with permission from [ACS Catal. 2023, 13, 12, 8262–8272]. Copyright [2023] American chemical Society".

6. Overall recap of the electrochemical reduction of N_2O by $[\text{Re}(\text{bpy})(\text{CO})_3\text{X}]^{n+}$ ($\text{X} = \text{CH}_3\text{CN}, \text{Cl}^-$ and OH^- , $n = 0$ or 1)

We have demonstrated that the bi-reduced species $[\text{Re}^0(\text{bpy}^{\bullet-})(\text{CO})_3]^-$ is the active catalytic species required for the electrochemical reduction of N_2O with a pseudo-first-order rate constant in the presence of N_2O saturated in acetonitrile solution and in the absence of proton source $k_{\text{ap}}^{\text{bi}} = 250$ s $^{-1}$. Considering pure kinetic conditions where N_2O is in excess in which the concentration of N_2O at the electrode surface is equal to the bulk concentration, the corresponding plateau current in CV can then be obtained by $i_{\text{pl}} = FSC_{\text{cat}}^0 \sqrt{2Dk_{\text{ap}}^{\text{bi}}} = 337$ μA which is the order of magnitude of the catalytic current observed experimentally (Figure IV.5 3). As observed in the previous Chapter, the addition of water is important because it shifts the onset of the catalytic wave towards less negative potential and also causes increase in the plateau current intensity. Water is actually important to regenerate the vacant coordination site on the bi-reduced species $[\text{Re}^0(\text{bpy}^{\bullet-})(\text{CO})_3]^-$ from $[\text{Re}^1(\text{bpy}^{\bullet-})(\text{CO})_3(\text{OH})]^-$ via a "PCET" type process. Also, water is involved in the N-O bond breaking by stabilizing the oxygen atom.

Scheme IV.6 1 shows the catalytic cycle for the reduction of N_2O by the bi-reduced species $[\text{Re}^0(\text{bpy}^{\bullet-})(\text{CO})_3]^-$.



Scheme IV.6 1 : Catalytic reduction of N_2O via $[Re^0(bpy^{\bullet-})(CO)_3]^-$.

Based on the activation driving force relationship build-up between the rate constant and the standard potential of the catalyst developed in Chapter II for homogeneous outersphere reduction of N_2O , the evaluated rate constant $k_{ap}^{bi} = 250 \text{ s}^{-1}$ would correspond to an electron donor with a standard potential of ca. -1.97 V which is more negative than the oxidation potential of $[Re^0(bpy^{\bullet-})(CO)_3]^-$ evaluated to be -1.36 V (Figure IV.6 2). This confirms that a vacant coordination site on the metal center is required for the binding of N_2O , which demands the release of OH^- from the precatalytic species $[Re^I(bpy^{\bullet-})(CO)_3(OH)]^-$ to trigger catalysis. Since the product formed from the innersphere activation of N_2O and the bi-reduced species $[Re^0(bpy^{\bullet-})(CO)_3]^-$ is the hydroxide complex then this confirms that the binding of N_2O to the metal center occurs via the oxygen atom and not through the central electrophilic nitrogen atom. Differently in the case of carbon dioxide reduction activation, the binding of CO_2 to the rhenium center occurs through the central electrophilic carbon atom.^{17,18,19,20}

However, reaching the bi-reduced species is not mandatory to reduce N_2O into N_2 . As shown in the previous section the monoreduced species $[Re^I(bpy^{\bullet-})(CO)_3]$ can also reduce N_2O but at slower rates compared to the bi-reduced species $[Re^0(bpy^{\bullet-})(CO)_3]^-$ $k_{ap}^{mono,ACN} \approx 10 \text{ s}^{-1}$ (pseudo-first order rate constant in N_2O saturated acetonitrile solution). Based on the standard potential of $[Re^I(bpy^{\bullet-})(CO)_3]$, (-1.23 V), we can deduce that the reduction of N_2O by $[Re^I(bpy^{\bullet-})(CO)_3]$ is much faster than the one predicted for an outersphere electron transfer.²¹ On the other hand $[Re^I(bpy^{\bullet-})(CO)_3(OH)]^-$ is able to reduce N_2O but with small rate constant

$k_{ap}^{mono,OH} = 0.04 \text{ s}^{-1}$ (pseudo-first order rate constant in N_2O saturated acetonitrile solution).

Taking into account that the standard potential of $[\text{Re}^{\text{I}}(\text{bpy})(\text{CO})_3(\text{OH})]^{0/-}$ is -1.43 V, it seems to align on the activation-driving force correlation predicted for an outersphere electron transfer process since it is difficult for N_2O to displace the strong hydroxide ligand, thus preventing the inner sphere activation of N_2O (Figure IV.6 2).

Concerning the mono-reduced species of $[\text{Re}^{\text{I}}(\text{bpy}^{\bullet-})(\text{CO})_3\text{Cl}]^-$ it is able to reduce N_2O with a rate constant of $k_{ap}^{mono,Cl} > 0.5 \text{ s}^{-1}$. This reaction of N_2O and the mono-reduced species is too slow to take place on the CV time scale but observed when running electrolysis of $[\text{Re}(\text{bpy})(\text{CO})_3\text{Cl}]$ in the presence of N_2O where no formation of the dimer is observed. This rate constant corresponds first to the loss of chloride then binding of N_2O to the vacant site. Taking into account the standard potential of $[\text{Re}^{\text{I}}(\text{bpy})(\text{CO})_3\text{Cl}]^{0/-}$ is -1.38 V, this indicates that the reaction is an innersphere electron transfer process rather than outersphere based on the rate constant and standard potential of the catalyst relationship. This demonstrates that hydroxide cannot be displaced by N_2O while chloride can be, but only after the $[\text{Re}(\text{bpy})(\text{CO})_3\text{Cl}]$ complex has been singly reduced. It is in accord with the fact that chloride is more labile than hydroxide as $[\text{Re}^{\text{I}}(\text{bpy}^{\bullet-})(\text{CO})_3(\text{OH})]^-$ is stable in solution whereas, due to spontaneous dechlorination, $[\text{Re}^{\text{I}}(\text{bpy}^{\bullet-})(\text{CO})_3\text{Cl}]^-$ evolves towards the formation of the dimer $[\text{Re}^0(\text{bpy})(\text{CO})_3]_2$. Therefore, catalysis of N_2O reduction via an innersphere process by $[\text{Re}^{\text{I}}(\text{bpy}^{\bullet-})(\text{CO})_3\text{Cl}]^-$ can be elongated by addition of excess of chlorides before switching into slower outersphere process due to the formation of $[\text{Re}(\text{bpy})(\text{CO})_3(\text{OH})]$. This is revealed by the exchange of OH^- by Cl^- upon addition of excess of chloride to electrogenerated solution of $[\text{Re}^{\text{I}}(\text{bpy}^{\bullet-})(\text{CO})_3(\text{OH})]^-$ forming the mono-reduced species $[\text{Re}^{\text{I}}(\text{bpy}^{\bullet-})(\text{CO})_3\text{Cl}]^-$ and later on evolves towards dimer $[\text{Re}^0(\text{bpy})(\text{CO})_3]_2$ formation (Figure IV.6 1). This illustrates the role of ligand exchange which can drive the catalytic process to move in a slower mode due to the generation of co-product (OH^-) during the reaction.

This illustrates the role of ligand exchange which can drive the catalytic process to move in a slower mode due to the generation of co-product (OH^-) during the reaction.

Figure IV.6 1 : UV-vis spectra of solution of 1 mM $[\text{Re}^{\text{I}}(\text{bpy}^{\ast-})(\text{CO})_3(\text{OH})]^-$ before (orange) and after addition of excess Et_4NCl 27 mM; after 5 s (blue) 10 s (red) then evolution towards formation of the dimer $[\text{Re}^0(\text{bpy})(\text{CO})_3]_2$ (green).

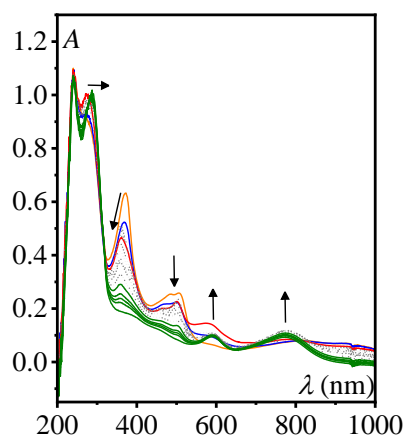
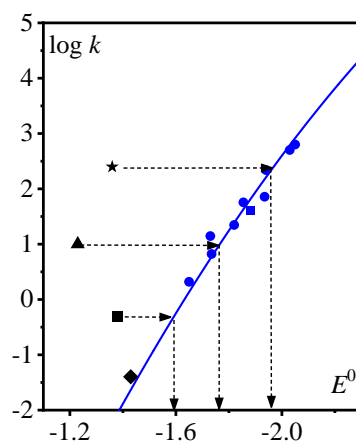
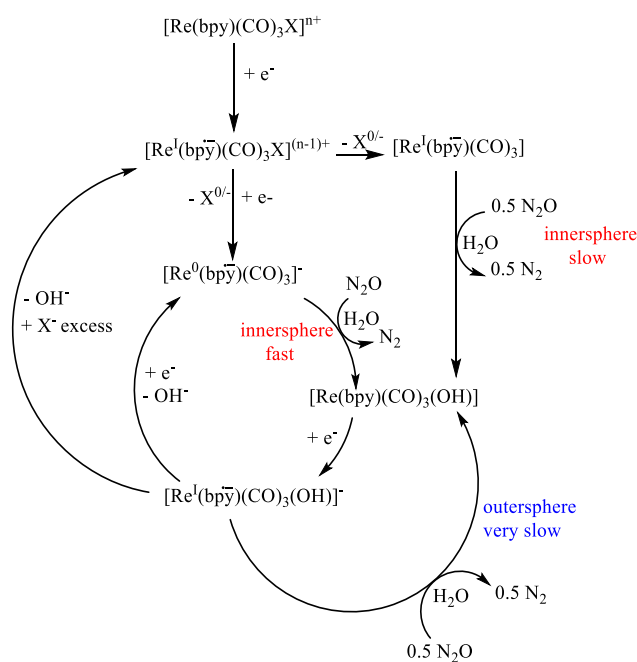


Figure IV.6 2 : Rate constant as a function of standard potential of the reductant E° in (V vs. SCE) for the homogeneous catalysis of N_2O reduction. Blue data corresponds to the reduction by electrogenerated organic aromatic radical anion or dianions and the blue line corresponds to the activation driving force plot predicted for an outersphere electron transfer. Reduction of $[\text{Re}^0(\text{bpy}^{\ast-})(\text{CO})_3]^-$ (black star), $[\text{Re}^{\text{I}}(\text{bpy}^{\ast-})(\text{CO})_3(\text{MeCN})]$ (black triangle), $[\text{Re}^{\text{I}}(\text{bpy}^{\ast-})(\text{CO})_3(\text{OH})]^-$ (black diamond) and $[\text{Re}^{\text{I}}(\text{bpy}^{\ast-})(\text{CO})_3\text{Cl}]^-$ (black square) ²¹. "Reprinted with permission from [ACS Catal. 2023, 13, 12, 8262–8272]. Copyright [2023] American chemical Society".



Based on the results discussed in this Chapter, a now well established mechanism of the electrochemical reduction of N_2O by $[\text{Re}(\text{bpy})(\text{CO})_3\text{X}]^{n+}$ ($\text{X} = \text{CH}_3\text{CN}, \text{Cl}^-$ $n = 0$ or 1) can be outlined as follow in Scheme IV.6 2 :



Scheme IV.6 2 : Global mechanism for the reduction of N_2O by $[\text{Re}(\text{bpy})(\text{CO})_3\text{X}]^{n+}$ complexes.

7. Conclusion

Through the use of spectroelectrochemistry measurements we were able to monitor direct reaction of N_2O with the bi-reduced species of $[Re(bpy)(CO)_3X]$ and to propose a catalytic mechanism for the reaction with N_2O as shown in Scheme IV.6 3. Two sequential one electron reductions of $[Re(bpy)(CO)_3Cl]$ lead to the catalytically-active state, $[Re^0(bpy^{\bullet-})(CO)_3]^-$, which can interact with N_2O through the O atom and form hydroxide, a strong ligand in $[Re(bpy)(CO)_3(OH)]$ which requires more negative potential for the release of OH^- thus shifting the catalytic wave towards more negative potential reflecting to a self-inhibition process. However generating the bi-reduced species is not the exclusive requirement for the reduction of N_2O . Mono-reduced species $[Re^I(bpy^{\bullet-})(CO)_3X]^{(n-1)+}$ ($X = CH_3CN, Cl^-$ and OH^- , $n = 0$ or 1) have shown to be less rapid compared to the bi-reduced species. An innersphere reduction of N_2O is achieved by the mono-reduced species in which N_2O can displace acetonitrile and chloride due to the lability of these ligands forming $[Re(bpy)(CO)_3(OH)]$ and since OH^- is a strong ligand the mono-reduced species $[Re^I(bpy^{\bullet-})(CO)_3(OH)]^-$ show an outersphere electron transfer making the catalytic process slower. This can be overcome by the addition of large concentration of chlorides salt enabling the displacement of hydroxide. This study highlights the role of ligand exchange on the electrocatalytic processes catalyzed by transition metal complexes and the role of potential co-product which can shift the process into a slower direction which can be detrimental for the catalyst thus demanding more energy for substrate activation.

References:

- (1) Froehlich, J. D.; Kubiak, C. P. The Homogeneous Reduction of CO₂ by [Ni(cyclam)]⁺: Increased Catalytic Rates with the Addition of a CO Scavenger. *Journal of the American Chemical Society* **2015**, *137* (10), 3565-3573. DOI: 10.1021/ja512575v.
- (2) Bruch, Q. J.; Malakar, S.; Goldman, A. S.; Miller, A. J. M. Mechanisms of Electrochemical N₂ Splitting by a Molybdenum Pincer Complex. *Inorganic Chemistry* **2022**, *61* (4), 2307-2318. DOI: 10.1021/acs.inorgchem.1c03698.
- (3) Lindley, B. M.; van Alten, R. S.; Finger, M.; Schendzielorz, F.; Würtele, C.; Miller, A. J. M.; Siewert, I.; Schneider, S. Mechanism of Chemical and Electrochemical N₂ Splitting by a Rhenium Pincer Complex. *Journal of the American Chemical Society* **2018**, *140* (25), 7922-7935. DOI: 10.1021/jacs.8b03755.
- (4) Ibrahim, A. F.; Garrido-Barros, P.; Peters, J. C. Electrocatalytic Nitrogen Reduction on a Molybdenum Complex Bearing a PNP Pincer Ligand. *ACS Catalysis* **2023**, *13* (1), 72-78. DOI: 10.1021/acscatal.2c04769.
- (5) Argüello, J. E.; Costentin, C.; Griveau, S.; Savéant, J.-M. Role of Protonation and of Axial Ligands in the Reductive Dechlorination of Alkyl Chlorides by Vitamin B12 Complexes. Reductive Cleavage of Chloroacetonitrile by Co(I) Cobalamins and Cobinamides. *Journal of the American Chemical Society* **2005**, *127* (14), 5049-5055. DOI: 10.1021/ja042940f.
- (6) Sampson, M. D.; Froehlich, J. D.; Smieja, J. M.; Benson, E. E.; Sharp, I. D.; Kubiak, C. P. Direct observation of the reduction of carbon dioxide by rhenium bipyridine catalysts. *Energy & Environmental Science* **2013**, *6* (12). DOI: 10.1039/c3ee42186d.
- (7) Grice, K. A.; Gu, N. X.; Sampson, M. D.; Kubiak, C. P. Carbon monoxide release catalysed by electron transfer: electrochemical and spectroscopic investigations of [Re(bpy-R)(CO)₄](OTf) complexes relevant to CO₂ reduction. *Dalton Transactions* **2013**, *42* (23), 8498-8503. DOI: 10.1039/C3DT50612F.
- (8) Smieja, J. M.; Kubiak, C. P. Re(bipy-tBu)(CO)₃Cl-improved catalytic activity for reduction of carbon dioxide: IR-spectroelectrochemical and mechanistic studies. *Inorg Chem* **2010**, *49* (20), 9283-9289. DOI: 10.1021/ic1008363.
- (9) Benson, E. E.; Grice, K. A.; Smieja, J. M.; Kubiak, C. P. Structural and spectroscopic studies of reduced [Re(bpy-R)(CO)₃]⁻¹ species relevant to CO₂ reduction. *Polyhedron* **2013**, *58*, 229-234. DOI: 10.1016/j.poly.2013.01.024.
- (10) Benson, E. E.; Kubiak, C. P. Structural investigations into the deactivation pathway of the CO₂ reduction electrocatalyst Re(bpy)(CO)₃Cl. *Chem Commun* **2012**, *48* (59), 7374-7376. DOI: 10.1039/c2cc32617e.
- (11) Timney, J. A.; Turner, J. J. The calculation of energy-factored force constants for fac-Re(CO)₃(N-N)(X) molecules and related complexes. *Vibrational Spectroscopy* **2022**, *120*. DOI: 10.1016/j.vibspec.2022.103374.
- (12) Worl, L. A.; Duesing, R.; Chen, P.; Ciana, L. D.; Meyer, T. J. Photophysical properties of polypyridyl carbonyl complexes of rhenium(I). *Journal of the Chemical Society, Dalton Transactions* **1991**. DOI: 10.1039/dt9910000849.
- (13) Johnson, F. P. A.; George, M. W.; Hartl, F.; Turner, J. J. Electrocatalytic Reduction of CO₂ Using the Complexes [Re(bpy)(CO)₃L]_n (n = +1, L = P(OEt)₃, CH₃CN; n = 0, L = Cl-, Otf-; bpy = 2,2'-Bipyridine; Otf- = CF₃SO₃) as Catalyst Precursors: Infrared Spectroelectrochemical Investigation. *Organometallics* **1996**, *15* (15), 3374-3387. DOI: 10.1021/om960044+.
- (14) Stor, G. J.; Hartl, F.; van Outersterp, J. W. M.; Stufkens, D. J. Spectroelectrochemical (IR, UV/Vis) Determination of the Reduction Pathways for a Series of [Re(CO)₃(α-diimine)L]^{0/+} (L' = Halide, OTf-, THF, MeCN, n-PrCN, PPh₃, P(OMe)₃) Complexes. **1995**, *14* (3), 1115-1131. DOI: 10.1021/om00003a013.
- (15) Bhugun, I.; Lexa, D.; Savéant, J.-M. Vacuum-Triggered Flash Desolubilization Method for Determining the Solubility of Gases in Pure and Mixed Solvents. Application to Carbon Dioxide. *Analytical Chemistry* **1994**, *66* (22), 3994-3996. DOI: 10.1021/ac00094a022.
- (16) Savéant, J.-M.; Costentin, C. Elements of Molecular and Biomolecular Electrochemistry. Vol. Chapter 2 2019; pp 130-133. John Wiley, 2019. ISBN: 978-1-119-29233-3.
- (17) Zeng, R.; Feller, M.; Ben-David, Y.; Milstein, D. Hydrogenation and Hydrosilylation of Nitrous Oxide Homogeneously Catalyzed by a Metal Complex. *J Am Chem Soc* **2017**, *139* (16), 5720-5723. DOI: 10.1021/jacs.7b02124.
- (18) Pauleta, S. R.; Carepo, M. S. P.; Moura, I. Source and reduction of nitrous oxide. *Coordination Chemistry Reviews* **2019**, *387*, 436-449. DOI: 10.1016/j.ccr.2019.02.005.
- (19) Vaughan, G. A.; Rupert, P. B.; Hillhouse, G. L. Selective O-atom transfer from nitrous oxide to hydride and aryl ligands of bis(pentamethylcyclopentadienyl)hafnium derivatives. *Journal of the American Chemical Society* **1987**, *109* (18), 5538-5539. DOI: 10.1021/ja00252a047.
- (20) Chen, P.; Gorelsky, S. I.; Ghosh, S.; Solomon, E. I. N₂O Reduction by the μ₄-Sulfide-Bridged Tetranuclear Cu₄Z Cluster Active Site. *Angewandte Chemie International Edition* **2004**, *43* (32), 4132-4140. DOI:10.1002/anie.200301734.

(21) Deeba, R.; Chardon-Noblat, S.; Costentin, C. Importance of Ligand Exchange in the Modulation of Molecular Catalysis: Mechanism of the Electrochemical Reduction of Nitrous Oxide with Rhenium Bipyridyl Carbonyl Complexes. *ACS Catalysis* **2023**, *13* (12), 8262-8272. DOI: 10.1021/acscatal.3c01495.

Chapter V: Extension to Catalysis of Pyridine N-Oxide Electrochemical Reduction

1. Introduction

As an extension of the previous work built on the field of deoxygenation of nitrous oxide using electrochemical molecular approach, we broadened our studies to the pyridine N-oxide (PNO). Why investigate on this molecule? This type of molecule occupies an important niche in organic chemistry, in essence they represent an important family of compounds with distinct biological properties. Moreover, they are commonly used as precursors in the synthesis of functionalized pyridines, by activating the heteroaromatic ring towards both nucleophilic and electrophilic reagents as they serve as an excellent directing group (DG) in C-H activation reactions, conferring enhanced reactivity and regioselectivity over their oxygen free counterparts.^{1,2,3,4} Consequently, deprotection i.e. removing the directing group, is an important task.

2. Properties of Pyridine N-oxide and the State of Art:

PNO is a heterocyclic compound with chemical formula C_5H_5NO (Figure V.2 1). It is colorless, hygroscopic solid, planar with N-O bond distance of 1.34 Å greater than that of N-O bond in N_2O (1.184 Å).⁵

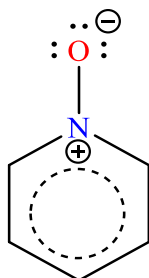
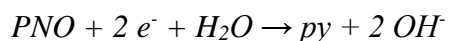


Figure V.2 1 : Chemical structure of pyridine N-oxide.

As opposed to nitrous oxide, pyridine N-oxide is a weak oxidant with a reduction potential of $E^0(\text{pyridine N-oxide/pyridine}) = -0.8 \text{ V vs. SCE}$. This molecule is thermodynamically difficult to reduce. Hence this represents a much greater challenge to activate pyridine N-oxide than N_2O .⁶ Previously it was reported deoxygenation of PNO and heterocyclic amine N-oxides using Pd and Cu catalyzed reduction^{7,8} or stoichiometric amount of a chemical reductant such as diboron reagents,⁹ or silanes.¹⁰ In addition photo-catalytic reduction was investigated by photo-induced catalyst free electron transfer upon blue-light irradiation in the presence of Hantzsch ester acting as electron donor and acceptor at the same time.¹¹ Metal catalyzed photo-

deoxygenation was additionally reported using ruthenium polypyridyl chloride as photocatalyst under blue light irradiation.¹² Another example was reported more recently by Cantat and coworkers, under ambient conditions using rhenium triscarbonyl bipyridyl complexes as photocatalysts giving quantitative production of pyridines (py).¹³ Furthermore, direct electrochemical reduction of N-oxides on diverse metallic electrodes at constant current in acetonitrile with water as co-solvent was reported. The yield and the selectivity of the reaction strongly depends on the nature of the metal used in the electrolysis.^{14,15} However this method has weak points: no control of the applied potential and the chemical properties of the electrode material used play an important role in selectivity and efficiency of the reaction. Hence, we decided to proceed towards an electrochemical homogeneous molecular catalytic approach leading to an innersphere activation of PNO by its interaction with the reduced form of a transition metal complex. Our ultimate goal would be to get a deep understanding of the mechanism.



3. Results and Discussion

We used the same family of transition metal complexes employed for the reduction of N₂O: rhenium triscarbonyl bipyridyl complexes, and applied the same mechanistic strategy analysis.

3.1 Cyclic Voltammetry Overview:

In contrast to N₂O, apparently, no reactivity is observed on the CV time scale in the presence of [Re(bpy)(CO)₃Cl] except increase in intensity (compare red to violet in Figure V.3.3.1 1). This increase in intensity observed could be a solubility issue. Addition of proton source (H₂O) in the presence of the Re catalyst, causes a shift of the reduction wave of pyridine N-oxide (green in Figure V.3.3.1 1) however this reduction occurs at the same potential as the direct reduction of pyridine N-oxide in the presence of 2 M H₂O in solution (blue in Figure V.3.3.1 1). Hence, it is not a catalytic wave.

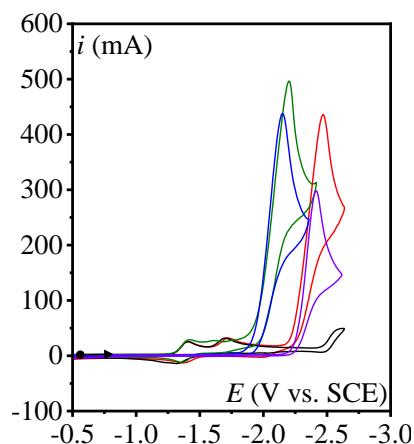


Figure V.3.3.1 1 : CVs of direct reduction of 10 mM PNO (violet) with 2 M H₂O (blue), 1 mM [Re(bpy)(CO)₃Cl]: under Ar (black), in the presence of 10.5 mM PNO (red), with addition of 2 M H₂O (green) in CH₃CN + 0.1M n-Bu₄NPF₆ at 0.1 V/s on a 3 mm diam. GCE.

However, switching to [Re(bpy)(CO)₃(MeCN)]PF₆ on the time scale of the CV, an interaction is observed with PNO. In Figure V.3.3.1 2, the first wave loses its reversibility in the presence of excess of PNO and increases in intensity. Also, the potential of the second wave slightly shifts towards more negative potential by 30 mV and increases in intensity (Figure V.3.3.1 3). This suggests that there is an interaction between the mono-reduced species [Re^I(bpy^{•-})(CO)₃(MeCN)] and PNO. To get more insights, SEC studies will be discussed in the following sections.

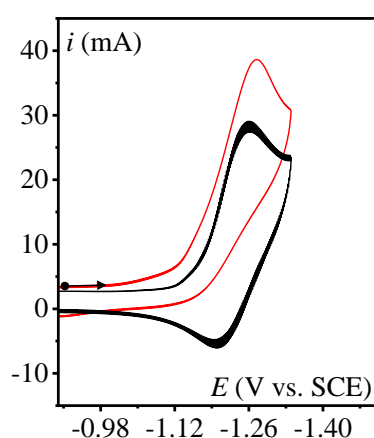


Figure V.3.3.1 2 : CVs of 1 mM [Re(bpy)(CO)₃(MeCN)]PF₆ under Ar (black), in the presence of excess PNO (red) in CH₃CN + 0.1 M n-Bu₄NPF₆ at 0.1 V/s on a 3 mm diam. GCE.

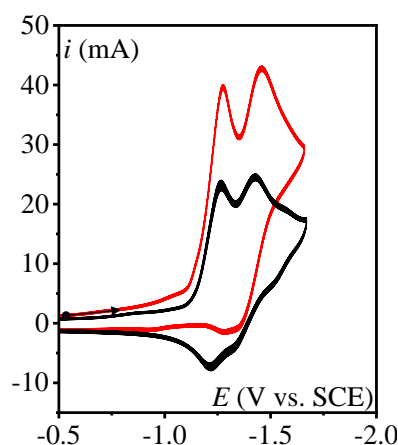


Figure V.3.3.1 3 : CVs of 1 mM [Re(bpy)(CO)₃(MeCN)]PF₆ under Ar (black), in the presence of excess PNO (red) in CH₃CN + 0.1 M n-Bu₄NPF₆ at 0.1 V/s on a 3 mm diam. GCE.

3.2 Reaction of PNO with the mono-reduced species

CPE was performed at -1.37 V, first reduction wave of the [Re(bpy)(CO)₃Cl] (Figure V.3.3.2 1) in the presence of 10 mole equivalents of PNO. Surprisingly we didn't

observe the formation of a dimer. This suggests that the reaction of PNO with the mono-reduced species is faster than its dimerization after loss of chloride. It was also noticed that the current passed as a function of time during electrolysis didn't reach zero when we have stopped the electrolysis after passing a charge of one electron per Re complex. Hence, we did not investigate a possible catalytic process at this potential on the electrolysis timescale but we cannot exclude a slow catalytic process.

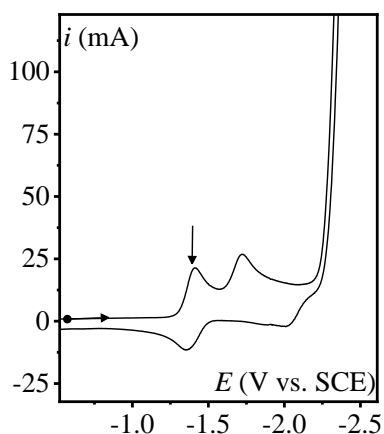


Figure V.3.3.2 1 : CV of 1 mM $[\text{Re}(\text{bpy})(\text{CO})_3\text{Cl}]$ + 10 mM PNO under Ar in CH_3CN + 0.1 M $n\text{-Bu}_4\text{NPF}_6$ at 0.1 V/s on a 3 mm diam. GCE.

CVs were run after electrolysis showed that a new complex was formed with characteristics different than the starting complex $[\text{Re}(\text{bpy})(\text{CO})_3\text{Cl}]$. Indeed, the complex formed gave a reversible reduction wave at $E_{1/2} = -1.42$ V and other waves at $E_{\text{pc}2} = -1.97$ V and $E_{\text{pc}3} = -2.11$ V similar to that of the $[\text{Re}(\text{bpy})(\text{CO})_3(\text{OH})]$ complex. It also shows that there is no reaction between the formed $[\text{Re}(\text{bpy})(\text{CO})_3(\text{OH})]$ and PNO nor after second reduction observed (on the time scale of the CV) (Figure V.3.3.2 2).

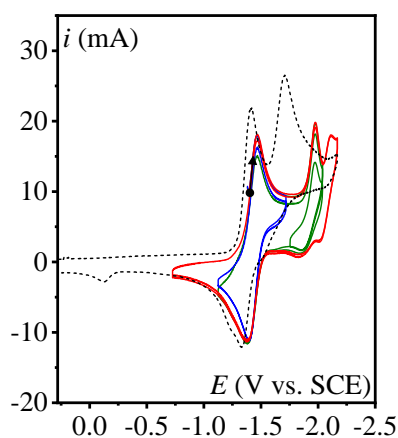


Figure V.3.3.2 2 : CVs of 1 mM $[\text{Re}(\text{bpy})(\text{CO})_3\text{Cl}]$ + 10 mM PNO (black short dash), after $E_{\text{app}} = -1.37$ V successive waves (blue), (green), (red) under Ar in CH_3CN + 0.1 M $n\text{-Bu}_4\text{NPF}_6$ at 0.1 V/s on a 3 mm diam. GCE.

Further characterization was made for the species obtained after $E_{app} = -1.37$ V. FTIR showed $\nu(\text{CO})$ with low intensity band at 2021 and other bands 2005, 1894 and 1874 cm^{-1} (Figure V.3.3.2 3) also UV-vis showing an absorption band at 382 nm (Figure V.3.3.2 4).

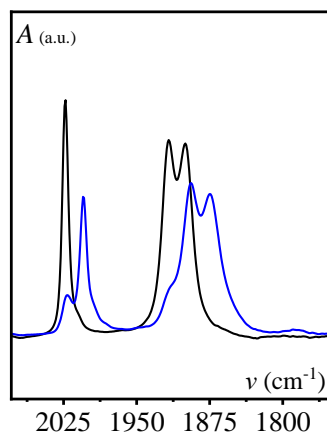


Figure V.3.3.2 3: FTIR spectra of 1 mM $[\text{Re}(\text{bpy})(\text{CO})_3\text{Cl}]$ before (black) and after $E_{app} = -1.37$ V (blue) in the presence 10 mM PNO in solution under inert atmosphere.

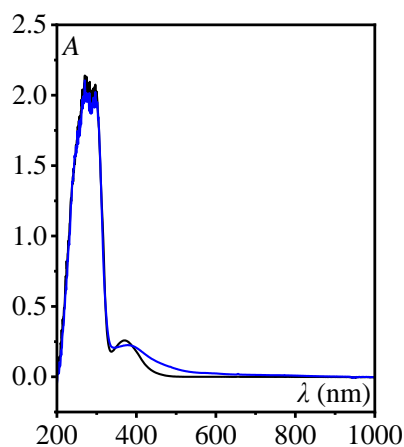
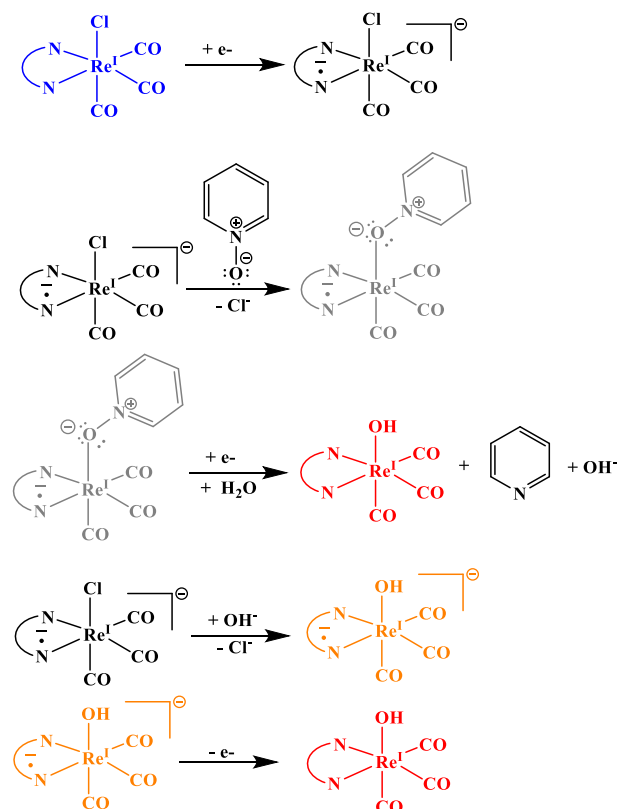


Figure V.3.3.2 4: UV-vis spectra of 1 mM $[\text{Re}(\text{bpy})(\text{CO})_3\text{Cl}]$ before (black) and after $E_{app} = -1.37$ V (blue) in the presence 10 mM PNO in solution, $l = 1$ mm quartz probe.

These characterizations give additional evidence supporting that the species obtained is $[\text{Re}(\text{bpy})(\text{CO})_3(\text{OH})]$ complex. But how is it formed? We suggest the mechanism in Scheme V.3.3.2 1 for the reaction of the $[\text{Re}^{\text{I}}(\text{bpy}^{\bullet-})(\text{CO})_3\text{Cl}]^-$ with PNO. We propose that, after the reductive dechlorination of the Re complex, pyridine N-oxide binds to the open coordination site and prevents the formation of the dimer via formation of an adduct in the presence of proton source which is then reduced by another electron to release py and OH^- thus forming the $[\text{Re}(\text{bpy})(\text{CO})_3(\text{OH})]$. This is in agreement with the above observation that $[\text{Re}^{\text{I}}(\text{bpy}^{\bullet-})(\text{CO})_3(\text{MeCN})]$ reacts with PNO on the timescale of CV. Also, formed hydroxide can replace the chloride on the mono-reduced species to form the $[\text{Re}^{\text{I}}(\text{bpy}^{\bullet-})(\text{CO})_3(\text{OH})]^-$ species. However, at the electrolysis applied potential of -1.37 V, the $[\text{Re}^{\text{I}}(\text{bpy}^{\bullet-})(\text{CO})_3(\text{OH})]^-$ is oxidized. It is the reason why a total of one electron per Re center is consumed to produce py at the level of the first reduction wave on the time scale of electrolysis.

After this first electrolysis, the potential was applied to -1.62 V passing a charge of one electron where no sustained current was observed, revealing the formation of the mono-reduced species of $[\text{Re}^{\text{I}}(\text{bpy}^{\bullet-})(\text{CO})_3(\text{OH})]^-$ characterized by FTIR with characteristic $\nu(\text{CO})/$ 2002, 1982, 1862 and 1848 cm^{-1} (Figure V.3.3.2 5) and UV-vis with absorption bands at 373, 483 and 509 nm (red) (Figure V.3.3.2 6).



Scheme V.3.3.2 1 : Proposed mechanism for the reaction of $[\text{Re}^{\text{I}}(\text{bpy}^{\bullet-})(\text{CO})_3\text{Cl}]$ with PNO on the time scale of electrolysis.

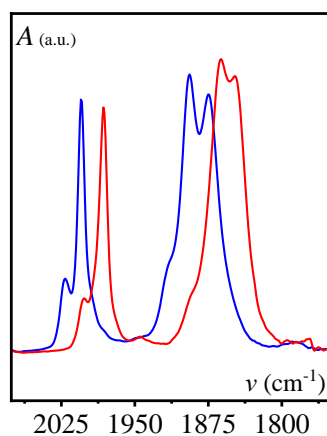


Figure V.3.3.2 5 : FTIR spectra of 1 mM $[\text{Re}(\text{bpy})(\text{CO})_3\text{Cl}]$ in the presence of 10 mM PNO after $E_{\text{app}} = -1.37$ V (blue) and $E_{\text{app}} = -1.62$ V (red) under Ar atmosphere.

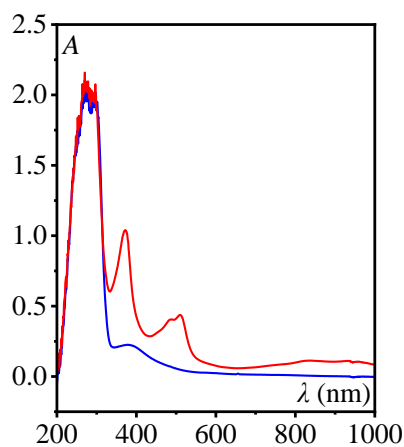


Figure V.3.3.2 6 : UV-vis spectra of 1 mM $[\text{Re}(\text{bpy})(\text{CO})_3\text{Cl}]$ in the presence of 10 mM PNO after $E_{\text{app}} = -1.37$ V (blue) $E_{\text{app}} = -1.62$ V (red), $l = 1$ mm quartz probe.

This shows that the interaction of PNO with the $[\text{Re}^{\text{I}}(\text{bpy}^{\bullet-})(\text{CO})_3(\text{OH})]^-$ is weak due to the difficulty of displacing OH^- by PNO. To confirm this hypothesis, we have electro-generated $[\text{Re}^{\text{I}}(\text{bpy}^{\bullet-})(\text{CO})_3(\text{OH})]^-$ and we have added PNO in excess (9.8 mM), in-situ UV-vis: little to no change was observed over a course of 19 min (Figure V.3.3.2 7).

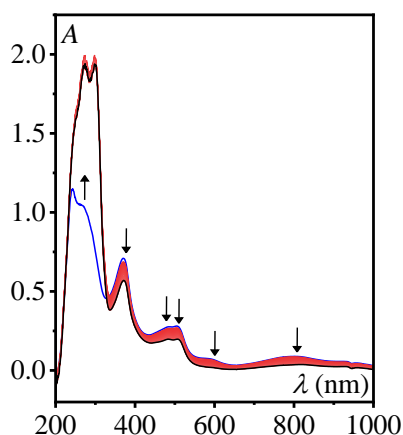


Figure V.3.3.2 7 : Evolution of UV-vis spectra (1 spectrum / 20 s) initial spectrum (blue) and final (black), $l = 1$ mm, 0.67 mM of $[\text{Re}^{\text{I}}(\text{bpy}^{\bullet-})(\text{CO})_3(\text{OH})]^-$ in $\text{CH}_3\text{CN} + 0.1$ M $n\text{-Bu}_4\text{NPF}_6$ with the addition of 9.8 mM of PNO.

3.3 Bi-reduced species with PNO

A solution of $[\text{Re}^0(\text{bpy}^{\bullet-})(\text{CO})_3]^-$ (1 mM) was electro-generated by two steps each, one electron reductive electrolysis from the $[\text{Re}(\text{bpy})(\text{CO})_3\text{Cl}]$. Then PNO was added in excess (10.5 mM) while monitoring the evolution of the species by in-situ UV-vis (1 spectrum / 20 s). It showed a slow decay of the absorption band of the bi-reduced species at 570 nm. Isosbestic points were observed at 491 and 746 nm showing clean transformation of the one species into another without the formation of intermediates (Figure V.3.3.3 1). What is the nature of the species formed ?

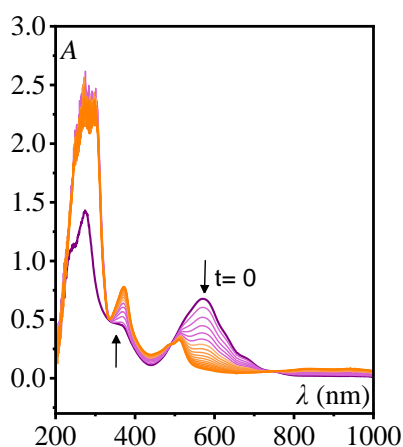


Figure V.3.3.3 1 : Evolution of UV-vis spectra scans were taken every 20 s, $l = 1$ mm, 0.67 mM solution of electrogenerated $[\text{Re}^0(\text{bpy}^{\bullet-})(\text{CO})_3]^-$ in $\text{CH}_3\text{CN} + 0.1$ M $n\text{-Bu}_4\text{NPF}_6$ with the addition of 12 mM of PNO.

The last spectrum observed after 6 min on Figure V.3.3.3 1 , peaks at 372, 483 and 509 nm did not evolve further nor do we observe the dimer. Hence, the species formed was stable inside the glovebox. CVs were run to characterize this species showing redox systems

corresponding to the $[\text{Re}(\text{bpy})(\text{CO})_3(\text{OH})]$: a reversible wave with $E_{1/2} = -1.43 \text{ V}$ (Figure V.3.3.3 2) followed by a second reduction wave of $E_{\text{pc}2} = -1.96$ and $E_{\text{pc}3} = -2.1 \text{ V}$ (Figure V.3.3.3 3). But what is the oxidation state of the $[\text{Re}(\text{bpy})(\text{CO})_3(\text{OH})]$ thus obtained, is it mono-reduced or neutral state species?

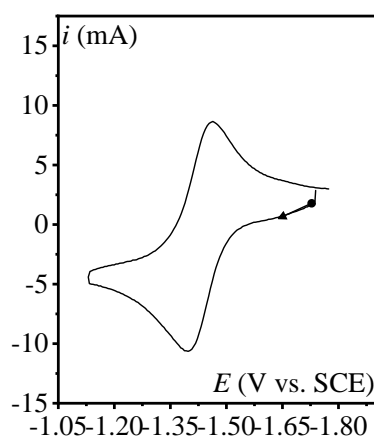


Figure V.3.3.3 2: CV of the reversible system obtained after addition of PNO to the bi-reduced species under Ar in $\text{CH}_3\text{CN} + 0.1 \text{ M } n\text{-Bu}_4\text{NPF}_6$ at 0.1 V/s on a 3 mm diam. GCE.

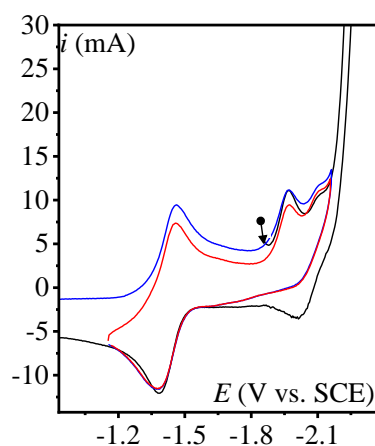


Figure V.3.3.3 3: Cyclic scans CVs of successive reduction waves followed by direct reduction of PNO at more negative potential $\approx -2.1 \text{ V}$ Cycle 1 (black), cycle 2 (blue) and cycle 3 (red) under Ar in $\text{CH}_3\text{CN} + 0.1 \text{ M } n\text{-Bu}_4\text{NPF}_6$ at 0.1 V/s on a 3 mm diam. GCE.

FTIR of the solution (Figure V.3.3.3 4) after addition of PNO to the bi-reduced species, showed a shift of the carbonyl bands towards higher wavenumber (higher energy) indicating decrease in the electron density on the $\text{Re}(\text{I})$ center (1982 , 1863 and 1846 cm^{-1}) at values very close to the ones of $\nu(\text{CO})$ of $[\text{Re}^{\text{I}}(\text{bpy}^{\bullet-})(\text{CO})_3(\text{OH})]^-$.

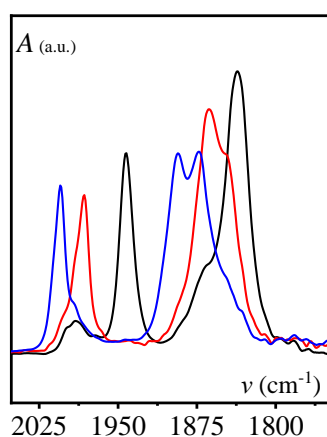


Figure V.3.3.3 4: FTIR spectra of $0.67 \text{ mM } [\text{Re}^0(\text{bpy}^{\bullet-})(\text{CO})_3]^-$ (black), after addition of 12 mM PNO (red) and after $E_{\text{app}} = -1.22 \text{ V}$ (blue) under Ar atmosphere.

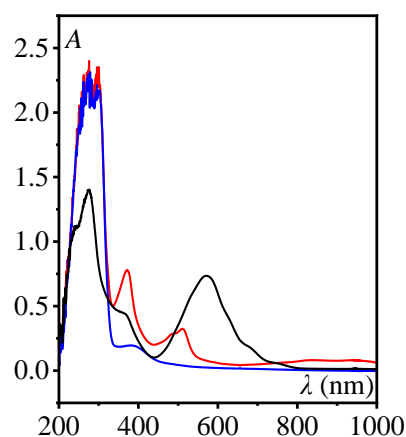
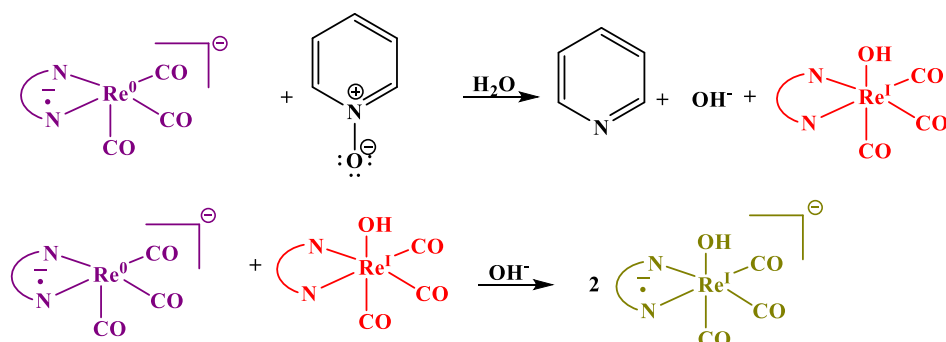


Figure V.3.3.3 5: UV-vis spectra of $0.67 \text{ mM } [\text{Re}^0(\text{bpy}^{\bullet-})(\text{CO})_3]^-$ (black), after addition of 12 mM PNO (red) and after $E_{\text{app}} = -1.22 \text{ V}$ (blue) under Ar atmosphere $l = 1 \text{ mm}$ quartz probe.

In order to confirm this, another electrolysis (oxidation) was performed at $E_{\text{app}} = -1.22 \text{ V}$. In-situ UV-vis showed decrease in the absorption intensity of the

$[\text{Re}^{\text{I}}(\text{bpy}^{\bullet-})(\text{CO})_3(\text{OH})]^-$ (Figure V.3.3.3 5), FTIR gave $\nu(\text{CO})/2005, 1893$ and 1874 cm^{-1} which characterizes $[\text{Re}(\text{bpy})(\text{CO})_3(\text{OH})]$ (Figure V.3.3.3 4).

Based on the above results we have proposed the mechanism of the reaction of the bi-reduced species with PNO (Scheme V.3.3.3 1). First step is a $2e^-$ reduction of PNO to py and hydroxide with the formation of $[\text{Re}(\text{bpy})(\text{CO})_3(\text{OH})]$; then, second step is the reaction of the bi-reduced species with $[\text{Re}(\text{bpy})(\text{CO})_3(\text{OH})]$ to form $[\text{Re}^{\text{I}}(\text{bpy}^{\bullet-})(\text{CO})_3(\text{OH})]^-$ solely observed in the solution. But why we didn't obtain a mixture of the mono-reduced and neutral species as observed after addition of N_2O on the bi-reduced species? We assume that after the formation of $[\text{Re}^{\text{I}}(\text{bpy}^{\bullet-})(\text{CO})_3(\text{OH})]^-$ the rate of the reaction with PNO is very slow because no change in the UV-vis absorption was observed. The second reason, is the slowness of the reaction of PNO with the bi-reduced species arises, a competition between the reaction of PNO or the reduction of $[\text{Re}(\text{bpy})(\text{CO})_3(\text{OH})]$ formed with the bi-reduced species, as shown in the proposed mechanism (Scheme V.3.3.3 1). The two reasons explain why we only observe $[\text{Re}^{\text{I}}(\text{bpy}^{\bullet-})(\text{CO})_3(\text{OH})]^-$ as reaction product of the bi-reduced species with PNO.



Scheme V.3.3.3 1 : Proposed mechanism for the reaction of PNO with $[\text{Re}^0(\text{bpy}^{\bullet-})(\text{CO})_3]^-$.

3.4 Controlled potential electrolysis: Product Analysis

In the absence of added source of proton:

After the observation of a reaction of the bi-reduced species with PNO we have run CPE at the potential of the second reduction wave of $[\text{Re}(\text{bpy})(\text{CO})_3\text{Cl}]$ (-1.82 V) in the presence of PNO (5 mM) with only residual amount of water from the electrolyte solution (Figure V.3.3.4 1) to observe the possibility of catalysis on the time scale of the electrolysis opposite to what was observed on the CV time scale. The current was not maintained constant; it dropped almost to zero after passing a charge corresponding to 2 moles of electrons per mole of Re complex (Figure V.3.3.4 2).

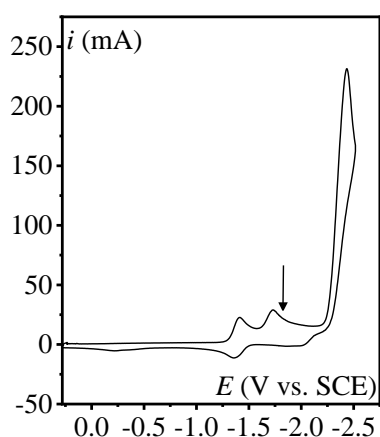


Figure V.3.3.4 1: CV of 1 mM $[\text{Re}(\text{bpy})(\text{CO})_3\text{Cl}]$ + 5 mM PNO under Ar in CH_3CN + 0.1 M $n\text{-Bu}_4\text{NPF}_6$ at 0.1 V/s on a 3 mm diam. GCE.

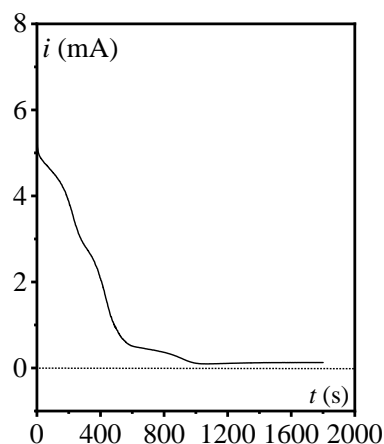


Figure V.3.3.4 2: Current vs. time for CPE at -1.82 V of 1 mM $[\text{Re}(\text{bpy})(\text{CO})_3\text{Cl}]$ + 5 mM PNO under Ar in CH_3CN + 0.1 M $n\text{-Bu}_4\text{NPF}_6$.

This experiment was performed while monitoring in-situ the UV-vis (Figure V.3.3.4 3). During the electrolysis we have observed the formation of $[\text{Re}^{\text{I}}(\text{bpy}^{\bullet-})(\text{CO})_3\text{Cl}]^-$, and then the dimer $[\text{Re}^0(\text{bpy})(\text{CO})_3]_2$. This shows that, to prevent the formation of the dimer, PNO has to be in large excess compared to the catalyst at least 10 times more (cf. above Reaction of PNO with the mono-reduced species). Then, during the CPE, the dimer was reduced and the Re-Re bonds broke giving $[\text{Re}^0(\text{bpy}^{\bullet-})(\text{CO})_3]^-$. After that, the bi-reduced species reacted with PNO giving $[\text{Re}(\text{bpy})(\text{CO})_3(\text{OH})]$, but at this applied potential of -1.82 V the $[\text{Re}(\text{bpy})(\text{CO})_3(\text{OH})]$ complex is reduced. Hence $[\text{Re}^{\text{I}}(\text{bpy}^{\bullet-})(\text{CO})_3(\text{OH})]^-$ was characterized by UV-vis as final species in the bulk of the electrolyte solution. All of these successive reactions are in agreement with the step by step shape of the curve i/s during the CPE (Figure V.3.3.4 2).

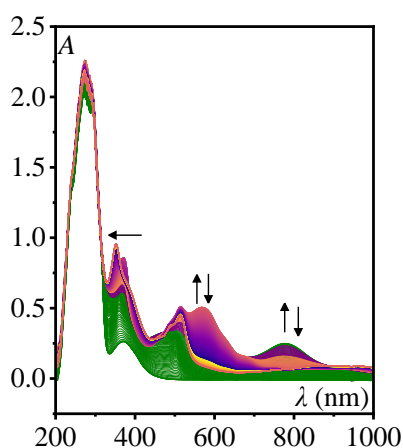


Figure V.3.3.4 3: In-situ UV-vis evolution of 1 mM $[\text{Re}(\text{bpy})(\text{CO})_3\text{Cl}]$ + 5 mM PNO under Ar + 0.1 M $n\text{-Bu}_4\text{NPF}_6$ at $E_{\text{app}} = -1.82$ V (1 spectrum / 5 s) starting from the green colored spectra passing by the purple and then ending with the orange.

The current dropped to zero at the end since no reaction takes place between $[\text{Re}^{\text{I}}(\text{bpy}^{\bullet-})(\text{CO})_3(\text{OH})]^-$ and PNO consistent with what was described in the previous sections. Therefore, the next goal would be to facilitate the removal of OH^- seeking the possibility to replace it by the substrate PNO and trigger catalysis.

In the presence of added water as a source of protons

We have run CPE at -1.67 V in the presence of water, $[\text{Re}(\text{bpy})(\text{CO})_3\text{Cl}]$ and PNO. Note that, in CV (Figure V.3.3.4 4) a shift of the reduction wave of PNO was observed towards less negative potential in the presence of water, however this wave is not catalytic since it occurs at the same potential for the direct reduction of PNO in the presence of water as already indicated in section 3.1 of this Chapter. Nonetheless, compared to the electrolysis run without added water, the current was maintained more or less constant passing a charge of 8 C over a course of $\sim 2\text{ hr}$ electrolysis. Note that a charge of 1.9 C is required to form the bi-reduced species (Figure V.3.3.4 5).

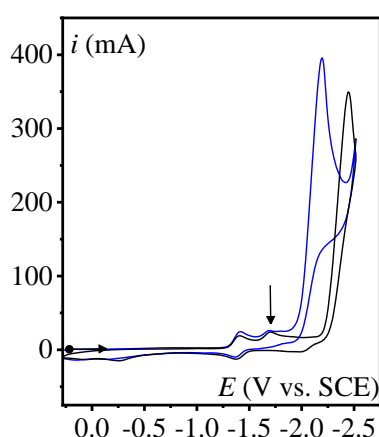


Figure V.3.3.4 4 : CVs of $1\text{ mM } [\text{Re}(\text{bpy})(\text{CO})_3\text{Cl}] + 11.4\text{ mM PNO}$ under Ar in the absence of water (black) with $1\text{ M H}_2\text{O}$ (blue) in $\text{CH}_3\text{CN} + 0.1\text{ M } n\text{-Bu}_4\text{NPF}_6$ at 0.1 V/s on a 3 mm diam. GCE .

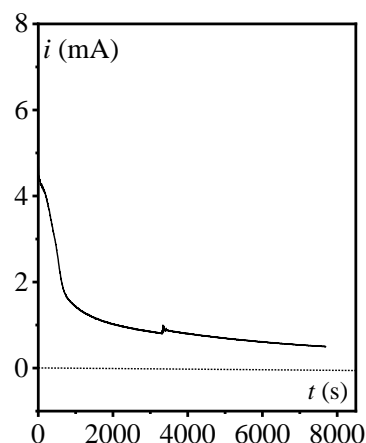


Figure V.3.3.4 5 : Current vs. time for CPE at -1.67 V of $1\text{ mM } [\text{Re}(\text{bpy})(\text{CO})_3\text{Cl}] + 11.4\text{ mM PNO}$ under Ar in $\text{CH}_3\text{CN} + 0.1\text{ M } n\text{-Bu}_4\text{NPF}_6$.

This electrolysis experiment was followed by in-situ UV-vis monitoring the nature of the species in the bulk of the solution. We have observed a growth of absorption bands at (368, 482 and 507 nm) which are slightly shifted from those of $[\text{Re}^{\text{I}}(\text{bpy}^{\bullet-})(\text{CO})_3(\text{OH})]^-$ (Figure V.3.3.4 6). Moreover, we have done CPE of $[\text{Re}(\text{bpy})(\text{CO})_3\text{Cl}]$ in the presence of water at the level of the first reduction wave and we have observed that the mono-reduced $[\text{Re}^{\text{I}}(\text{bpy}^{\bullet-})(\text{CO})_3(\text{OH}_2)]$ species has absorption peaks at 368, 481 and 506 nm (Figure V.3.3.4 7). This suggests that the resting state species during CPE in the presence of PNO and H_2O is the aqua $[\text{Re}^{\text{I}}(\text{bpy}^{\bullet-})(\text{CO})_3(\text{OH}_2)]$ complex and not the bi-reduced species

$[\text{Re}^0(\text{bpy}^{\bullet-})(\text{CO})_3]^-$ nor $[\text{Re}^I(\text{bpy}^{\bullet-})(\text{CO})_3(\text{OH})]^-$. We propose that when water is present in the solution in large excess, the protonation of OH^- is facilitated or makes easier to displace of OH^- by H_2O ligand giving $[\text{Re}^I(\text{bpy}^{\bullet-})(\text{CO})_3(\text{OH}_2)]$ which diffuses to the bulk solution where the UV-vis absorption measurements are carried out with the optical probe.

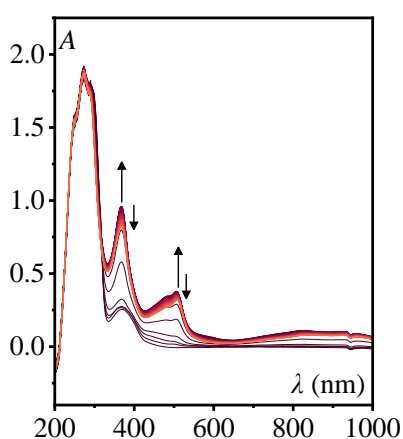


Figure V.3.3.4 6 : In-situ UV-vis evolution of of 1 mM $[\text{Re}(\text{bpy})(\text{CO})_3\text{Cl}] + 11.4 \text{ mM PNO} + 1 \text{ M H}_2\text{O} + 0.1 \text{ M n-Bu}_4\text{NPF}_6$ during $E_{\text{app}} = -1.67 \text{ V}$ under Ar. (1 spectrum / 100 s)

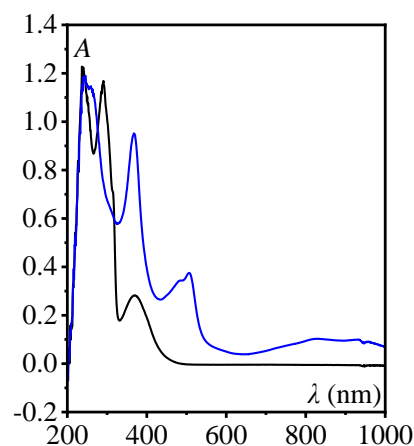


Figure V.3.3.4 7 : UV-vis spectrum of 1 mM $[\text{Re}(\text{bpy})(\text{CO})_3\text{Cl}] + 500 \text{ mM H}_2\text{O}$ before electrolysis (black) and after $E_{\text{app}} = -1.52 \text{ V}$ (blue) + 0.1 M $\text{n-Bu}_4\text{NPF}_6$ in CH_3CN .

Solution samples were taken over the course of the electrolysis and analyzed by high performance liquid chromatography (HPLC: cf. experimental section). A decrease in the concentration of PNO and an increase in the concentration of py was observed. However, the reduction of PNO and the production of py did not follow a 1:1 stoichiometry (quantity of PNO reduced is higher than that of pyridine produced): the faradaic yield of the transformation is 39 %. CVs run after the electrolysis showed a decrease in the current intensity of the direct reduction of PNO confirming consumption of PNO (Figure V.3.3.4 8).

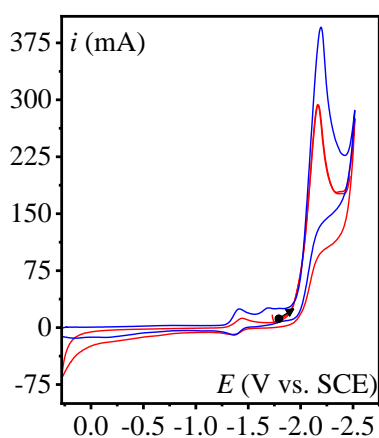


Figure V.3.3.4 8 : CVs of 1 mM $[\text{Re}(\text{bpy})(\text{CO})_3\text{Cl}] + 11.4 \text{ mM PNO}$ under Ar with 1 M H_2O (blue) and after $E_{\text{app}} = -1.67 \text{ V}$ (red) in $\text{CH}_3\text{CN} + 0.1 \text{ M n-Bu}_4\text{NPF}_6$ at 0.1 V/s on a 3 mm diam. GCE.

In addition, control experiment for the electrolysis of a solution of PNO containing 2 M H₂O was made at $E_{app} = -1.62$ V passing a charge of 4.5 C over a course of 100 min showed lower current density compared to the experiment carried in the presence of the Re catalyst (Figure V.3.3.4 10). CVs run before and after electrolysis showed very small decrease of the intensity of the direct reduction of PNO (Figure V.3.3.4 9). Hence this shows the important role of the catalyst in the reduction of PNO.

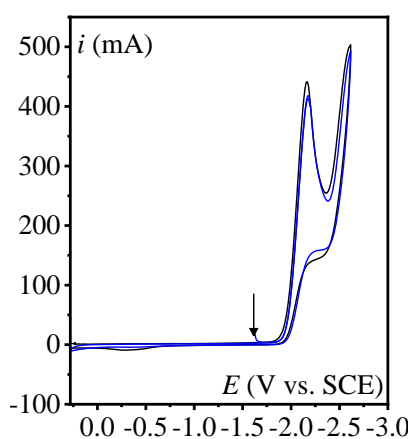


Figure V.3.3.4 9 : CVs of 10 mM PNO + 2 M H₂O before (black) and after $E_{app} = -1.62$ V (blue) under Ar in CH₃CN + 0.1 M n-Bu₄NPF₆ at 0.1 V/s on a 3 mm diameter GCE.

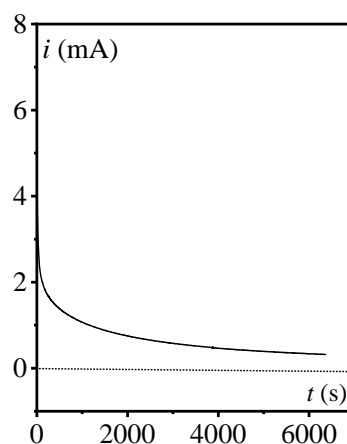


Figure V.3.3.4 10 : Current vs. time for controlled potential electrolysis at -1.62 V of 10 mM PNO + 2 M H₂O under Ar in CH₃CN + 0.1 M n-Bu₄NPF₆.

Several control experiments were made to investigate the low faradaic yield of pyridine produced. We did the electrolysis in a closed tight cell under the same conditions in the presence of H₂O, following the experiment by gas analysis but no hydrogen gas was detected. We also thought that the py produced could be reduced at the potential we applied for the electrolysis of PNO in the presence of the catalyst and water. We have performed CPE at -1.62 V for pyridine in the presence of the Re catalyst and water and we confirmed that py is not reduced at this applied potential also the CV of the direct reduction of py in the presence of H₂O shows that there is no current at this applied potential (Figure V.3.3.4 11). Hence the low yield detected for py needs to be ameliorated in the future.

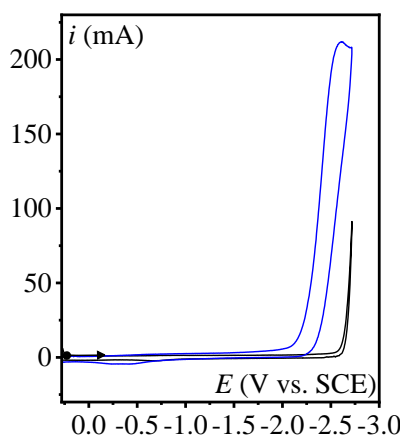


Figure V.3.3.4 11 : CVs of 5 mM py under Ar black, with 2 M H₂O (blue) in CH₃CN + 0.1 M n-Bu₄NPF₆ at 0.1 V/s on a 3 mm diam. GCE.

4. Conclusion :

A new electrochemical molecular approach has been developed for the deoxygenation of PNO under ambient conditions, inspired by the reduction of N₂O using the rhenium tricarbonyl bipyridine complexes. We have observed that both N₂O and PNO react with the mono-reduced species [Re^I(bpy^{•-})(CO)₃Cl]⁻, [Re^I(bpy^{•-})(CO)₃(MeCN)] and bi-reduced species [Re⁰(bpy^{•-})(CO)₃]⁻. However, the kinetics of the reaction with N₂O is faster compared to PNO. On the CV time scale; no catalytic current is observed in the presence of PNO while a catalytic wave is present with the Re complex under N₂O. This difference can be attributed to the difference in the bond dissociation energy of PNO (63.3 kcal.mol⁻¹)¹⁶ N₂O (39 kcal.mol⁻¹)¹⁷ which explains the difficulty in activating N-O bond breaking in PNO compared to N₂O. In addition, after the reduction of both oxide substrates a strong OH⁻ coordinating ligand is formed as a co-product playing a role in the self-modulation of the catalytic process as discussed in the Chapter IV.

References:

-
- (1) Wu, J.; Cui, X.; Chen, L.; Jiang, G.; Wu, Y. Palladium-Catalyzed Alkenylation of Quinoline-N-oxides via C–H Activation under External-Oxidant-Free Conditions. *Journal of the American Chemical Society* **2009**, *131* (39), 13888-13889. DOI: 10.1021/ja902762a.
 - (2) Londregan, A. T.; Jennings, S.; Wei, L. Mild Addition of Nucleophiles to Pyridine-N-Oxides. *Organic Letters* **2011**, *13* (7), 1840-1843. DOI: 10.1021/ol200352g.
 - (3) Sharma, U.; Park, Y.; Chang, S. Rh(III)-Catalyzed Traceless Coupling of Quinoline N-Oxides with Internal Diarylalkynes. *The Journal of Organic Chemistry* **2014**, *79* (20), 9899-9906. DOI: 10.1021/jo501995c.
 - (4) Zhang, X.; Qi, Z.; Li, X. Rhodium(III)-Catalyzed C-C and C-O Coupling of Quinoline N-Oxides with Alkynes: Combination of C-H Activation with O-Atom Transfer. *Angewandte Chemie International Edition* **2014**, *53* (40), 10794-10798. DOI:10.1002/anie.201406747.
 - (5) Ülkü, D.; Huddle, B. P.; Morrow, J. C. The crystal structure of pyridine 1-oxide. *Acta Crystallographica Section B* **1971**, *27* (2), 432-436. DOI:10.1107/S0567740871002334.
 - (6) Tanekazu, K.; Hiroshi, M. The Effect of Substituents on the Half-Wave Potential of the Polarographic Reduction of Pyridine N-Oxide Derivatives. *Bulletin of the Chemical Society of Japan* **1966**, *39* (10), 2057-2062. DOI: 10.1246/bcsj.39.2057.
 - (7) Fuentes, J. A.; Clarke, M. L. Deoxygenation of Pyridine N-Oxides by Palladium-Catalysed Transfer -Oxidation of Trialkylamines. *Synlett* **2008**, *2008* (17), 2579-2582. DOI: 10.1055/s-0028-1083508.
 - (8) Jeong, J.; Lee, D.; Chang, S. Copper-catalyzed oxygen atom transfer of N-oxides leading to a facile deoxygenation procedure applicable to both heterocyclic and amine N-oxides. *Chemical Communications* **2015**, *51* (32), 7035-7038. DOI: 10.1039/C5CC01739D.
 - (9) Kokatla, H. P.; Thomson, P. F.; Bae, S.; Doddi, V. R.; Lakshman, M. K. Reduction of Amine N-Oxides by Diboron Reagents. *The Journal of Organic Chemistry* **2011**, *76* (19), 7842-7848. DOI: 10.1021/jo201192c.
 - (10) Chandrasekhar, S.; Reddy, C. R.; Rao, R. J.; Rao, J. M. Efficient and Chemoselective Deoxygenation of Amine N-Oxides Using Polymethylhydrosiloxane. *Synlett* **2002**, *2002* (02), 0349-0351. DOI: 10.1055/s-2002-19751.
 - (11) Konev, M. O.; Cardinale, L.; Jacobi von Wangelin, A. Catalyst-Free N-Deoxygenation by Photoexcitation of Hantzsch Ester. *Organic Letters* **2020**, *22* (4), 1316-1320. DOI: 10.1021/acs.orglett.9b04632.
 - (12) Kim, K. D.; Lee, J. H. Visible-Light Photocatalyzed Deoxygenation of N-Heterocyclic N-Oxides. **2018**, *20* (23), 7712-7716. DOI: 10.1021/acs.orglett.8b03446.
 - (13) Kjellberg, M.; Ohleier, A.; Thuéry, P.; Nicolas, E.; Anthore-Dalion, L.; Cantat, T. Photocatalytic deoxygenation of N–O bonds with rhenium complexes: from the reduction of nitrous oxide to pyridine N-oxides. *Chemical Science* **2021**, *12* (30), 10266-10272. DOI: 10.1039/D1SC01974K.
 - (14) Xu, P.; Xu, H. C. Electrochemical Deoxygenation of N-Heteroaromatic N-Oxides. *Synlett* **2019**, *30* (10), 1219-1221. DOI: 10.1055/s-0037-1611541.
 - (15) Fukazawa, Y.; Rubtsov, A. E.; Malkov, A. V. A Mild Method for Electrochemical Reduction of Heterocyclic N-Oxides. *European Journal of Organic Chemistry* **2020**, *2020* (22), 3317-3319. DOI:10.1002/ejoc.202000377.
 - (16) Bach, R. D.; Schlegel, H. B. The Bond Dissociation Energy of the N–O Bond. *The Journal of Physical Chemistry A* **2021**, *125* (23), 5014-5021. DOI: 10.1021/acs.jpca.1c02741.
 - (17) Dean, J. A. Lange's Handbook of Chemistry. In *Lange's Handbook of Chemistry*, Properties of atoms radicals and bonds, fifteenth edition.

Chapter VI: Conclusions and Perspectives

This thesis tackles different fields, under the headline of homogeneous electrochemical molecular catalysis for the activation of N-O bond in two oxide substrates (N₂O and pyridine N-oxide) in organic solvents under ambient conditions using electrons as an external energy source. A field which was still underexplored.

In Chapter I we have gave a general introduction of N₂O and the mitigation strategies to reduce this molecule, following we have illustrated the principles of molecular catalysis of electrochemical reactions which will be the main principle used in our study throughout this thesis.

In Chapter II we have studied the activation of N₂O via an outersphere electron transfer from electrogenerated organic aromatic radical anions and dianions leading to the deoxygenation of N₂O via formation of N₂O^{•-} as an intermediate. Showing the selectivity of these organic redox catalysts yielding exclusively nitrogen gas in quantitative faradaic yields. We have also investigated a deactivation pathway for 4-cyanopyridine used as a redox catalyst showing a competition between the reduction of N₂O and the protonation of 4-cyanopyridine radical anion by water used as a co-substrate.

In Chapter III we have studied chemical catalysis of N₂O deoxygenation using homogeneous electrochemical molecular approach. Inspired by the molecular catalysts which showed to be efficient for the reduction of CO₂, we did screening for a large range of well known transition metal based complexes: [Re(R-bpy)(CO)₃X], [Mn(R-bpy)(CO)₃Br] and FeTPPCl which have the ability of storing more than one electron at potentials which is less than -1.72 V and in addition, the availability of one open coordination site after their reduction. We used cyclic voltammetry as an analytical tool to evaluate the catalytic efficiency towards N₂O reduction in the presence and absence of proton donors (H₂O and PhOH) which showed to be beneficial in enhancing the catalytic rates. These complexes showed to be selective catalysts for the reduction of N₂O giving quantitative faradaic yield for N₂ production even in the presence of proton source. Preliminary studies were made on Ru, Os and Rh complexes. This study which will open new directions in the future for the development of polypyrrole metal carbonyl modified electrode films.

Chapter IV has focused on deep mechanistic analysis for the reduction of N₂O by rhenium carbonyl bipyridine complexes. This was achieved with the help of well-established electrochemical methods such as cyclic voltammetry, controlled potential electrolysis along with spectroelectrochemical measurements. Focusing on knowing what is occurring on each

reduction wave of the Re complex under N_2O atmosphere, leading finally to a full proposed mechanism allowing us to see differences between the reduction of N_2O and CO_2 . Even though they both are isoelectronic and have a central electrophilic center, differences still exist. From this deep mechanistic analysis, we were able to call attention to the role of ligand exchange in the modulation of homogeneous chemical catalysis. We have observed that the reduction of N_2O by the bi-reduced Re complex produces hydroxide. The latter acts as a strong coordinating ligand and thus, demands more energy potential to decoordinate it to create a vacant coordination site for the binding of N_2O . The consequence is thus shifting the catalytic wave towards more negative potential than the potential of formation of the bi-reduced complex.

Chapter V takes insights from what was studied and developed in chapters III and IV. We have studied the deoxygenation of PNO using rhenium transition metal complexes. In spite of the difficulty in activating pyridine N-oxide compared to N_2O as attested from the CV run of the rhenium complex in the presence of PNO where no catalysis was observed. On the electrolysis time scale we were able to reduce PNO into pyridine with faradaic yields that need to be further improved in the future. A proposed mechanism for the reduction of PNO by the rhenium complex has been suggested based on mechanistic analysis by SEC measurements in which we have observed as in the case of N_2O the production of hydroxide anions which plays a role in the self modulation of molecular catalysis. In the future it would be interesting to screen a wide range of N-oxides with different substituents (EWG and EDG) on the ring followed by kinetic analysis to determine rate constants.

Our promising results and methodology used in our studies will open new directions in the future for the studying in depth reaction mechanism for instance, FeTPPCL towards N_2O reduction. The question which arises will it follow the same mechanism as the reduction of carbon dioxide?

Moreover, it will also be interesting to extend our studies for the activation of S-O bond in sulfoxides or sulfones using molecular catalysis. This type of molecules is thermodynamically difficult to reduce as pyridine N-oxide, which will be a new challenge to tackle.

Chapter VII: Experimental Part

Methods and Instrumentation

Acetonitrile (Fisher Chemical, > 99.9 %, HPLC Gradient Grade), tetrabutylammonium hexafluorophosphate ($n\text{-Bu}_4\text{NPF}_6$, Aldrich 99%) were used as received. All other chemical reagents used in the synthetic routes were obtained from commercial sources as guaranteed-grade reagents and used without further purification. The water utilized in most measurements and synthetic procedures was Milli-Q filtered (18.2 M Ω ·cm at 25 °C). Proton nuclear magnetic resonance (^1H NMR) spectra were recorded at room temperature on Bruker Advance 400 MHz spectrometers.

1. Cyclic voltammetry

Cyclic voltammograms were obtained by use of CHI 750E bipotentiostat and XM Solartron Analytical Instrument potentiostat (Echem Lab AMETEK) with XM-studio ECS as software and a standard three-electrode cell. The working electrode was a commercial 3 mm diameter glassy carbon disk. Prior to the acquisition of each CV, the WE was polished using 2 μm monocrystalline diamond paste PM (Presi) followed by rinsing with methanol. The counter-electrode was a platinum wire and the reference electrode was Ag^+/Ag (AgNO_3 10 mM) electrode in acetonitrile + 0.1 M $n\text{-NBu}_4\text{PF}_6$ in acetonitrile. The potentials are then reported vs. SCE according to: $E(\text{vs. SCE}) = E(\text{vs. Ag}^+/\text{Ag}) + 0.28 \text{ V}$. All experiments were carried out under argon or N_2O (Air Liquid) at room temperature (293 K). Ohmic drop was compensated using the positive feedback compensation implemented in the instrument.

2. Linear scan voltammetry

The LSV experiments were performed using CHI750E bipotentiostat connected to a Pine Research MSR Rotator with glassy carbon rotating disk electrode of diameter 5 mm, auxiliary electrode and the reference electrode are the same as for the CV. The LSV experiments were run with scan rate of 10 mV/s and rotation rate of 1000 rpm.

3. Exhaustive electrolysis at controlled potential for SEC

Bulk electrolysis experiments were carried out under an argon atmosphere in a glovebox at room temperature using carbon felt with apparent surface area (S_{app}) of 6.53 cm^2 as the WE and platinum wire as counter electrode isolated from the electrolytic working solution through an CH_3CN + 0.1 M $n\text{-NBu}_4\text{PF}_6$ solution bridge. The reference electrode was an Ag^+/Ag (AgNO_3 10mM) electrode in CH_3CN + 0.1 M $n\text{-NBu}_4\text{PF}_6$. The process of electrolysis was followed by monitoring the changes in the UV-Vis spectra of the solution by (SEC) absorption measurements at RT using a XM Solartron Analytical Instrument potentiostat (Echem Lab

AMETEK) with XM-studio ECS as software to perform electrochemical measurements (CV and bulk electrolysis) coupled with an MCS 501 UV-NIR (Carl Zeiss) diode array spectrophotometer equipped with an automatic shutter. The light sources are halogen (CLH 500 20 W) and deuterium lamps (CLD 500) with optic fibers (041.002–UV SN012105) using an additional $l = 1$ mm quartz immersion probe (Hellma). Ex-situ IR spectra were recorded using a PerkinElmer Two FT-IR Spectrometer 0.5 mm path length cell with KBr windows for solution analysis. The IR is given after subtracting the IR of the electrolyte solution used.

4. Controlled potential electrolysis described in (Chapter II and III)

Electrolysis were performed using a Solartron Analytical Instrument potentiostat (Modulab XM MTS) using XM-studio software. The experiments were carried out in an airtight conventional three-electrode cell (25 mL) with a GC plate working electrode (1 cm^2), the volume of the solution was 9 mL and hence the headspace 16 mL. The reference electrode was a Ag^+/Ag (AgNO_3 10 mM) in acetonitrile + 0.1 M $n\text{-NBu}_4\text{PF}_6$ and the counter electrode a platinum wire in a bridge separated from the electrolytic cell by a glass frit, containing a 0.1M $n\text{-NBu}_4\text{PF}_6$ acetonitrile solution. The electrolyte solution was purged with Ar then N_2O during 1h prior to electrolysis. To prevent any light induced process, the cell was covered by an aluminum foil and the stirring rate was 900 rpm.

Controlled potential electrolysis described in (chapter IV): The experiments were carried out in a sealed conventional three-electrode cell (48.5 mL) with a carbon felt WE with apparent surface area (S_{app}) of 6.53 cm^2 , the volume of the solution CH_3CN was 14 mL and hence the headspace 34.5 mL. The electrolyte solution was purged first with argon and then with N_2O during 60 min prior to electrolysis with stirring rate of 900 rpm.

5. Determination of solubility of N_2O

The solubility of N_2O in CH_3CN was determined according to the method described in reference.¹ Vacuum was first established in the chamber using a vacuum pump. Then the stopcock was closed and disconnecting the vacuum pump. A volume V_s taken from the saturated acetonitrile solution with N_2O using gas tight Hamilton Microsyringe was rapidly introduced into the chamber through the rubber septum. The sample then pulverized into small droplets that infuse mostly into the fritted glass disk. Then after removal of the syringe from the rubber septum, vacuum was broken by the opening the stopcock allowing the admission of atmospheric air. The stopcock was opened and closed twice allowing the passage of the dissolved gas into the gas phase. After 10 s a gas phase sample V_g was extracted from the gas phase of the

desolubilization chamber through the rubber septum using gas tight Hamilton Microsyringe and finally injected into the GC. The surface area of N₂O on the thermal conductivity detector (TCD) was integrated and the solubility was calculated based on the equation below. A schematic representation of the gas desolubilization chamber is given below (Figure VII 1):

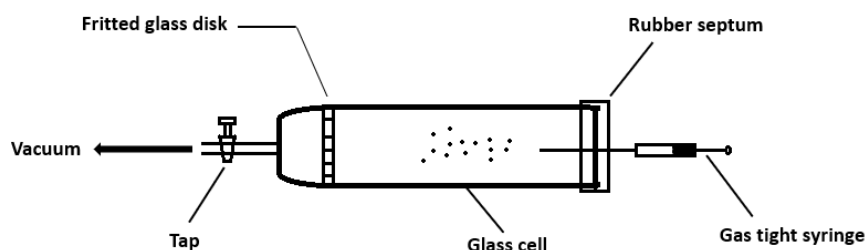


Figure VII 1 : Gas desolubilization chamber. ¹

The concentration was calculated based on the following equation:

$$C = \frac{A}{SV_m} \times \frac{273.15}{273.15 + t_c} \times \frac{V_c}{V_g \times V_s}$$

where A: integrated area of N₂O sample injected into the TCD (here, A =2189199)

S: slope of the calibration curve (S =1268872091 from Figure VII 2)

t_c: temperature in degree Celsius (21°C)

V_c: volume of the desolubilization chamber (39 mL)

V_m: molar volume of the gas under standard conditions (22.4 L/mol)

V_g: volume extracted from the gas phase of the desolubilization chamber injected in the GC for analysis (100 μL)

V_s: volume sampled from the saturated solution introduced into the chamber (100 μL)

Calibration curve was plotted by preparing mixture samples of 1, 2 and 3 mL respectively of N₂O gas adding them into a 64 mL bottle containing air and then injecting 100 μL of each sample into the GC. The obtained curve is given in (Figure VII 2).

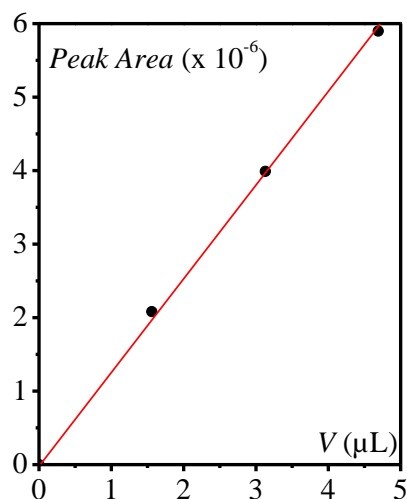


Figure VII 2 : Calibration curve: surface area of the N₂O peak (TCD detector) as function of the injected volume of N₂O.

6. Quantification of electrolysis reaction product of N₂O reduction

Calculation of faradaic yield

Gas analysis for N₂ was performed using GC/MS gas chromatography (Perkin Elmer Clarus 560) instrument with MS column fitted with GS-QPlot column from Agilent. Temperature was held at 80 °C for the oven. The carrier gas was Helium. Manual injections (100 μL) were performed at intervals during the experiment via a gas tight Hamilton microsyringe. Calibration was made by injecting a gas sample from a 5 % N₂ in N₂O obtained from a commercial gas bottle. Both Mass Spectrometry and TCD were used to detect and quantify N₂ gas.

At a given charge passed Q (in C), the % of N₂ in the gas phase was obtained from a peak area GC measurement from a 100 μL sample of the headspace. The volume of N₂ in the headspace is then obtained by: $v_{N_2}(\text{mL}) = v_H \times (\%N_2)_{\text{sample}} / 100$ knowing that the volume of the headspace v_H . Then, considering that all the N₂ produced is in the gas phase, we obtained the quantity of N₂ produced by: $n_{N_2} = v_{N_2}(\text{mL}) / 22400(\text{mL/mol})$. Hence the faradaic yield is:

$$FY(N_2) = \frac{2n_{N_2}}{Q/F}$$

Checking the cell tightness was made by monitoring the quantity of oxygen level in the cell from the GC analysis, and also by leaving the cell closed overnight without applying potential to check if the quantity of N₂ in the headspace has increased.

7. Quantification of electrolysis reaction product of pyridine N-oxide reduction

Calculation of faradaic yield:

The product of pyridine N-oxide reduction (pyridine) was detected using a Perkin Elmer liquid chromatograph equipped with an UV-vis detector set at 254 nm and a column (Epic C18 150 x 4.6 mm 5 μ m pore size and 20 μ l volume automatic injector). Best separation between PNO and pyridine were achieved with an eluent of 50/50 mixture of (H₂O / CH₃CN) with a flow rate of 0.5 mL/min. Solution samples were taken at different intervals of time and at a given charge passed Q (in C) the peak surface area of pyridine was integrated and the concentration was deduced based on calibration curve obtained with known concentration of pyridine (Figure VII 3). Hence the faradaic yield was calculated based on $FY_{py} = \frac{n(py)_{experimental}}{n(py)_{theoretical}}$ where the $n(py)$ theoretical is calculated based on the charge passed.

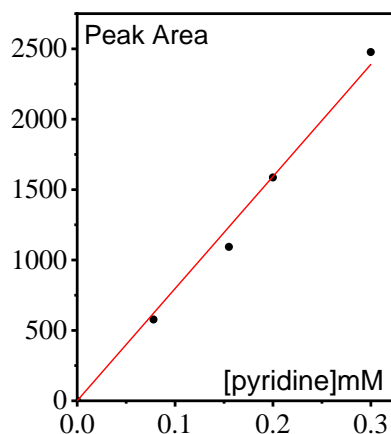
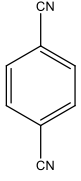
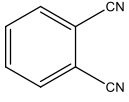


Figure VII 3 : Calibration curve for pyridine using Perkin Elmer HPLC with a UV-vis detector.

Chapter II

1. Aromatic redox catalysts

Catalyst	Structure
Terephthalonitrile	
Phthalonitrile	

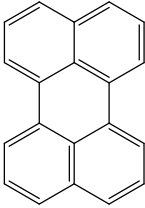
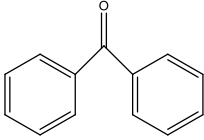
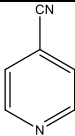
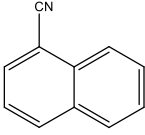
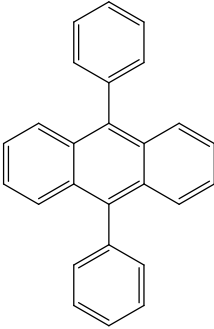
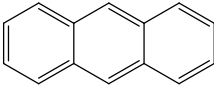
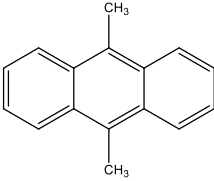
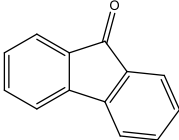
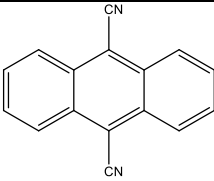
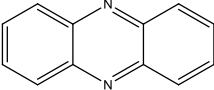
Perylene	
Benzophenone	
4-cyanopyridine	
1-naphthonitrile	
9,10-diphenylanthracene	
Anthracene	
9,10-dimethylantracene	
Fluorenone	
9,10-dicyanoanthracene	
Phenazine	

Table VII 1 : Names with structures of the organic aromatic molecules.

2. Ohmic drop correction

The resistance between the working electrode and the reference electrode is evaluated using the manual positive feedback compensation of the potentiostat. The positive feedback was manually increased until sustained oscillations are observed upon scanning in a range of potential where there is only capacitive current. The obtained value is $R_u = 120 \Omega$. A correction of $R_u \times i$ was applied on the potential axis of the raw data.

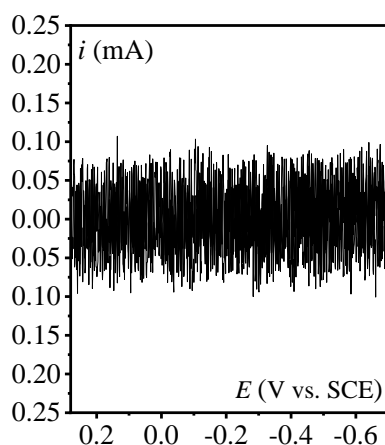


Figure VII 4 : Oscillatory behavior arising upon positive feedback compensation of the ohmic drop. $v = 5 \text{ V/s}$, $S = 0.07 \text{ cm}^2$.

Chapter III

Synthesis and characterization

All complex synthesis have already been described in the literature. We have reproduced or modified slightly the reported protocol.

Synthesis of $[\text{Re}(2,2'\text{-bpy})(\text{CO})_3\text{Cl}]$

This complex was synthesized with slight modifications to the literature.² An equimolar amount of $[\text{Re}(\text{CO})_5\text{Cl}]$ (0.3 g, 0.83 mmol) and 2,2'-bipyridine (0.136 g, 0.83 mmol) was dissolved in toluene (40 mL) and heated to 115 °C. The reaction mixture was stirred under reflux for 4 h under Ar and covered from light. Afterwards the solution was removed from the heat source and cooled down at RT and then placing it in the freezer. The product precipitated from solution as yellow powder and was filtered off and washed with diethyl ether. Pure product was isolated from the reaction and dried in desiccator with an overall yield of (74%).

$^1\text{H NMR}$ (CD_3CN , 298 K, 400 MHz) δ_{H} in ppm 7.64 (2H, m), 8.20 (2H, m), 8.43 (2H, d), 9.02 (2H, d)

FTIR in- CH_3CN ν (CO) in cm^{-1} : 2023, 1917, 1897

Synthesis of [Re(2,2'-bpy)(CO)₃Br]

Same procedure was used for the synthesis of this complex as for the chloride one. An equimolar amount of [Re(CO)₅Br] (0.205 g, 0.505 mmol) and 2,2'-bipyridine (0.084 g, 0.543 mmol) was dissolved in toluene (40 mL) and heated to 115 °C. The reaction mixture was stirred under reflux for 3 h. Afterwards the solution was removed from the heat source and cooled at RT and then placed in the freezer. The product precipitated from solution as yellow powder and was filtered off and washed with diethyl ether. Pure product was isolated from the reaction and dried in desiccator with an overall yield of (89 %).

¹H NMR (CD₃CN, 298 K, 400 MHz) δ_H in ppm 7.63 (2H, m), 8.19 (2H, m), 8.43 (2H, d), 9.04 (2H, d)

Synthesis of [Re(2,2'-bpy)(CO)₃(MeCN)]PF₆

A mixture of [Re(CO)₃(bpy)Br] (0.1 mg, 0.197 mmol) and AgOtf with Otf = trifluoromethanesulfonate (0.053 g, 0.207 mmol) were dissolved in 36 mL of acetonitrile and the mixture was refluxed under Ar covered from light for 8 h at 85 °C. The flask was kept to cool and the solution was filtered on celite to remove the precipitated AgCl salt. After 4 mL of saturated aqueous solution of NH₄PF₆ was added to the filtrate collected. Filtration was made to remove insoluble NH₄PF₆ salt. The filtrate was evaporated and the complex was dissolved in minimum (V: 1 / 1 / 1) of ethanol-water-acetone containing small quantity of NH₄PF₆. The solvent was evaporated and the complex was dissolved again in minimum quantity of dry dichloromethane, precipitation of white crystals of NH₄PF₆ was observed. Filtration was made and the filtrate collected was evaporated slowly to give green smooth solid dried after in the desiccator with an overall yield of (80 %).

¹H NMR (CD₃CN, 298 K, 400 MHz) δ_H in ppm 2.04 (3H, s), 7.72 (2H, m), 8.29 (2H, m), 8.48 (2H, d), 9.03 (2H, d)

FTIR in-CH₃CN ν (CO) in cm⁻¹: 2040, 1937 (br)

Synthesis of [Re(2,2'-bpy)(CO)₃(Otf)]

[Re(bpy)(CO)₃Br] (0.126 g, 0.25 mmol) was dissolved in acetone (22 mL). AgCF₃SO₃ (0.075g, 0.294 mmol) was added and the solution was refluxed under argon in dark for 1 h at 56 °C, the solution was filtered on celite to remove precipitated AgBr and the filtrate was evaporated then dried in the desiccator to give [Re(bpy)(CO)₃(Otf)] with an overall yield of (90 %).³

¹H NMR (CD₃CN, 298 K, 400 MHz) δ_H in ppm 7.72 (2H, m), 8.29 (2H, m), 8.48 (2H, d), 9.03 (2H, d)

Synthesis of [Re(2,2'-bpy)(CO)₃(OH)].2H₂O

A mixture of [Re(bpy)(CO)₃(OTf)] (OTf = trifluoromethanesulfonate) (0.149 g, 0.25 mmol) and KOH (1.94 mL, 4 M solution) in water (10.5 mL) and acetone (4.5 mL) was refluxed for 21 h and gave a red solution. The solution was cooled to room temperature and then concentrated to precipitate a yellow product. The solid was collected by filtration and washed with water. The product was then dried in the desiccator giving an orange colored product with an overall yield: 48 mg, 46%.^{4,5}

¹H NMR (CD₂Cl₂, 298 K, 400 MHz) δ_H in ppm 9.02 (2H, d), 8.22 (2H, d), 8.10 (2H, m), 7.55 (2H, m), 1.50 [s (br), OH and 2H₂O]

FTIR in-CH₃CN ν (CO) in cm⁻¹ : 2005, 1894, 1875

% Anal. Calcd. for C₁₃H₉N₂O₄Re.2H₂O: C, 32.56; H, 2.73; N, 5.84. found: C, 32.84; H, 2.54; N, 5.86

ESI-HRMS calculated m/z = 445.02 for [M+H]⁺ C₁₃H₁₀N₂O₄Re, found 445.02

Synthesis of [Re(4,4'-OMebpy)(CO)₃Cl]

Re(CO)₅Cl (0.105 g, 0.28 mmol) was dissolved in 50 mL of toluene. An equimolar amount of 4,4-dimethoxy-2,2-bipyridine (0.062 g, 0.28 mmol) and heated to 110 °C. After 5 min of stirring with heat, the reaction mixture started to turn yellow. Reflux was continued for 2 h 30 min, and the reaction mixture was allowed to cool. The solution was put in a freezer for 1h 30 min to precipitate the product. The yellow solid was filtered and washed with pentane before being dried under vacuum giving a product with an overall yield: 110 mg, 75 %.⁶

¹H NMR (CD₃CN, 298 K, 400 MHz) δ_H in ppm 4.04 (6H, s), 7.13 (2H, m), 7.88 (2H, d), 8.77 (2H, d)

FTIR in-CH₃CN ν (CO) in cm⁻¹ : 2020, 1913, 1893

Synthesis of [Re(4,4'-CO₂Mebpy)(CO)₃Cl]

This complex was synthesized by my colleague from our team lab Mélanie Guyot (PhD student).⁷

Synthesis of [Re(6,6'-dmbpy)(CO)₃Cl], [Re(4,4'-Bubpy)(CO)₃Cl] and [Re(4,4'-OMebpy)(CO)₃Cl]

These complexes were synthesized by our collaborators in CEA Saclay by a former PhD student Marianne Kjellberg.⁸

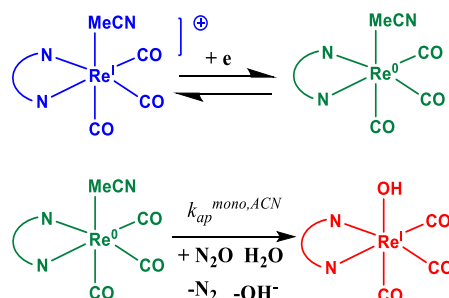
Synthesis of other transition metal complexes studied:

These complexes were synthesized by former PhD students and researchers in the team; [Re(terpy)(CO)₃Cl], [Re(4,4'-dmbpy)(CO)₃Cl], [Mn(bpy)(CO)₃Cl], [Mn(dmbpy)(CO)₃Cl], [Ru(bpy)(CO)₂Cl₂], [Ru(4,4'-dmbpy)(CO)₂Cl₂], [Ru(CO₂-isobpby)(CO)₂Cl₂], [Ru(bpy)(CO)Cl₃], [Os(bpy)₂(CO)Cl]PF₆ and [Rh(phen)(Cp*)]ClO₄.

Chapter IV: Evaluation of rate constants

Evaluation of $k_{ap}^{mono,ACN}$:

The rate constant for the reaction of N₂O with [Re^I(bpy^{*-})(CO)₃(MeCN)] was evaluated by considering EC mechanism (Scheme VII 1).



Scheme VII 1 : EC mechanism for the reaction of N₂O with the [Re^I(bpy^{-})(CO)₃(MeCN)].*

Transitioning from KP (irreversible) to KO (reversible) upon increasing the scan rate from 0.05 to 1 V/s which increases the reversibility of the wave as shown in (Figure VII 5). This indicates

that $\log\left(\frac{k_{ap}^{mono,ACN}}{Fv/RT}\right)$ varies from ca. 0.5 to -0.5, i.e. $k_{ap}^{mono,ACN} \approx 10 \text{ s}^{-1}$.⁹

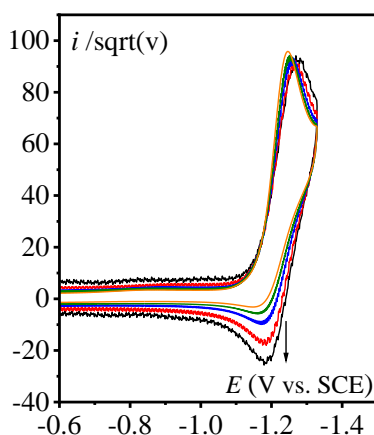


Figure VII 5 : Normalized CVs by (\sqrt{v}) of 1 mM $[\text{Re}(\text{bpy})(\text{CO})_3(\text{MeCN})]\text{PF}_6$ in $\text{CH}_3\text{CN} + 0.1 \text{ M } n\text{-Bu}_4\text{NPF}_6$ on a 3 mm diameter GCE under N_2O atmosphere at 0.05 (orange), 0.1 (green), 0.2 (blue), 0.5 (red) and 1 (black) V/s.

Evaluation of $k_{ap}^{\text{mono,OH}}$:

The rate constant for the reaction of N_2O with $[\text{Re}^{\text{I}}(\text{bpy}^{\bullet-})(\text{CO})_3(\text{OH})]$ was determined by electrogenerating a solution of the mono-reduced species by one step one electron electrolysis of $[\text{Re}(\text{bpy})(\text{CO})_3(\text{OH})]$ at -1.52 V in the glovebox (Figure VII 6).

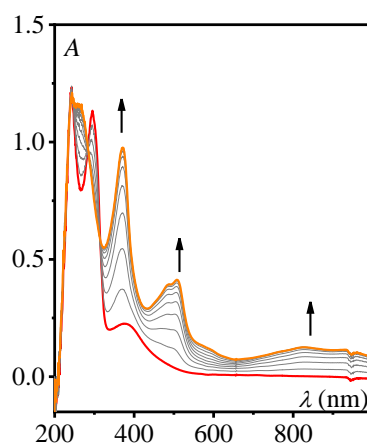


Figure VII 6 : UV-vis evolution of 0.8 mM of $[\text{Re}(\text{bpy})(\text{CO})_3(\text{OH})]$ in $\text{CH}_3\text{CN} + 0.1 \text{ M } n\text{Bu}_4\text{NPF}_6$ at $E_{app} = -1.52 \text{ V}$ on carbon felt inside the glove box.

Then a solution of CH_3CN saturated with N_2O (50 μL) was added using gas tight Hamilton Microsyringe to the solution of the mono-reduced species while monitoring the UV-vis evolution of the species in-situ using cyclic scan (1 spectrum / 40 s). Following the absorbance at 508 nm showed first a fast decay attributed to the reaction of N_2O with the bi-reduced species due to over reduction of the complex but then after slow decay was observed

which corresponds to the reaction of N_2O with the mono-reduced species $[Re^I(bpy^{\bullet-})(CO)_3(OH)]^-$ giving a value of $k_{ap}^{mono,OH} = 0.04 \text{ s}^{-1}$ (Figure VII 7).

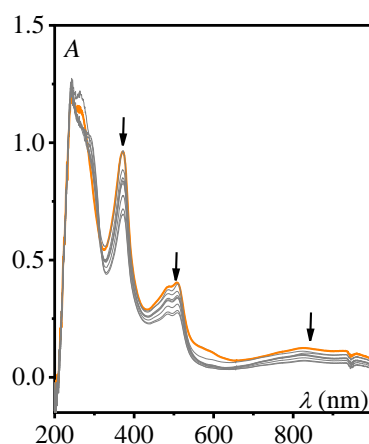


Figure VII 7 : UV-vis evolution of the mono-reduced species after addition of 1.16 mM N_2O in CH_3CN (1 spectrum / 40 s.)

Considering a second order reaction between $[Re^I(bpy^{\bullet-})(CO)_3(OH)]^-$ (0.80 mM) and N_2O (1.16 mM) the rate constant was evaluated by following the absorption at 508 nm (Figure VII 8).

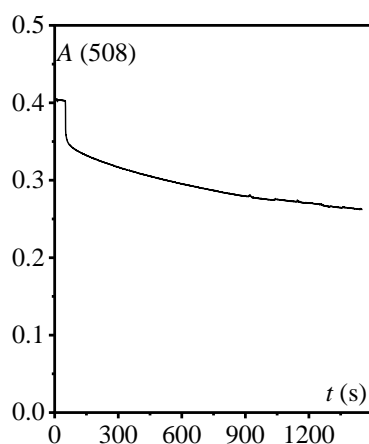
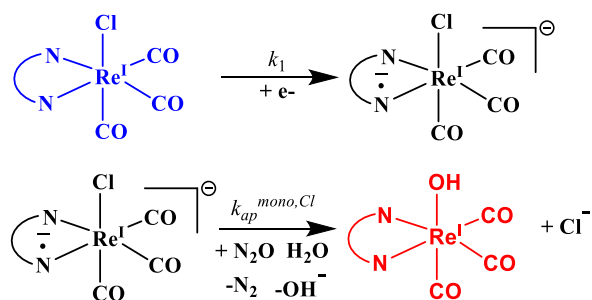


Figure VII 8 : Time evolution of absorbance at 508 nm.

Evaluation of $k_{ap}^{mono,Cl}$:

For the evaluation of the $k_{ap}^{mono,Cl}$ we consider reaction of N_2O with $[Re^I(bpy^{\bullet-})(CO)_3Cl]^-$ without formation of the dimer based on the following scheme:



Scheme VII 2 : EC mechanism for the reaction of N_2O with $[Re^I(bpy^{\bullet-})(CO)_3Cl]^-$.

First we have to determine t_{cell} which corresponds to time constant of the electrochemical cell following the one-electron electrolysis of $[Re(bpy)(CO)_3Cl]$ under Ar.

The concentration of $[Re(bpy)(CO)_3Cl]$ in the bulk is evaluated from the charge passed Q at a given time of the electrolysis:

$$[[Re(bpy)(CO)_3Cl]] = 1(\text{mM}) - \frac{Q}{FV} \quad (F \text{ is the Faraday constant}).$$

And the concentration of the dimer $[Re^0(bpy)(CO)_3]_2$ at any time is given by A_{775} / A_{775}^0

Hence the concentration of the mono-reduced species $[Re^I(bpy^{\bullet-})(CO)_3Cl]^-$ at any time is given by: (Figure VII 9 and Figure VII 10)

$$\left[[Re(bpy^{\bullet-})(CO)_3Cl]^- \right] = 1(\text{mM}) - [[Re(bpy)(CO)_3Cl]] - 2[[Re(bpy)(CO)_3]_2]$$

The rate of conversion of $[Re(bpy)(CO)_3Cl]$ into the mono-reduced species given by k_1 corresponds to the $1/t_{cell}$ where $t_{cell} = 500$ s evaluated from either the initial decay of $[Re(bpy)(CO)_3Cl]$ or the initial growth of $[Re(bpy^{\bullet-})(CO)_3Cl]^-$.

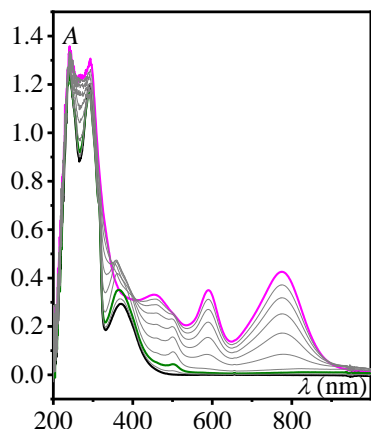


Figure VII 9: UV-vis evolution of spectra during $E_{app} = -1.42$ V on carbon felt (1 spectrum / 125 s) in $CH_3CN + 0.1$ M $n-Bu_4NPF_6$ inside the glove box.

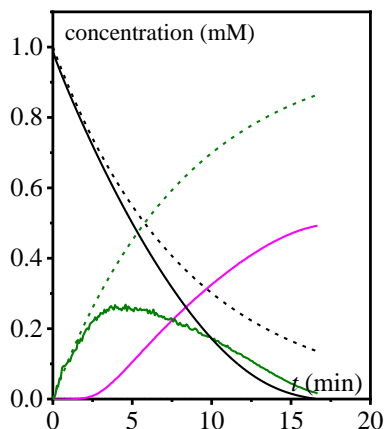


Figure VII 10: Time evolution of concentration of $[Re(bpy)(CO)_3Cl]$ (black), $[Re^I(bpy^{\bullet-})(CO)_3Cl]^-$ (green), $[Re(bpy)(CO)_3]_2$ (magenta), dotted curves growth of $[Re^I(bpy^{\bullet-})(CO)_3Cl]^-$ and decay of $[Re(bpy)(CO)_3Cl]$ corresponding to first order constant k_1 with $t_{cell} = 500$ s.

From the electrolysis of 0.83 mM $[Re(bpy)(CO)_3Cl]$ under N_2O at -1.37 V we were able to evaluate $k_{ap}^{mono,Cl}$. UV-vis monitoring of the bulk of the solution shows slow conversion of $[Re(bpy)(CO)_3Cl]$ but no dimer formation. The broad band at 650 nm corresponds to the degraded catalyst which also has contribution on the band at 500 nm. Moreover the $[Re(bpy)(CO)_3(OH)]$ complex also absorbs at 500 nm. Hence, we can write $A_{500} = [[Re(bpy)(CO)_3(OH)]] \times 0.045 + [degraded] \times 0.2$ and so the the initial concentration of the catalyst is equal to the sum of the $[Re(bpy)(CO)_3(OH)] + degraded catalysts + [Re(bpy)(CO)_3Cl]_t$ (Figure VII 11)

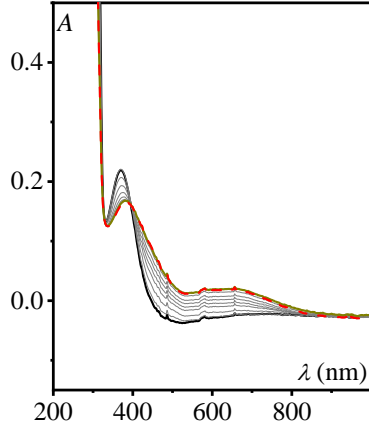


Figure VII 11 : UV-vis evolution of 0.83 mM $[\text{Re}(\text{bpy})(\text{CO})_3\text{Cl}]$ at $E_{\text{app}} = -1.37$ V under the flux of N_2O on carbon felt in $\text{CH}_3\text{CN} + 0.1$ M $n\text{-Bu}_4\text{NPF}_6$ (1 scan / 500 s).

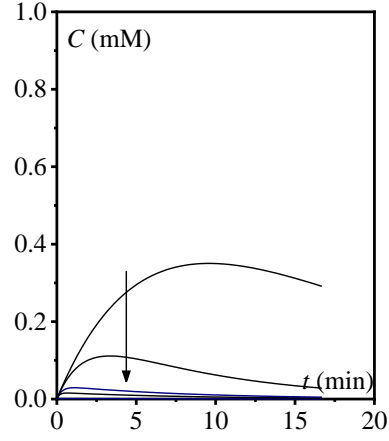


Figure VII 12 : Simulations of the time evolution of the concentration of $[\text{Re}(\text{bpy}^{\bullet-})(\text{CO})_3\text{Cl}]^-$ according to the (Scheme VII 2) with $t_{\text{cell}} = 1 / k_1 = 500$ s and $k_{\text{ap}}^{\text{mono,Cl}} = 0.0015, 0.002, 0.01, 0.05, 0.1$ s^{-1} .

Considering the reaction depicted in (Scheme VII 2):

$$[[\text{Re}(\text{bpy})(\text{CO})_3\text{Cl}]] = [[\text{Re}(\text{bpy})(\text{CO})_3\text{Cl}]]_{t=0} \exp(-k_1 t)$$

$$\frac{d[[\text{Re}(\text{bpy})(\text{CO})_3(\text{OH})]]}{dt} = k_{\text{ap}}^{\text{mono,Cl}} [[\text{Re}(\text{bpy}^{\bullet-})(\text{CO})_3\text{Cl}]^-]$$

which resolution indicates the maximal concentration of the intermediate $[\text{Re}^{\text{I}}(\text{bpy}^{\bullet-})(\text{CO})_3\text{Cl}]^-$ is:

$$[[\text{Re}(\text{bpy}^{\bullet-})(\text{CO})_3\text{Cl}]^-] = [[\text{Re}(\text{bpy})(\text{CO})_3\text{Cl}]]_{t=0} \frac{k_1}{k_{\text{ap}}^{\text{mono,Cl}} - k_1} \left[\exp(-k_1 t) - \exp(-k_{\text{ap}}^{\text{mono,Cl}} t) \right]$$

Based on the above expression plotting the concentration of the mono-reduced species $[\text{Re}(\text{bpy}^{\bullet-})(\text{CO})_3\text{Cl}]^-$ at different values of $k_{\text{ap}}^{\text{mono,Cl}}$ (Figure VII 12) shows that when $k_{\text{ap}}^{\text{mono,Cl}}$

> 0.5 s^{-1} , the concentration of $[[\text{Re}(\text{bpy}^{\bullet-})(\text{CO})_3\text{Cl}]^-]$ is small enough so that it is not seen experimentally.

References

- (1) Bhugun, I.; Lexa, D.; Savéant, J.-M. Vacuum-Triggered Flash Desolubilization Method for Determining the Solubility of Gases in Pure and Mixed Solvents. Application to Carbon Dioxide. *Analytical Chemistry* **1994**, *66* (22), 3994-3996. DOI: 10.1021/ac00094a022.
- (2) Worl, L. A.; Duesing, R.; Chen, P.; Ciana, L. D.; Meyer, T. J. Photophysical properties of polypyridyl carbonyl complexes of rhenium(I). *Journal of the Chemical Society, Dalton Transactions* **1991**, (S). DOI: 10.1039/dt9910000849.
- (3) Johnson, F. P. A.; George, M. W.; Hartl, F.; Turner, J. J. Electrocatalytic Reduction of CO₂ Using the Complexes [Re(bpy)(CO)₃L]_n (n = +1, L = P(OEt)₃, CH₃CN; n = 0, L = Cl⁻, Otf⁻; bpy = 2,2'-Bipyridine; Otf⁻ = CF₃SO₃) as Catalyst Precursors: Infrared Spectroelectrochemical Investigation. *Organometallics* **1996**, *15* (15), 3374-3387. DOI: 10.1021/om960044+.
- (4) Gibson, D. H.; Yin, X. Synthesis and Reactions of fac-Re(dmbpy)(CO)₃X (dmbpy = 4,4'-dimethyl-2,2'-bipyridyl; X = COOH, COOMe, H, OH, and OCHO). *Journal of the American Chemical Society* **1998**, *120* (43), 11200-11201. DOI: 10.1021/ja982284h.
- (5) Gibson, D. H.; Yin, X.; He, H.; Mashuta, M. S. Synthesis and Reactions of fac-[Re(dmbpy)(CO)₃X] (dmbpy = 4,4'-Dimethyl-2,2'-bipyridine; X = COOH, CHO) and Their Derivatives. *Organometallics* **2003**, *22* (2), 337-346. DOI: 10.1021/om020677q.
- (6) Smieja, J. M.; Kubiak, C. P. Re(bipy-tBu)(CO)₃Cl-improved catalytic activity for reduction of carbon dioxide: IR-spectroelectrochemical and mechanistic studies. *Inorg. Chem.* **2010**, *49* (20), 9283-9289. DOI: 10.1021/ic1008363.
- (7) Guyot, M.; Lalloz, M.-N.; Aguirre-Araque, J. S.; Rogez, G.; Costentin, C.; Chardon-Noblat, S. Rhenium Carbonyl Molecular Catalysts for CO₂ Electroreduction: Effects on Catalysis of Bipyridine Substituents Mimicking Anchorage Functions to Modify Electrodes. *Inorganic Chemistry* **2022**, *61* (40), 16072-16080. DOI: 10.1021/acs.inorgchem.2c02473.
- (8) Kjellberg, M.; Ohleier, A.; Thuéry, P.; Nicolas, E.; Anthore-Dalio, L.; Cantat, T. Photocatalytic deoxygenation of N-O bonds with rhenium complexes: from the reduction of nitrous oxide to pyridine N-oxides. *Chemical Science* **2021**, *12* (30), 10266-10272. DOI: 10.1039/D1SC01974K.
- (9) Savéant, J.-M. Costentin, C. Elements of Molecular and Biomolecular Electrochemistry. Chapter 2; John Wiley, 2019. ISBN: 978-1-119-29233-3.

Résumé :

En raison des préoccupations croissantes concernant le réchauffement climatique, l'intérêt pour la réduction du $N_2O(g)$ s'est progressivement accru ces dernières années. Le N_2O est considéré comme le principal responsable de la dégradation de la couche d'ozone stratosphérique et comme le troisième gaz à effet de serre anthropique le plus important. La réduction du N_2O en gaz N_2 est donc intéressante. Bien qu'il soit un bon oxydant thermodynamiquement parlant, le N_2O est une molécule cinétiquement inerte. Son utilisation en tant qu'oxydant nécessite donc une catalyse hétérogène dans des conditions difficiles ($> 200^\circ C$). Des enzymes, à savoir les N_2O réductases, ont été signalées comme étant capables de réduire l'oxyde nitreux, et des molécules à base de Cu, modèles des sites actifs de ces enzymes, ont été proposés et utilisés comme réactifs stœchiométriques pour réduire le N_2O . Plus généralement, la liaison et l'activation du N_2O au niveau des centres métalliques des complexes de métaux de transition ont été étudiées et examinées, mais seuls quelques exemples de réactions avec le N_2O se produisent dans des conditions de réaction homogènes et douces. Dans la plupart des cas, le N_2O réagit avec des espèces organométalliques très réactives par transfert d'atomes d'oxygène. Cette réactivité a permis le développement de transformations catalysées par des métaux de transition où le N_2O est désoxygéné en présence de réducteurs tels que les réactifs de Grignard, les phosphines, les aldéhydes, les alcools ou le CO. Il est surprenant de constater qu'en dehors de ces quelques exemples, il y a eu très peu de tentatives pour catalyser la réduction électrochimique de N_2O en N_2 à l'aide de catalyseurs moléculaires, car elle cette méthode peut également être considérée comme un exemple de prototype de réaction de désoxygénation de la liaison N-O. Pour cette raison, nous avons décidé dans cette thèse de procéder à une étude approfondie de la conversion électrochimique de N_2O en N_2 avec une approche de catalyse moléculaire dans des conditions ambiantes dans un solvant organique et d'effectuer une analyse mécanistique approfondie en utilisant des techniques spectroélectrochimiques. Notre raisonnement initial est basé sur des analogies entre le N_2O et le CO_2 (les deux molécules sont isoélectroniques avec un atome électrophile central). Le N_2O devrait se lier au site vacant du métal de la forme réduite d'un complexe de métaux de transition (rhénium et manganèse) et le transfert d'électrons devrait se produire du métal vers le centre électrophile du N_2O en présence d'un acide agissant comme source de protons pour faciliter la rupture de la liaison N-O tout en stabilisant l'oxygène. Dans ce contexte, les électrons utilisés pour la réduction du N_2O sont obtenus par voie électrochimique via l'utilisation de catalyseurs moléculaires en solutions homogènes agissant comme des navettes d'électrons de l'électrode au substrat (N_2O) lié à la forme réduite du catalyseur. Une catalyse homogène plus simple a également été réalisée par l'utilisation de catalyseurs redox (molécules aromatiques organiques) qui acquièrent les électrons, via un transfert en sphère externe, de l'électrode agissant de manière hétérogène et les délivrent, sans interaction chimique au N_2O via une réaction en sphère externe). Cela permet d'apporter une réaction électrochimique de référence en catalyse. Cependant, la catalyse chimique est plus intéressante dans le sens où le catalyseur doit être conçu pour permettre une interaction chimique entre la forme active réduite du catalyseur et le substrat.

Absract :

Due to increasing concerns regarding global warming an interest in $N_2O(g)$ reduction is gradually increasing in the recent days. N_2O has been categorized as the greatest contributor to the stratospheric ozone depletion and is regarded as the third most significant anthropogenic greenhouse gas. Reduction of N_2O to N_2 gas is therefore of interest. Despite being a thermodynamically good oxidant, N_2O is a kinetically inert molecule. Hence its use as an oxidant requires harsh conditions ($> 200^\circ C$) heterogeneous catalysis. Enzymes, namely N_2O reductase enzymes, have been reported to be able to reduce nitrous oxide, and Cu based molecular models of these enzymes active sites have been proposed and used as stoichiometric reagents to reduce N_2O . More generally, binding and activation of N_2O at transition metal complex centers has been studied and reviewed, but only few examples of reactions with N_2O occur under homogeneous and mild reaction conditions. In most cases, N_2O reacts with highly reactive organometallic species via oxygen atom transfer. This reactivity has enabled the development of transition metal-catalyzed transformations where N_2O is deoxygenated in the presence of reductants such as Grignard reagents, phosphines, aldehydes, alcohols, or CO. It is surprising to observe that, besides these few examples, there have been very few attempts to catalyze the electrochemical reduction of N_2O to N_2 with molecular catalysts as it can also be viewed as a prototypical example of N-O bond deoxygenation. For that reason, we have decided in this thesis to undergo a thorough investigation of the N_2O to N_2 electrochemical conversion with a molecular catalytic approach under ambient conditions in organic solvent and performing in depth mechanistic analysis using spectroelectrochemical techniques. Our initial reasoning is based on analogies between N_2O and CO_2 (both molecules are isoelectronic with a central electrophilic atom). N_2O should bind to the open coordination site on reduced form of a transition metal complex (rhenium and manganese) and transfer of electrons should occur from the metal to the electrophilic center of N_2O in the presence of an acid acting as proton source to facilitate the breaking of the N-O bond while stabilizing the oxygen. In this context the electrons used for the reduction of N_2O were obtained electrochemically via the use of homogenous molecular catalysts acting as electron shuttles from the electrode to the substrate and creating open coordination site for (N_2O) binding to the reduced form of the catalyst. Simpler homogeneous catalysis was also be realized by the use of redox catalysts (organic aromatic molecules) in which the catalyst acquires the electrons via an outer-sphere manner from the electrode acting heterogeneously and delivers them via an outersphere manner with no chemical interaction with N_2O . This allows to set a benchmark for catalysis. However chemical catalysis is more interesting in the sense that the catalyst should be designed to allow chemical interaction between the reduced active form of the catalyst and the substrate.